

Evolution of Hadrosaurs in the Campanian of Laramidia:
New Information from the Skull Roof and Braincase

by

Bradley McFeeters

A thesis submitted to the Faculty of Graduate and Postdoctoral
Affairs in partial fulfillment of the requirements for the degree of

Doctor of Philosophy

in

Earth Sciences

Carleton University
Ottawa, Ontario

© 2022, Bradley McFeeters

Abstract

This project seeks to investigate the morphology, ontogeny, and evolution of skull roof and braincase characters in hadrosaurids from the Campanian of northern Laramidia (Alberta and Montana), a setting in which they have been historically recognized as having a high abundance and diversity. New material is evaluated to clarify the distribution and informativeness of morphological character states, allowing for further testing of previous hypotheses about how the ontogenetic development of these characters evolved within clades, and enabling the identification of previously unrecorded taxa. Five partial skulls of *Maiasaura peeblesorum* are described from a bone bed in the Two Medicine Formation of Montana, providing the basis for a description of the braincase morphology of this taxon, and an ontogenetic series allowing the development of the crest to be compared to related taxa. Two new partial skulls from the middle unit of the Oldman Formation at the Milk River Ridge Reservoir near Warner, southern Alberta both represent first occurrences for taxa in that unit. The first is described as the first diagnostic occurrence of *Maiasaura* in Canada.

Maiasaura and *Brachylophosaurus* in the middle unit of the Oldman Formation are the first example of co-occurring brachylophosaurins. The second is described as a new taxon of Parasaurolophini, and is the oldest diagnostic lambeosaurine in Alberta. A phylogenetic analysis using maximum parsimony and Bayesian methods supports these identifications, and also reidentifies a previously described specimen from the Dinosaur Park Formation as the geologically youngest brachylophosaurin in Alberta.

Statement of Contributions

A version of Chapter 2 was published in *Acta Palaeontologica Polonica* with coauthors David Evans and Hillary Maddin (McFeeters et al. 2021b). This is an open-access article distributed under the terms of the Creative Commons Attribution License, which permits unrestricted use, distribution, and reproduction in any medium, provided the original author and source are credited. I collected the observations and wrote the draft of the manuscript. David Evans provided access to the fossil material and offered some initial ideas in the conception of the study. Hillary Maddin provided helpful comments on the manuscript and guidance with integrating this project into the thesis.

A version of Chapter 3 was published in the *Canadian Journal of Earth Sciences* with coauthors David Evans, Michael Ryan, and Hillary Maddin (McFeeters et al. 2021a). Copyright remains with the author(s) or their institution(s). I collected the observations and wrote the draft of the manuscript. David Evans and Michael Ryan provided access to the fossil material associated with the Southern Alberta Dinosaur Project, and are the sources of firsthand knowledge about the geological setting of the Milk River Ridge Reservoir locality. Hillary Maddin provided helpful comments on the manuscript and guidance with integrating this project into the thesis.

The other chapters have never been submitted for publication. A version of Chapter 4 is intended to be eventually be submitted for a publication with the same authorship as Chapter 3.

Acknowledgements

I thank my advisor Hillary Maddin for welcoming me into the lab and helping this PhD project to completion, Michael Ryan and David Evans for encouraging my involvement in dinosaur research and providing opportunities through Southern Alberta Dinosaur Project, Wendy Sloboda for finding and collecting the Alberta specimens described herein, and Brandon Strilisky at the Royal Tyrrell Museum of Palaeontology for allowing their loan and use in this project. I also thank David Evans, Kevin Seymour, Ian Morrison, and Brian Iwama (ROM), Margaret Currie, Jordan Mallon, Scott Rufolo, Alan McDonald, and Shyong En Pan (CMN), and Jade Atkins and Dana Korniesel (Maddin Lab, Carleton University) for assistance with access to specimens, Shino Sugimoto of the Royal Ontario Museum for specimen preparation, and Tom Dudgeon for help with travel accommodation and discussions. Alex Prieditis (Carleton University) provided expert additional photography of ROM 60261 and ROM 66180 (Chapter 2), and Thais Condez helped with troubleshooting the phylogenetic analyses (Chapter 5). Bucky Gates, Liz Freedman Fowler, Craig Scott, and anonymous others gave constructive reviews of the chapters submitted for publication. This work also benefitted from correspondence with Liz Freedman Fowler, Denver Fowler, and Hai Xing. Thanks also to all friends and family who offered their support and encouragement. This research was funded by an NSERC Alexander Graham Bell Canada Graduate Scholarship (2016-2018), Ontario Graduate Scholarship (2019), and Dr. George A. Jeletzky Memorial Scholarship (2019).

Table of Contents

Abstract	ii
Statement of Contributions.....	iii
Acknowledgements	iv
Table of Contents.....	v
List of Tables	viii
List of Appendices	xvii
Chapter 1: Introduction.....	1
1.1 General Background	1
1.2 Research Focus	5
1.3 Thesis Structure	12
1.4 Nomenclatural Note	13
Chapter 2: Ontogeny and variation in the skull roof and braincase of the hadrosaurid dinosaur <i>Maiasaura peeblesorum</i> from the Upper Cretaceous of Montana, USA	16
2.1 Introduction.....	17
2.2 Materials and Methods.....	20
2.3 Description	28
2.4 Discussion.....	65
2.5 Conclusions.....	79

Chapter 3: First occurrence of <i>Maiasaura</i> (Dinosauria, Hadrosauridae) from the Upper Cretaceous Oldman Formation of southern Alberta, Canada	81
3.1 Introduction.....	82
3.2 Systematic Palaeontology	86
3.3 Description	87
3.4 Discussion.....	104
3.5 Conclusions.....	116
Chapter 4: A new parasaurolophin (Hadrosauridae: Lambeosaurinae) from the Oldman Formation of southern Alberta	117
4.1 Introduction.....	118
4.2 Systematic Palaeontology	122
4.3 Description and Comparisons	123
4.4 Discussion.....	154
4.5 Conclusions.....	167
Chapter 5: Phylogenetic Analysis of Distinctive Hadrosaurid Skull Roof and Braincase Material from the Belly River Group (Upper Cretaceous, Campanian) of Alberta.....	169
5.1 Introduction.....	169
5.2 Materials and Methods.....	173
5.3 Results.....	198
5.4 Discussion and Conclusions.....	202
Chapter 6: Conclusions.....	210
6.1 New Findings on Skull Roof and Braincase Morphology	211
6.2 New Findings on Distributions and Palaeoecology	214

6.3	New Findings on Ontogeny and Heterochrony	218
6.4	Discussion and Conclusions.....	221
	Appendices	223
	References	269

List of Tables

Table 2.1 Cranial measurements (mm) of <i>Maiasaura peeblesorum</i>	21
Table 2.2 Selected cranial measurements of <i>Maiasaura peeblesorum</i> expressed as a percentage of the maximum recorded value in this study. Underlined values exceed 85% and are suggestive of “adult” dimensions (Evans 2010).	68

List of Figures

- Figure 2.1** Hadrosaurid dinosaur *Maiasaura peeblesorum* Horner and Makela, 1979, from the Two Medicine Formation (Campanian), Linster Quarry, Montana, USA; partial crania in right lateral view. A. ROM 66182. B. ROM 66181. C. ROM 60261. D. ROM 60260. E. ROM 66180.....25
- Figure 2.2** Hadrosaurid dinosaur *Maiasaura peeblesorum* Horner and Makela, 1979, from the Two Medicine Formation (Campanian), Linster Quarry, Montana, USA; partial crania in dorsal view. A. ROM 66182. B. ROM 66181. C. ROM 66180. D. ROM 60261. E. ROM 60260.....26
- Figure 2.3** Hadrosaurid dinosaur *Maiasaura peeblesorum* Horner and Makela, 1979 (ROM 66182) from the Two Medicine Formation (Campanian), Linster Quarry, Montana, USA; disarticulated partial nasals. A. Paired posterior parts of nasals in dorsal (A1), anterior (A2), ventral (A3), and medial (A4) views. B. Middle part of a nasal in lateral view. C. Anterior part of a nasal in lateral view.....27
- Figure 2.4** Hadrosaurid dinosaur *Maiasaura peeblesorum* Horner and Makela, 1979 (ROM 66180), from the Two Medicine Formation (Campanian), Linster Quarry, Montana, USA; partial skull of in anterior (A1) and anterodorsal (A2) views, with schematic interpretation of prefrontal–nasal crest morphology.29
- Figure 2.5** Hadrosaurid dinosaur *Maiasaura peeblesorum* Horner and Makela, 1979 from the Two Medicine Formation (Campanian), Linster Quarry, Montana, USA; detail of frontal morphology showing the variable development of frontal depressions. A. ROM

66182, in anterodorsal view. B. ROM 66181, in oblique right anterodorsal view. C. ROM 66180, in oblique right posterodorsal view. Scale bars 20 mm.....29

Figure 2.6 Hadrosaurid dinosaur *Maiasaura peeblesorum* Horner and Makela, 1979 from the Two Medicine Formation (Campanian), Linster Quarry, Montana, USA (A–C) and *Brachylophosaurus canadensis* Sternberg, 1953, from Oldman Formation (Campanian) of Alberta, Little Sandhill Creek, Canada (D); detail of anterior margins of

dorsotemporal fenestrae showing the variable development of overhanging ledges. A.

ROM 66181, in oblique left posterodorsal view. B. ROM 60260, in oblique right

posterodorsal view. C. ROM 66180, in posterodorsal view. D. CMN 8893, in oblique

right posteroventral view, detail of overhanging ledge viewed through the right lateral

temporal fenestra. Scale bars 20 mm.....39

Figure 2.7 Dorsotemporal bar of hadrosaurid dinosaur *Maiasaura peeblesorum* Horner and Makela, 1979 (ROM 60261 A; ROM 66180, C), from the Two Medicine Formation (Campanian), Linster Quarry, Montana, USA; compared to *Brachylophosaurus*

canadensis Sternberg, 1953 (CMN 8893, B) from the Oldman Formation (Campanian) of Alberta, Little Sandhill Creek, Canada. A, B1 in right lateral view; B2, C in dorsal view.

Scale bars 20 mm.....43

Figure 2.8 Hadrosaurid dinosaur *Maiasaura peeblesorum* Horner and Makela, 1979, from the Two Medicine Formation (Campanian), Linster Quarry, Montana, USA; partial skull of ROM 60261 in anterior view.....48

Figure 2.9 Hadrosaurid dinosaur *Maiasaura peeblesorum* Horner and Makela, 1979, from the Two Medicine Formation (Campanian), Linster Quarry, Montana, USA; partial skull of ROM 60261 in left lateral view.....49

Figure 2.10 Hadrosaurid dinosaur *Maiasaura peeblesorum* Horner and Makela, 1979 (ROM 60261), from the Two Medicine Formation (Campanian), Linster Quarry, Montana, USA; lateral wall of neurocranium showing possible variation in the position of cranial nerve VII in left lateral (A1) and right lateral (A2) views.....53

Figure 2.11 Hadrosaurid dinosaur *Maiasaura peeblesorum* Horner and Makela, 1979 (ROM 66180), from the Two Medicine Formation (Campanian), Linster Quarry, Montana, USA; lateral wall of neurocranium showing the prominent overhang of the crista prootica in right lateral (A1) and oblique right posteroventral (A2) views.55

Figure 2.12 Hadrosaurid dinosaur *Maiasaura peeblesorum* Horner and Makela, 1979, from the Two Medicine Formation (Campanian), Linster Quarry, Montana, USA; skulls in posterior view A. ROM 60261. B. ROM 66180. ROM 66180 is photographed in a slightly more posterodorsal perspective than58

Figure 2.13 Hadrosaurid dinosaur *Maiasaura peeblesorum* Horner and Makela, 1979, from the Two Medicine Formation (Campanian), Linster Quarry, Montana, USA; basicrania in ventral view. A. ROM 66182. B. ROM 60261. C. ROM 60260. D. ROM 66180. Arrows point to the contact between the basisphenoid (anterior) and basioccipital (posterior), and illustrate the variable orientation of this contact. Scale bars 20 mm.64

Figure 3.1 Geographic distribution of fossil localities in Alberta and Montana that have produced *Maiasaura* (diamonds) and *Brachylophosaurus* (triangles). Solid symbols indicate type localities. The map was created using Adobe Photoshop CS5 Extended version 12.0 x 64, using data from Freedman Fowler and Horner (2015: fig. 2). Base map adapted from Google Maps.84

- Figure 3.2** Stratigraphic distribution of *Maiasaura* (diamonds), *Brachylophosaurus* (triangles), and other brachylophosaurins (inverted triangles) in Alberta and Montana. Solid symbols indicate type localities. Modified from Thompson et al. (2021).85
- Figure 3.3** Braincase and left supratemporal arch of TMP 2010.077.0030 in left lateral (A, B), right lateral (C, D), and dorsal (E, F) views. alp, base of alar process; bpp, basiptyergoid process; crpr, crista prootica; CN III–XII, cranial nerve foramina; cup, cultriform process; dtf, dorsotemporal fenestra; ecc, endocranial cavity; fr, frontal; frcr, base of frontal crest; frd, frontal depression; ibpp, interbasiptergoid process; ica, foramen for internal carotid artery; pa, parietal; pf, prefrontal; po, postorbital; prcp, precotyloid process; prvp, prootic ventrolateral pit, qc, quadrate cotylus; sq, squamosal.88
- Figure 3.4** Nasal fragments of TMP 2010.077.0030 in lateral (A, C) and medial (B, D) views. adp, anterodorsal process; avp, anteroventral process; nf, narial fenestra; pdp, contact with posterodorsal process of premaxilla; plp, contact with posterolateral process of premaxilla. Dashed line represents the reconstructed margin of the narial fenestra.89
- Figure 3.5** Prefrontal and frontal margin of left orbital rim of TMP 2010.077.0030 in left ventrolateral (A) and medial (B) views; right orbital rim of ROM 66180 (*Maiasaura peeblesorum*) in ventrolateral view (C); close-up of right prefrontal–frontal contact of ROM 66180 in ventral view (D). fr, frontal; pf, prefrontal; po, postorbital.92
- Figure 3.6** Posterior frontals of TMP 2010.077.0030 in (A) right lateral (cross-sectional) view and (B) dorsal view. fr, frontal; frd, frontal depression; pa, parietal; pf, prefrontal; po, postorbital; t, tesserae-like bone texture.94
- Figure 3.7** Supratemporal bar of TMP 2010.077.0030 in left lateral view (A); of ROM 60261 (*Maiasaura peeblesorum*) in right lateral view, reversed (B); and of CMN 8893

<i>(Brachylophosaurus canadensis)</i> in left lateral view (C). Not to scale. pa, parietal; po, postorbital; prcf, precotyloid fossa;.....	97
Figure 3.8 Anteroventral region of neurocranium lateral wall of TMP 2010.077.0030, in left lateral view. alp, alar process; bpp, basipterygoid process; bsp, basisphenoid; CN V, trigeminal foramen (cranial nerve V); fov, fenestra ovalis; fro, fenestra rotunda; ibpp, interbasipterygoid process; lbsr, lateral ridges on basisphenoid; lsp, laterosphenoid; opc, orbital canal; prvp, prootic ventrolateral pit; wf, wedge-shaped	100
Figure 3.9 Posterior view of the occipital region in (A) TMP 2010.077.0030 and (B) CMN 8893 (<i>Brachylophosaurus canadensis</i>). bo, basioccipital; exc, exoccipital condyloid; exs, exoccipital shelf; fm, foramen magnum; nac, nasal crest; pop, paroccipital process of exoccipital; sq, squamosal.....	108
Figure 4.1 Map showing the location of the Milk River Ridge Reservoir bone bed in southern Alberta, Canada. Modified from Figure. 2 of Ryan and Russell (2005).	121
Figure 4.2 Overview of the partial skull roof and braincase TMP 2016.023.0039 in A) right lateral; and B) left lateral view.....	124
Figure 4.3 Overview of the partial skull roof and braincase TMP 2016.023.0039 in A) dorsal; and B) ventral view. The dorsal view was taken from a photo of only the upper part of the specimen.....	125
Figure 4.4 Overview of the partial skull roof and braincase TMP 2016.023.0039 in A) anterior; and B) posterior view.....	126
Figure 4.5 Detail of the prefrontal-postorbital articulation in TMP 2016.023.0039: A) right postorbital region in oblique latero-dorsal view; B) right prefrontal and postorbital in lateral view, and compared to C), left prefrontal and postorbital of <i>Parasaurolophus</i>	

<i>walkeri</i> (ROM 768), reversed, with red line highlighting how the posterior limit of the prefrontal does or does not overlie the jugal process; D) detail of posterior surface of right postorbital. Not to scale.	128
Figure 4.6 Detail of frontal platform of A) TMP 2016.023.0039 in anterior view, compared to B) <i>Parasaurolophus</i> sp. (Belly River Group), CMN 8502, and C) right frontal of <i>Parasaurolophus</i> sp. (Kaiparowits Formation), UCMP 556168.....	132
Figure 4.7 Detail of features of the middle skull roof (frontal and parietal) of TMP 2016.023.0039 in dorsal view.	134
Figure 4.8 Middle skull roof of A) TMP 2016.023.0039, and B) <i>Parasaurolophus walkeri</i> ROM 768 compared in oblique left postero-lateral view; C) same region of ROM 768 in left lateral view (compare to Figure 4.2). Not to scale.	136
Figure 4.9 Detail of neurocranial features of TMP 2016.023.0039, in A) left antero-lateral view, photographed in articulation with the skull roof; B) right lateral view,	141
Figure 4.10 Corythosaurian skull roofs in ventral view, showing the orientation of the postorbital process of the laterosphenoid, indicated by an arrow: A) TMP 2016.023.0039; B) <i>Parasaurolophus</i> sp. CMN 8502; C) <i>Velafrons coahualiensis</i> , cast of CPC-59; D) Lambeosaurini indet. ROM 23903; E) Lambeosaurini indet. ROM 694; F) Lambeosaurini indet. ROM 1940; G) <i>Hypacrosaurus altispinus</i> CMN 8675. Scale bars = 5 cm.	143
Figure 4.11 Comparison of parabasisphenoid morphology in various corythosaurians, in left lateral view: A) <i>Parasaurolophus</i> cf. <i>cyrtocristatus</i> UCMP 143270; B) <i>Parasaurolophus tubicen</i> , ROM 65650 (right lateral view, reversed); C) <i>Lambeosaurus lambei</i> , CMN 8703; D) <i>Corythosaurus casuarius</i> , ROM 1933; E) <i>Hypacrosaurus altispinus</i> , ROM 702. Not to scale. Abbreviations: ap = alar process;	146

Figure 4.12 Comparison of corythinosaurian braincases in posterior view, illustrating the variation in the arching of the ventral margin of the otoccipital: A) TMP 2016.023.0039; B) *Parasaurolophus walkeri* ROM 768; C) *Parasaurolophus* cf. *cyrtocristatus* UCMP 143270; dD) *Hypacrosaurus altispinus* CMN 8675; E) *Lambeosaurus lambei* ROM 794; F) *Corythosaurus intermedius* ROM 776; g) Lambeosaurini indet. ROM 1940. Not to scale. See references in text for additional 151

Figure 4.13 Detail of supraoccipital in TMP 2016.023.0039, in oblique postero-dorsal view. 153

Figure 5.1 Illustrations of new character states scored in the phylogenetic analysis. Numbers correspond to numbers in the text and data file. Drawings are schematic and do not represent actual specimens. 174

Figure 5.2 Illustrations of potential character states not scored in the phylogenetic analysis, in the order discussed in the text: A) thickness of the prefrontal rim; B) anterodorsal slope of the frontal; C) elevation of the median ascending process of the supraoccipital relative to the squamosal bosses; D) length and arching of the otoccipital ‘neck’ of the paroccipital processes; E) reduction of the alar process of the parabasisphenoid; F) distal swelling and lateral groove on the basiptyergoid process; G) prootic forming a pit or pocket above the basal tubera. Drawings are schematic and do not represent actual specimens. 176

Figure 5.3 Comparison of hadrosaurid braincases, showing differences in the inclination of the frontal platform (red lines): A) CMN 8502 (*Parasaurolophus* sp.) in left lateral view, showing a high angled frontal platform (character 166, state 3); B) CMN 52845 (Brachylophosaurini) in posterior view, showing distortion of the braincase; C)

CMN 52845 in right lateral view, showing a lower angled frontal platform (character 166, state 1).	197
Figure 5.4 Consensus trees of the maximum parsimony analysis: A) strict consensus tree; B) 50% majority-rule consensus tree. Bootstrap supports over 50% are shown below nodes.	199
Figure 5.5 Majority-rule consensus tree of the Bayesian phylogenetic analysis, with posterior probabilities displayed at nodes.	201
Figure 5.6 Brachylophosaurin skull roofs in dorsal view: A) CMN 52845; B) MOR 720, from Freedman Fowler and Horner 2015: Fig. 11E, reproduced under the terms of the Creative Commons Attribution License.	208

List of Appendices

Appendix 5.1. Overview of published phylogenetic analyses with a member of Hadrosauridae as the main taxon of interest, 2010 to present.....	223
Appendix 5.2. List of modifications to the matrix of Ramírez Velasco (2022).....	226
Appendix 5.3. Taxon-character matrix used in this analysis.....	233

Chapter 1: Introduction

1.1 General Background

Hadrosaurs (Hadrosauridae) are a monophyletic group of ornithischian dinosaurs impressive for their success as widespread and abundant large herbivores, their sophisticated and extravagant derived cranial anatomies, and the outstanding quality of their fossil record (Horner et al. 2004). Among the first Mesozoic dinosaurs to be scientifically described in North America was the hadrosaur *Hadrosaurus* (Leidy 1858), and for more than the past century, hadrosaurs have remained among the best known and most studied ornithischians. Their documented geographic distribution now includes most continents, and as “duckbills,” they are among the few groups of ornithischians with a widely recognized English common name. Recent research involving fossils of hadrosaurs and close relatives spans topics as varied as osteohistological analysis of growth rates and life history (Serrano et al. 2021; Wosik and Evans 2022), palaeoecological reconstruction from isotope signatures (Cullen et al. 2022; Martin et al. 2022), ontogenetic dietary shifts from tooth microwear (Wyenberg-Henzler et al. 2022), classification of eggs and embryos (L. Xing et al. 2022; Zhu et al. 2022), palaeobiological implications of palaeopathologies (Bertoazzo et al. 2021, 2022; Cruzado-Caballero et al. 2021; Słowiak et al. 2021), and even experimental music creation (Brown 2022).

The earliest members of the broader clade Hadrosauroidea evolved from an *Iguanodon*-like ornithopod in the Early Cretaceous, and their evolutionary transformation into the more derived Hadrosauridae of the Late Cretaceous is now fairly well documented (e.g., Sues and Averianov 2009; Tsogtbataar et al. 2019). A major

evolutionary radiation of ‘true hadrosaurs,’ the Euhadrosauria, encompasses the majority of known members of Hadrosauridae (or possibly all, see nomenclatural note in section 1.4), and has a fossil record restricted to the final 20 million years of the Late Cretaceous (Santonian–Maastrichtian). Norman (2014) identified the origin of this diverse clade as the one the key events in the narrative of hadrosaur evolution, following a stage characterized by anatomically conservative basal hadrosauromorphs. Euhadrosaurian novelties include functional changes to the jaws related to further development of the chewing apparatus, and a more robust temporal region to withstand the added stresses (Norman 2014). Another major difference between euhadrosaurians and other hadrosauroids is their propensity to evolve diverse, elaborate cranial crests, which in several lineages incorporate or overhang elements of the braincase. Although this crest morphology is highly variable, Hopson (1975) and later Prieto-Márquez et al. (2020) suggested that the general condition of crestedness in the solid-crested Saurolophinae and hollow-crested Lambeosaurinae is a homologous state present as the base of Euhadrosauria, with the ancestral state being a simple *Gryposaurus*-like nasal arch, and crestless saurolophines with a flat skull roof (such as *Acristavus* and *Edmontosaurus*) are secondarily derived. This remains contentious, however, and euhadrosaurian crests could alternatively be viewed as an example of parallel evolution, with various states of crestedness evolving from flat-headed ancestors multiple times. The diversification of euhadrosaurian crests brought variation in the contributing cranial elements. In addition to modified nasals, as in the earlier-diverging hadrosauroids that bore crests, crests of lambeosaurines incorporated the premaxillae, and, especially pertinent to this research, some members of both Lambeosaurinae and Saurolophinae had crests incorporating the

frontals. How this diversity of crests arose is poorly understood. There is no unambiguous transitional series of one major crest shape (as categorized by Prieto-Márquez et al. 2020: fig. 21) transforming into another ontogenetically or phylogenetically, and although some divergent crest morphologies uncontestedly arose from a crested common ancestor (such as lambeosaurins and parasaurolophins within the hollow-crested Lambeosaurinae; Evans 2006), ancestral crest morphology is unclear for some parts of the phylogeny (Ramírez-Velasco et al. 2021). Part of this problem is that the earlier stages of the euhadrosaur radiation have a relatively poor fossil record (Prieto-Márquez et al. 2020; Thompson et al. 2021), with the majority of abundant fossils coming from long after the major subclades had split.

A recent investigation into the rate of character evolution in hadrosaurs found different evolutionary patterns when cranial characters were divided into facial, crest, and mandibular/dental regions (Stubbs et al. 2019). Characters related to the feeding apparatus had a single main burst of elevated character change on the branch leading to euhadrosaurs, indicative of a key adaptive innovation, whereas multiple bursts occurred within euhadrosaurs for crest characters hypothesized to be related to socio-sexual display. Braincase characters were not included as a category, however (Stubbs et al. 2019). The braincase occupies an interesting position in the euhadrosaur skull at the junction of these different evolutionary narratives. Functional/morphological changes could involve recruitment of frontals into growing a more elaborate bony crest (social function), or modification of cranial muscle attachments or stress dissipation in response to refinement of chewing apparatus (feeding function), in addition to the braincase's obvious function of containing the brain, which was relatively large with a derived

morphology in members of this clade (Evans et al. 2009b; Lauters et al. 2013). The topic of character evolution in the hadrosaur braincase thus leads to some interesting questions. Is character evolution in hadrosaur braincase dominated by a particular functional factor? How evolutionarily independent are braincase characters? And how is this potential interaction of different selective pressures on the braincase and skull roof reflected in the evolution of ontogeny in hadrosaurs?

Knowledge of the hadrosaur braincase has a long history, with the first examples being described early in the 20th century (e.g., Brown 1914a; Lambe 1920). Ostrom (1961a) published a landmark study describing the complete cranial anatomy of hadrosaurs, with special reference to the lambeosaurine *Corythosaurus*, and attempted a thorough reconstruction of the muscles, nerves, and other soft tissues of the head, as inferred from comparisons to living reptiles. Around the same time, Langston (1960) also made a detailed analysis of the cranial nerves and inner ear. Yet as recently as the early 21st century, Horner et al. (2004: 450) were able to state in a review chapter, “Because it is not often prepared, the braincase in hadrosaurs is incompletely known.” Progress on this front has been considerable since then; many hadrosaur taxa now have detailed braincase descriptions, and a picture is forming of the braincase variation within the clade (e.g., Bell 2011a, 2011b; Brink et al. 2014; Bolotsky and Godefroit 2004; Cuthbertson and Holmes 2010; Evans 2010; Evans et al. 2007; Freedman Fowler and Horner 2015; Gates and Scheetz 2015; Gates et al. 2021; Godefroit et al. 2004a, 2004b, 2008, 2012a, 2012b; McDonald et al. 2021; Pereda-Suberbiola et al. 2009; Prieto-Márquez 2005, 2010d; Prieto-Márquez and Salinas 2010; Ramírez Velasco et al. 2021; Xing et al. 2017, 2022). However, there has been comparatively little information published on individual

and ontogenetic variation in the braincase of hadrosaurs, and some otherwise well-known taxa lack detailed braincase descriptions. Braincase characters also remain a relatively minor component of hadrosaur phylogenetic datasets, compared to other cranial characters, so are potentially undersampled as a source of phylogenetic data. For example, of the 235 cranial characters used by Xing et al. (2017), fewer than 20 describe any element of the neurocranium, versus over 20 characters each for the premaxilla, maxilla, and dentary. Gates et al. (2021: 27) noted “An interesting trend in the preservation of most *Parasaurolophus* cranial material is the prevalence of articulated skull roofs ... Growth of the large cranial crest may require that the skull become reinforced from an early ontogenetic stage, which in part may explain the prevalence of these skull sections being preserved with such frequency.” A statistical study has not yet been done to compare skull roof taphonomy in various crested vs non-crested hadrosaurs, but collections visits (CMN, ROM, pers. obs.) suggest that this taphonomic mode of articulated partial skull roofs with at least part of the braincase attached is not uncommon in other hadrosaurs, to at least some degree. The skull roof/braincase unit appears to form a significant component of the hadrosaur fossil record, with the potential for contributing important new information on their evolution.

1.2 Research Focus

This thesis focuses on the skull roof and braincase anatomy of hadrosaurs from the Campanian of Alberta, Canada, and Montana, USA. This area has among the longest histories of hadrosaur fossil collecting and research (Christison et al. 2020), and has produced excellent material of many famous taxa. During the Campanian (late Late

Cretaceous; 83.6–72.1 million years ago), North America was divided by the north-south Western Interior Seaway, with the western land mass forming the continent Laramidia. In the study area, regressions and transgressions of the western shore of the seaway are preserved in cyclical deposits of terrestrial and marine rocks. It was in this dynamic setting that Laramidian hadrosaurs appear to have been at their greatest taxonomic diversity. Hadrosaurs are the most abundant dinosaurs in the Dinosaur Park Formation in Alberta, which is the youngest of three formations that make up the Belly River Group (Eberth 2005), and has produced the greatest number of valid hadrosaur species of any formation globally (Ryan and Evans 2005). Lambeosaurines are represented in the Dinosaur Park Formation by the iconic parasaurolophin *Parasaurolophus walkeri* (Parks 1922), characterized by a long, tubular crest, and the lambeosaurins *Corythosaurus* spp. and *Lambeosaurus* spp., with varying forms of helmet-like hollow crests. Species turnover among the lambeosaurin genera occurs in the formation (Evans and Reisz 2007; Mallon et al. 2012), but has not been shown in *Parasaurolophus*, which is a less common taxon. Saurolophines are represented by the kritosaurin *Gryposaurus notabilis* in the lower part of the formation, and the saurolophin *Prosaurolophus maximus* in the upper part of the formation, with no stratigraphic overlap (Lowi-Merri and Evans 2020). The edmontosaurin *Edmontosaurus regalis* appears in the latest Campanian part of the lower Horseshoe Canyon Formation (Eberth et al. 2013), separated from the Dinosaur Park Formation by the Bearpaw transgression, but the edmontosaurin clade is so far unknown from the Belly River Group. Belly River Group hadrosaurs are less abundantly known and have a lower described diversity below the Dinosaur Park Formation. The Oldman Formation, which is time-equivalent to the lower Dinosaur Park Formation in its upper

unit, produces the brachylophosaurin *Brachylophosaurus canadensis* in its middle unit, which is a clade not recognized in the Dinosaur Park Formation (Ryan and Evans 2005). *Gryposaurus* is also present in the lower Oldman Formation (Scott et al. 2022), but lambeosaurines are practically unknown from the middle or lower Oldman, in contrast to their abundance in the Dinosaur Park Formation. Hadrosaurs are poorly known in the lowest formation of the Belly River Group, the Foremost Formation, but are represented by postcranial material referred to the brachylophosaurin *Probrachylophosaurus* (Thompson et al. 2021), originally described from the Judith River Formation in Montana (Freedman Fowler and Horner 2015). The Judith River Formation in central Montana spans a time range approximately equivalent to the entire Belly River Group (Freedman Fowler and Horner 2015; Ryan et al. 2017), and also produces material of *Brachylophosaurus* (Prieto-Márquez 2005). To the west in Montana, the Two Medicine Formation is another extensive formation deposited over approximately the same span of time but farther removed from marine influence, and contains some different hadrosaur taxa. The lower Two Medicine Formation, which is slightly older than the Foremost Formation of the Belly River Group, produces the crestless brachylophosaurin *Acristavus gagslarsoni* and another *Gryposaurus* species, *G. latidens*, which are among the oldest named hadrosaurids in Laramidia (Gates et al. 2011; Prieto-Márquez et al. 2012), although slightly older unnamed hadrosauroid material from the Santonian Milk River Formation in southern Alberta may also be hadrosaurid or euhadrosaurian (Larson et al. 2014). Higher in the Two Medicine Formation, equivalent in age to the upper Belly River Group, hadrosaurs are represented by the crested brachylophosaurin *Maiasaura peeblesorum* (Horner and Makela 1979; Horner 1983), the lambeosaurin *Hypacrosaurus*

stebingeri (Horner and Currie 1994; Brink et al. 2014), and the same species of *Prosaurolophus* that is known from the Dinosaur Park Formation (McGarrity et al. 2013).

The early 21st century had been a remarkably busy time for diagnosing new ceratopsid ornithischians from northern Laramidia, especially in the Belly River Group, where they are the most abundant large herbivorous dinosaurs after hadrosaurs. New taxa, or taxa new for the Belly River Group, that have been proposed since 2000 on the basis of both new and previously collected material include *Chasmosaurus* (or *Vagaceratops*) *irvinensis* (Holmes et al. 2001; Sampson et al. 2010), *Coronosaurus brinkmani* (Ryan and Russell 2005; Ryan et al. 2012), *Albertaceratops nesmoi* (Ryan 2007), the Dinosaur Park Formation pachyrhinosaurin (Ryan et al. 2010), *Mojoceratops perifania* (Longrich 2010; disputed by Maidment and Barrett 2011 and Campbell et al. 2016), *Spinops sternbergorum* (Farke et al. 2011), *Xenoceratops foremostensis* (Ryan et al. 2012), *Mercuriceratops gemini* (Ryan et al. 2014), *Kosmoceratops* sp. (Longrich 2014; disputed by Campbell et al. 2016), *Pentaceratops aquilonius* (Longrich 2014; disputed by Mallon et al. 2016), *Wendiceratops pinhornensis* (Evans and Ryan 2015), and the Oldman Formation nasutoceratopsin (Ryan et al. 2017). In contrast, no new hadrosaurs have been named on the basis of material from the Belly River Group in this century. The last new hadrosaur taxon named with a holotype from the Oldman Formation was *Brachylophosaurus canadensis* (Sternberg 1953), and from the Dinosaur Park Formation, *Lambeosaurus magnicristatus* (Sternberg 1935). Only very recently have updates to the diversity of the Belly River Group dinosaur assemblages once again included hadrosaurs, represented by material that is so far indeterminate at the species level (Thompson et al. 2021; Scott et al. 2022), although new hadrosaur species have

been recently named from the nearby Two Medicine (Gates et al. 2011) and Judith River (Freedman Fowler and Horner 2015) formations. The difference in the recent research histories of ceratopsids and hadrosaurs in the Belly River Group is unlikely to be entirely explained by the taxonomic diversity of hadrosaurs in these formations being already perfectly known, especially given that they remain relatively poorly known from units lower than the Dinosaur Park Formation. It is predicted that continued description of hadrosaurid material from this area will likely lead to significant new discoveries, and that by paying particular attention to the skull roof and braincase, we may gain new insights into the evolutionary questions raised in the section above, and an improved understanding of historically underappreciated characters that may aid in the taxonomic diagnosis of less complete cranial specimens.

Ongoing focused collecting efforts under the organization of the Southern Alberta Dinosaur Project, led by David C. Evans and Michael J. Ryan, has recovered new diagnostic hadrosaur cranial material from the Comrey Sandstone Zone of the Oldman Formation. Two partial skulls representing different hadrosaur taxa were both found by Wendy Sloboda at the Milk River Ridge Reservoir locality near Warner, Alberta, and are described here. Proper interpretation of this material requires solid grounding in the phylogenetic distribution, individual variability, and ontogenetic development of morphological characters. To this end, examination of material from bone beds that preserve the same element from multiple simultaneously buried individuals can be especially instructive, if there can be reasonable confidence that only one hadrosaur taxon is present (Prieto-Márquez and Gutarra 2016; Fondevilla et al. 2018). A previously

undescribed series of partial skulls of *Maiasaura peeblesorum* from the Linster Quarry bone bed in the Two Medicine Formation in Teton County, Montana, is described here.

The reconstruction of evolutionary diversification of a clade from the fossil record, although involving a large element of chance discovery, can also be seen as a test of the predictions made by previous hypotheses, such as the following:

Phylogenies make predictions of “ghost lineages” whenever the stratigraphic sequence of known taxa does not match the inferred sequence of phylogenetic divergence (Norell 1993). For example, the brachylophosaurin *Maiasaura peeblesorum* is geologically younger than *Brachylophosaurus canadensis*, but *B. canadensis* is generally considered to share a more recent common ancestry with the geologically older *Probrachylophosaurus bergei* (Freedman Fowler and Horner 2015). Thus, earlier members of the *Maiasaura* clade are predicted to have existed separately from the *Brachylophosaurus* clade since before the occurrence of *P. bergei*, and may be discoverable in the fossil record. Geographic range extensions of fossil taxa may also be predictable, if similar-aged outcrops are known from neighbouring areas, and barriers to taxa moving freely between those areas are not. For example, the hadrosaurs *Brachylophosaurus canadensis* and *Prosaurolophus maximus* have geographic ranges that include different formations on either side of the Canada/USA border (Prieto-Márquez 2005; McGarrity et al. 2013), so it can be predicted that this was also the case for additional hadrosaur taxa presently known from only one of these formations. If, on the other hand, further discoveries increase the taxonomic differences between these hadrosaur assemblages, some additional factor could be proposed to explain this.

Another prediction that can be made from phylogenetic hypotheses is that the morphological distance between hypothesized sister clades with long ghost lineages will decrease as stratigraphically lower, earlier-diverging members of either clade are discovered, since that taxon would have had less time to accumulate character changes after its divergence from their most recent common ancestor. For example, lambeosaurin and parasaurolophin lambeosaurines are both known from the lower Dinosaur Park Formation, and the skull roofs of *Corythosaurus* and *Parasaurolophus* are readily distinguishable from each other. If *Adelolophus*, without a known skull roof, is a parasaurolophin (Ramírez Velasco 2022), the members of those clades in the Dinosaur Park Formation must have lived millions of years after their most recent common ancestor. A new lambeosaurin or parasaurolophin that fills part of either ghost lineage could be predicted to probably be a more basal taxon with a more plesiomorphic skull roof morphology, which would provide evidence on the sequence and direction of character state changes.

Proposed heterochronic mechanisms of evolutionary change also make predictions about the morphologies of undiscovered taxa. Peramorphic development of the cranial crest has been hypothesized for both *Brachylophosaurus* (Freedman Fowler and Horner 2015) and *Parasaurolophus* (Evans et al. 2007; Farke et al. 2013). In the case of *Brachylophosaurus*, this was supported by the discovery of *Probrachylophosaurus*, a potentially ancestral taxon with an adult skull roof morphology reminiscent of an immature *Brachylophosaurus*, and an immature skull roof morphology reminiscent of adult *Acristavus*, a potential earlier ancestral taxon (Freedman Fowler and Horner 2015). No such sequence has been proposed for *Parasaurolophus*, in which the peramorphic

nature of the crest was inferred from comparison to contemporaneous lambeosaurins of an equivalent ontogenetic stage (Evans et al. 2007; Farke et al. 2013). However, it could be predicted that an earlier, more plesiomorphic parasaurolophin could have an adult skull roof morphology reminiscent of an immature *Parasaurolophus* individual.

1.3 Thesis Structure

This thesis includes three chapters describing new fossil material, followed by a further chapter of additional data analysis.

In Chapter 2, I describe five partial skulls referred to the brachylophosaurin *Maiasaura peeblesorum* from the Linster Quarry bone bed. Despite the overall significance of this taxon in hadrosaur research, and its unique crest morphology incorporating modified frontals, a full description of the braincase of *M. peeblesorum* had not previously appeared in the peer-reviewed literature, and a revised diagnosis of the taxon is provided. An ontogenetic series is proposed that documents the development of the nasal-frontal crest, and ontogeny in *Maiasaura* is compared to related taxa. Individual variation in the sample is also assessed.

In Chapter 3, I describe the partial skull TMP 2010.077.0030 from the Milk River Ridge Reservoir locality, and assign it to *Maiasaura* sp. This specimen represents the first documented occurrence of *Maiasaura* in Alberta, and the second brachylophosaurin taxon in the Comrey Sandstone Zone of the Oldman Formation. Implications for cladogenesis, paleobiogeographic distribution, and habitat partitioning in brachylophosaurins are discussed.

In Chapter 4, I describe the partial skull TMP 2016.023.0039 from the Milk River Ridge Reservoir locality, and assign it to a proposed new taxon within Parasaurolophini. This proposed new taxon is the oldest parasaurolophin with the skull roof and braincase preserved, and the first occurrence of this clade documented in the Oldman Formation. The diagnosis includes a unique combination of character states, including some shared with lambeosaurins. Implications for heterochrony in Parasaurolophini are discussed.

In Chapter 5, I further test the phylogenetic positions of the two Milk River Ridge Reservoir specimens by adding them to a modified version of a published hadrosaur character-taxon matrix (Ramírez Velasco 2022). New morphological characters noted over the course of this project are added or discussed. Preliminary results of both the maximum parsimony and Bayesian analyses support TMP 2010.077.0030 as a member of the *Maiasaura* clade, and TMP 2016.023.0039 as a parasaurolophin outside of *Parasaurolophus*. A novel phylogenetic position is also recovered in both analyses for CMN 52845, an enigmatic hadrosaur braincase previously described as cf. *Parasaurolophus* sp. (Evans et al. 2009a), increasing the hadrosaur diversity of the Dinosaur Park Formation.

Finally, a short concluding chapter provides a summary and synthesis of the results from the preceding chapters, and suggests directions for further research.

1.4 Nomenclatural Note

Phylogenetic nomenclature throughout this thesis follows the definitions in Madzia et al. (2021), with the reference phylogeny being the 50% majority-rule consensus tree of the maximum parsimony analysis described in Chapter 5. Thus, for the

purposes of this discussion I recognize a valid Euhadrosauria defined as the most inclusive clade containing *Lambeosaurus lambei* and *Saurolophus osborni* but not *Hadrosaurus foulkii*, and Saurolophinae (rather than Hadrosaurinae) as the name of the major euhadrosaurian clade sharing a more recent common ancestor with *Saurolophus osborni* than with *Lambeosaurus lambei*. However, I recognize this outcome is influenced by the dataset chosen as the starting point of that analysis (Ramírez Velasco 2022). The novel results of this research are not expected to have a large impact on whether or not future analyses recover a valid Euhadrosauria or Saurolophinae, because this is essentially dependent on the labile position of *Hadrosaurus foulkii*, a taxon based on a holotype that preserves no anatomical overlap with any of the specimens I describe (Prieto-Márquez et al. 2006). The publications arising from Chapters 2 and 3 (McFeeters et al. 2021a, 2021b) used the traditional “Hadrosaurinae” for the clade including such taxa as *Saurolophus*, *Edmontosaurus*, *Gryposaurus*, and *Maiasaura*. For the reason explained above these chapters use “Saurolophinae” for that clade in the thesis, but at this point I do not have strong convictions that the phylogenetic hypothesis implied in either name is unreasonable.

In publications stemming from this thesis, McFeeters et al. (2021a, 2021b) noted that the taxon Maiosaurinae (Horner 1992) can be considered effectively a senior synonym of Brachylophosaurini (Gates et al. 2011), and proposed that the name of this taxon be amended to “Maiosaurini,” attributed to Horner (1992). This follows the same Principle of Coordination for “family-group” names governed by the International Code of Zoological Nomenclature (ICZN) that is commonly invoked to justify the priority of Hadrosaurinae (attributed to Cope 1869, rather than Lambe 1918) over Saurolophinae

(Brown 1914b) in phylogenetic scenarios in which they are equivalent (Madzia et al. 2021). However, the Principle of Coordination does not exist under the International Code of Phylogenetic Nomenclature (PhyloCode), and Madzia et al. (2021) opted to retain the widely used name Brachylophosaurini, rejecting “Maiosaurini.” I agree with Madzia et al. (2021) on the benefits of establishing a more stable, formal phylogenetic nomenclature for Ornithischia, and have amended those chapters to use Brachylophosaurini, as defined by them.

Chapter 2: Ontogeny and variation in the skull roof and braincase of the hadrosaurid dinosaur *Maiasaura peeblesorum* from the Upper Cretaceous of Montana, USA

Abstract— Five new partial skulls of the hadrosaurid dinosaur *Maiasaura peeblesorum* from the Linster Quarry bone bed (Two Medicine Formation, Campanian) in Montana, USA, provide the basis for a description of the skull roof and braincase morphology of this taxon. These skulls additionally form an ontogenetic series consisting of one subadult, two small “intermediate adults”, and two larger “mature adults”. The subadult skull is approximately two thirds as wide as the largest adult and lacks a nasofrontal crest, suggesting that the crest formed relatively late in ontogeny compared to some other hadrosaurids. As in closely related taxa, larger skulls of *M. peeblesorum* have a proportionately wider braincase and a larger, more rugosely ridged nasal–frontal contact for supporting a larger crest. In the two largest adults, the skull roof incipiently overhangs the anterior margin of the dorsotemporal fenestrae. In the largest skull examined, the crest is semicircular in anterior view and incorporates flared, anteriorly concave prefrontals in its lateral margins. Intraspecific variation in *M. peeblesorum* is observed in cranial characters previously discussed as interspecific variation in related taxa, including the prominence of dorsal depressions on the frontal, and the position of the foramen for the facial nerve (CN VII). Although cranial ontogeny in *Maiasaura* shares some trends with *Brachylophosaurus* and *Probrachylophosaurus*, it deviates in other ways from the previous heterochronic model proposed for the evolution of Brachylophosaurini.

2.1 Introduction

The hadrosaurid *Maiasaura peeblesorum* was originally described by Horner and Makela (1979) in a brief paper reporting the holotype adult skull (YPM-PU 22405) and referred perinate material (YPM-PU 22400). Horner and Makela (1979) also described the first known hadrosaurid nest, containing the referred perinate material, and their study was revolutionary in its inferences regarding family life in a non-avian dinosaur. Horner (1983) later published a detailed description of YPM-PU 22405, and Prieto-Márquez and Guenther (2018) provided a detailed description of the nestlings YPM-PU 22400. Following its initial discovery, *Maiasaura peeblesorum* has become abundantly represented by referred bone bed material (Varricchio and Horner 1993; Schmitt et al. 2014), leading to this taxon figuring prominently in studies of hadrosaurid growth (Horner et al. 2000; Dilkes 2001; Baziak 2008; Guenther et al. 2018; Heck and Woodward 2018; Heck and Woodward Ballard 2019; Woodward 2019) and population biology (Woodward et al. 2015; Wosik et al. 2020).

Despite the abundance and significance of this taxon, the details of its skull roof and braincase anatomy, and the ontogenetic development and variation affecting cranial characters, are incompletely documented in comparison to most closely related brachylophosaurin taxa (Prieto- Márquez 2005; Cuthbertson and Holmes 2010; Gates et al. 2011; Freedman Fowler and Horner 2015), and Laramidian hadrosaurids more generally (Waldman 1969; Dodson 1975; Evans et al. 2005, 2007; Gates and Sampson 2007; Gates et al. 2007; Evans 2010; Brink et al. 2011; Campione and Evans 2011; Farke et al. 2013; McGarrity et al. 2013; Farke and Herrero 2014; Drysdale et al. 2019; Lowi-

Merri and Evans 2020; Takasaki et al. 2020). The skull roof of the holotype is imperfectly preserved, and much of the braincase is obscured or missing (Horner 1983). A few additional skeletons with skulls have since been referred to *Maiasaura peeblesorum*. Trexler (1995) described the skull of OTM F138 in an unpublished M.Sc. thesis. ROM 44770, a specimen with a nearly complete skull, is widely referenced in the comparative literature on hadrosaurids (Gates et al. 2011; Prieto-Márquez and Serrano-Brañas 2012; Campione et al. 2013; McGarrity et al. 2013; Bell 2014; 2014; Xing et al. 2017; Kobayashi et al. 2019; Takasaki et al. 2020), but has never been comprehensively described. Gates et al. (2011) figured the skull of TCM1 2001.89.2 as a line drawing. No skull roof or braincase elements of very small *Maiasaura* individuals have been described or figured, except for a single perinate parietal (Horner 1999: fig. 2E). Cranial elements of *Maiasaura* perinates in the YPM-PU 22400 collection are limited to maxillae, quadrates, jugals, and dentaries (Prieto-Márquez and Guenther 2018; contra Horner 1992, who cited this collection as including fused exoccipital–opisthotics).

The skull of *Maiasaura peeblesorum* is unique among hadrosaurids in the possession of a transversely-oriented solid crest that rises vertically above the skull roof, formed by the nasals, prefrontals, and frontals (Horner 1983). The currently known successive sister taxa to *Maiasaura* do not record the gradual acquisition of an increasingly *Maiasaura*-like crest morphology. Rather, although solid cranial crests are also present in the brachylophosaurin taxa most closely related to *Maiasaura* (*Brachylophosaurus* and *Probrachylophosaurus*; Freedman Fowler and Horner 2015), the crests of these taxa strongly differ from *Maiasaura* in both their orientation and composition, and the next most closely related taxon, *Acristavus*, is crestless as an adult

(Gates et al. 2011). Subadult specimens of *Maiasaura* with incomplete stages of crest development have also not been previously described. How *Maiasaura* acquired its unique cranial anatomy, from both an ontogenetic and phylogenetic perspective, thus remains open to further study.

I describe here five new partial skulls of *Maiasaura peeblesorum*, ranging from subadult to adult stages. Collectively, this material allows us to describe for the first time the ontogenetic acquisition of the crest in this taxon, and changes to the surrounding cranial elements. I also describe the anatomy of the braincase and other elements incompletely preserved in the holotype skull, and document variation in this region of *Maiasaura*. The cranial anatomy and variation is compared to other brachylophosaurins, and cranial characters previously proposed to vary between brachylophosaurin taxa are evaluated. Ontogenetic changes to the skull in *Maiasaura* and other brachylophosaurins are compared, and implications for the evolutionary history of *Maiasaura* are discussed.

Institutional abbreviations— **CMN**, Canadian Museum of Nature, Ottawa, Ontario, Canada; **MOR**, Museum of the Rockies, Bozeman, Montana, USA; **OTM**, Old Trail Museum, Choteau, Montana, USA; **ROM**, Royal Ontario Museum, Toronto, Ontario, Canada; **TCMI**, The Children’s Museum of Indianapolis, Indianapolis, Indiana, USA; **UMNHVP**, Utah Museum of Natural History Vertebrate Paleontology, Salt Lake City, Utah, USA; **YPM-PU**, Princeton University collection at the Yale Peabody Museum, New Haven, Connecticut, USA.

Other abbreviations— CN, cranial nerve.

2.2 Materials and Methods

The partial skulls ROM 60260, 60261, 66180, 66181, and 66182 were collected from the Linster Quarry locality in upper Campanian (Upper Cretaceous) strata of the Two Medicine Formation in Teton County, northwestern Montana, USA (48° 0'51.56" N, 112° 33'36.56" W). The fossil vertebrate assemblage at this locality includes additional hadrosaurid material referable to *Maiasaura peeblesorum* (including TCMI 2001.89.2; Gates et al. 2011: fig. 2B), undescribed tyrannosaurid material, and the holotype and referred material of the dromaeosaurid *Bambiraptor feinbergi* (Burnham et al. 1997, 2000). Referral of the new material to *Maiasaura peeblesorum* can be based on the presence in the adult skulls of a transversely oriented crest projecting vertically at the nasal–frontal contact (Horner and Makela 1979). Although the skull identified as subadult does not exhibit this diagnostic character, the morphology of its nasal–frontal contact can be reasonably interpreted as an ontogenetic precursor, and there is no evidence for a second hadrosaurid taxon in this bonebed.

Relative ontogenetic stage was estimated using a combination of linear measurements taken with a measuring tape (Table 2.1), and the relative development of cranial ornamentation and fusion. Quantitative definitions of “juvenile”, “subadult”, and “adult” stages, referring to individuals with linear cranial dimensions less than 50%, 50–85%, and over 85% of the greatest recorded measurement for the species, respectively, are modified from Evans (2010), using the consensus of various linear measurements on

Table 2.1 Cranial measurements (mm) of *Maiasaura peeblesorum*.

	ROM 66182		ROM 66181		ROM 60261		ROM 60260		ROM 66180	
	R	L	R	L	R	L	R	L	R	L
Length of nasofrontal contact, along its incline	48		>47		62		80		?	
Maximum width of nasofrontal contact platform	71		75		31	NA	125		~130	
Width of both frontals across the orbits	132		147		64	NA	180		198	
Dorsoventral thickness of frontals posterior to nasofrontal contact	32		42		62		>70		?	
Length of parietal sagittal crest	85		112		112		115		110	
Posterior skull roof width across squamosals	120		144		69	NA	166		194	
Maximum preserved width of orbit	73	98	NA	80?	NA	NA	NA	NA	80+	96
Length of dorsotemporal fenestra	85	86	103	102	112	NA	117	116	105	104
Width of dorsotemporal	37	38	52	52	43	NA	43	60	62	61

fenestra										
Neurocranium length, from CN II to basioccipital process of exoccipital	103	99	123	122	106	105	110	110		112
“Middle” neurocranium length, from anterior edge of CN V to posterior edge of CN XII	60	53	67	67	61	66	77e	71		72
Width across basioccipital processes of exoccipitals	53		67		49		70		83	
Width across basisphenoid- basioccipital contact	47		NA		53		65		84	
Ventral length of basioccipital	48		NA		51		60		74	
Width across occipital condyle of basioccipital	46		NA		52		69		74	

the skull roof and braincase instead of total skull length (Table 2.1). I recognize that the stage determined by this approach is an approximation and may not always perfectly correspond to the stage determined by total skull length, because allometric elongation of the snout is not accounted for, but I consider it the most reasonable approach available given the incompleteness of the skulls under consideration. Absolute individual ages could not be estimated, since all of the specimens lack suitable associated postcrania for histological sampling.

Systematic palaeontology

Ornithischia Seeley, 1887

Ornithopoda Marsh, 1881

Iguanodontia Baur, 1891

Hadrosauriformes Sereno, 1997

Hadrosauridae Cope, 1869

Saurolophinae Brown 1914b

Brachylophosaurini Gates et al. 2011

Maiasaura Horner and Makela, 1979

Type species: *Maiasaura peeblesorum* Horner and Makela, 1979; Two Medicine Formation, Montana; Upper Cretaceous, Campanian.

Maiasaura peeblesorum Horner and Makela, 1979, figures. 2.1–2.13.

Holotype: PU 22405; James and John Peebles ranch, Teton County, Montana; upper Two Medicine Formation, Campanian, Upper Cretaceous.

Material— ROM 66182, relatively small skull roof and braincase including articulated prefrontals (Figs. 2.1A, 2.2A); additional material (from the same bonebed but not all from the same individual) including disarticulated partial nasals (Fig. 2.3), lacrimal, and palatine. ROM 66181, intermediate-sized posterior skull roof and dorsolateral portion of the braincase, lacking the basisphenoid and basioccipital (Figs. 2.1B, 2.2B). ROM 60261, intermediate-sized right half of posterior skull roof, and both sides of neurocranium (Figs. 2.1C, 2.2D). ROM 60260, large, heavily fractured posterior skull roof and braincase (Figs. 2.1D, 2.2E). ROM 66180, large skull roof and braincase including articulated nasals and prefrontals (Figs. 2.1E, 2.2C). All from the Two Medicine Formation of the Linster Quarry bone bed locality in Teton Country, Montana.

Amended diagnosis— Brachylophosaurin saurolophine characterized by a short naris separated from the anterior margin of the orbit by an elongated mid-facial region; elongate facial region wide in transverse section; and nasals concave anterior to articulation with frontals (modified from Horner and Makela 1979). In the mature ontogimorph, additional autapomorphies include lateral expansion of the prefrontals as part of a dish-like, semicircular nasal–prefrontal–frontal crest; extensive thickening and fusion of the frontals, with a dorsally extending arcade that buttresses the nasal and forms the back part of the crest; and a markedly overhanging crista prootica with a defined

Figure 2.1 Hadrosaurid dinosaur *Maiasaura peeblesorum* Horner and Makela, 1979, from the Two Medicine Formation (Campanian), Linster Quarry, Montana, USA; partial crania in right lateral view. A. ROM 66182. B. ROM 66181. C. ROM 60261. D. ROM 60260. E. ROM 66180.

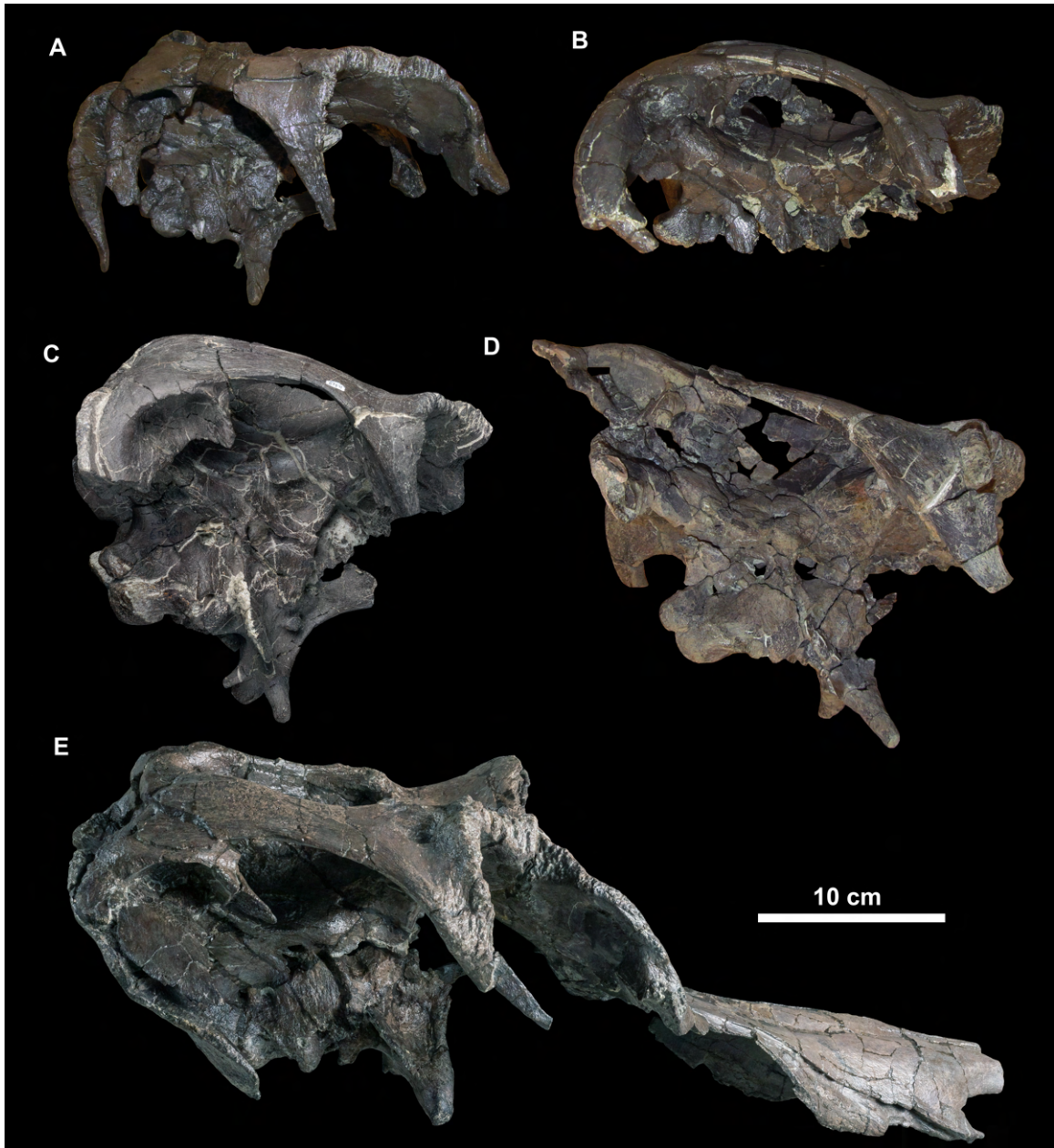


Figure 2.2 Hadrosaurid dinosaur *Maiasaura peeblesorum* Horner and Makela, 1979, from the Two Medicine Formation (Campanian), Linster Quarry, Montana, USA; partial crania in dorsal view. A. ROM 66182. B. ROM 66181. C. ROM 66180. D. ROM 60261. E. ROM 60260.

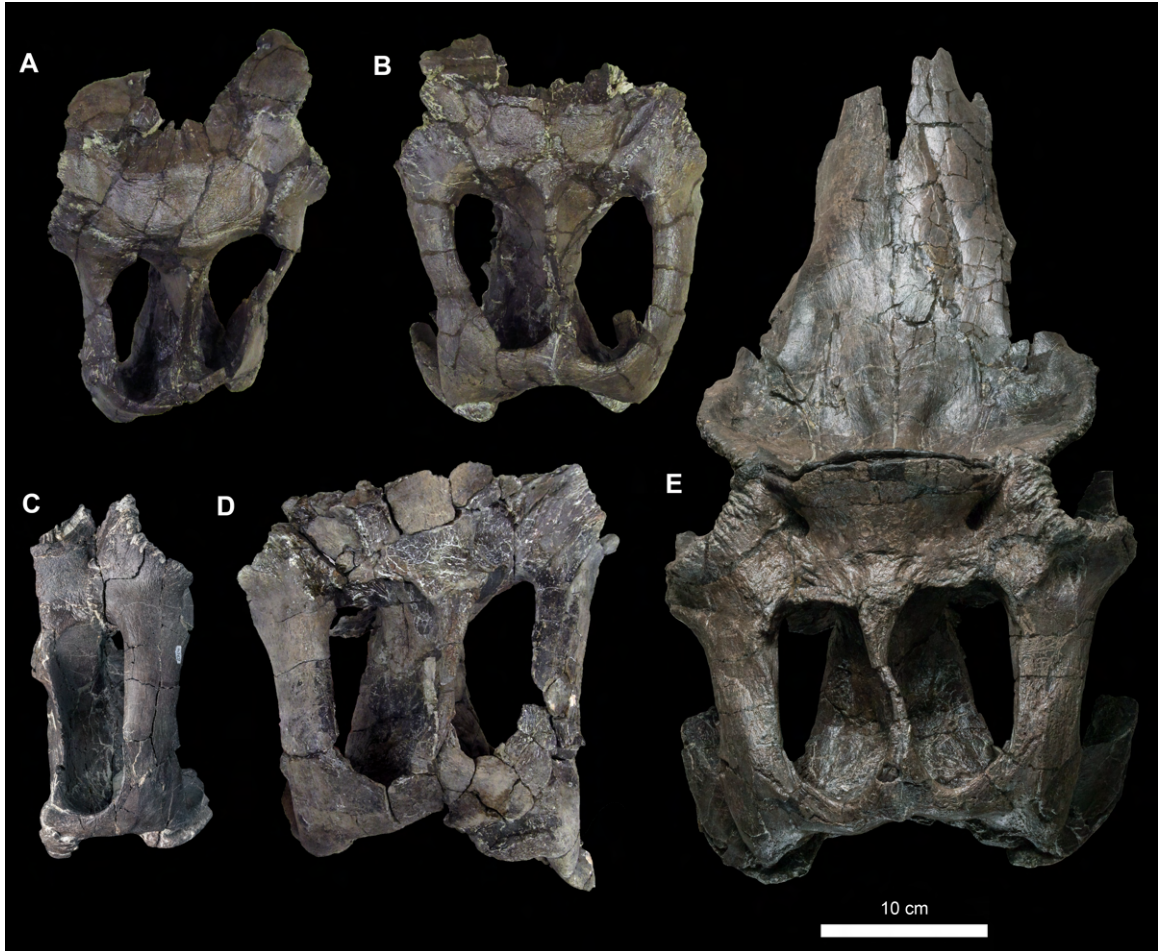
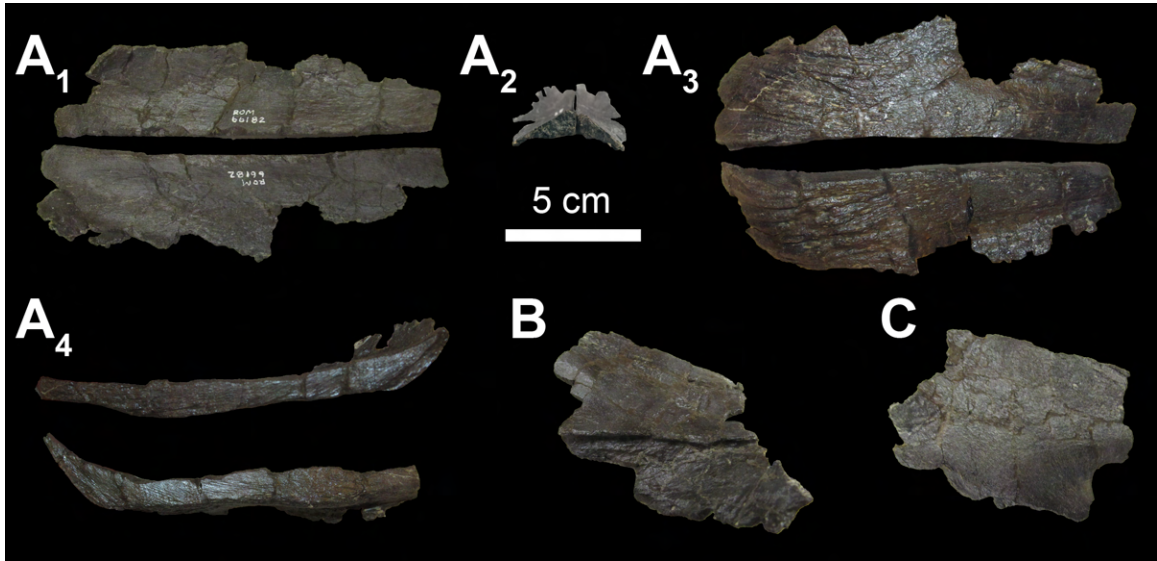


Figure 2.3 Hadrosaurid dinosaur *Maiasaura peeblesorum* Horner and Makela, 1979 (ROM 66182) from the Two Medicine Formation (Campanian), Linster Quarry, Montana, USA; disarticulated partial nasals. A. Paired posterior parts of nasals in dorsal (A1), anterior (A2), ventral (A3), and medial (A4) views. B. Middle part of a nasal in lateral view. C. Anterior part of a nasal in lateral view.



ventral channel. Skull roof differs from *Acristavus* in the anteroposteriorly less elongate dorsal exposure of the frontals and presence of an elevated solid crest at the nasal–frontal contact; from *Acristavus* and *Brachylophosaurus* in the posterior elevation of the squamosal process of the postorbital; from *Brachylophosaurus* and *Probrachylophosaurus* in that the expansion of the posterior nasal is directed dorsally rather than posteriorly, and in the incorporation of the prefrontals and frontals into the dorsally exposed surface of the crest; and from *Brachylophosaurus* in the relatively flattened dorsotemporal bar, and relatively dorsoventrally deep posterior squamosals.

2.3 Description

Dermatocranium

Nasal— Nearly complete paired nasals are preserved in articulation in ROM 66180 (Fig. 2.4), and a small posterolateral fragment of the left nasal is preserved in articulation with the ROM 66182 partial cranium (Fig. 2.5A). Additionally, four disarticulated partial nasal pieces are also catalogued under ROM 66182 (Fig. 2.3). The left and right posterior nasal pieces catalogued under ROM 66182 are compatible with being parts of the same individual, but cannot be articulated comfortably with the ROM 66182 partial cranium, and in the case of the left nasal cannot belong to it because an overlapping part of that element is already attached. However, these pieces do articulate well with the frontals of ROM 66181, and could represent the nasals of that individual (or another of the same size). The other two disarticulated nasal pieces catalogued under ROM 66182 cannot be manipulated into articulation. One is a flat middle part of a nasal with part of the contact surface for the posterolateral process of the premaxilla (Fig.

Figure 2.4 Hadrosaurid dinosaur *Maiasaura peeblesorum* Horner and Makela, 1979 (ROM 66180), from the Two Medicine Formation (Campanian), Linster Quarry, Montana, USA; partial skull of in anterior (A1) and anterodorsal (A2) views, with schematic interpretation of prefrontal–nasal crest morphology.

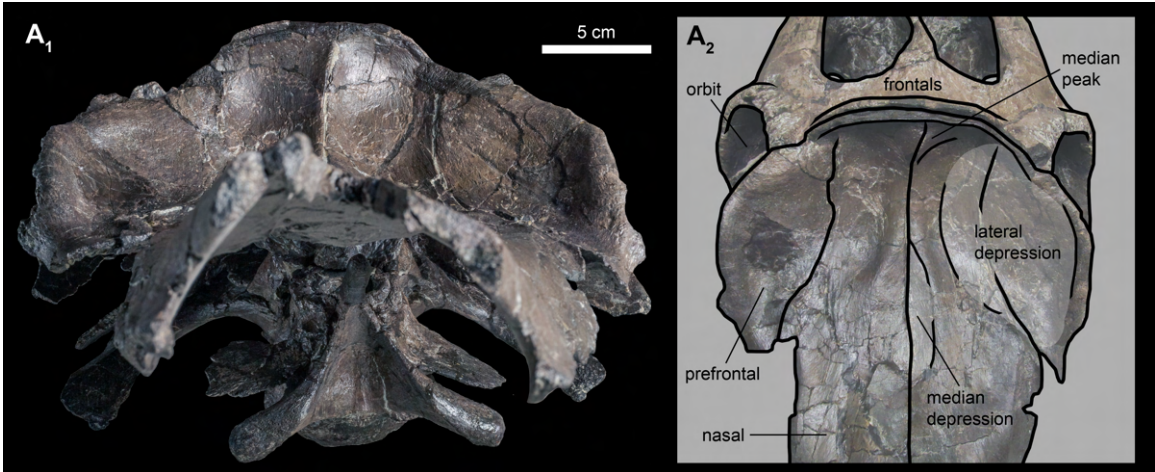
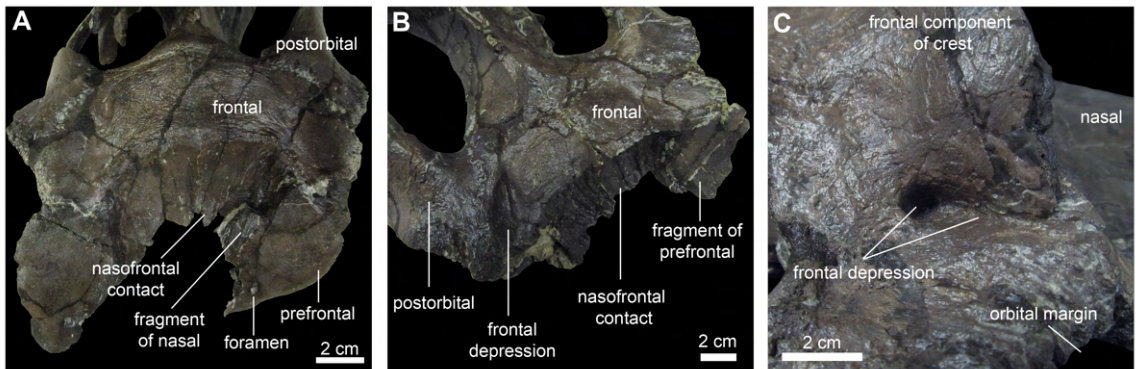


Figure 2.5 Hadrosaurid dinosaur *Maiasaura peeblesorum* Horner and Makela, 1979 from the Two Medicine Formation (Campanian), Linster Quarry, Montana, USA; detail of frontal morphology showing the variable development of frontal depressions. A. ROM 66182, in anterodorsal view. B. ROM 66181, in oblique right anterodorsal view. C. ROM 66180, in oblique right posterodorsal view. Scale bars 20 mm.



2.3B). The other is an anterior part of a right nasal including the posterior border of the narial fenestra (Fig. 2.3C).

The nasals of ROM 66180 are diagnostic of this taxon, contributing to both the elongate facial region that distances the external naris from the orbit, and participating in the composition of the distinctive forward-facing crest (Horner and Makela 1979). In both ROM 66180 and 66182 partial crania, the dorsal surfaces of the articulated nasals descend anteroventrally, unlike the *Acristavus* specimen MOR 1155 (Gates et al. 2011: fig. 4A) and *Brachylophosaurus* (Sternberg 1953), in which the horizontal dorsal surface of the nasal is approximately level with the frontal. The nasals of ROM 66180 resemble those of YPM-PU 22405 in being broad in dorsal view and dorsoventrally shallow in lateral view (Horner 1983). The nasals are broadest and flattest at mid-length, directly anterior to the prefrontal–lacrimial contact. The contact surface for the posterolateral process of the premaxilla is separated from the external surface of the nasal by a pronounced ridge, which is low and rounded posteriorly and becomes an enlarged, sharply defined overhang anteriorly, until merging with the anteroventral process beneath the narial fenestra. The posterior end of the contact surface is exposed dorsolaterally, and tapers to a point medial to the prefrontal–lacrimial contact. The dorsal exposure of the contact decreases anteriorly until it is hidden from view by the overhanging ridge, occurring at approximately the same distance along the nasals as the posterior end of a triangular gap between the nasals that held the posterodorsal processes of the premaxillae. Anteriorly, the nasals curve lateroventrally, giving the rostrum a rounded, tubular cross-section (Fig. 2.4). The outer boundary of the circumnarial fossa is not defined as a distinct depression in the region surrounding the narial fenestra, but the

lateral side of the nasal is flattened in the region indicated as the fossa by Horner (1983: fig. 1B).

The posterior ends of the nasals are inclined vertically in ROM 66180 to form the anteromedial surface of the crest (Fig. 2.4). The combined width of the nasal contribution to the crest is 100 mm. Numerous small foramina are present near the ends of the nasals, as in YPM-PU 22405 (Horner 1983: fig. 2E). The nasals in this region of ROM 66180 are thickest medially, forming a median peak with a triangular cross-section. Laterally, each nasal is slightly concave transversely, as in *Brachylophosaurus* (CMN 8893; Cuthbertson and Holmes 2010). The peaked median edge of each nasal becomes more rounded anteriorly, and expands laterally as the dorsal surface of the nasals transitions from vertically oriented to horizontally oriented, eventually reaching the lateral margin of each nasal and restricting the transverse concavities to the crest region. Anteroventral to the crest region, the arms of the median ridge diverge to define a shallow, ovoid median depression on the dorsal surface of the nasals measuring approximately 70 mm long and 40 mm wide. The posterior margin of the nasal contribution to the crest appears to have been shallowly curved in ROM 66180, versus more pointed in YPM-PU 22405 (Horner 1983: fig. 2E). The posterior edges of the nasals in ROM 66180 are reconstructed, but the dorsal margin of the naso-frontal contact on the frontal is partially preserved, giving some sense of their probable shape. ROM 66180 differs from ROM 44770 in that the latter has an appreciably more distinct median ridge along the internasal contact directly anterior to the crest, flanked by correspondingly deeper concavities, superficially recalling this region of the nasals in *Prosaurolophus* (Brown 1916: fig. 3; McGarrity et al. 2013: fig. 4). ROM 44770 further differs from ROM 66180 in that the dorsal margin of the nasals

between the prefrontal region and the external naris is slightly convex in lateral view. However, ROM 44770 is strongly compressed mediolaterally, and these differences may be diagenetic in origin.

The smaller, disarticulated, posterior partial nasals problematically catalogued with ROM 66182 (but not referable to the ROM 66182 partial cranium, and possibly belonging to the same individual as ROM 66181) present a less complex dorsal topography (Fig. 2.3A). These nasals have a triangular cross-section over most of their preserved length, formed by a thick medial edge smoothly grading to a thin lateral edge. The dorsal angle measured in anterior view is 107° (Fig. 2.2E). The medial surface, forming the internasal contact, is flat and vertical (Fig. 2.2D). The thin lateral margins are incompletely preserved. The posterior part of the nasal curves dorsally. The posterodorsal extremity of the nasal is relatively flatter and slightly transversely concave. The ventral side of the dorsally curved posterior region is characterized by anteroposterior striations for articulation with the frontal, resembling this contact on the subadult nasal of *Probrachylophosaurus* (MOR 1097, Freedman Fowler and Horner 2015: fig. 8F). Although the posterior margins of the small nasals are incompletely preserved, there is no indication of the nasal crest extending farther posteriorly than the nasal–frontal contact in any specimen of *Maiasaura*, unlike *Brachylophosaurus* and *Probrachylophosaurus*.

Prefrontal— The hadrosaurid prefrontal is considered a fusion of the ancestral prefrontal with the supraorbital elements (Maryńska and Osmólska 1979; Horner et al. 2004). A boundary between these ancestral components was not observed in any of the material examined, and the total element is herein referred to simply as the prefrontal. The pre-frontal contacts the frontal posteriorly, the nasal medially, and the lacrimal

ventrally. In at least one specimen referred to *Maiasaura*, ROM 44770, the posterolateral process of the premaxilla also reaches the prefrontal laterally, separating the nasal from the lacrimal, as in *Brachylophosaurus* (Prieto-Márquez 2005: fig. 6A; Cuthbertson and Holmes 2010: fig. 2B), but apparently not in *Acristavus* (Gates et al 2011: fig. 4C). No premaxilla–prefrontal contact is shown in the published figures of YPM-PU 22405 (Horner 1983: fig. 1B) or TCMI 2001.89.2 (Gates et al. 2011: fig. 2B), possibly due to breakage. Complete pairs of prefrontals are preserved in articulation with the frontals and nasals in ROM 66180 (Fig. 2.4), and with the frontals in ROM 66182 (Fig. 2.5A). A portion of the left prefrontal is preserved in articulation with the frontal in ROM 66181 (Fig. 2.5B). The anteroventral portion of the prefrontal forms a complex articulation with the lacrimal. In both ROM 66180 and 66182, this surface is subtriangular in ventral view, with a large socket-like depression for receiving the lacrimal on the medial side, and a smaller, shallower contact on the lateral side. In ROM 66180, the anterior tip of the ventral articular surface is elongate and tapered, with a series of parallel, anteroposterior ridges and grooves, which extend as far posteriorly as the posterior margin of the medial depression. The flat posterolateral corner of the articular surface is inclined posterodorsally towards the orbit, and bordered posteriorly by a pronounced transverse lip. The lateral side of the lacrimal directly dorsal to this flat surface is very rugose. Posteromedial to the lacrimal contact on the ventral surface of the skull roof, there is a fusiform depression enclosed by a prominently protruding rim (at least on the left side, where this region is better prepared), incorporating at least the medial edge of the prefrontal, and possibly the posterior edge of the nasal. In ROM 66182, the anteroventral surface of the prefrontal is proportionately shorter anteroposteriorly, and the rugosity on

the lateral surface dorsal to the lacrimal contact is absent. The right prefrontal of ROM 66182 can be connected to a disarticulated right lacrimal sharing the same specimen number, and possibly belonging to this individual. The long axis of the lacrimal in ROM 66182, when articulated with the prefrontal, is steeply angled anteroventrally, maintaining approximately the same inclination as the anteroventral portion of the prefrontal. In larger specimens of *Maiasaura*, including YPM-PU 22405 (Horner 1983: fig. 1) and ROM 44770, the long axis of the lacrimal is nearly horizontal.

Horner (1983: 31) was unable to determine the shape of the prefrontal in YPM-PU 22405, but noted that it appeared to form “a portion of the lateral surface” of the nasofrontal crest. The prefrontal in ROM 66180 is confirmed to participate extensively in the anterolateral surface of the crest, contributing an anteriorly directed surface continuous with and comparable in area to that of the posterior nasals. The area of the crest formed by the prefrontals is weakly concave anteriorly with a convex dorsolateral rim, producing an approximately semi-circular, dish-like overall crest morphology in anterior view. Like the nasal, the tilted posterodorsal portion of the prefrontal is broad mediolaterally and thin dorsoventrally. It descends steeply anteroventrally from the dorsal edge of the crest, and its convex lateral edge projects laterally from its contact with the frontal, attaining a maximum width in dorsal view that is greater than the frontals, comparable to that of the squamosals, and only slightly less than that of the postorbitals. As with the other bones forming the dorsal margin of the orbit, the lateral margin of the prefrontal is rugosely textured, particularly on a flat, posterolaterally-facing triangular surface directly anterior to the prefrontal–frontal contact, but also continuing

anteroventrally along the lateral rim of the crest. The anteroventral end of the lateral rim of the crest overhangs the posterior end of the lacrimal contact.

The dorsal portion of the prefrontal is also anteroposteriorly elongate and steeply tilted with curved lateral margins in ROM 44770 and 66182, but its anterodorsal surface is relatively flat, so the dish-like crest morphology is not expressed. In ROM 66182, the dorsal surface of each prefrontal is pierced by a supraorbital foramen, positioned towards the medial side of the element approximately two-thirds of the total length from its posterior margin, a short distance posterior to the point at which it narrows to its minimum breadth and twists laterally (Fig. 2.5A). On the ventral side of the prefrontal, the foramen is positioned more posteriorly, close to the visible interdigitating contact with the frontal. Definitive prefrontal foramina were not observed in ROM 44770 or 66180, possibly due to preservational factors. A small foramen may be visible towards the medial edge of the ventral surface of the left prefrontal in ROM 66180.

Frontal— The frontals contact the nasals and prefrontals anteriorly, the postorbitals and parietal posteriorly, and the neurocranium ventrally. The contact between the left and right frontals is visible in ROM 66181 and 66182 (Fig. 2.5A, B), but it is less prominent than in subadult *Brachylophosaurus* (Freedman Fowler and Horner 2015: fig. 11). In ROM 60260 and 66180, the frontals are indistinguishably fused into a single element, unlike in other saurolophines. The state of this character is obscured by breakage in ROM 60261. Horner (1983) characterized the frontals of YPM-PU 22405 as short and massive, which is corroborated by the new material. The frontals are proportionately wider and thicker in the larger individuals, relative to their length.

The anterior surface of the frontal forms a broad, continuous contact with the nasal and prefrontal. In dorsal view, the external frontal margin of the contact produces a weakly pronounced apex inserting between the individual nasal contact surfaces in ROM 66182 (Fig. 2.5A), whereas the midline of the nasal–frontal contact is transversely straight in dorsal view in ROM 60260 and 66181 (Fig. 2.5B). At its lateral limits, the nasal–frontal contact curves slightly anteriorly in ROM 60261, 66181, and 66182, whereas the entire contact is straight in dorsal view in ROM 60260 and 66180. Among saurolophines, a relatively straight transverse nasal–frontal contact is also present in *Edmontosaurus*, but differs from *Maiasaura* in being distinctly crenulated (Xing et al. 2017). The nasal contact is flat and only partially inclined in ROM 66182, but is anteroposteriorly concave and approximately vertical in ROM 60260, 60261, 66180, and 66181. The contact surface is relatively finely grooved in ROM 66182, more deeply grooved in ROM 66181 and 60261, and very strongly grooved in ROM 60260. In ROM 60261, the prominence of the grooves increases medially. In dorsal view, the contact between the nasals and frontals is slightly bowed posteriorly in ROM 44770, 60261, 66181, and 66182, and essentially straight in ROM 60260 and 66180. Elevation of the frontal immediately posterior to the nasal contact is slight in ROM 66181 and 66182, but distinctly present in ROM 60261. The flat dorsal surface of the frontal in ROM 66181 and 66182 has a slightly wrinkled, pebbly texture. The dorsal surface appears to be damaged in ROM 60261. The anterior frontal is highly elevated posterior to the nasals in ROM 60260 and 66180, and the dorsal surface across the paired frontals is convex transversely. A lesser, but distinct elevation also occurs at the posterior margin of the

frontal in ROM 60260 and 66180, so in lateral view the dorsal surface of the frontal is concave.

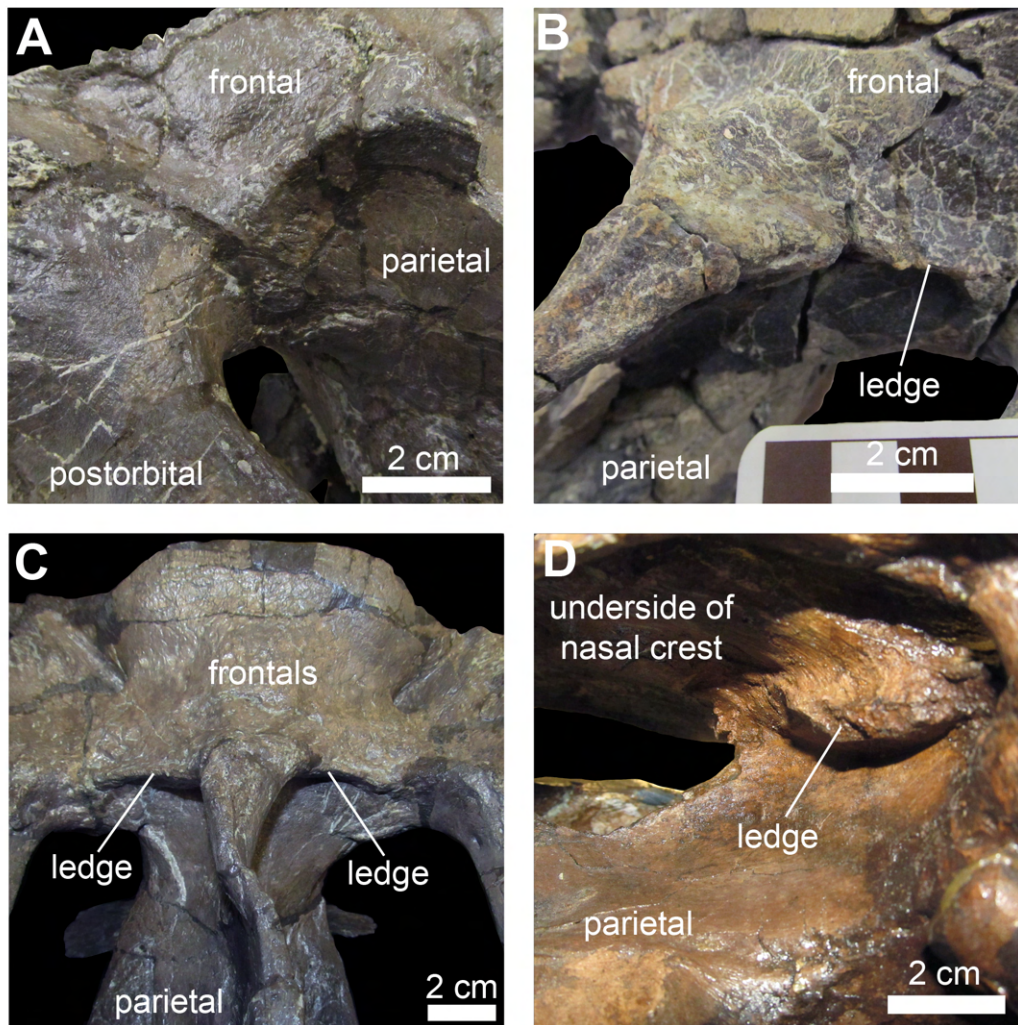
Frontal depressions, previously noted to occur in other brachylophosaurins (Horner 1988; Freedman Fowler and Horner 2015), are essentially absent in ROM 66182 (Fig. 2.5A). The posterior corner of a shallow, incomplete incipient frontal depression may be present on the right frontal, if this indentation is a true anatomical feature. Frontal depressions in ROM 60261 and 66181 are narrow and elongate, oriented diagonally, and projecting posteromedially between the nasal–frontal contact and the orbital rim (Fig. 2.5B). The frontal depressions are situated close to (though not contacting), and parallel to, the interdigitating frontal–postorbital sutures. In ROM 66181, the distance between the frontal depression and the parietal is slightly less than the length of the depression, and a projection of the long axis of the depression would contact the middle of the midline parietal bar. In ROM 60261, the distance between the frontal depression and the parietal exceeds the length of the depression, and a projection of the long axis of the depression would contact the anterior end of the midline parietal bar. In ROM 66180, the frontal depressions are relatively deep (over 10 mm), but constricted anteriorly, so that the dorsal openings are smaller and more circular than in the other specimens (Fig. 2.5C). The frontal depressions may also be constricted in ROM 60260, but damage to this region makes their morphology, if present, unclear.

Horner (1983) described the frontal of YPM-PU 22405 as contacting supraorbital elements laterally, though most descriptions of brachylophosaurin skulls do not mention these elements and describe the frontal as contributing directly to the dorsal margin of the orbit (Sternberg 1953; Prieto-Márquez 2005; Cuthbertson and Holmes 2010; Gates et al.

2011; Freedman Fowler and Horner 2015). Definitive supraorbitals were not observed in any of the *Maiasaura* specimens examined in this study, but the contacts may be obscured by imperfect preservation. A possible example of a supraorbital is visible in ventral view in the right orbit of ROM 66180, based on comparison to the figure of YPM-PU 22405 (Horner 1983: fig. 2G). The small foramen described by Horner (1983) as entering the dorsal surface of the skull medial to the orbit was also not observed in the specimens examined, though prominent foramina are visible ventrally near the orbital rims. The exposed lateral edge of the frontal is heavily rugose, with thick columnar ridges. In dorsal view, the orbital margin of the frontal is recessed medially from the lateral edge of the postorbital (and prefrontal, when preserved), as in some specimens of *Brachylophosaurus canadensis*, and unlike *Acristavus gagslarsoni* and *Probrachylophosaurus bergei* (Freedman Fowler and Horner 2015). The contact between the frontal and postorbital is an open interdigitating suture in ROM 60261, 66181, and 66182. In ROM 66180, this suture is fused (or at least, not obviously detectable), but a raised ridge that is absent in ROM 60261, 66181, and 66182 marks the location of the contact. The region is too damaged in ROM 60260 to determine whether this ridge was present or absent.

Posteriorly, the contact between the frontal and parietal is most clearly visible in ROM 66182, resembling the contact in other brachylophosaurins (Freedman Fowler and Horner 2015: fig. 11). In this specimen the skull roof slopes gently from the frontal–parietal contact to the dorsotemporal fenestra, with no ridge or overhanging structure (Fig. 2.6A). A slight ridge is present in ROM 60261 in the same position as the frontal–parietal contact in ROM 66182, and also very slightly in ROM 66181, particularly on the

Figure 2.6 Hadrosaurid dinosaur *Maiasaura peeblesorum* Horner and Makela, 1979 from the Two Medicine Formation (Campanian), Linster Quarry, Montana, USA (A–C) and *Brachylophosaurus canadensis* Sternberg, 1953, from Oldman Formation (Campanian) of Alberta, Little Sandhill Creek, Canada (D); detail of anterior margins of dorsotemporal fenestrae showing the variable development of overhanging ledges. A. ROM 66181, in oblique left posterodorsal view. B. ROM 60260, in oblique right posterodorsal view. C. ROM 66180, in posterodorsal view. D. CMN 8893, in oblique right posteroventral view, detail of overhanging ledge viewed through the right lateral temporal fenestra. Scale bars 20 mm.



left side. In ROM 60260 and 66180, the skull roof has a short ledge (averaging approximately 10 mm in ROM 66180) overhanging the anterior margin of each dorsotemporal fenestra, at approximately the same position as the frontal–parietal contact in ROM 66182, and the slight ridge in ROM 60261. Because the boundary between the frontal and parietal is not clearly visible on these larger specimens, it is not absolutely certain whether these overhangs are extensions of the frontal, the parietal, or both elements (Fig. 2.6B, C). In *Brachylophosaurus* (Fig. 2.6D), a similar but more extensive (2–5 cm) overhang onto the dorsotemporal fenestrae is reported to be variably composed of the prefrontals and frontals (Freedman Fowler and Horner 2015). However, ROM 60260 and 60261 differ from *Brachylophosaurus* in that in the latter taxon the overhang buttresses the nasal crest, and is only developed in individuals in which the nasal crest overlies the entire anteroposterior length of the frontals (Freedman Fowler and Horner 2015).

Postorbital— The postorbitals form the lateral margin of the skull roof posterior to the frontals. They contact the frontals anteromedially, the parietals medially, the laterosphenoids anteroventrally, and the squamosals posteroventrally. The anterodorsal edge of the postorbital, forming the posterodorsal margin of the orbit, is crenulated and rugose in the manner of the frontal. The anteriorly directed sheet of bone that covers the posterodorsal corner of the orbit in *Acristavus* (Gates et al. 2011) is absent, though the interior space of the orbit extends posteriorly onto the recessed anteromedial surface of the postorbital, which is hidden in lateral view posteromedial to the orbital margin. This concavity does not take the form of a hypertrophied, strongly demarcated “pocket”, as it does in *Edmontosaurus regalis* (Xing et al. 2017: fig. 12). In ROM 60260, 60261, 66181,

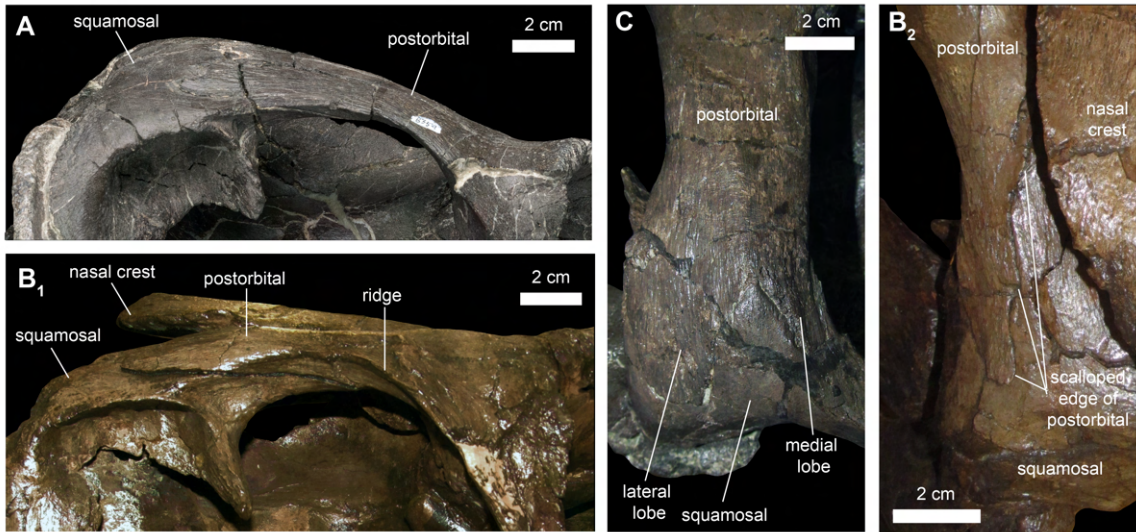
and 66182, the rugose texture on the postorbital is restricted to the orbital margin, and the dorsolateral surface of the triangular jugal process is smooth. Farther ventrally, the lateral surface of the jugal process in ROM 60261 and 66182 is lightly striated. In ROM 66180, the anterodorsal and posterodorsal margins of the jugal process are connected lateroventrally by an irregular, U-shaped rugosity covering the middle of the jugal process (Fig. 2.1E). The ventral part of the jugal process, in contrast, is smooth. The right postorbital of ROM 66180 also has an anomalous circular depression on the dorsal surface between the jugal and squamosal processes (Fig. 2.2C); a pathological circular depression has been reported on the same element in the *Brachylophosaurus* specimen TMP 1990.104.0001 (Freedman Fowler and Horner 2015). The dorsal part of the jugal process is triangular in cross-section with well-defined corners, broad anterior and posterior surfaces, and a narrower lateral surface. The ventral part of the jugal process has an L-shaped cross-section, with the anterior and posterior surfaces compressed to a transverse sheet forming the longer side of the L, and the lateral surface forming the shorter side of the L projecting as a ridge posteriorly from the transverse sheet. The jugal process is relatively straight in ROM 60261, 66181, and 66182, whereas its ventral part is bent strongly anteriorly in ROM 60260 and 66180, though this difference may be a preservational artefact. In at least ROM 66180, a small circular foramen perforates the posteroventral surface of the main body of the postorbital, between the jugal and squamosal processes. A small foramen also opens at the approximately same level on the anterior side of the right postorbital in this specimen, but is not observed on the left.

The squamosal process is approximately horizontal in ROM 66182, as in *Acristavus* (Gates et al. 2011) and *Brachylophosaurus* (Sternberg 1953), so the skull roof

is not strongly elevated posteriorly. In ROM 44770, 60260, 60261, 66180, and 66181, the squamosal process is arched dorsally, and its posterior end is elevated with respect to the main body of the postorbital. The squamosal process is dorsoventrally flattened, with a dorsal surface that is gently convex mediolaterally. The lateral and medial edges separating the dorsal and ventral surfaces are well defined. The lateral ridge is continuous with the posterolateral ridge on the jugal process, and forms the ventral edge of the dorsotemporal bar in lateral view (Fig. 2.7A). In *Brachylophosaurus* (CMN 8893), in contrast, this ridge continues to rise dorsolaterally on the squamosal process, and a portion of this process ventral to the ridge is visible in lateral view (Fig. 2.7B). The posterior end of the squamosal process overlying the squamosal is bifurcated (Fig. 2.7C), with a broad lateral branch and a narrow medial branch (“mitten shaped”), as in *Saurolophus angustirostris* (Bell 2011a: fig. 1). This differs from the condition in *Brachylophosaurus* (CMN 8893; Fig. 2.7B) and *Probrachylophosaurus* (Freedman Fowler and Horner 2015: fig. 13B) in which the posterior end of the squamosal process is scalloped and diagonally oriented. The squamosal process is also deeply bifurcated in *Gryposaurus notabilis* (Prieto-Márquez 2010d: fig. 3), but in that taxon both branches are narrow. In ROM 66180, the dorsal surface of the squamosal process has a faint diagonal ridge that ends at the point of this bifurcation, and distinguishes the dorsal surface (terminating in the narrow medial branch) from the dorsolateral surface (terminating in the broad lateral branch).

Parietal— The parietal forms the midline bar between the dorsotemporal fenestrae, and overlies the posterior part of the endocranial cavity. It is expanded laterally at its anterior and posterior ends. At the anterior end, the contact with the postorbital

Figure 2.7 Dorsotemporal bar of hadrosaurid dinosaur *Maiasaura peeblesorum* Horner and Makela, 1979 (ROM 60261 A; ROM 66180, C), from the Two Medicine Formation (Campanian), Linster Quarry, Montana, USA; compared to *Brachylophosaurus canadensis* Sternberg, 1953 (CMN 8893, B) from the Oldman Formation (Campanian) of Alberta, Little Sandhill Creek, Canada. A, B₁ in right lateral view; B₂, C in dorsal view. Scale bars 20 mm.



occurs immediately lateral to the main body of the parietal in ROM 60261, related to the relative narrowness of the dorsotemporal fenestrae. In individuals with relatively broader dorsotemporal fenestrae, including ROM 66180 and 66181, the parietal has short anterolateral processes extending between the main body and the postorbital; however, the precise location of the boundary between the parietal and postorbital in ROM 66180 is unclear (Fig. 2.6C).

The region of the skull roof joining the midline bar of the parietal to the frontal forms a posteriorly directed triangle. This triangular region is relatively low and unornamented in ROM 60261 and 66181, but is an elevated, roughened mound in ROM 60260, 66180, and 66182, as previously noted for the posterior-most frontal region of YPM-PU 22405 (Horner 1983). The triangular platform is anteroposteriorly short in ROM 60261, 66181, and 66182. It is elongated posteriorly in ROM 60260, flanking either side of the dorsally protruding sagittal crest. This elongated condition is asymmetrically present on the right side of ROM 66180, which has experienced some deformation of the parietal midline. Dorsally, the edge of the parietal is thin in ROM 60261, 66181, and 66182, but is somewhat more robust in ROM 60260 and 66180. The parietal continues as a mediolaterally narrow plate considerably ventral to the level of the skull roof, with the expansion for the endocranial cavity reaching farthest dorsally towards the anterior end of the parietal. Posteriorly, the parietal thins out and wedges between the squamosals. The lateral surfaces of the parietal are commonly cracked and poorly preserved, making detailed description of this region difficult. Ventrally, the contact between the parietal and neurocranium follows a straight line. There is no

indication of a foramen at the intersection of the laterosphenoid, prootic, and parietal, which was described in *Acristavus* (Gates et al. 2011).

Squamosal— The squamosals form the posterolateral corners and posterior margin of the dorsal skull roof. The postorbital ramus of the squamosal is a flattened triangular sheet that underlies, and is depressed into, the ventromedial surface of the squamosal ramus of the postorbital. The tapered anterior end of the postorbital ramus terminates posteriorly to the anterior margin of the dorsotemporal fenestra. The postorbital ramus is connected to the prequadratic process by a short, diagonal strut that spans the posterodorsal corner of the lateral temporal fenestra, and defines a laterally concave pocket in the squamosal anterodorsal to the prequadratic process. This subtly contrasts with the condition in *Brachylophosaurus* (CMN 8893), in which the postorbital ramus is exposed laterally for its entire length along the dorsal margin of the lateral temporal fenestra, rather than only in the posterodorsal corner.

The prequadratic process is spike-like with a flattened, approximately triangular cross-section. Its orientation is approximately parallel to the jugal ramus of the postorbital. The posterolateral surface of the prequadratic process adjoining the quadratic condyle is large and flat, with sharply defined edges. The anterolateral surface, facing the lateral temporal fenestra, is the narrowest surface of the prequadratic process, and has a rounded transition to the broad anteromedial surface. The prequadratic process is dorsoventrally longer than mediolaterally wide, whereas these dimensions are reported to be equal in the stouter prequadratic processes of *Probrachylophosaurus* and subadult *Brachylophosaurus* (Freedman Fowler and Horner 2015). The prominent quadrate cotyle is longer anteroposteriorly than mediolaterally. Both quadrate cotyles are compressed

anteroposteriorly in ROM 66180, such that the prequadratic and postquadratic processes meet in a sharp “V” in ventral view. In less distorted specimens, such as ROM 60261, the angle between the processes is much broader. The postquadratic process has a compressed, blade-like shape, with an anterolaterally facing external surface and a posteromedially facing internal surface. The posterior margin of the postquadratic process closely follows the curve of the paroccipital process of the exoccipital.

The hook-shaped medial ramus of the squamosal is bowed posteriorly, and curls anteromedially with an anteriorly directed extension appressed to the lateral surface of the parietal. In ROM 60261 (Fig. 2.2D) and ROM 66180 (Fig. 2.2C), the minimum breadth of the medial ramus of the squamosal in dorsal view is considerably less than that of the dorsotemporal bar, as in *Edmontosaurus regalis* (Xing et al. 2017: fig. 10) and *Prosaurolophus maximus* (McGarrity et al. 2013: fig. 4), whereas in ROM 66181 (Fig. 2.2B) these dimensions are subequal, as in *Acristavus gagslarsoni* (Gates et al. 2011: fig. 4). The squamosals contact each other at the midline posteriorly in ROM 60260, 60261, and 66180–66182, as in *Acristavus* and *Probrachylophosaurus* (Freedman Fowler and Horner 2015), but are separated by the parietal in ROM 44770, as in *Brachylophosaurus* (CMN 8893).

Neurocranium

Presphenoid— Partially preserved presphenoids (sensu Evans 2006) are visible in ROM 60260, 60261, and 66182, but little morphological detail is recorded, and the boundary between this element and the orbitosphenoid is unclear in all specimens analysed. The presphenoid bridges the space between the ventral side of the frontal and

the anterodorsal side of the orbitosphenoid. It is a thin, plate-like element that encloses the olfactory channel laterally and ventrally.

Orbitosphenoid— Orbitosphenoids are preserved in ROM 60260, 60261, 66181, and 66182. The paired orbitosphenoids contact each other and the presphenoids anteriorly, the frontals dorsally, the laterosphenoids posteriorly, and the parabasisphenoid ventrally. In ROM 60260, the poorly preserved orbitosphenoid appears to be fused to the frontal. In ROM 66182, the contact between the frontal and orbitosphenoid is unfused, while fusion to the laterosphenoid is indeterminate. The contact between the orbitosphenoid and laterosphenoid is visible on the left side in ROM 66181, occurring anteromedial to the vertical ridge that marks the posterior limit of the interior space of the orbit. The general morphology of the orbitosphenoid is best observed on the left side of ROM 60261 (Figs. 2.8, 2.9). The exposed upper portion of the orbitosphenoid is rectangular in lateral view, as in *Brachylophosaurus* (CMN 8893). The orbitosphenoid lacks an obvious separate foramen for the trochlear nerve (CN IV) in the same region that it exits in CMN 8893, where instead only a small, horizontal groove is observed in ROM 60261. However, this small foramen may be obscured by a crack in the latter specimen immediately posterior to the groove, and thus not greatly different in position from closely related taxa. The groove for the trochlear nerve fades out above the foramen for the optic nerve (CN II), rather than remaining distinct up to the anterior edge of the orbitosphenoid, as figured for *Kerberosaurus* (Bolotsky and Godefroit 2004: fig. 3A). The region ventral to the rectangular body of the orbitosphenoid is a web of struts enclosing three larger foramina. The most anterodorsal of these, forming the exit for the optic nerve, opens laterally and has an anteroposteriorly elongate ovoid shape. The optic

Figure 2.8 Hadrosaurid dinosaur *Maiasaura peeblesorum* Horner and Makela, 1979, from the Two Medicine Formation (Campanian), Linster Quarry, Montana, USA; partial skull of ROM 60261 in anterior view.

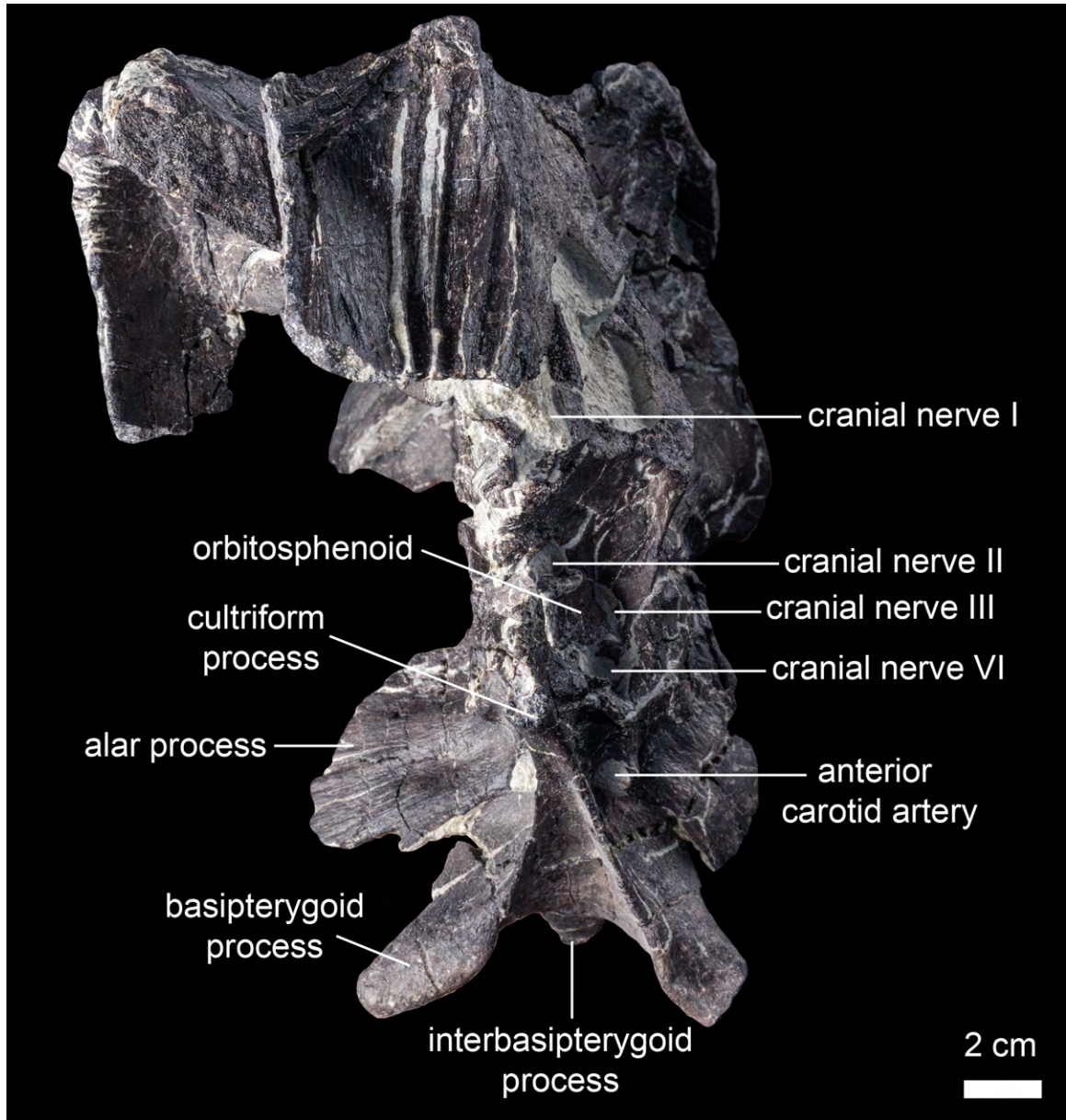
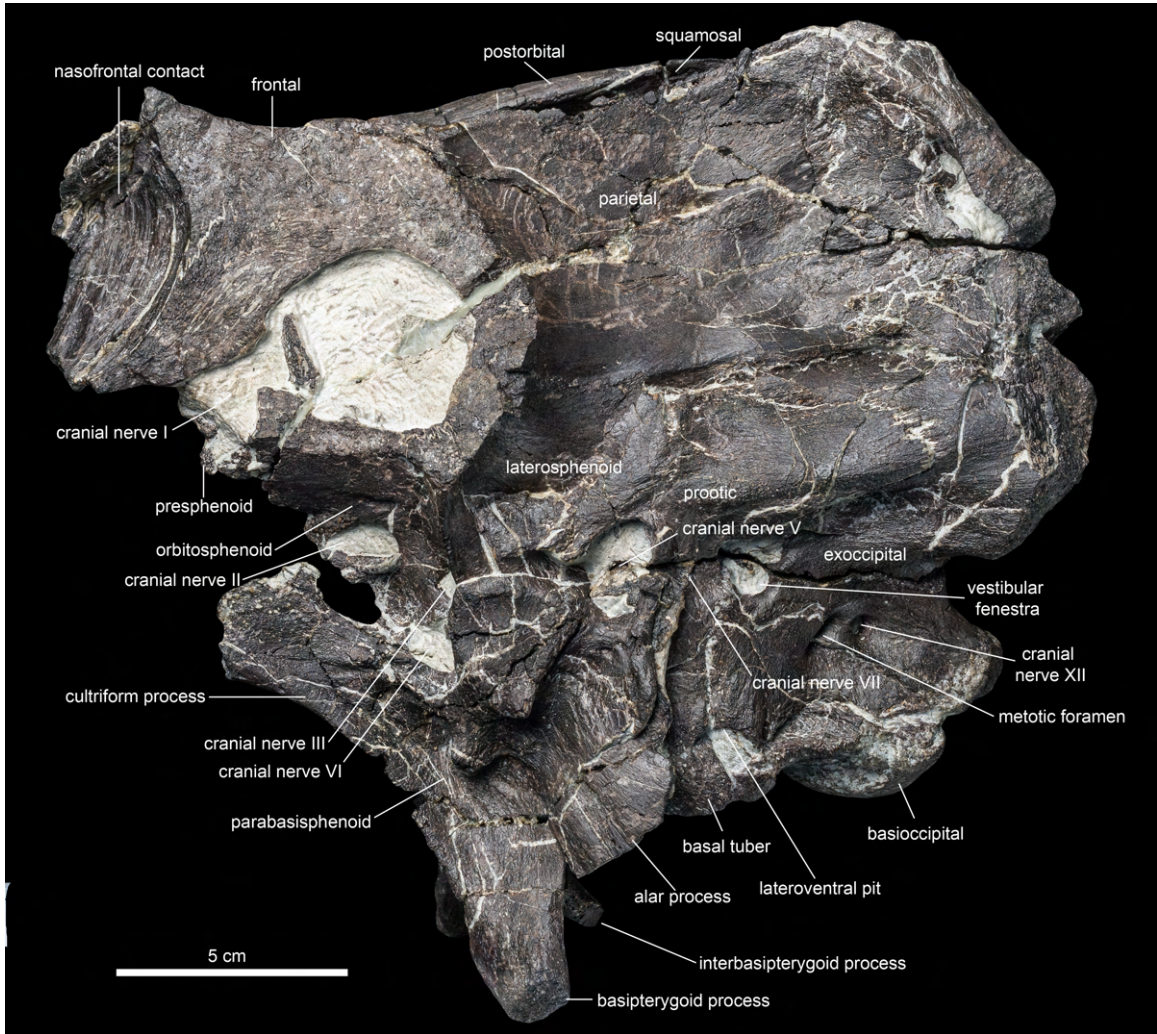


Figure 2.9 Hadrosaurid dinosaur *Maiasaura peeblesorum* Horner and Makela, 1979, from the Two Medicine Formation (Campanian), Linster Quarry, Montana, USA; partial skull of ROM 60261 in left lateral view.



nerve foramen is more completely ossified around and more laterally facing than in specimens of *Brachylophosaurus* (Prieto-Márquez 2005; Cuthbertson and Holmes 2010) and *Gryposaurus* (Prieto- Márquez 2010d), in which the optic nerve exits anteriorly into the hypophyseal cavity. The dorsal and ventral borders nearly connect anteriorly, but given the broken state of the available material it cannot be definitively determined whether the foramen was fully enclosed by bone on each side, as in adult *Edmontosaurus* (Xing et al. 2017), *Saurolophus* (Bell 2011a: fig. 11), and lambeosaurines (Ostrom 1961a; Godefroit et al. 2004b; Evans 2010). The two other posteroventral foramina, forming the exits for the oculomotor nerve (CN III) dorsally and abducens nerve (CN VI) ventrally, are more anteriorly directed, and separated by a bar projecting from the laterosphenoid. The presence of separate foramina for CN III and CN VI differs from the condition in edmontosaurines (Bolotsky and Godefroit 2004; Godefroit et al. 2012; Xing et al. 2017) and lambeosaurines (Ostrom 1961a; Godefroit et al. 2004; Pereda-Suberbiola et al. 2009; Evans 2010), in which these nerves exit through a single, merged foramen. The foramen for CN III is bordered by the orbitosphenoid anteriorly and the laterosphenoid posteroventrally, while the foramen for CN VI is bordered by the orbitosphenoid anterodorsally, the laterosphenoid posterodorsally, and the parabasisphenoid ventrally, with the contact between the orbitosphenoid and the cultriform process occurring at the anterior point on this foramen.

Laterosphenoid— The paired laterosphenoids are the anterior elements of the lateral walls of the braincase (Fig. 2.9). They contact the orbitosphenoids anteriorly, the frontals, postorbitals, and parietal dorsally, the basisphenoid ventrally, and the prootics

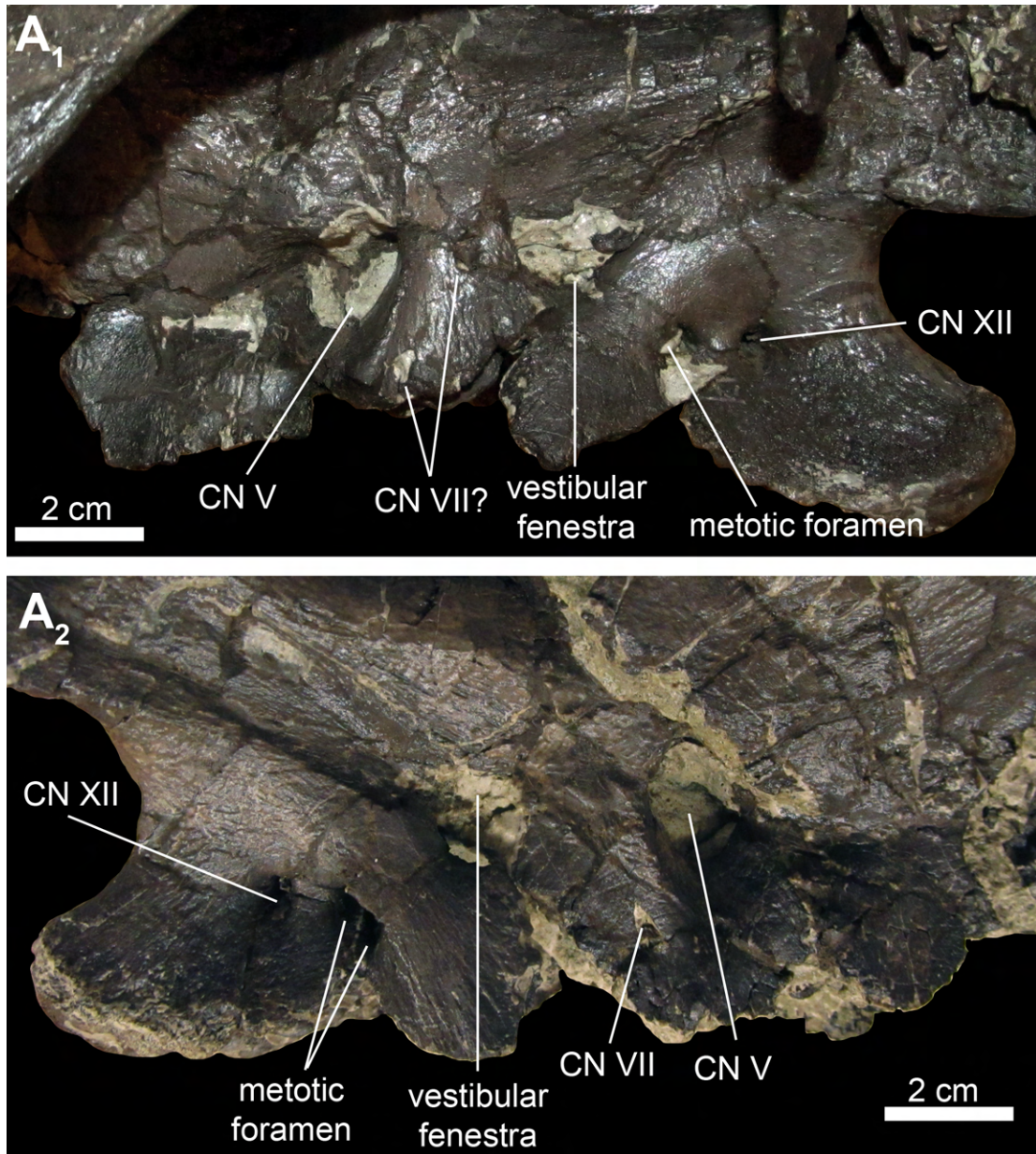
posteriorly. The contact with the prootic is visible along the posterior border of the laterosphenoid in ROM 60261, 66181, and 66182, while the laterosphenoid is fused to both the basisphenoid and the prootic in ROM 60260 and 66180. The laterosphenoid is approximately triangular in shape, broad dorsally and tapering ventrally. Anteriorly the laterosphenoid forms a sharply defined vertical edge, defining the border between the orbit and the lateral wall of the braincase. Dorsolaterally, this edge is continuous with the posteromedial edge of the postorbital. The dorsal contact between the laterosphenoid and parietal is straight. The posterior border of the laterosphenoid contributes to the anterior border of the large foramen for the trigeminal nerve (CN V). From the trigeminal foramen, a horizontal groove for the ophthalmic ramus (CN V1) continues along the lateral face of the laterosphenoid to the anterior corner of the lateral wall of the braincase. In ROM 60261, a small tab is preserved projecting ventrally from the laterosphenoid along the dorsal edge of this groove, close to the edge of the trigeminal foramen, indicating the attachment of the musculus levator pterygoideus (Holliday 2009). Ventrally, a process of the laterosphenoid overlies a laterally projecting pedestal formed by the basisphenoid, as in *Brachylophosaurus* (CMN 8893).

Prootic— The paired prootics are the middle elements of the lateral wall of the braincase (Fig. 2.9). They contact the laterosphenoids anteriorly, the parietal dorsally, the opisthotic–exoccipitals posteriorly, and the basisphenoid ventrally. The prootic is unfused to either the parietal or the exoccipital–opisthotic complex in ROM 60261, 66181, and 66182, and fused to both elements in ROM 60260 and 66180. The ventral margin of the prootic, along with the opisthotic–exoccipital complex, contributes to a distinct pit or pocket on the lateral side of the braincase immediately dorsal to the basal tubera, as in

Brachylophosaurus (CMN 8893), in all of the examined specimens of *Maiasaura* that are adequately preserved to evaluate this character (ROM 60260, 60261, 66180, and 66182).

The anterior border of the prootic is mediolaterally broad where it encloses the posterior part of the trigeminal foramen. The trigeminal foramen has a rounded subtriangular outline similar to that of *Brachylophosaurus* (CMN 8893), rather than the more angular condition described for *Acristavus* (Gates et al. 2011). In ROM 60261 and 66182, the prootic ventral to the trigeminal foramen forms a slight horizontal bar, as in *Brachylophosaurus* (Godefroit et al. 2012), but a distinct pocket is not developed ventral to the bar as in *Kerberosaurus* (Bolotsky and Godefroit 2004). In ROM 60260 and 66180, the bar is absent, and the ventrolateral surface of the prootic is smooth. A pronounced groove posterodorsal to the trigeminal foramen is observed in ROM 60261. The small foramen for the facial nerve (CN VII) is contained entirely within the prootic, separated from the trigeminal foramen by a posterodorsally inclined ridge confluent with the alar process. The facial nerve exits through a singular foramen on each side positioned directly posterior to the trigeminal foramen in ROM 60260, 66180, and 66182, as in *Brachylophosaurus* (CMN 8893). In ROM 66181, the facial nerve foramen is displaced ventrally on both sides, such that it does not overlap the trigeminal foramen horizontally (Fig. 2.10). On the left prootic of ROM 66181, but not the right, a small hole directly posterior to the trigeminal nerve may be a second exit for the facial nerve, or merely damage to the prootic. The position of the facial nerve foramen is obscured by breakage in ROM 60261. A groove for the palatine branch of the facial nerve runs anteroventrally from the facial nerve foramen following the posterior margin of the alar process.

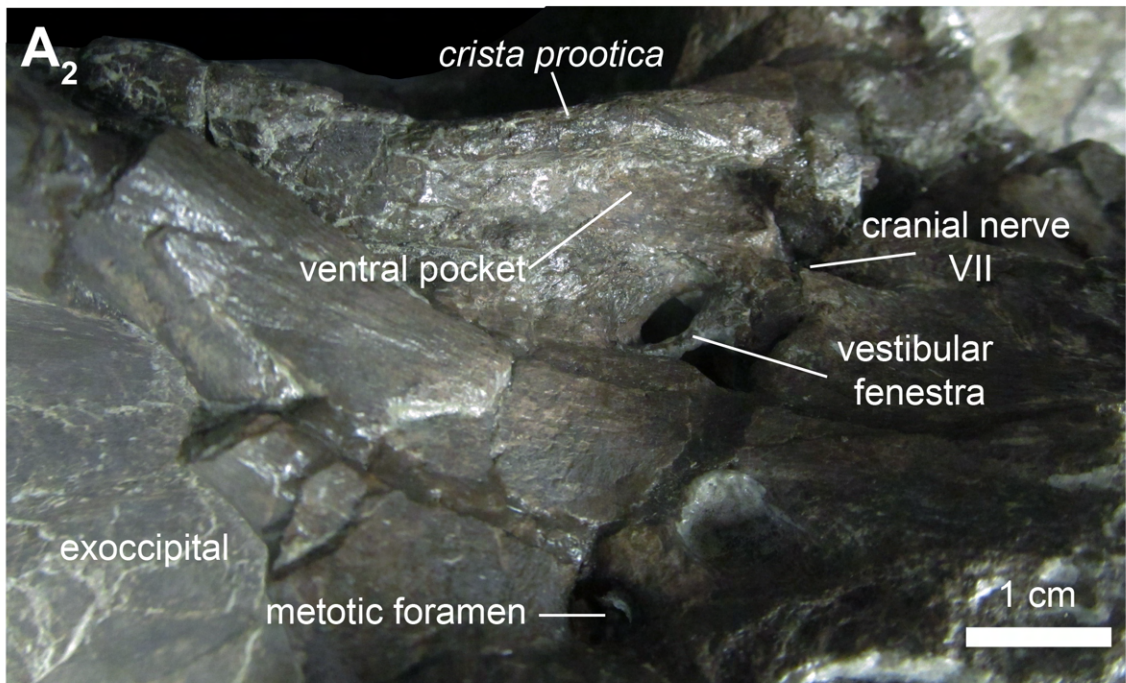
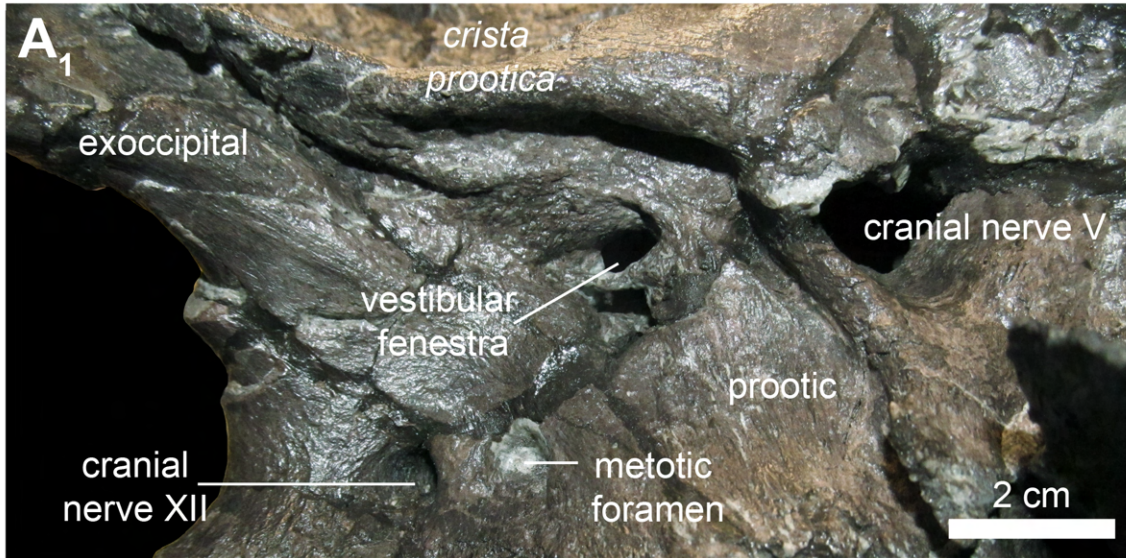
Figure 2.10 Hadrosaurid dinosaur *Maiasaura peeblesorum* Horner and Makela, 1979 (ROM 60261), from the Two Medicine Formation (Campanian), Linster Quarry, Montana, USA; lateral wall of neurocranium showing possible variation in the position of cranial nerve VII in left lateral (A1) and right lateral (A2) views.



The vestibular fenestra opens along the contact between the prootic and the opisthotic–exoccipital complex, with the majority of this fenestra positioned over the basioccipital contribution to the basal tubera, though in ROM 60261 it partly straddles the basisphenoid–basioccipital boundary. The vestibular fenestra is much larger than the facial nerve foramen, but smaller than the trigeminal foramen. In ROM 66180 it has the same height as the trigeminal foramen, but is not as wide anteroposteriorly. A thin bony septum, the crista interfenestralis, divides the vestibular fenestra into its dorsal and ventral components (Fig. 2.11). These two openings have been variously identified in other hadrosaurids as the fenestra ovalis and fenestra rotunda (Bolotsky and Godefroit 2004), or fenestra ovalis and glossopharyngeal (CN IX) foramen (Langston 1960), respectively. The crista interfenestralis has a posterodorsal-to-anteroventral diagonal orientation in ROM 60260, 66182, and possibly 66181, based on a fragment visible on the right side. It is only slightly inclined from the horizontal in ROM 66180, in which it parallels the nearly horizontal crista prootica in this region of that specimen (Fig. 2.11). The crista prootica of ROM 60261 is also nearly horizontal, but may be slightly inclined in the opposite direction (posteroventral-to-anterodorsal); however, the bone is fragmented in this region and may not reflect the original orientation. On the right side of ROM 60261, a vertical septum further subdivides the fenestra ovalis. This septum was not observed in the other specimens.

Opisthotic–exoccipital complex— The opisthotic and exoccipital are indistinguishably fused in all specimens. By convention, the term exoccipital is used for the description of this element (Evans 2010; alternatively “otoccipital” in some sources).

Figure 2.11 Hadrosaurid dinosaur *Maiasaura peeblesorum* Horner and Makela, 1979 (ROM 66180), from the Two Medicine Formation (Campanian), Linster Quarry, Montana, USA; lateral wall of neurocranium showing the prominent overhang of the crista prootica in right lateral (A1) and oblique right posteroventral (A2) views.



The exoccipitals contact the prootic anteriorly, the parietal, squamosals, and supraoccipital dorsally, and the basioccipital ventrally. The contact between the exoccipital and basioccipital is visible in all examined specimens for which both elements are preserved. It is relatively high in ROM 60261 and 66182, and very low in ROM 60260 and 66180, with little exposure of the basioccipital in lateral view.

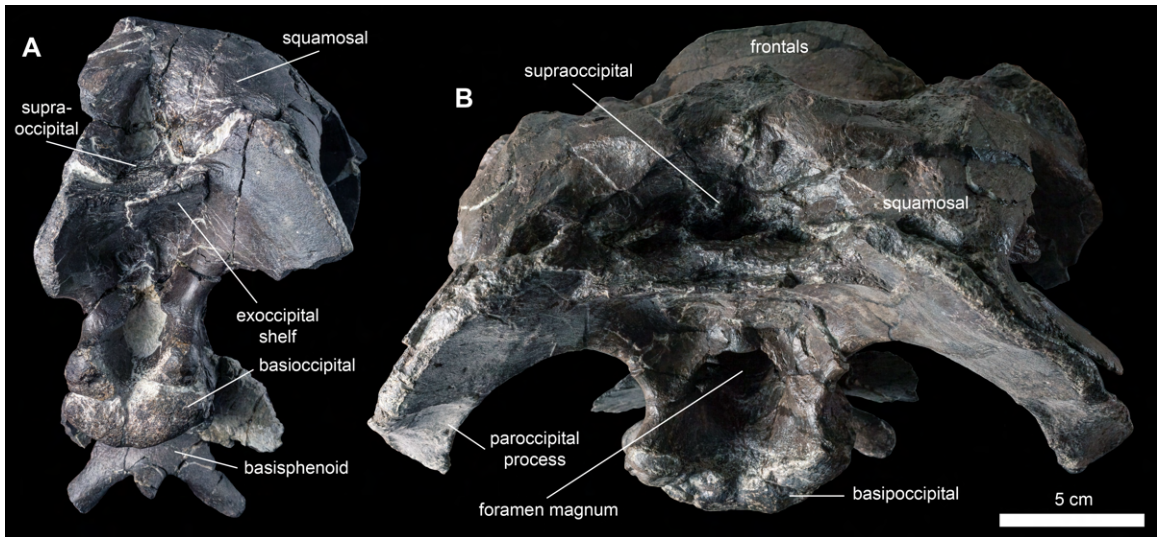
The metotic strut is indistinct from the rest of the lateral wall of the braincase, beyond forming the posterior border of the vestibular fenestra and the anterior border of the metotic foramen. A broad groove extending posterodorsally from the vestibular foramen is well defined in ROM 66180 and on the right side of 66181. Posterior to the metotic strut, the lateral surface of the exoccipital is pierced by two foramina, as in *Probrachylophosaurus* (Freedman Fowler and Horner 2015: fig. 15) and the type specimen of *Brachylophosaurus canadensis* (Cuthbertson and Holmes 2010: fig. 4). A third foramen is variably present in *Brachylophosaurus* from Montana (Prieto-Márquez 2005: fig. 8), but is not present in any of the *Maiasaura* specimens for which this character was observed (ROM 44770, 60260, 60261, 66180–66182). The opening of the metotic foramen is oriented primarily laterally in ROM 44770, 66180, and 66182, posterolaterally in ROM 60260 and 66181, and posteriorly in ROM 60261. It is positioned more ventrally on the side of the braincase than the vestibular fenestra, and does not overlap with it horizontally, except for slightly on the right side of ROM 66181. The metotic foramen is semi-divided by a small septum projecting from its posterior margin in at least ROM 60261. The metotic foramen may also preserve a remnant of a septum on the left side of ROM 66180, and the right side of ROM 66181 (Fig. 2.10). The metotic foramen appears to be a single, round foramen in ROM 66182, but this is

difficult to confirm as the actual condition, rather than a preservational artefact. The more posterior foramen is an exit for the hypoglossal nerve (CN XII). The metotic and hypoglossal foramina are at the same horizontal level. The distance between the posterior edge of the hypoglossal foramen and the posterior edge of the exoccipital (measured straight back from the foramen) is considerably greater than the distance between the posterior edge of the hypoglossal foramen and the anterior edge of the metotic foramen in ROM 60261, but not in ROM 44770, 60260, 66180–66182.

The posterodorsally angled crista prootica is strongly pronounced, and variable in form. In ROM 66181 and 66182, there is no gap between this ridge and the dorsal margin of the vestibular foramen, and there is no distinct pocket or overhang ventral to the ridge. In ROM 60261, a conspicuous pocket is present ventral to the crista prootica, dorsal to the metotic and hypoglossal foramina, but not extending as far anteriorly as the vestibular fenestra. In ROM 60260 and 66180, this pocket is elaborated to form a laterally enclosed, ventrally open channel on the underside of the crista prootica (Fig. 2.11). This channel extends farther anteriorly over the vestibular fenestra, which is separated from the crista prootica by a distinct gap. In ROM 66180 this channel contains a lateral groove, connecting to the dorsal groove from the facial nerve foramen on the prootic, and a medial groove, connecting to the dorsal groove from the vestibular foramen, separated by a small ridge where they come together below the posterior extent of the crista prootica.

The exoccipitals meet posteriorly, forming a shelf that supports the supraoccipital dorsally, and overhangs the foramen magnum ventrally (Fig. 2.12). The underside of the shelf has a ridge along the contact between the exoccipitals in ROM 66181, as in *Brachylophosaurus* (CMN 8893). This ridge is absent or only very faintly present in

Figure 2.12 Hadrosaurid dinosaur *Maiasaura peeblesorum* Horner and Makela, 1979, from the Two Medicine Formation (Campanian), Linster Quarry, Montana, USA; skulls in posterior view A. ROM 60261. B. ROM 66180. ROM 66180 is photographed in a slightly more posterodorsal perspective than ROM 60261; in actuality, the basiptyergoid processes of both specimens project ventral to the occipital condyle.



ROM 60260, 66180, and 66182. In ROM 60261 the exoccipitals were slightly pushed together during diagenesis, so the “ridge” cannot be reliably assessed. Between this shelf and the foramen magnum are a pair of depressions that serve as the insertion sites of the musculus rectus capitus posterior (Ostrom 1961a). These depressions are quite shallow in ROM 60260, 66180, and 66182, and relatively deep in ROM 60261 and 66181. The diamond-shaped foramen magnum is enclosed by the exoccipitals. A small ridge overhangs each side of the foramen magnum dorsolaterally. These are most prominent in ROM 60261 and 66182, and slight in 66180. The posteroventral protrusions of the exoccipital condyloids project farther posteriorly than the occipital condyle of the basioccipital. The paroccipital processes are anteroposteriorly compressed. A small tuberosity is present on the medial edge of the paroccipital process. The ventral extremities of both paroccipital processes are preserved in ROM 66180, in which each is capped by a small, roughened protrusion on the anteroventral corner (Fig. 2.12).

Supraoccipital— The supraoccipital is a median element exposed on the posterior surface of the braincase, ventral to the squamosals and dorsal to the exoccipitals (Fig. 2.12). As in other hadrosauriforms, the supraoccipital is excluded from the foramen magnum. The exposed region of the supraoccipital is somewhat variable in form, which can be partly attributed to differential deformation among the sample. The ventral body of the supraoccipital is a relatively shallow, flat plate in ROM 66180–66182, while it is thicker in ROM 44770, 60260, and 60261. The posterior edge of the plate-like body is transversely striated in ROM 66182, as in *Acristavus* (Gates et al. 2011), but not in other specimens of *Maiasaura* (e.g., ROM 66180). The triangular nuchal pit is relatively shallow in ROM 66182, and excessively shallow in ROM 66181, although in at least the

latter specimen this is the result of the pit being post-depositionally collapsed. In contrast, the nuchal pit is dorsoventrally high in ROM 44770 and 60261, and in at least the former specimen (the latter is infilled by matrix), anteroposteriorly very deep. In ROM 60260 and 66180, the nuchal pit has a tripartite structure, with a large median depression flanked on either side by a smaller lateral depression. The laminae that separate these depressions are oriented dorsolaterally to ventromedially. One of these laminae is possibly also visible on the right side in ROM 60261, though the entire tripartite structure is not clear in that specimen. In ROM 66180, the laminae meet ventrally to form a roughened, semicircular platform posteroventral to the median depression. The large median depression in ROM 66180 is fairly deep anteroposteriorly but relatively low dorsoventrally, though this could be the result of dorsoventral compression. Following the soft tissue reconstructions of the hadrosaurid head by Ostrom (1961a), the larger median pit likely corresponds to the attachment area of the nuchal ligament, and the two smaller lateral pits likely correspond to the insertions of the musculus spinalis capitis. However, the relative sizes of these landmarks are the inverse of those illustrated by Ostrom (1961a: fig. 53) for *Hypacrosaurus*.

Parabasisphenoid— The parasphenoid and basisphenoid are indistinguishably fused into a parabasisphenoid in all of the examined specimens. The parasphenoid is the more anterior of the two elements, and forms the cultriform process. The basisphenoid contacts the laterosphenoid and prootic dorsally, and the basioccipital posteriorly. The cultriform process is best preserved in ROM 60261 and 66182. In ROM 66180, this process is artificially reconstructed, and should not be used as a basis for morphological comparisons. The cultriform process projects anterodorsally. It is subrectangular in lateral

view, with approximately parallel dorsal and ventral margins at its mid-length.

Anteriorly, the cultriform process is slightly expanded dorsally in ROM 60261, but no contact with the presphenoid is preserved. The cultriform process is teardrop-shaped in cross-section, with a mediolaterally compressed sheet forming the dorsal part and a more robust, rounded ventral part. Posteriorly, the rounded lateroventral edges of the cultriform process give rise to sharp-edged laminae, which diverge posterolaterally and connect the cultriform process to the basiptyergoid processes. The triangular region of the basisphenoid between these laminae is concave. The anterior foramen for the internal carotid artery pierces the basisphenoid posteroventral to the cultriform process, anteroventral to the pedestal for the basisphenoid–laterosphenoid contact, anterior to the alar process, and dorsal to the basiptyergoid process (Fig. 2.8). This foramen is shielded laterally by a small, anteroventrally projecting tab-like process of the basisphenoid (Fig. 2.9).

The paired basiptyergoid processes project ventrolaterally and slightly posteriorly in ROM 66182, and ventrolaterally and slightly anteriorly in ROM 60260, 60261, and 66180. The degree of ventrolateral orientation of the basiptyergoid processes is variable, ranging from more ventrally oriented in ROM 66182 to more laterally oriented in ROM 66180. The basiptyergoid processes are subtriangular in cross-section. They consist of a proximal region bound by the descending lamina of the cultriform process anteriorly and the interbasiptyergoid ridge posteromedially, and a freely projecting distal region. The posterodorsal edge of each basiptyergoid process is well defined in ROM 60260 and 66182, but is more rounded in ROM 60261 and 66180. The smaller interbasiptyergoid process is flattened along a posterodorsal to anteroventral axis, and the distal end tapers

medially. It is oriented posteroventrally, approximately parallel to the cultriform process in ROM 60261 (Fig. 2.9), but more ventrally in ROM 66182.

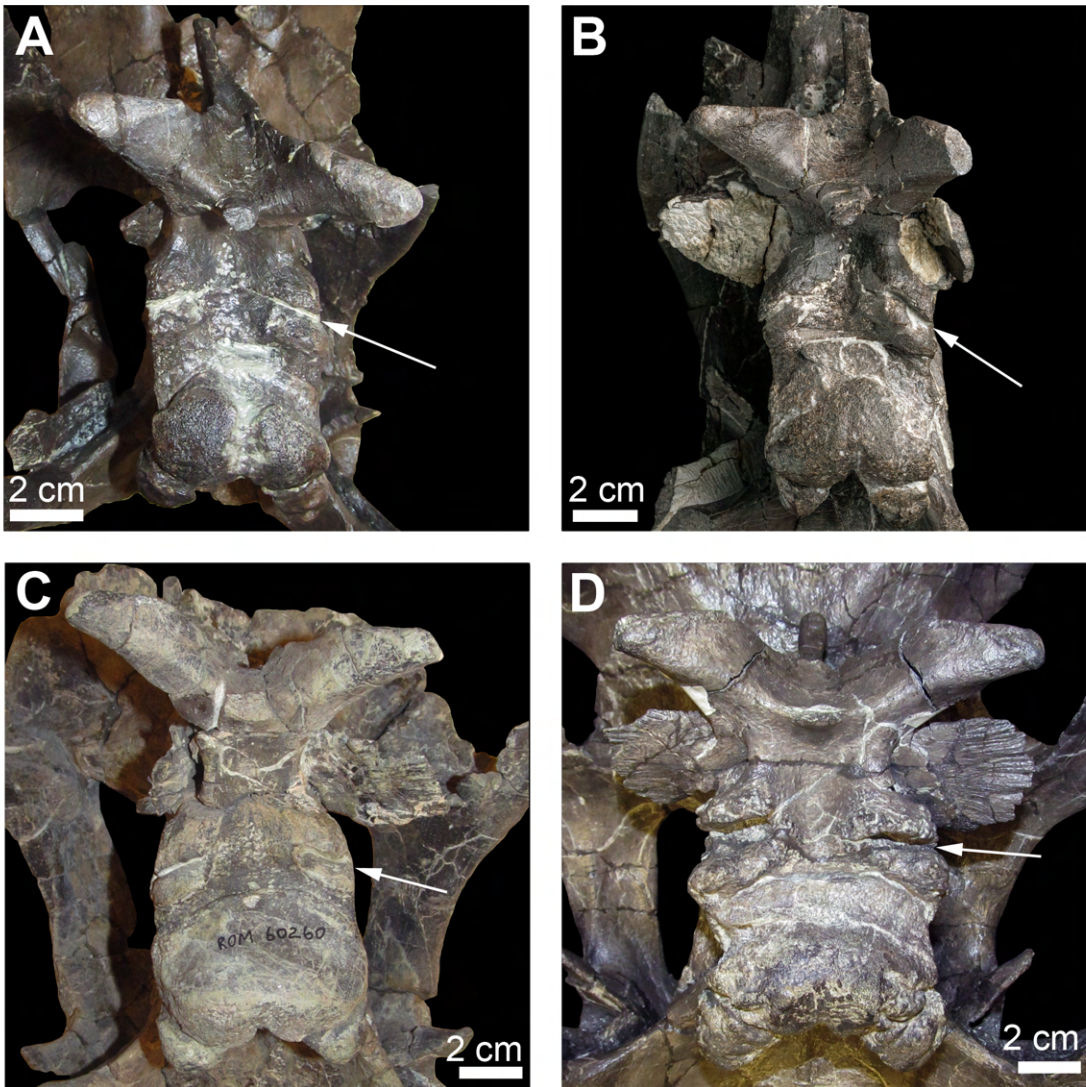
The paired alar processes are large, thin sheets of bone formed mostly by the basisphenoid, except for a small, medial section of the dorsal edge that was possibly formed by the prootic (ROM 60261, 66181). The alar process of each side projects laterally from the braincase and is posterodorsally inclined. The anterodorsal and posteroventral surfaces have lightly striated or fluted textures. The anteroventral edge of the alar process is distinctly pendent below the ventral extent of the basal tubera in ROM 60261, and just slightly so in ROM 60260. The alar processes do not extend ventrally past the basal tubera in ROM 66180 and 66182, but the ends of the processes are broken. In ROM 60260, 60261, and 66182, the alar process is approximately coplanar with the posterodorsal edge of the basipterygoid process, such that extending the plane of the alar process anteroventrally would bisect the basipterygoid process along its length. The anterior face of the alar process is oriented slightly more dorsally in ROM 66180, compared to other specimens of *Maiasaura*, but this could be a preservational artefact. Immediately ventral to the alar process, and posterodorsal to the basipterygoid process, the lateral surface of the basisphenoid is pierced by the posterior foramen for the internal carotid artery. This foramen is hidden behind the alar process in lateral view.

Posterior to the basipterygoid and alar processes, the basisphenoid is hourglass-shaped in ventral view. Several tiny foramina are present in the median concavity of the ventral surface of the basisphenoid posterior to the interbasipterygoid ridge in ROM 60261 and 66182, but are absent in ROM 60260 and 66180. The basisphenoids form the

anterior half of the basal tubera, with a rather loose connection to the posterior halves formed by the basioccipital. In ventral view, the boundary between the basisphenoid and basioccipital contributions to the basal tubera is strongly angled anteromedially in ROM 60261 and 66182, only slightly angled in ROM 60260, and nearly straight transversely in ROM 66180 (Fig. 2.13). A V-shaped contact between the basisphenoid and basioccipital is visible medial to the basal tubera in ROM 60261, where the basisphenoid receives an anteriorly projecting triangular process of the basioccipital. This V-shaped contact is not visible in ROM 66180, where the boundary between the basisphenoid and basioccipital is distinct ventrally only on the basal tubera.

Basioccipital— The basioccipital forms the posteroventral region of the braincase. It contacts the basisphenoid anteriorly, and the exoccipitals dorsally. In ventral view, the basioccipital is approximately square in ROM 60261 and 66182, whereas it is distinctly wider than long in ROM 60260 and 66180 (Fig. 2.13). The width of the basioccipital is approximately the same across the basal tubera as across the occipital condyle. Posterior and medial to the basal tubera, an abrupt “step” transversely crosses the ventral surface of the basioccipital, with the surface posterior to this step extending farther ventrally. The paired small excavations possibly occurring medial to the basal tubera on the basioccipital of *Acristavus* (Gates et al. 2011: fig. 9C, D), similar to *Gobihadros* (Tsogtbaatar et al. 2019: fig. 8B), are not observed in any individual of *Maiasaura*. The underside of the occipital condyle projects further ventrally still, and may be separated from the rest of the ventral surface by a transverse sulcus, as in ROM 66182. The portion of the occipital condyle formed by the basioccipital is separate from that formed by the exoccipital condyloids, and is directed posteroventrally. In ROM

Figure 2.13 Hadrosaurid dinosaur *Maiasaura peeblesorum* Horner and Makela, 1979, from the Two Medicine Formation (Campanian), Linster Quarry, Montana, USA; basicrania in ventral view. A. ROM 66182. B. ROM 60261. C. ROM 60260. D. ROM 66180. Arrows point to the contact between the basisphenoid (anterior) and basioccipital (posterior), and illustrate the variable orientation of this contact. Scale bars 20 mm.



66182, the condyle is cleft posteriorly along its midline, to a greater extent than seen in ROM 60260, 60261, and 66180, although this may be a result of damage. The lateroventral surfaces of the occipital condyle are deeply furrowed in ROM 66180, whereas they are smooth in ROM 60260, 60261, and 66182.

2.4 Discussion

Ontogenetic and individual variation in *Maiasaura peeblesorum*— Although the individual ages of the specimens at their times of death are unknown, ontogeny is a plausible explanation for a considerable amount of anatomical and size variation in this sample (Table 2.3). As in ontogenetic series of other hadrosaurids, visible sutures between cranial elements are obliterated with increasing skull size, and cranial ornamentation is proportionately enlarged (e.g., Evans 2010; Bell 2011b; Freedman Fowler and Horner 2015). Prieto-Márquez (2005) suggested that ontogeny in *Brachylophosaurus* is characterized by negative allometry of the orbital cavity and neurocranial foramina, and positive allometry of neurocranial width, and this appears to also be the case in *Maiasaura*, based on the contrast between the smallest (ROM 66182) and largest (ROM 66180) individuals. However, quantifying size-related variation is confounded by the absence of total skull lengths, potentially variable compression of the skulls (in both direction and degree), and diagenetic distortion potentially altering the dimensions and orientation of the structure or opening being measured. These confounding factors can lead to disagreements in the literature over seemingly simple questions such as whether the individuals being compared differ in size, as in the case of the proposed “slender” and “robust” adults of *Brachylophosaurus* (Prieto-Márquez 2005;

Cuthbertson and Holmes 2010; Freedman Fowler and Horner 2015). Nonetheless, it is possible to loosely rank the specimens in this study in order of relative skull size.

The specimen ROM 66182 is the smallest skull in this sample. In most transverse skull roof and braincase measurements (interorbital width across frontals, dorsotemporal fenestra width, posterior skull width across squamosals, and occipital condyle width), as well as basioccipital ventral length, ROM 66182 is between 61–67% of the size of ROM 66180 (Tables 2.1, 2.2). However, the anteroposterior lengths of the lateral wall of the braincase and of the supratemporal fenestrae are between 81–82% of the size of ROM 66180, and the largest preserved anteroposterior diameter of the orbit is approximately equal to that of ROM 66180. Aside from the maximum width of the orbit, a suspected negatively allometric character that is easily distorted and varies between sides of the specimen, linear dimensions of ROM 66182 consistently fall within the range of 50–85% of the highest values recorded in this study, so I interpret it as a subadult *sensu* Evans (2010).

Most contacts between cranial elements are visible in ROM 66182. The flat nasal–frontal contact is relatively shallowly inclined, and only weakly grooved (Fig. 2.5A). It does not rise above the height of the middle of the frontal. The dorsoventral thickness of the frontal is less than half that of large adults, with a flat dorsal surface and no frontal depressions. The absence of a crest in ROM 66182 indicates that the crest formed relatively late in the growth of *Maiasaura*, after the animal had reached subadult size, as in the closely related *Probrachylophosaurus* (Freedman Fowler and Horner 2015). In contrast, a distinct crest is already present in juveniles less than half of the greatest recorded adult size in the saurolophins *Prosaurolophus* (Drysdale et al. 2019)

and *Saurolophus* (Bell 2011b), and the lambeosaurine *Parasaurolophus* (Evans et al. 2007; Farke et al. 2013). Posterior to the frontals, the skull roof of ROM 66182 is relatively horizontal (Fig. 2.1A), as in other brachylophosaurin genera, but unlike larger specimens of *Maiasaura*. The increased elevation of the posterior skull roof with increasing skull size is also seen in *Gryposaurus* (Farke and Herrero 2014). ROM 60261 and 66181 are intermediate in both size and morphology between the subadult skull and the largest specimens. The anteroposterior lengths of the parietal and of the braincase lateral wall are at least 85% of (or may even slightly exceed) that of the largest braincases (Table 2.2), but the width of the skull is considerably less (approximately 74% of the width of ROM 66180 in ROM 66181), as is the ventral length of the basioccipital (approximately 69% of the length of ROM 66180 in ROM 60261). I interpret these specimens as (young) adults sensu Evans (2010), giving higher priority to the anteroposterior measurements as a stand-in for total skull length. In most measurements, ROM 66181 is slightly larger than ROM 60261, although ROM 60261 has anteroposteriorly longer dorsotemporal fenestrae (Table 2.1).

As in ROM 66182, most contacts between the cranial elements are visible in ROM 60261 and 66181. In ROM 66181, the connection between the lateral wall of the neurocranium and the basicranium was sufficiently loose that these regions became disarticulated after death, and the latter was lost. In both specimens, the nasal–frontal contact is concave and nearly vertically oriented. The grooves and ridges on the contact surface of the frontal are strongly pronounced medially, and weaker laterally (Fig. 2.8). The contact surface is dorsoventrally higher in ROM 60261 than in ROM 66181, and more distinctly rises above the rest of the frontal (Fig. 2.9), suggesting that ROM 60261

Table 2.2 Selected cranial measurements of *Maiasaura peeblesorum* expressed as a percentage of the maximum recorded value in this study. Underlined values exceed 85% and are suggestive of “adult” dimensions (Evans 2010).

	ROM 66182	ROM 66181	ROM 60261	ROM 60260	ROM 66180
Width of nasofrontal suture	55	58	?	<u>96</u>	<u>100</u>
Width of both frontals across the orbits	67	74	?	<u>91</u>	<u>100</u>
Length of parietal sagittal crest	74	<u>97</u>	<u>97</u>	<u>100</u>	<u>96</u>
Posterior skull roof width across squamosals	62	74	71e	<u>86</u>	<u>100</u>
Length of dorsotemporal fenestra	73–74	<u>87–88</u>	<u>96</u>	<u>99–100</u>	<u>89–90</u>
Width of dorsotemporal fenestra	60–61	84	69	69– <u>97</u>	<u>98–100</u>
Neurocranium length, from CN II to basioccipital process of exoccipital	80–84	<u>99–100</u>	<u>85–86</u>	<u>89</u>	<u>91</u>
“Middle” neurocranium	69–78	<u>87</u>	79– <u>86</u>	<u>92–100</u>	<u>94</u>

length, from anterior edge of CN V to posterior edge of CN XII					
Width across basioccipital processes of exoccipitals	64	80	59	84	<u>100</u>
Width across basisphenoid-basioccipital contact	56	NA	63	77	<u>100</u>
Ventral length of basioccipital	65	NA	69	81	<u>100</u>
Width across occipital condyle of basioccipital	62	NA	70	<u>93</u>	<u>100</u>

represents a slightly more mature individual in terms of crest development, despite not being larger overall. The frontal depressions are relatively shallow and anteroposteriorly elongate (Fig. 2.5B), as in *Acristavus*, *Probrachylophosaurus*, and subadult *Brachylophosaurus* (Freedman Fowler and Horner 2015). The posterior skull roof is elevated, as in the larger adults (Fig. 2.1).

The specimens ROM 60260 and 66180 are the largest skulls in this sample, and are interpreted as “mature adults”, with the majority of linear measurements (lengths and widths) being within 85–100% of the highest recorded values (Table 2.2). Dorsal skull roof measurements of ROM 60260 are approximately 85–90% as wide as ROM 66180, though the two specimens are similar in lateral braincase wall length, and the dorsotemporal fenestrae are anteroposteriorly longer in ROM 60260. Contacts between most neurocranial elements are obliterated by fusion in both specimens, with the basisphenoid–basioccipital contacts across the basal tubera being a notable exception. The sutures between the left and right frontals, and the frontals and parietal, are also obliterated. The concave nasal–frontal contact, which remains unfused, is greatly enlarged, vertically oriented, and substantially elevated above the base level of the frontal, and covered by deep grooves and ridges. Posterior to the nasal contact, the frontal is anteroposteriorly short, and dorsoventrally thick. The raised buttress of the nasal–frontal crest contributes to a medially convex transverse profile of the frontals. This contrasts with the ontogenetic trajectory in *Saurolophus*, in which the dorsal surface of the frontal is domed in juveniles and flattens in adults (Bell 2011b). The ontogenetic obliteration of both the interfrontal and frontal–parietal sutures, along with the increasing thickness and transverse convexity of the frontal region, is unique to *Maiasaura* among

saurolophines, and is convergent with the ontogenetic trajectory of pachycephalosaurids (Schott et al. 2011). The frontal depressions (at least in ROM 66180) are relatively deep while being constricted to small, round openings, related to the overall growth and thickening of the frontals (Fig. 2.5C). Along the region of the presumed frontal–parietal contact, a short ledge overhangs the anterior margin of each dorsotemporal fenestra (Fig. 2.6), as in adult *Brachylophosaurus* (Freedman Fowler and Horner 2015). The rugosity on the lateral surface of the postorbital is more extensive in ROM 66180 than in ROM 60261, supporting the interpretation of the wider skull as more mature. On the neurocranium, the channel beneath the overhanging crista prootica is incipiently developed posteriorly in the intermediate adult stage (ROM 60261), but is not fully expressed until the mature adult stage, especially in ROM 66180 (Fig. 2.11). The relatively broader neurocranium of the mature adult stage is especially evident in the proportions of the basioccipital, which is considerably wider transversely than long anteroposteriorly in both ROM 60260 and 66180 (Fig. 2.13). In contrast, the basioccipital is proportionately narrower in CMN 8893, a presumably adult individual of *Brachylophosaurus* with a well-developed crest, more closely resembling the basioccipital of the incipiently crested *Maiasaura*. The basisphenoid–basioccipital contacts on the basal tubera also become more transversely oriented in ventral view with increasing skull size in *Maiasaura* (Fig. 2.13). Bullar et al. (2019) reported a somewhat similar ontogenetic trend in the orientation and composition of the basal tubera in a ceratopsian, *Psittacosaurus*. Further research may establish this trend to have a broad phylogenetic significance.

Specimen ROM 44770 has been previously regarded as an exemplary “adult” individual of *Maiasaura peeblesorum* (Trexler 2001: 303; Prieto-Márquez 2010d: 497; Campione et al. 2013: 67; Freedman Fowler and Horner 2015: table 2; Prieto-Márquez and Guenther 2018: 4). Woodward et al. (2015: 509) regarded ROM 44770 as “likely a skeletally mature individual,” based on their histological analysis showing an external fundamental system (EFS) in tibiae from similar-sized individuals. However, ROM 44770 lacks some characters of the most mature adult ontogimorph identified in this study, including a fully enlarged semi-circular crest incorporating flared prefrontals, a high degree of vertical elevation of the frontals at the nasal–frontal contact with respect to the mid-frontal surface, an especially rugose ventrolateral surface of the postorbital, and a prominently overhanging crista prootica with a ventrally open channel. Other characters, such as the form of the frontal depressions and the presence or absence of an overhanging ridge on the anterior border of the dorsotemporal fenestrae, cannot be determined due to poor preservation. An objective size comparison of ROM 44770 to the other specimens in this study is hampered by the broken and strongly mediolaterally compressed condition of the braincase and posterior skull roof. The posterior width of the skull is 130 mm as preserved, intermediately between that of ROM 66182 and 60261. The basioccipital is small in ROM 44770, with an estimated ventral length of 49 mm, also intermediate between that in ROM 66182 and 60261. However, the distance on the lateral wall of the braincase from the posterior margin of the trigeminal foramen to the posterior edge of the braincase is relatively long, at approximately 8 cm, exceeding the “large adult” specimens ROM 60260 and 66180 (approximately 70 mm).

The total skull length of ROM 44770, from premaxilla to paroccipital process, is approximately 710 mm, compared to 820 mm in the holotype YPM-PU 22405 (Horner 1983). Although further work is needed to definitively establish the ontogenetic stage of this individual, ROM 44770 may belong to the “intermediate” stage of incipiently-crested subadult individuals identified in this study. Alternatively, ROM 44770 could represent a different sex, population, or chronospecies exhibiting a more plesiomorphic cranial morphology at maturity (e.g., Freedman Fowler and Horner 2015). According to Trexler (2001), ROM 44770 was discovered lower in section relative to YPM-PU 22405 and OTM F138, but the absolute difference in the geological ages of these specimens is unknown (Freedman Fowler and Horner 2015).

At least one aspect of variation observed in this study does not appear to be related to size or ontogeny, but contributes new data to the range of individual variation in brachylophosaurin cranial anatomy. The position of the foramen for CN VII on the lateral wall of the braincase, relative to the other cranial nerve foramina, has been considered to be of possible taxonomic significance in brachylophosaurins (Gates et al. 2011). However, the relatively low position of this foramen in the intermediate-aged ROM 66181 (Fig. 2.10) varies more from other specimens of *Maiasaura* than the position of this foramen is reported to vary between other brachylophosaurin taxa (Gates et al. 2011; Freedman Fowler and Horner 2015). The number of foramina for CN VII varies between one and two per side in hadrosaurids, sometimes even within a species (Evans 2010). The singular CN VII foramen observed in most specimens of *Maiasaura* is positioned most similarly to the foramen for the hyomandibular ramus in hadrosaurids

with two CN VII foramina, but in ROM 66181 the entire nerve appears to exit in the position taken by the palatine ramus when both foramina are present.

It is unknown whether any of the observed variation is due to sexual dimorphism. Analysis of *Maiasaura* bonebed material is compatible with dimorphism in body mass (Saitta et al. 2020). However, sexual dimorphism in cranial anatomy has not been confirmed in any ornithischian dinosaur to date (Mallon 2017). The sample size necessary to statistically demonstrate sexual dimorphism is predicted to be much greater than presently available for skulls of *Maiasaura peeblesorum* (Hone and Mallon 2017).

Implications for brachylophosaurin evolution— Although *Maiasaura* shares the condition of a solid cranial crest with the brachylophosaurins *Brachylophosaurus* and *Probrachylophosaurus*, the forms of these crests differ, and it is unclear what shape of solid crest, if any, was present in their most recent common ancestor. Horner (1983: 37) considered it “likely that *Brachylophosaurus* was derived from a hadrosaur closely resembling *Maiasaura*,” despite recognizing *Brachylophosaurus* as the stratigraphically earlier of the two (Horner 1983: fig. 6), but *Acristavus* and *Probrachylophosaurus* were unknown at that time. Freedman Fowler and Horner (2015) proposed a heterochronic model of brachylophosaurin cranial evolution in which the subadult morphology of *Brachylophosaurus* retains adult characters of its apparent ancestor, *Probrachylophosaurus*, which in turn as a subadult retains adult characters of its apparent ancestor, *Acristavus*. They reported conflicting evidence for the phylogenetic position of *Maiasaura*, which depending on the matrix used could be recovered as either the sister taxon of *Brachylophosaurus* (suggesting descent from a *Probrachylophosaurus*-like ancestor), or immediately outside of the *Probrachylophosaurus*–*Brachylophosaurus*

clade (Freedman Fowler and Horner 2015); most subsequent analyses that include the relevant taxa have favoured the latter topology (Xing et al. 2017; Kobayashi et al. 2019; Prieto-Márquez et al. 2019, 2020; Zhang et al. 2020; Takasaki et al. 2020).

The subadult *Maiasaura* ROM 66182 resembles the adult forms of other brachylophosaurins in having a relatively horizontal posterior skull roof. As in *Acristavus*, the posterior corners of the nasal–frontal contact are square (Gates et al. 2011). However, the anteroventrally inclined orientation of the nasal–frontal contact and adhering nasal fragment, along with the orientation of the correspondingly sized and potentially associated lacrimal, suggest an anteroventrally sloping preorbital region as reconstructed for small juveniles of this taxon (Carpenter 1999: fig. 12.5), rather than an approximately horizontal posterior nasal as in adult *Acristavus*, *Brachylophosaurus*, and *Probrachylophosaurus*. Gates et al. (2011) described the nasal–frontal contact of *Acristavus* (UMNHVP 16607) as posteriorly deep and oriented at 90 degrees to the floor of the contact, as in ROM 44770, with an upturned lip of the frontal along the dorsal boundary of the contact. The least mature specimen of *Maiasaura* in this study with a vertical nasal–frontal contact, ROM 66181, is similar to *Acristavus* in that the frontal along the dorsal boundary of the contact forms only a slightly raised lip, rather than the greater elevation in more mature individuals of *Maiasaura*. However, *Maiasaura* at the ontogenetic stage represented by ROM 66181 differs from *Acristavus* in that the correspondingly sized and potentially associated partial nasals are curved posterodorsally, and their steep deflection from the dorsal surface of the frontals when articulated with ROM 66181 forms an incipient crest surface. At no point in its known ontogeny, then, does *Maiasaura* recapitulate the flat, horizontally oriented posterior nasals of *Acristavus*

gagslarsoni (MOR 1155). Alternatively, the strong similarity in the frontal side of the contact between ROM 66181 and UMNHVP 16607 could suggest that the unknown nasals of the latter more closely resembled those of an incipiently crested *Maiasaura* than they did the nasals of the *Acristavus gagslarsoni* holotype (in which the orientation of the contact cannot be determined from the figures of the articulated skull).

Also at no point in its ontogeny does *Maiasaura* possess a flattened, posteriorly directed, paddle-like crest, which characterizes adult *Probrachylophosaurus* and *Brachylophosaurus*. However, the ontogeny of the nasal and frontal in *Maiasaura* does resemble these taxa in that the grooves and ridges of the frontal–nasal contact become progressively deeper as the contact surface enlarges, and length of the frontal posterior to the contact becomes proportionately shorter anteroposteriorly (Freedman Fowler and Horner 2015). The partial nasals corresponding in size with, and potentially belonging to, ROM 66181 have a distinctly triangular cross-section, as in adult *Probrachylophosaurus* and subadult *Brachylophosaurus*, while the nasals of the large adult ROM 66180 are more flattened along their midline, as in adult *Brachylophosaurus* (Freedman Fowler and Horner 2015). The “mature adult” ontogimorph of *Maiasaura* also shares with adult *Brachylophosaurus*, but not with any known ontogimorph of *Probrachylophosaurus*, a short overhang of the skull roof over the anterior margins of the dorsotemporal fenestrae. If these rudimentary ledges in *Maiasaura* are homologous to those that buttress the posteriorly directed nasal crest in *Brachylophosaurus*, a perturbation in the relative timing of crest formation in the *Maiasaura* lineage may have allowed for the novel onset of vertically directed crest growth to effectively preempt the ancestral onset of posteriorly directed crest growth, while not physically impeding the growth of the now vestigial

supporting ledges at the posterior end of the frontal. However, this scenario remains highly speculative given the absence of visible boundaries between the surrounding elements in *Maiasaura* individuals that exhibit this character, and the recently recognized complexity of soft tissue correlates in the dorsotemporal region of many dinosaurs (Holliday et al. 2020).

The problematic brachylophosaurin taxon “*Brachylophosaurus goodwini*” (Horner 1988) is based on a single specimen, UCMP 130139, from stratigraphically slightly lower in the Judith River Formation than the holotype of *Probrachylophosaurus bergei* (Freedman Folwer and Horner 2015). In recent decades “*Brachylophosaurus goodwini*” has variously been considered a junior synonym of *Brachylophosaurus canadensis* (Horner et al. 2004; Prieto-Márquez 2005), or potentially representing a new genus, if diagnostic (Freedman Fowler and Horner 2015). Freedman Fowler and Horner (2015) considered the exceptionally deep frontal depressions of UCMP 130139 as potentially distinguishing it from *Probrachylophosaurus bergei*. Given the variation in frontal depression depths described herein across the ontogenetic series of *Maiasaura peeblesorum*, I consider it possible that this difference between “*Brachylophosaurus goodwini*” and *Probrachylophosaurus bergei* may also be ontogenetic. However, I refrain from formally proposing the synonymy of these taxa here, given that no shared characters have been found to unite them, and also considering the questionable diagnostic value of UCMP 130139 owing to its preservational condition (Freedman Fowler and Horner 2015).

Implications for life appearance— The life appearance of *Maiasaura* is a popular subject in paleoart (e.g., Henderson in Wallace 1987; Kish in Russell 1989; Barlowe in Dodson 1995; Paul in Carpenter 1999). Although a detailed iconographic history of this species, as given by Bertozzo et al. (2017) for *Gryposaurus*, is beyond the scope of this study, I note that there has been some past and present confusion over the precise shape of the cranial ornamentation, which Horner (1983: 29) once described as a “crest or horn-like structure between the orbits”. Depiction of the ornamentation as a conical, “horn-like” structure has occasionally persisted even in professional artwork in the recent peer-reviewed literature (Bonadonna in Romano and Farlow 2018), but is not compatible with the known cranial morphology.

The remarkably wide, semi-circular prefrontal–nasal–frontal crest morphology of ROM 66180 documented here contributes new information on the striking visual appearance of one of the most iconic saurolophines. The topography of the nasal–prefrontal surface in ROM 66180, with a pair of large depressions that together span nearly the entire width of the crest (Fig. 2.4), is more complex than in smaller, incipiently crested individuals (Fig. 2.3), and may correlate with the presence of a soft tissue structure that was more developed in mature individuals. The breadth, position, and orientation of the crest surface on the skull of ROM 66180 is superficially suggestive of an odontocete melon (McKenna et al. 2012), but the extreme ecological differences between *Maiasaura* and echolocating toothed whales, and the ontogenetically late development of the crest in *Maiasaura*, make the presence of any analogous sensory organ implausible. Within Saurolophinae, a soft tissue visual display structure was preserved on the head of *Edmontosaurus* (Bell et al. 2014), and more broadly in this

subfamily, the presence of an inflatable soft tissue display structure has been inferred from the circumnarial depression on the facial skeleton (Hopson 1975). The latter soft tissue display structure has been proposed to have existed in conjunction with, and been supported by, a solid bony crest in Saurolophini (Hopson 1975; Drysdale et al. 2019). The subtlety of the transition in ROM 66180 between the flat surface that Horner (1983: fig. 1) identified as the “circumnarial depression” and the rest of the nasal may suggest that the lateral depressions on the crest are correlated with the same contiguous display organ, as reconstructed by Hopson (1975) for saurolophins, but this remains to be tested. Trexler (1995) reported possible preservation of the integument on the crest of OTM F138, but a later review by Bell (2014) could not confirm this identification.

2.5 Conclusions

The skull roof and braincase of *Maiasaura peeblesorum* are fully described from multiple individuals, complementing earlier descriptions of cranial anatomy in this taxon by Horner (1983) and Trexler (1995), and enabling further comparisons of this informative anatomical region to other hadrosaur taxa. The ontogenetic development of the cranial ornamentation is described in *Maiasaura* for the first time, allowing comparison of ontogenies between this and related taxa. The “mature adult” ontogimorph exhibits some potentially diagnostic characters not previously recognized in *Maiasaura*, and illustrates the extent of the prefrontal involvement in the mature crest. However, some individual variation observed did not appear to follow an ontogenetic trend. Sample sizes are still insufficient to assess evolutionary or sexually dimorphic variation in

Maiasaura, and further progress on these topics may clarify or modify the interpretation of ontogenetic and individual variation outlined here.

The ontogeny of the crest in *Maiasaura* shares similarities with *Brachylophosaurus* and *Probrachylophosaurus*, consistent with their derivation from a solid-crested common ancestor, but it is uncertain what the shape of the ancestral crest was. The discovery of rudimentary ledges, of unknown functional significance, projecting over the dorsotemporal fenestrae in only the largest specimens of *Maiasaura* suggest the hypothesis that the nasal crest growth was ancestrally directed posteriorly, as in *Brachylophosaurus*, before vertical nasal growth took over in the *Maiasaura* lineage. This hypothesis could be supported or refuted by the discovery of more plesiomorphic sister taxa to *Maiasaura*. *Maiasaura* resembles other brachylophosaurins, and differs from saurolophins and lambeosaurines, in delaying the formation of an incipient solid crest until well after the skull reaches half of its mature adult size. This difference in ornament growth strategy between the various clades of hadrosaurs, along with recently detected variation in overall growth dynamics (Słowiak et al. 2020), may point to clade-specific differences in behaviour and ecology that are as-yet unappreciated in the fossil record. Further attention to this type of variation may help explain changes in the taxonomic content of hadrosaur assemblages, in response to varying palaeoenvironmental, palaeogeographic, or behavioural conditions.

Chapter 3: First occurrence of *Maiasaura* (Dinosauria, Hadrosauridae) from the Upper Cretaceous Oldman Formation of southern Alberta, Canada

Abstract— I describe a new partial skull with braincase of a brachylophosaurin hadrosaurid from the Milk River Ridge Reservoir near Warner, southern Alberta, as the first diagnostic occurrence of *Maiasaura* in Canada. This material was collected in the Oldman Formation, at approximately the same stratigraphic level as a nearby bonebed of the ceratopsid *Coronosaurus brinkmani*. The assignment of this specimen to *Maiasaura*, rather than to *Brachylophosaurus*, is supported by the narrow and acute posterior margin of the external naris, the relationship between the postorbital and squamosal in the supratemporal bar, and the morphology of the frontals, which are greatly thickened and elevated anteriorly, with the dorsal surface not completely covered by the nasofrontal contact at adult size. The occurrence of both *Maiasaura* and *Brachylophosaurus* in approximately similar-aged deposits of the Comrey Sandstone zone in southern Alberta provides support for some cladogenesis in the evolutionary history of Brachylophosaurini. Geographically, the more western distribution of *Maiasaura* localities with respect to all *Brachylophosaurus* localities is consistent with the hypothesis that a preference for more inland versus seaway-adjacent habitats may have influenced the phylogenetic divergence of these taxa.

3.1 Introduction

Brachylophosaurini are recognized as the earliest-diverging clade of saurolophines (or hadrosaurines, depending on the favoured phylogeny) present in Laramidia, and include both solid-crested and non-crested species (Gates et al. 2011; Xing et al. 2017). Notably, these large herbivores have figured prominently in discussions of the roles of palaeogeography and heterochrony in dinosaur speciation (Horner 1983; Gates et al. 2011; Freedman Fowler and Horner 2015).

Brachylophosaurins are particularly well known from Montana, USA, where they are represented by at least four stratigraphically discrete taxa: *Acristavus gagslarsoni* (Gates et al. 2011) from the lower Two Medicine Formation, *Probrachylophosaurus bergei* (Freedman Fowler and Horner 2015) from the lower Judith River Formation, *Brachylophosaurus canadensis* (Sternberg 1953) from higher in the Judith River Formation (Prieto-Márquez 2005, 2007; Murphy et al. 2007), and *Maiasaura peeblesorum* (Horner and Makela 1979) from higher in the Two Medicine Formation (Horner 1983; Prieto-Márquez and Guenther 2018). The latter two of these are represented by abundant bone bed material. A possible fifth Montanan taxon, “*Brachylophosaurus goodwini*” (Horner 1988) from the Judith River Formation, is of uncertain validity (Freedman Fowler and Horner 2015). Additional recently recovered material from the Judith River Formation of Montana could represent another new taxon, stratigraphically and morphologically intermediate between *Probrachylophosaurus* and *Brachylophosaurus* (McDonald et al. 2019). In contrast, the record of diagnostic brachylophosaurin material from Alberta, Canada, has so far been restricted to a single identified species, *B. canadensis* from the Oldman Formation (Sternberg 1953;

Cuthbertson and Holmes 2010), and material recently identified as *Probrachylophosaurus* sp. indet. from the underlying Foremost Formation (Thompson et al. 2020). Although Reid (1990) mentioned the existence of fragmentary material indicating the presence of *Maiasaura* in southern Alberta, Ryan and Russell (2001) noted that this purported occurrence (of “cf. *Maiasaura peeblesorum*”) in the Oldman Formation of Alberta was based only on uncatalogued phalanges in the collections of the Royal Tyrrell Museum (TMP), of which the identifying character (midline ridge on the ventral surface of pedal unguals) is also present in those of *Brachylophosaurus*. As such, they considered the phalanges more likely referable to *Brachylophosaurus*, the better-known and more abundantly represented hadrosaur from the Oldman Formation. Brown et al. (2015) also did not recognize *Maiasaura* from Alberta.

In 2010, Wendy Sloboda discovered a new partial skull of a brachylophosaurin hadrosaur, TMP 2010.077.0030, while prospecting for the Southern Alberta Dinosaur Project along the south end of the Milk River Ridge Reservoir near Warner, southern Alberta (Fig. 3.1). This locality is best known for producing bone bed material that has been referred to the ceratopsian *Coronosaurus brinkmani* (Ryan and Russell 2005; Ryan et al. 2012; Ryan and Chiba 2020). TMP 2010.077.0030 was collected from approximately the same stratigraphic level as the *Coronosaurus* bone bed, placing it within the Comrey Sandstone Zone (informal middle unit) of the Oldman Formation (Eberth 2005) (Fig. 3.2), in which the holotype of *B. canadensis* from Dinosaur Provincial Park (CMN 8893), and the *B. canadensis* referred specimen TMP 1990.104.0001 from southern Alberta (Ryan and Evans 2005) were discovered. In this Chapter I describe the anatomy of TMP 2010.077.0030, compare the

Figure 3.1 Geographic distribution of fossil localities in Alberta and Montana that have produced *Maiasaura* (diamonds) and *Brachylophosaurus* (triangles). Solid symbols indicate type localities. The map was created using Adobe Photoshop CS5 Extended version 12.0 x 64, using data from Freedman Fowler and Horner (2015: fig. 2). Base map adapted from Google Maps.

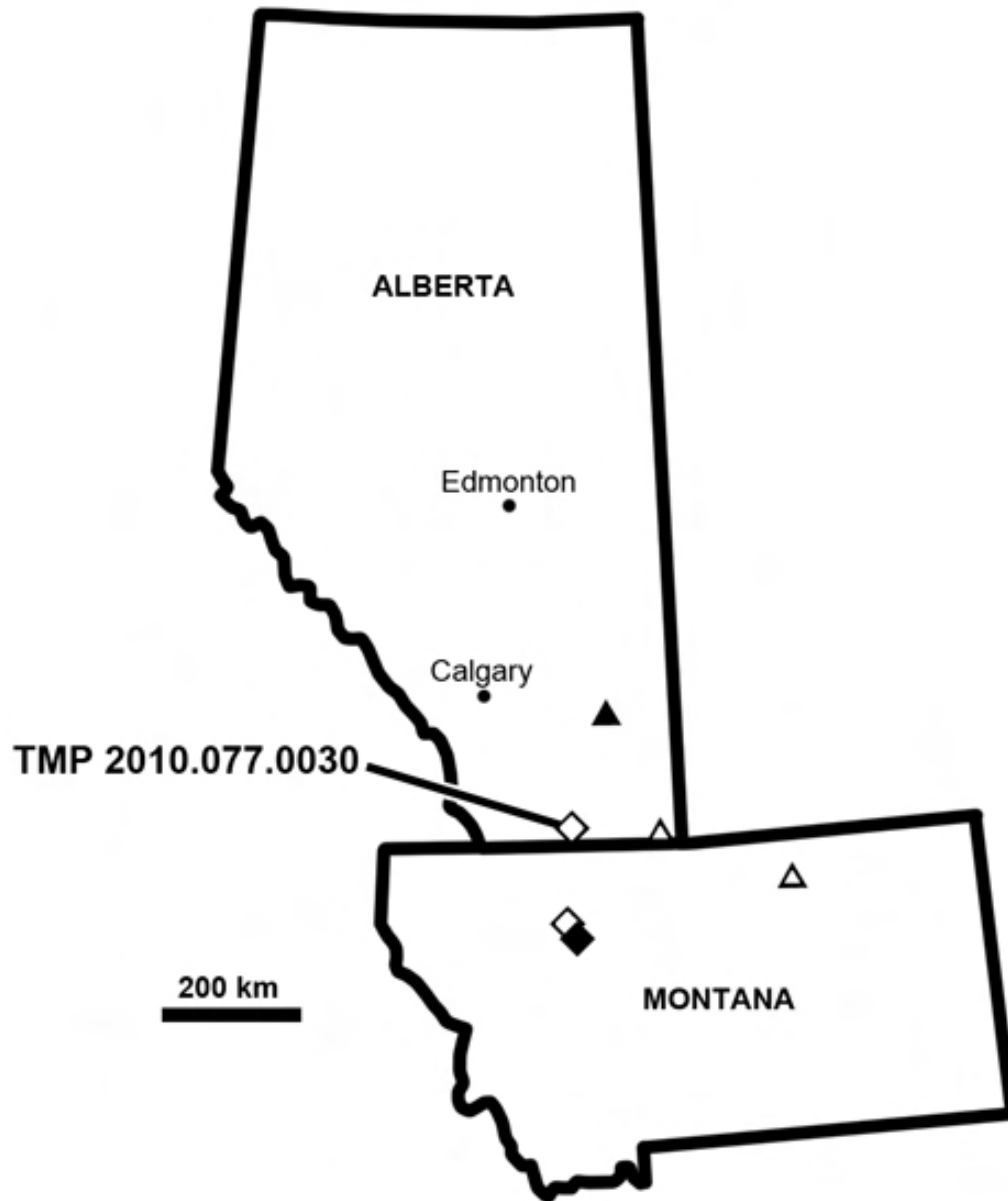
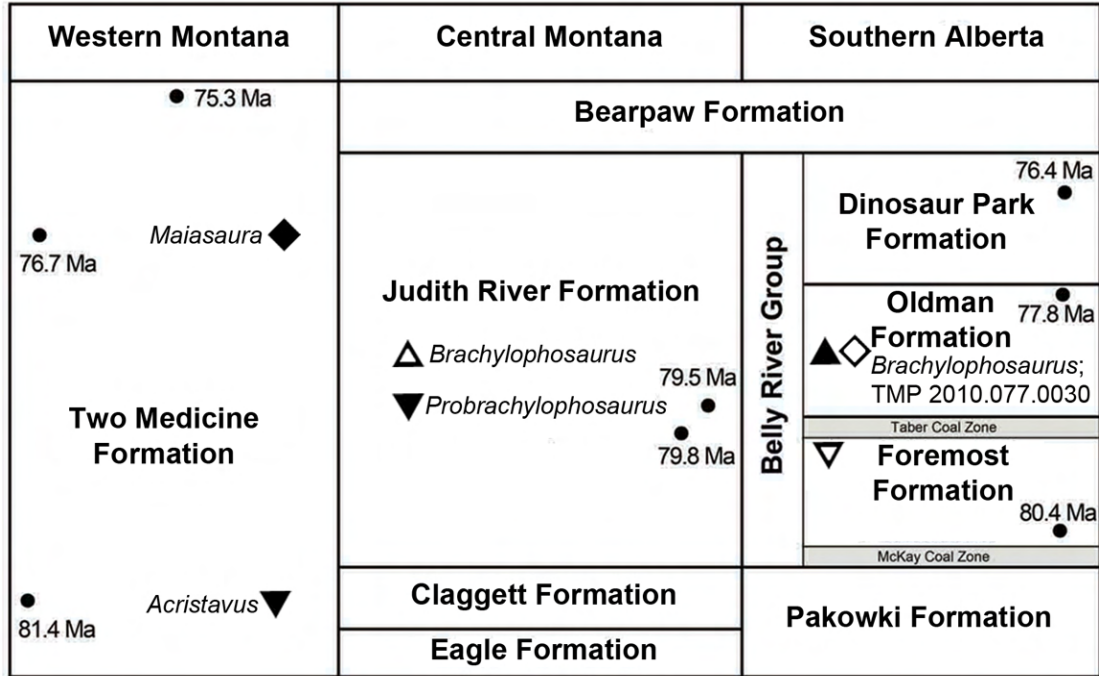


Figure 3.2 Stratigraphic distribution of *Maiasaura* (diamonds), *Brachylophosaurus* (triangles), and other brachylophosaurins (inverted triangles) in Alberta and Montana. Taxa reported from southern Alberta are *Probrachylophosaurus* sp. in the Foremost Formation, and *Brachylophosaurus canadensis* and *Maiasaura* sp. in the Oldman Formation. Solid symbols indicate type localities. Modified from Thompson et al. (2021).



skull with that of other brachylophosaurins, and discuss its significance for understanding the distribution and evolution of Brachylophosaurini.

Institutional abbreviations— **CMN**, Canadian Museum of Nature, Ottawa, Ontario, Canada; **MOR**, Museum of the Rockies, Bozeman, Montana, USA; **ROM**, Royal Ontario Museum, Toronto, Ontario, Canada; **TMP**, Royal Tyrrell Museum of Palaeontology, Drumheller, Alberta, Canada; **UMNHVP**, Utah Museum of Natural History Vertebrate Paleontology, Salt Lake City, Utah, USA.; **YPM-PU**, Princeton University collection at the Yale Peabody Museum, New Haven, Connecticut, USA.

3.2 Systematic Palaeontology

Ornithopoda Marsh, 1881

Iguanodontia Dollo, 1888

Hadrosauridae Cope, 1869

Saurolophinae Brown, 1914b

Brachylophosaurini Gates et al., 2011

Maiasaura Horner and Makela, 1979

Maiasaura sp. indet.

New Material— TMP2010.077.0030, partial skull.

Locality and Horizon— Comrey Sandstone Zone of the Oldman Formation, Milk River Ridge Reservoir, near Warner, Alberta, Canada. GPS coordinates are on file at the TMP. The age is Campanian, approximately 77 Ma (Eberth 2005). Approximately 100 m to the south of the documented *Coronosaurus* bonebed of Ryan and Russell (2005), and at the same stratigraphic level.

3.3 Description

TMP 2010.077.0030 consists primarily of the braincase and articulated left supratemporal arch (Fig. 3.3). Additionally, two morphologically informative fragments of the nasals are identified (Fig. 3.4). Over 160 unidentified small bone fragments are also included in TMP 2010.077.0030, most showing no characteristic morphology.

Nasal— The larger and more anterior fragment is from the right nasal (Fig. 3.4A–B). The total preserved length of this fragment is 124 mm, and its height is 62 mm. This region of the nasal is gently curved mediolaterally between the flattened narial region, including the ovoid posterior margin of the narial fenestra, and the supranarial region. The anterior ends of both the anterodorsal and anteroventral processes are broken. The margin of the narial fenestra is gently rounded, rather than sharp-edged, between the lateral and medial faces of the nasal. A small triangular section of the nasal along the posterior margin of the narial fenestra has been lost to breakage, but this does not substantially detract from knowledge of the shape of the fenestra in this region (estimated in Fig. 3.4A), which is relatively shallow with a depth of approximately 25 mm at the anteriormost preserved point on the anteroventral process. The small, subtriangular anteroventral process is asymmetrical in lateral view, with a concave dorsal edge and a

Figure 3.3 Braincase and left supratemporal arch of TMP 2010.077.0030 in left lateral (A, B), right lateral (C, D), and dorsal (E, F) views. alp, base of alar process; bpp, basiptyergoid process; crpr, crista prootica; CN III–XII, cranial nerve foramina; cup, cultriform process; dtf, dorsotemporal fenestra; ecc, endocranial cavity; fr, frontal; frcr, base of frontal crest; frd, frontal depression; ibpp, interbasiptyergoid process; ica, foramen for internal carotid artery; pa, parietal; pf, prefrontal; po, postorbital; prcp, precotyloid process; prvp, prootic ventrolateral pit, qc, quadrate cotylus; sq, squamosal.

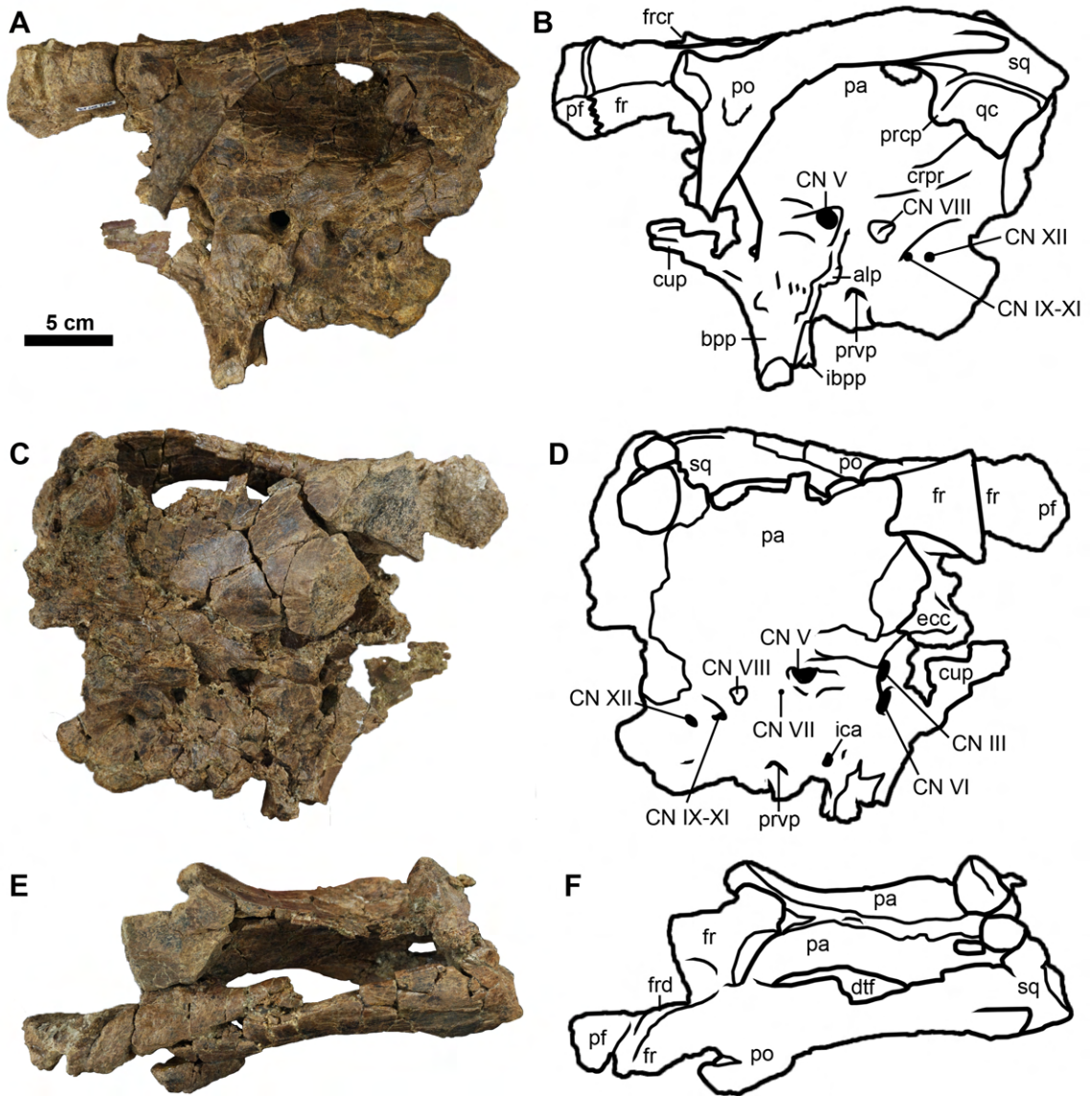
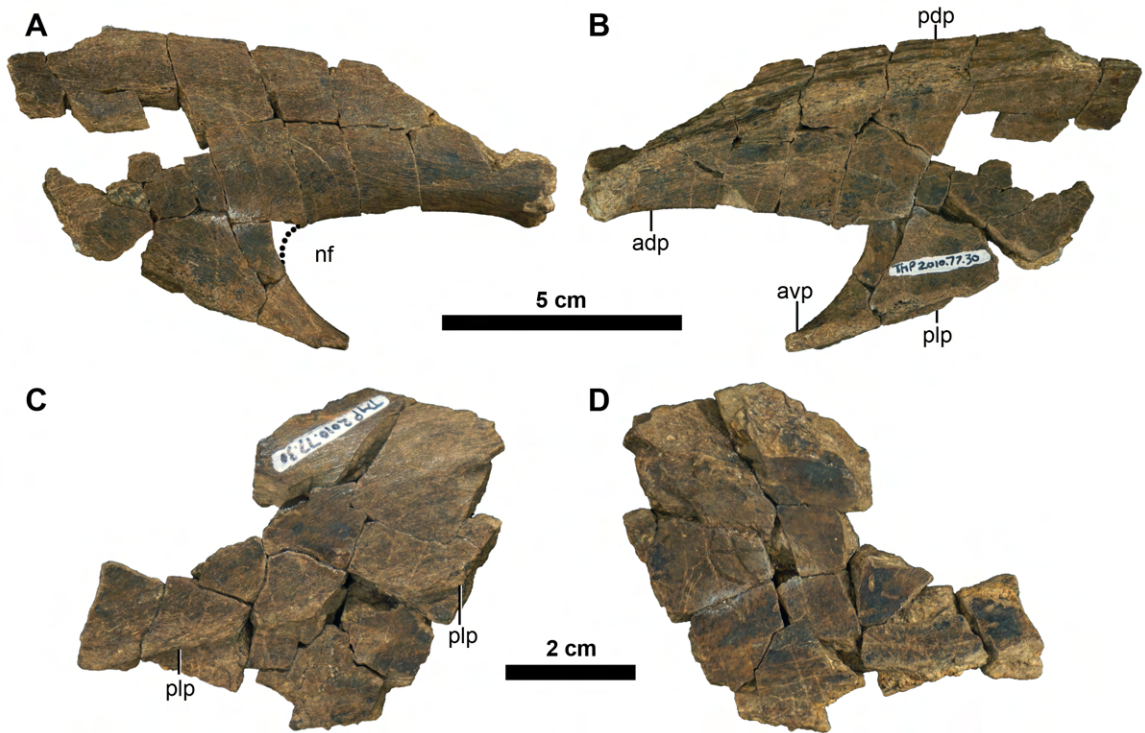


Figure 3.4 Nasal fragments of TMP 2010.077.0030 in lateral (A, C) and medial (B, D) views. adp, anterodorsal process; avp, anteroventral process; nf, narial fenestra; pdp, contact with posterodorsal process of premaxilla; plp, contact with posterolateral process of premaxilla. Dashed line represents the reconstructed margin of the narial fenestra.



straight ventral edge. A shallow, “V”-shaped groove for articulation with the posterolateral process of the premaxilla runs the length of the ventral surface of the anteroventral process. The groove becomes shallower towards the anterior end of the process. The dorsal part of the medial surface of the nasal has a long, flat contact with the posterodorsal process of the premaxilla, which is 11 to 15 mm deep, depending on the position measured. This contact is textured with faint, anteroposteriorly directed ridges and grooves lengthwise, and a smooth depression anteriorly. If the orientation of the medial contact is assumed to be vertical, the lower part of the nasal fragment containing the narial fenestra is oriented in a diagonal plane, with the narial fenestra facing slightly dorsolaterally.

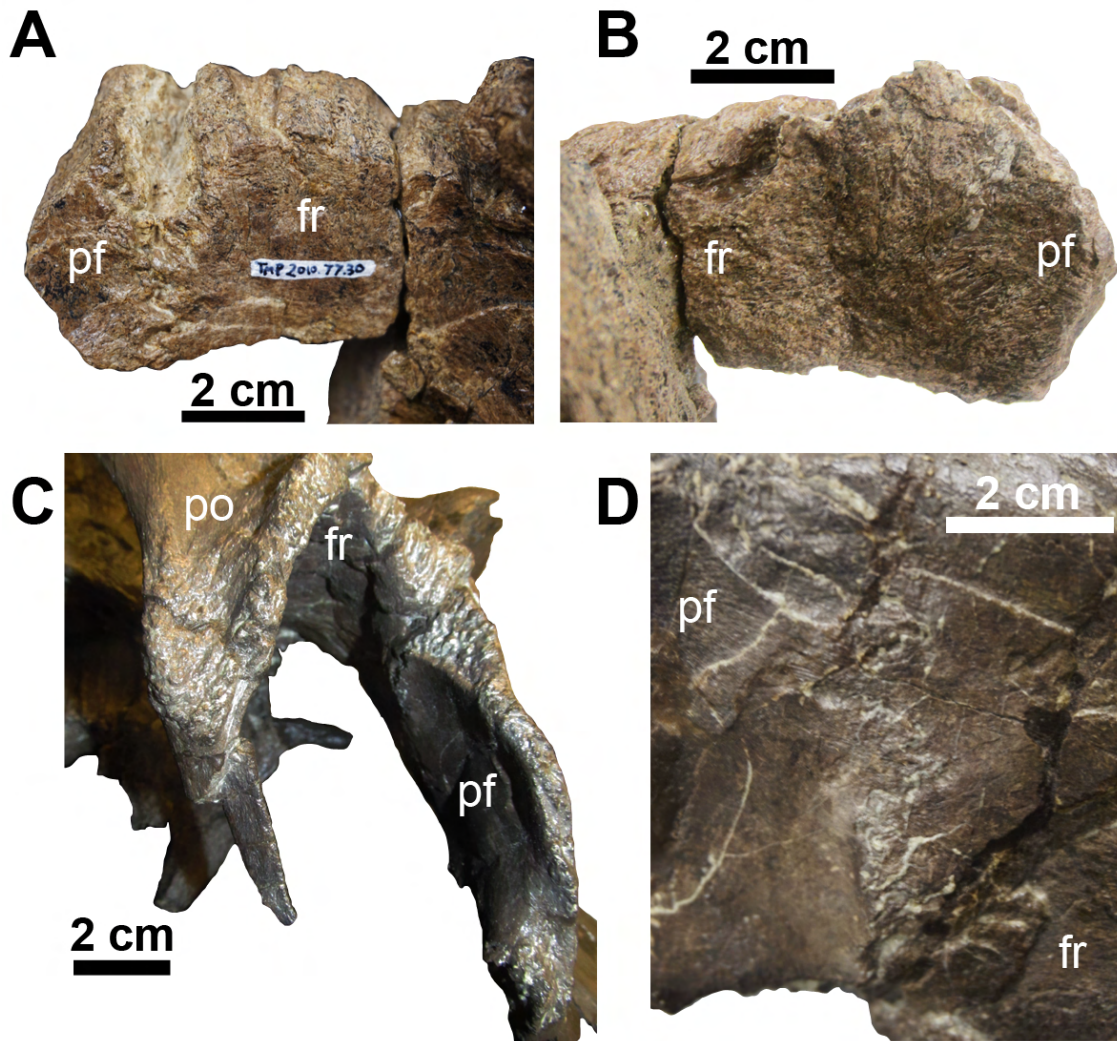
The smaller and more posterior nasal fragment is more difficult to definitively assign to either the left or right side, though it is most similar to the morphology of the left nasal of ROM 66180 (*M. peeblesorum*). In any case, it preserves no point of connection to the other nasal fragment (Fig. 3.4C–D). Its preserved length is 67 mm, and its height is 45 mm. This region of the nasal is plate-like and slightly curved, with a convex lateral side and a concave medial side. The only notable anatomical feature visible on this fragment is the abrupt straight edge on the lateral side that divides the thicker (7 mm thick) upper region from the laterally recessed (5 mm thick) lower surface that contacts the medial side of the posterolateral process of the premaxilla. No contacts with other bones are present on the medial side.

Prefrontal— Only the posteriormost region of the left prefrontal, forming the anterodorsal region of the orbit, is preserved. The preserved length of this element is 20 mm, and its maximum depth is 48 mm. The external boundary between the prefrontal and

the frontal is identifiable as a deeply interdigitating contact between a line of prominent, simple triangular projections, which is visible for a length of 25 mm along the ventrolateral surface within the orbit (Fig. 3.5A). Above this contact, on the lateral surface of the orbital rim, a deep vertical fissure occurs between the prefrontal and the frontal, inset up to approximately 10 mm from the orbital rim (Fig. 3.3E), but there is no distinct boundary between these elements within the fissure. The depth of the orbital rim at this location is 28 mm. The prefrontal contribution to the lateral rim of the orbit anterior to the fissure is lost to breakage. What is present of the dorsal surface of the prefrontal is narrow and poorly preserved, but the dorsolateral edge appears to be slightly raised with respect to the remainder of the dorsal surface. In medial view, the prefrontal contributes to a flat breakage surface continuous with the frontal. The absence of an internal boundary between these elements indicates that they were fused in life.

Frontal— The broken frontals can be described as essentially two regions, the anteriorly projecting left lateral region and the more posterior central region. The frontal contribution to the left orbital rim is at least 19 mm long posterior to the prefrontal–frontal fissure, or 31 mm including it. The depth of the frontal at the orbital rim is at least 20 mm. The orbital rim of the frontal is furrowed. A narrow frontal depression runs diagonally across the dorsal surface posterior to the prefrontal–frontal fissure, but does not reach the lateral edge of the orbital rim. In medial view, the thickness of this region of the frontal beneath the frontal depression is 24 mm. In contrast, its thickness opposite the prefrontal–frontal furrow (the deepest preserved part of the orbital region) is 48 mm. The frontal depression continues posteromedially to the junction of the lateral and posterior frontal fragments, where it becomes broad, ovoid, and shallow. In anterior view, the

Figure 3.5 Prefrontal and frontal margin of left orbital rim of TMP 2010.077.0030 in left ventrolateral (A) and medial (B) views; right orbital rim of ROM 66180 (*Maiasaura peeblesorum*) in ventrolateral view (C); close-up of right prefrontal–frontal contact of ROM 66180 in ventral view (D). fr, frontal; pf, prefrontal; po, postorbital.

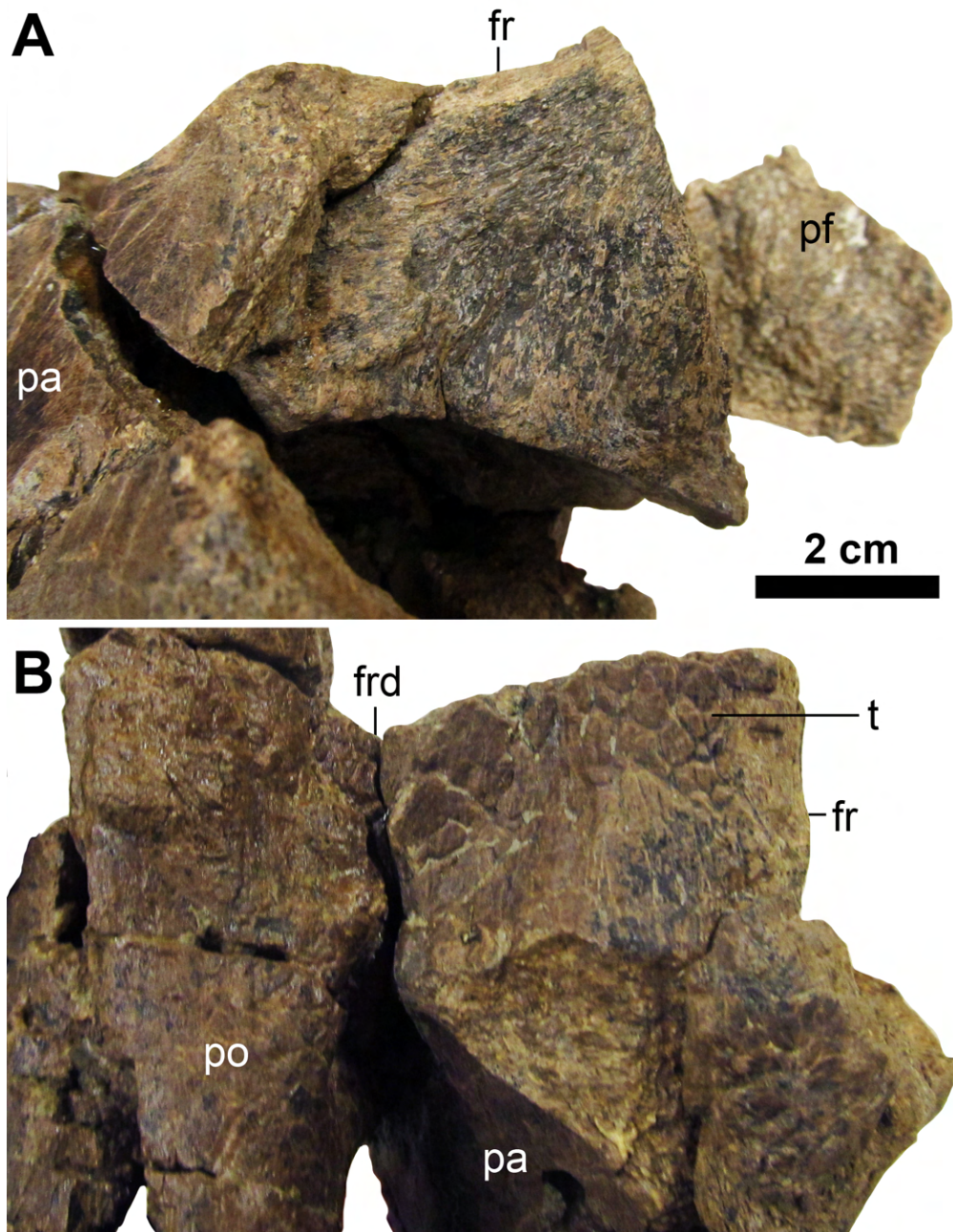


thickness of the central part of the frontal beneath the frontal depression is 35 mm. No obvious contact between the frontal and the postorbital is observed on the skull roof, probably due to breakage and poor preservation in this region, or potentially to fusion of these elements.

The central region of the frontals is roughly pentagonal in dorsal view (Fig. 3.6B), with an estimated length of approximately 50 mm. I estimate that when the frontals were complete, they were no shorter than approximately 80 mm, including the unpreserved nasal–frontal contact. The central region is broken along two almost perpendicular planes: an approximately transverse plane that cuts off the nasal–frontal contact and an approximately sagittal plane down the midline (Fig. 3.6A). The dorsal surface is elevated anteriorly (Fig. 3.6A), reaching a vertical thickness of at least 48 mm above the exposed endocranial cavity (57 mm measured along the anterior breakage surface, which is inclined slightly posterodorsally). The elevated region of the frontal is highest medially, descending laterally to form a rounded transverse section. The dorsal surface in this region has a lightly defined mosaic-like texture not seen elsewhere on the preserved elements, with individual tesserae up to 5 mm in diameter (Fig. 3.6B). Posteriorly, the region of the frontal–parietal contact is broken on both sides. Although the left frontal is represented best, a small posteromedial portion of the right frontal is preserved to the right of the parietal sagittal crest. The left and right frontals are fused, with the interfrontal suture having been nearly or completely obliterated.

Parietal— The parietal is a singular, elongate, hourglass-shaped bone forming the middle part of the posterior skull roof, as in other saurolophines (Fig. 3.3E–F). Its length is estimated to be approximately 140 mm. Most of this element is preserved, but the

Figure 3.6 Posterior frontals of TMP 2010.077.0030 in (A) right lateral (cross-sectional) view and (B) dorsal view. fr, frontal; frd, frontal depression; pa, parietal; pf, prefrontal; po, postorbital; t, tesserae-like bone texture.



dorsal margin of the sagittal crest is broken, and damage obscures the posterior contacts with the squamosals and supraoccipital. The sagittal crest is smooth and thin, with a thickness of 2 mm at its thinnest. Ventrally, the parietal is fused to the lateral walls of the neurocranium.

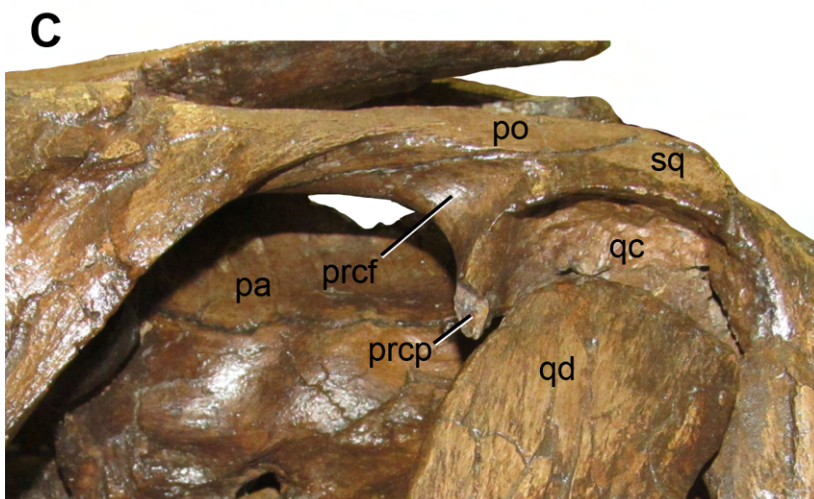
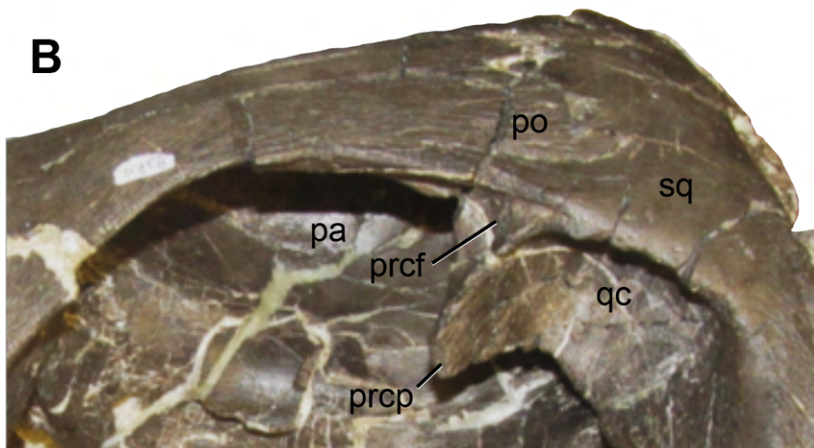
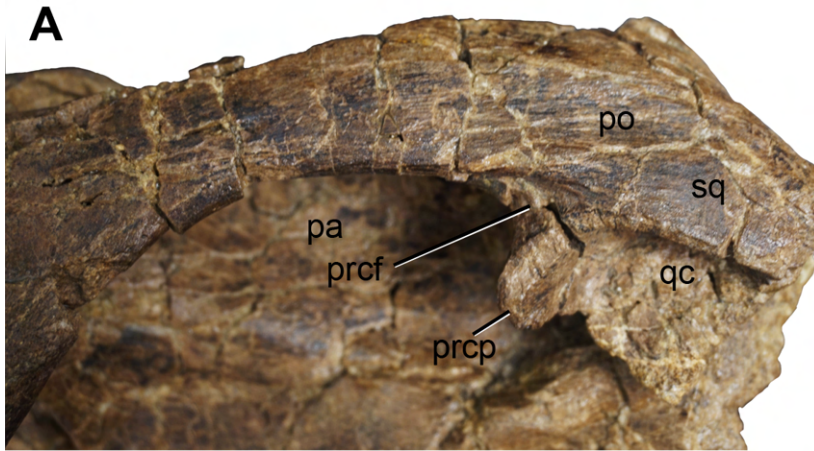
Postorbital— Most of the left postorbital is preserved, but its contacts with other elements, aside from the squamosal, are unclear due to breakage. Damage to the ventral part of the postorbital obscures the ridge that would join the postorbital and laterosphenoid, as well any presence of a postorbital foramen. The anterior process is also lost to breakage, as is the ventral extremity of the jugal process. The total preserved anteroposterior length of the postorbital is approximately 170 mm. The jugal process is directed anteroventrally and has a preserved length of approximately 70 mm. A “Y”-shaped rugosity occurs dorsally on the anterolateral and posterolateral margins of the jugal process; the two arms of the “Y” converge farther ventrally on the middle of the lateral side, and continue along the length of the process. This rugosity contributes to a slightly bulbous lateral surface of the jugal process. Although rugose, the texture of the jugal process lacks linear features such as ridges or furrows. The transition from the rugose lateral surface of the jugal process to the posterior surface is gradual, rather than abrupt. The lateral surface of the postorbital body between the fork of the “Y” is relatively smooth, but not depressed in relation to the squamosal process.

The squamosal process appears as a flattened bar with laterodorsally and ventromedially directed faces, and forms the dorsal margin of the lateral fenestra (Fig. 3.7). It is directed slightly posterodorsally in relation to the orbital rim. The posterior termination is dorsal to the quadrate cotylus of the squamosal. Measured dorsal to the

precotyloid process of the squamosal, the squamosal process of the postorbital is a narrow strap, 23 mm in width, with a dorsal exposure approximately equal to the width of the squamosal medial to it. Whether the squamosal process was bifurcated, with the other ramus situated more medially, is unclear due to poor preservation. The contact between the dorsomedial edge of the posterior tip of the squamosal process and the squamosal is flat and straight.

Squamosal— The left squamosal is mostly complete, with the exception of the precotyloid process. There is some breakage along the dorsolateral rim of the quadrate cotylus, and at the tip of the precotyloid process. The anterior process of the squamosal contacts the postorbital ventromedially, and is hidden by the postorbital in lateral view. The straight contact between these elements is visible on the ventromedial surface of the supratemporal bar. The precotyloid fossa occupies a small, triangular sheet of bone at the posterodorsal corner of the lateral temporal fenestra between the precotyloid process and the postorbital, with the fossa being restricted to the squamosal (Fig. 3.7). The triangular precotyloid process projects anteriorly, laterally, and ventrally. As preserved, it is relatively stout, being approximately as broad as long; however, it may have been slightly longer when complete. Its lateral surface is flat and continuous with the quadrate cotylus, whereas the dorsomedial side is convex. The quadrate cotylus is longer anteroposteriorly than mediolaterally, and the highest point in the cotylus is anterior to the midpoint of its length. The medial side of the squamosal is smooth and generally flat, with a slight convexity on the reverse side of the quadrate cotylus. The posterodorsal surface of the squamosal medial to the posterior termination of the squamosal process of the postorbital is smooth, flat, and essentially horizontal. More posteriorly, it is steeply sloped to form

Figure 3.7 Supratemporal bar of TMP 2010.077.0030 in left lateral view (A); of ROM 60261 (*Maiasaura peeblesorum*) in right lateral view, reversed (B); and of CMN 8893 (*Brachylophosaurus canadensis*) in left lateral view (C). Not to scale. pa, parietal; po, postorbital; prcf, precotyloid fossa; prcp, precotyloid process; qc, quadrate cotylus of squamosal; qd, quadrate; sq, squamosal.



the posterior squamosal surface. In posterior view the dorsal surface of the squamosal rises medially, reaching a height of approximately 30 mm above the quadrate cotylus.

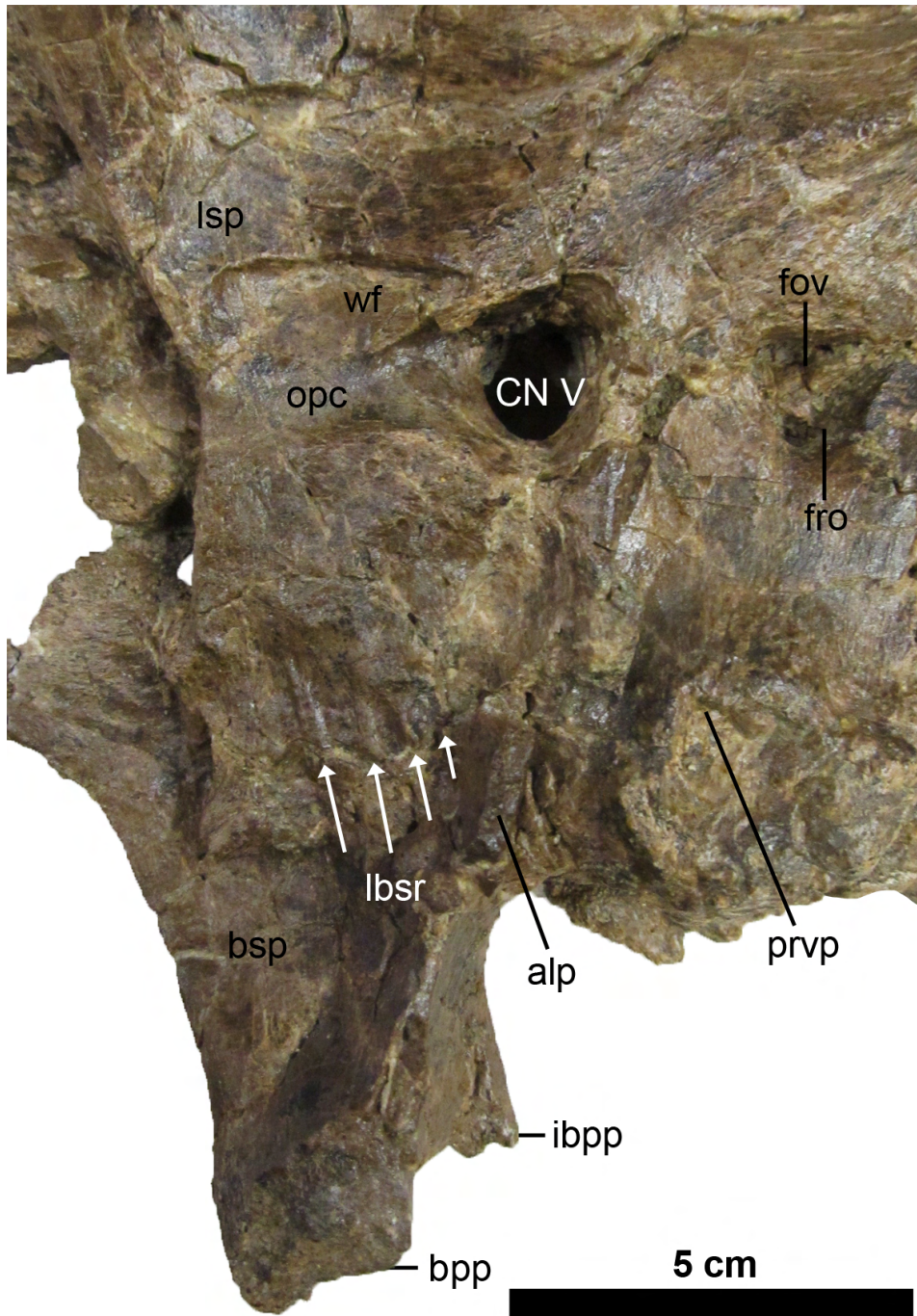
The posterior margin of the dorsal skull roof is poorly preserved, and it cannot be determined whether the left and right squamosals contacted each other, or were separated by the parietal. A featureless fragment of bone located at approximately the midline of the skull roof posterior to the parietal sagittal crest could belong to either the parietal, or the posteromedial process of the squamosal. A larger, rounded bone fragment on the right side of the posterior skull roof is in the appropriate position to pertain to the right squamosal, but does not mirror any of the preserved morphology of the left squamosal.

Neurocranium— Because the contacts between individual neurocranial elements are generally not visible in TMP 2010.077.0030, and because features of interest often occur where multiple elements meet, these elements (and the parasphenoid, which is seamlessly fused to the basisphenoid) will be described under a single heading. The correlation of foramina to soft tissue anatomy follows Ostrom (1961a). Anterodorsally, the orbitosphenoid–presphenoid complex is broken anteriorly. On the left side, a small (~3 mm) foramen for the trochlear nerve (CN IV) is possibly preserved near the probable boundary of the plate-like orbitosphenoid and the laterosphenoid. The optic foramen (for CN II) is anteriorly facing, positioned on the midline, and is an inverted trapezoid in outline, directly ventral to the large, broken opening of the endocranial cavity and foramen for the olfactory nerve (CN I). The foramina for the oculomotor nerve (CN III) and abducens nerve (CN VI) are arranged vertically ventrolateral to the optic foramen on either side, and dorsolateral to the cultriform process. The oculomotor foramen is positioned directly anteromedial to the canal for the ophthalmic ramus of the trigeminal

nerve (CN VI) on the braincase lateral wall, whereas the abducens foramen is entirely ventral to the level of this canal. The foramen for the oculomotor nerve is fully separated from that for the abducens nerve by a dorsomedially oriented strut of bone 7 mm wide. A very thin bridge of bone encloses the abducens nerve foramina anteriorly, separating the left and right foramina, and joins the base of the cultriform process to the anteriorly convergent anterolateral walls that separate the oculomotor and optic foramina.

A pronounced ridge on the laterosphenoid divides the orbital cavity, anteriorly, from the lateral wall of the braincase, posteriorly. This ridge is flexed in lateral view, with its inflection point located directly above the ophthalmic canal (Fig. 3.8). The minimum length of the braincase lateral wall, from the anterior margin of the ophthalmic canal to the anteriormost point on the posterior margin of the exoccipital, is 118 mm. The height of the ophthalmic canal is 10 mm. The ophthalmic canal is shallowly defined, and is bounded by a distinct ridge for only the posterior half of its length dorsally, and the posterior two thirds of its length ventrally. The dorsal ridge is continuous with the external margin of the trigeminal (CN V) foramen. This foramen is circular in outline internally, but has a subtriangular profile externally, due to its strongly arched posterodorsal margin. The canal for the maxillary and mandibular rami (CN V2&3) of the trigeminal nerve may have prevented the ventral margin of the ophthalmic canal and the posteroventral margin of the trigeminal nerve foramen from forming an uninterrupted ventral bar, but this is difficult to definitively determine due to breakage. A wedge-shaped fossa, 30 mm long and 11 mm high, is present directly dorsal to the ophthalmic canal (Fig. 3.8). It has a well-defined dorsal rim, and is bounded posteroventrally by the ridge overhanging the trigeminal foramen and ophthalmic canal.

Figure 3.8 Anteroventral region of neurocranium lateral wall of TMP 2010.077.0030, in left lateral view. alp, alar process; bpp, basipterygoid process; bsp, basisphenoid; CN V, trigeminal foramen (cranial nerve V); fov, fenestra ovalis; fro, fenestra rotunda; ibpp, interbasipterygoid process; lbsr; lateral ridges on basisphenoid; lsp, laterosphenoid; opc, ophthalmic canal; prvp, prootic ventrolateral pit; wf, wedge-shaped fossa.



The posterior margin of the trigeminal nerve foramen is continuous with the base of the alar process, which has a thickness of 4 mm. Most of the alar process is broken off on the left side, and on the right side it is not preserved at all. The alar process is angled approximately 65° from the horizontal. A small (~3 mm) facial nerve (CN VII) foramen is positioned at the posterior margin of the alar process, at approximately the same level as the ventral edge of the trigeminal nerve foramen, and is best seen on the right side. More ventrally along the posterior margin of the alar process is a larger foramen for the passage of the internal carotid artery. The ventral boundary between the prootic and the basisphenoid is indicated by a pit-like structure dorsal to the basal tuber of the basisphenoid. The dorsal margin of the pit, apparently corresponding to the ventral margin of the prootic, has a hooded or folded appearance with a pointed peak (Fig. 3.8). The subtriangular vestibular fenestra is best seen on the left side. Within this foramen, there is a septum dividing the anterodorsal half (the fenestra ovalis) from the posteroventral half (the fenestra rotunda). The vestibular fenestra is slightly more ventral than the trigeminal foramen. A robust crista prootica extends diagonally from the posterodorsal corner of the braincase, and merges smoothly into the lateral braincase wall dorsal to the vestibular fenestra. There is a wedge-like indentation following the ventral margin of the crista prootica anteriorly (dorsal to the vestibular fenestra), but not posteriorly.

The metotic strut is weakly defined from the rest of the lateral surface of the opisthotic–exoccipital complex (otoccipital or simply “exoccipital,” following Evans 2010). There are two round, laterally facing foramina, of approximately equal diameter

(~5 mm), in the anterior half of the exoccipital. They are separated by a vertical strut 6 mm wide. The dorsal margins of these foramina are ventral to the ventral margin of the fenestra rotunda, and their ventral margins are approximately level with the posteriormost point of the exoccipital condyloid. The more anterior of the two foramina contacts the metotic strut, and possibly contained the passage of the glossopharyngeal (CN IX), vagus (CN X), and accessory (CN XI) nerves, as well as the jugular vein. It is divided by a fine septum internally, which runs anterodorsal–posteroventral, separating the cranial nerves from the jugular vein (Ostrom 1961a). The more posterior of the two foramina is identified as the hypoglossal nerve (CN XII) foramen. The triangular exoccipital condyloids project farther posteriorly than the occipital condyle of the basioccipital. The exoccipital–basioccipital contact is poorly preserved, but is faintly visible in places, and is low on the braincase lateral wall.

The posterior aspect of the neurocranium is poorly preserved. The supraoccipital is completely fragmented, and preserves no morphological information. The base of the paroccipital process of the exoccipital projects posterolaterally, but this process is lost to breakage on both sides. Below the supraoccipital, the exoccipitals join to form a shelf with a straight posterior margin. The underside of the exoccipital shelf is angled posterodorsally, and extends for a distance of approximately 50 mm beyond the dorsal margin of the foramen magnum. Between the exoccipital shelf and the foramen magnum are a pair of tall ovoid depressions, separated by a stout ridge that continues along the underside of the exoccipital shelf; these depressions represent the area of insertion of the *M. rectus capitis posterior* (Ostrom 1961a). Another ridge on the medial surface of each exoccipital descends posteroventrally from the dorsal margin of the foramen magnum,

and terminates in a blunt knob anterodorsal to the level of the exoccipital condyloids. The ventral margin of the foramen magnum and the posterior floor of the endocranial cavity are unpreserved.

The cultriform process of the parasphenoid–basisphenoid complex is thin, fragile, and poorly preserved, with a horizontally projecting anterior sheet. Its ventral margin descends posteriorly and connects with the laminae forming the anterior edges of the lateroventrally projecting basipterygoid processes. The recessed anterior surface of the basisphenoid between these laminae is deep and triangular. The left basipterygoid process is broken distally, and the right one is not preserved. The posteroventrally projecting interbasipterygoid process is stout with a flattened, oblate cross-section, but is also broken distally. Posteriorly, the basipterygoid and interbasipterygoid processes are connected to a steep surface that descends ventrally approximately 30 mm relative to the dorsal-most point on the ventral surface of the basisphenoid.

The lateral surface of the basisphenoid is not strongly inset below the basisphenoid process of the laterosphenoid, as if to form a laterally projecting pedestal for the laterosphenoid, although it is difficult to rule out diagenetic compression as enhancing the flatness of this region. Directly ventral to the basisphenoid process of the laterosphenoid, the lateral surface of the basisphenoid has a set of four small, subvertical columns or ridges (Fig. 3.8), which can be seen on both sides of the braincase. These ridges are approximately 2 mm wide, up to 15 mm long, and are spaced 3–5 mm apart. Anteroventral to these ridges, the basisphenoid has a small triangular process that laterally shields the foramen for the palatine artery. There is a shallow ovoid depression on the basisphenoid ventral to the trigeminal foramen, anterior to the alar process. The

contact between the basisphenoid and basioccipital contributions to the basal tubera is clearly visible for a short distance in lateral view, but is not visible in ventral view due to breakage. The main body of the basisphenoid is hourglass-shaped in ventral view.

The basioccipital is a poorly preserved rectangular element measuring approximately 60 mm long. It is broken lengthwise into two parts, with a large gap between the left and right sides. As preserved, the basioccipital is longer than wide.

3.4 Discussion

Comparisons and identification— The Oldman Formation of Alberta has so far produced only two named hadrosaurids, the saurolophine *B. canadensis* (Sternberg 1953) and the lambeosaurin lambeosaurine *Hypacrosaurus stebingeri* (Horner and Currie 1994). Another specimen, TMP 2016.023.0039, represents a parasaurolophin lambeosaurine (Chapter 4). TMP 2010.077.0030 can be confidently excluded from Lambeosaurinae on the basis of the narial fenestra bordered by the nasal, and the anteroposteriorly elongate parietal (Horner et al. 2004). Referral of TMP 2010.077.0030 to Brachylophosaurini is supported by the preserved portion of the alar process of the basisphenoid, which is large and highly angled, in the same plane as the basiptyergoid process (Gates et al. 2011). The basiptyergoid and interbasiptyergoid processes, though incompletely preserved, are also consistent with the morphology exhibited by members of this clade. The presence of a distinct pit on the lateral braincase wall dorsal to the basal tubera is also characteristic of at least some brachylophosaurins, being first proposed as an autapomorphy of *M. peeblesorum* (Hickie et al. 2015), but also present in *Brachylophosaurus* (CMN 8893). A similar pit is also potentially present in figured

material of *Kundurosaurus nagorny* (Godefroit et al. 2012: fig. 11B), a possible edmontosaurin, but I have not confirmed this with direct observation. The morphology of the shortened and anteriorly thickened frontal precludes inclusion in the edmontosaur clade. Detailed comparisons will, therefore, focus on establishing the affinities of TMP 2010.077.0030 within Brachylophosaurini. I directly compared TMP 2010.077.0030 to specimens of *Brachylophosaurus* (CMN 8893) and *Maiasaura* (ROM 44770, ROM 60260, ROM 60261, ROM 66180, ROM 66181, and ROM 66182), with the remaining comparisons being based on the literature. *Wulagasaurus dongi* (Godefroit et al. 2008) from the Maastrichtian Yuliangzi Formation in Heilongjiang Province, China, has been recovered as an early-diverging brachylophosaurin in some recent phylogenetic analyses, but its known material includes no elements in common with TMP 2010.077.0030 (Xing et al. 2012), so they cannot be compared.

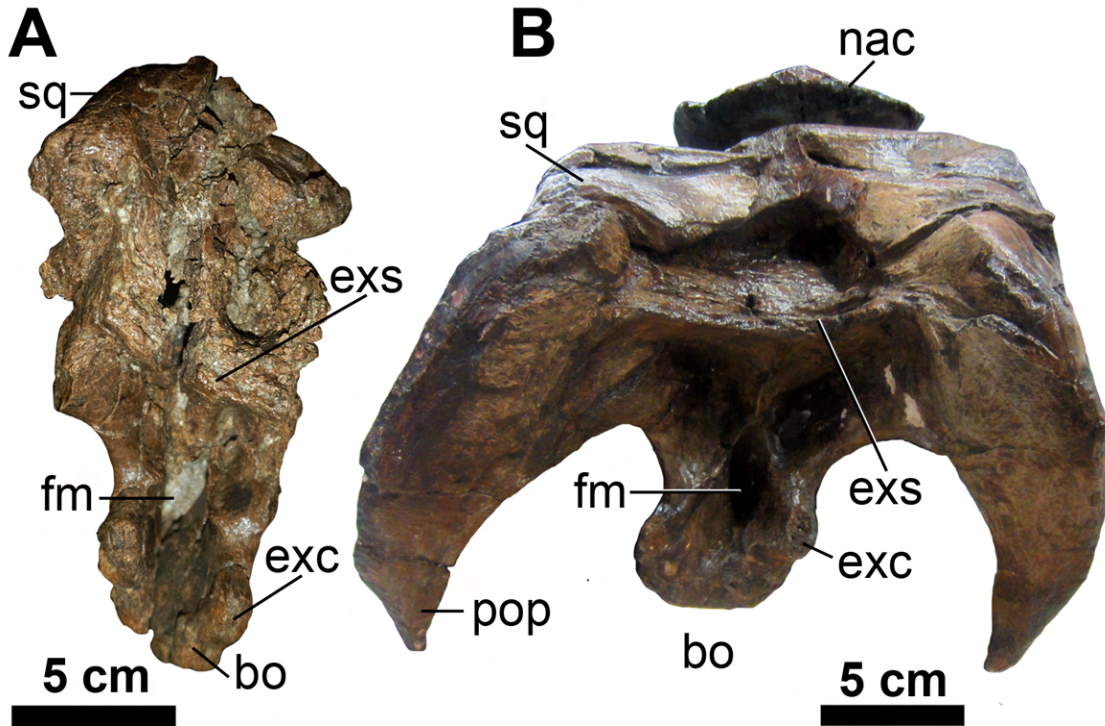
Although *B. canadensis* is the only brachylophosaurin well established to occur in the middle unit of the Oldman Formation, multiple characters indicate that TMP 2010.077.0030 is not referable to that taxon. In CMN 8893, the holotype of *B. canadensis*, the dorsal margin of the anteroventral process of the nasal is straighter than in TMP 2010.077.0030, and the posterior height of the narial fenestra is much greater (Cuthbertson and Holmes 2010: fig. 3), being more than twice that in TMP 2010.077.0030, despite the dimensions of the posterior skull roof and braincase indicating that these individuals had roughly similar-sized skulls. The relative dorsoventral expansion of the narial fenestra shows some variation among specimens of *Brachylophosaurus*, however, being most pronounced in CMN 8893 and more modest in TMP 1990.104.0011 (Cuthbertson and Holmes 2010: fig. 17) and MOR 794 (Prieto-

Márquez 2005: fig. 6), so this character by itself may not definitively preclude TMP 2010.077.0030 from being *Brachylophosaurus*. The dorsal margin of the orbit (prefrontal and frontal) is relatively thin in *Brachylophosaurus* compared with TMP 2010.077.0030. The skull roof in adult specimens of *Brachylophosaurus* differ drastically from that of TMP 2010.077.0030, in having a subhorizontal deeply grooved nasal–frontal contact that covers the entire length of the frontals (Freedman Fowler and Horner 2015: fig. 11D–E). The frontals of subadult *Brachylophosaurus* have a posterior region of the dorsal surface not covered by the nasal–frontal contact, but differ from TMP 2010.077.0030 in having a prominent unfused contact between the left and right frontals (Freedman Fowler and Horner 2015: fig. 11B–C). The lateral surface of the jugal process of the postorbital in CMN 8893 is smooth and slightly concave, whereas in TMP 2010.077.0030 it is rugose and slightly convex. However, Freedman Fowler and Horner (2015) noted that the lateral surface of the jugal process is highly intraspecifically variable in *B. canadensis*, and therefore may not be taxonomically significant. The supratemporal bar in CMN 8893 is oriented horizontally with a long lateral exposure of the postorbital–squamosal contact, such that the squamosal forms a significant part of the dorsal margin of the lateral temporal fenestra in lateral view, and the precotyloid fossa extends onto the lateral surface of the squamosal process of the postorbital; in all of these characters, the supratemporal bar differs from that in TMP 2010.077.0030, in which the supratemporal bar is elevated posterodorsally, the contribution of the squamosal to the dorsal margin of the lateral temporal fenestra in lateral view is relatively short, and the precotyloid fossa is restricted to the squamosal (Fig. 3.7). In posterior view, the dorsal surface of the squamosal in CMN 8893 is low and flat relative to the condition in TMP 2010.077.0030

(Fig. 3.9). The sharply rimmed wedge-shaped fossa on the braincase dorsal to the orbital canal in TMP 2010.077.0030 is similar to that in a juvenile specimen of *Brachylophosaurus* from the MOR 1071 bone bed (Holliday 2009: fig. 2A). This fossa is also weakly present in CMN 8893; however, its distribution and taxonomic significance among brachylophosaurins has not been established, and it does not appear to uniformly characterize *Brachylophosaurus*, being absent in an adult MOR 1071 braincase (Prieto-Márquez 2005: fig. 8; Holliday 2009: fig. 2B). Most significantly, TMP 2010.077.0030 differs in the much greater thickness and structure of the frontal at the anterior margin of the orbits where it buttresses the nasal, which reflects the much taller, dorsally directed crest in *Maiasaura* relative to the much thinner, more horizontal platform for the posteriorly directed nasal crest in *Brachylophosaurus*.

Acristavus gagslarsoni is the geologically oldest named brachylophosaurin, occurring in the lower Two Medicine Formation of Montana, USA, and in the Wahweap Formation of Utah, USA (Gates et al. 2011). Gates et al. (2011) claimed the swelling of the interdigitate prefrontal–frontal suture is diagnostic of *Acristavus*, but this is difficult to compare from published photographs. The dorsal surface of the frontal in the characteristically flat-headed *Acristavus* is essentially horizontal for most of its length. At the nasal–frontal contact, it rises to a slight peak positioned over the mid-length of the orbit (Gates et al. 2011: fig. 4A). In contrast, the dorsal surface of the frontal in TMP 2010.077.0030 has an anteriorly ascending slope that is visible much farther posteriorly, and is well-developed dorsal to the jugal process of the postorbital (Fig. 3.3). Although there is some breakage to the anterior edge of the postorbital in TMP 2010.077.0030, there is no indication of an enlarged sheet of bone covering the posterodorsal corner of

Figure 3.9 Posterior view of the occipital region in (A) TMP 2010.077.0030 and (B) CMN 8893 (*Brachylophosaurus canadensis*). bo, basioccipital; exc, exoccipital condyloid; exs, exoccipital shelf; fm, foramen magnum; nac, nasal crest; pop, paroccipital process of exoccipital; sq, squamosal.



the orbit, which is a characteristic of *Acristavus*, and especially pronounced in UMNHVP 16607 (Gates et al. 2011). Although both *Acristavus* and TMP 2010.077.0030 possess rugose postorbitals, TMP 2010.077.0030 lacks the diagnostic deep depression on the lateral surface of the postorbital jugal process (Gates et al. 2011: fig. 7B); rather, the massive rugosity spans the entire lateral surface in this region. The supratemporal bar in *Acristavus* is flattened as in TMP 2010.077.0030, but is oriented horizontally as in *Brachylophosaurus* (Gates et al. 2011). The foramen that pierces the lateral wall of the braincase at the contact between the parietal, laterosphenoid, and prootic in *Acristavus* (Gates et al. 2011: fig. 9B) is absent in TMP 2010.077.0030. The distance between the posterior extent of the basioccipital and the dorsal margin of the foramen magnum is claimed to be greater in *Acristavus* than in other saurolophines (Gates et al. 2011), but cannot be evaluated from the published figures. On the basis of the observed differences, it is unlikely that TMP 2010.077.0030 is referable to *Acristavus*.

Probrachylophosaurus bergei is also geologically older than TMP 2010.077.0030, but younger than *Acristavus*, occurring in deposits equivalent to the informal lower unit of the Oldman Formation (Freedman Fowler and Horner 2015). Unfortunately, the characters used by Freedman Fowler and Horner (2015) to diagnose this species cannot be evaluated in TMP 2010.077.0030, and several characters distinguishing TMP 2010.077.0030 from *Brachylophosaurus*, such as the depth of the posterior margin of the external naris, cannot be evaluated in *Probrachylophosaurus*. As in TMP 2010.077.0030, cranial sutures in the holotype of *Probrachylophosaurus bergei*, MOR 2919, are often faint or obscured due to fusion and remodelling (Freedman Fowler and Horner 2015). The thickness of the lateral region of the frontal in MOR 2919, as

reported by Freedman Fowler and Horner (2015) at the orbital rim and below the frontal depressions, is also similar to TMP 2010.077.0030. In dorsal view, the preserved posteromedial region of the frontals in TMP 2010.077.0030 is proportionally similar to the region of the frontals posterior to the nasal–frontal contact in MOR 2919. It is possible that the missing nasal–frontal contact in TMP 2010.077.0030 originally resembled that of *Probrachylophosaurus*, although there is no indication on the preserved part of the highly rugose and pitted posterior margin that characterizes the nasal–frontal contact of MOR 2919. Unlike TMP.2010.077.0030, the midline of the frontals directly posterior to the nasal–frontal contact in MOR 2919 does not visibly rise above the orbital rim in lateral view (Freedman Fowler and Horner 2015: fig. 3A). The posterior end of the postorbital in MOR 2919 articulates with a deep, prominently scalloped lip of the squamosal (Freedman Fowler and Horner 2015: fig. 13B), which is not developed in TMP 2010.077.0030 (Fig. 3.7). At present, while there are no unambiguous derived characters that would uniquely support the referral of TMP 2010.077.0030 to *Probrachylophosaurus*, the evidence against such a possibility is far from extensive. This situation will hopefully improve as more material is found.

Maiasaura peeblesorum is the geologically youngest named brachylophosaurin from Laramidia, based on material from the upper Two Medicine Formation, and is therefore slightly younger than TMP 2010.077.0030 (Freedman Fowler and Horner 2015). Horner and Makela (1979) identified a relatively small narial fenestra as a diagnostic feature of this taxon based on their study of the holotype, YPM-PU 22405, and the same state is confirmed in both subadult (ROM 66182) and adult (ROM 66180) material from the Linster Quarry bone bed (see Chapter 2). The nasal fragments of TMP

2010.077.0030 are essentially identical to the corresponding regions in ROM 66180, including the margin of the narial fenestra. The similarity in curvature of the posterior nasal fragment of TMP 2010.077.0030 to that in ROM 66180, while not in itself diagnostic, is consistent with the presence of a long, wide post-narial region of the face, another feature of *Maiasaura* (Horner and Makela 1979). While the nasal–frontal contact itself is missing in TMP 2010.077.0030, the dorsal elevation of the central region of the frontals towards their anterior end suggests that it extended above the horizontal, with the frontals contributing the posterior side of a solid crest, an autapomorphy of *Maiasaura* (Horner and Makela 1979). The obliteration of the interfrontal contact and the faint mosaic-like texture on the raised central region are typical of large individuals of *Maiasaura* (e.g., ROM 60260, ROM 66180). The great thickness of the frontals over the endocranial cavity in TMP 2010.077.0030 compares favourably with ROM 60261, a specimen of *Maiasaura* in which the braincase is broken along a similar plane. The “Y”-shaped ornamentation on the lateral surface of the postorbital is shared with ROM 66180, although as noted earlier this character has questionable diagnostic value. The form of the supratemporal bar in TMP 2010.077.0030 agrees with that in *Maiasaura* in every way that it differs from *Brachylophosaurus*: the supratemporal bar rises posterodorsally; the squamosal process of the postorbital is flattened and forms the dorsal margin of the lateral temporal fenestra, hiding the anterior process of the squamosal in lateral view; and the precotyloid fossas restricted to the squamosal (Fig. 3.7). The relatively deep posteromedial height of the squamosals in TMP 2010.077.0030 is also like that in *Maiasaura* (ROM 60261, ROM 66180), and unlike that in *Brachylophosaurus* (CMN 8893).

Although agreeing with *M. peeblesorum* in most respects, TMP 2010.077.0030 also has some characters that are unexpected for that species. The extreme thickness of the preserved posterior region of the prefrontal, the large size of the triangular interdigitations forming the ventrolateral prefrontal–frontal contact, and the deep dorsolateral fissure or notch between the prefrontal and frontal all differ from other examined specimens of *Maiasaura* (Fig. 3.5). The prefrontal in ROM 66180 is a laterally flared, dorsoventrally flattened element that is angled anteroventrally from the frontal, such that the dorsal surface is continuous with the nasal contribution to the crest, and the interdigitated frontal–prefrontal contact is oriented ventrally rather than ventrolaterally. The ventral interdigitations of the contact are complex and irregular, rather than simple interlocking triangles (Fig. 3.3D). The prefrontal is less modified to contribute to the crest in ROM 44770, but still lacks the unusual features of TMP 2010.077.0030. The pronounced ridge defining the dorsal margin of a wedge-shaped fossa on the laterosphenoid has not been previously noted in *M. peeblesorum*, and is absent in at least some individuals (ROM 60261), although possible variation in this character was noted earlier for *B. canadensis*. The series of small, subvertical ridges on the lateral surface of the basisphenoid, anterior to the alar process (Fig. 3.8), are also unknown in *M. peeblesorum*, and have not been described in any closely related taxon. It is possible that TMP 2010.077.0030 represents a new species of *Maiasaura*, given its occurrence in slightly older deposits, and in a different formation from the type locality of *M. peeblesorum*. At present I elect not to name a new taxon for this material, given its incompleteness, though further work may eventually necessitate such action.

Evolutionary and palaeoecological implications— The identification of TMP 2010.077.0300 as a specimen of *Maiasaura* from a stratigraphic unit that has also produced *B. canadensis* is significant in demonstrating that there was no major temporal gap between the stratigraphic ranges of these taxa. Previously, all valid brachylophosaurin taxa were stratigraphically segregated, at least when the ages of specimens were comparable (Freedman Fowler and Horner 2015). The *Maiasaura* specimen ROM 44770 is from stratigraphically lower in the Two Medicine Formation than the type locality of *M. peeblesorum*, but its absolute age or relative correlation with other formations has not yet been well established (Trexler 2001; Freedman Fowler and Horner 2015). Freedman Fowler and Horner (2015) hypothesized that *A. gagslarsoni*, *Probrachylophosaurus bergei*, and *B. canadensis* were members of a single anagenetic lineage, consistent with their lack of stratigraphic overlap. The origin of *Maiasaura* was hypothesized to have most likely involved a cladogenic divergence from this lineage at an uncertain time, though Freedman Fowler and Horner (2015) did note that in the phylogenetic analysis where *Brachylophosaurus* was recovered as the sister taxon of *Maiasaura*, it could also be possible that the latter was descended from the former. Most recent phylogenetic analyses have agreed in supporting *Probrachylophosaurus*, rather than *Maiasaura*, as the sister taxon of *Brachylophosaurus* (Kobayashi et al. 2019; Prieto-Márquez et al. 2019), and consequently, predict a cladogenic origin of the *Maiasaura* lineage prior to the existence of *Probrachylophosaurus*. TMP 2010.077.0030 contributes to filling in this “ghost lineage” for *Maiasaura*, and provides physical evidence independent of the phylogenetic analyses that *Maiasaura* is not the anagenetic descendant of *B. canadensis*.

The occurrence of more than one saurolophine taxon at the same stratigraphic level within a formation is unusual in the Upper Cretaceous of western North America, and the presence of two brachylophosaurin taxa in the informal middle unit of the Oldman Formation may be the first reported example from Canada, although their stratigraphic equivalence is approximate. In Alberta, the Dinosaur Park Formation contains *Gryposaurus* in its lower part, and *Prosaurolophus* in its upper part (Ryan and Evans 2005). The marine Bearpaw Formation contains a single identified saurolophine taxon, *Prosaurolophus* (Drysdale et al. 2019). In the Horseshoe Canyon Formation, *Saurolophus* occurs higher than *Edmontosaurus* (Eberth et al. 2013). It is notable that the total replacement of *Edmontosaurus* by *Saurolophus* in the Horseshoe Canyon Formation evidently did not involve the extinction of the former, which later reappears in southwestern Canada as the sole saurolophine taxon in the Frenchman Formation of Saskatchewan (Campione and Evans 2011).

Horner (1983) considered *M. peeblesorum* an endemic resident of upland palaeoenvironments. In Horner's (1983) hypothesis of saurolophine evolution, the common ancestor of *Brachylophosaurus* and *Maiasaura* was an upland dweller morphologically more similar to *Maiasaura*, with a relatively small narial fenestra. The acquisition of a greatly enlarged narial fenestra in *Brachylophosaurus* was, in Horner's view, possibly related to the more seaward, lowland palaeoenvironments preferred by this taxon. Gates and Scheetz (2015) invoked a similar hypothesis of habitat partitioning among closely related saurolophines between upland versus coastal lowland palaeoenvironments to explain the possibly coeval occurrences of *Rhinorex condrupus* (Gates and Scheetz 2015) and *Gryposaurus monumentensis* (Gates and Sampson 2007)

only 250 km apart in central and southern Utah. Cullen and Evans (2016) demonstrated that the broad composition of dinosaur taxa in microsite assemblages is generally stable across varying palaeoenvironments in the Upper Cretaceous of Alberta, and questioned the role of environmental sensitivity as a driver of dinosaur distribution in Laramidia. However, that study was focused on large-scale statistical analyses of microsite material with necessarily coarser taxonomic resolution, since hadrosaurid species cannot be reliably distinguished on the basis of isolated teeth (Coombs 1988). I therefore find no conflict between the results of Cullen and Evans (2016) and the possibility of habitat partitioning among hadrosaurids at a finer taxonomic scale, such as between *Maiasaura* and *Brachylophosaurus* in the Oldman Formation. The geographic locality near Warner, Alberta where TMP 2010.077.0030 was discovered is consistent with the trend of all *Maiasaura* localities being more western than all *Brachylophosaurus* localities, in both Alberta and Montana (Fig. 3.1). This may have significance given that all else being equal, a more western locality will tend to be more inland with respect to the shore of the Western Interior Seaway. However, this will not necessarily be the case for localities deposited at different times, due to the regression and transgression of the seaway. Further geological analysis of the Milk River Ridge Reservoir locality may be able to determine whether or not it represents a more upland depositional environment than the localities in the Oldman Formation that have produced fossils of *Brachylophosaurus*. Regardless of whether *Maiasaura* and *Brachylophosaurus* had different habitat preferences, the relatively small geographic distances between the various localities would have perhaps made at least occasional encounters between the two taxa inevitable. *Maiasaura* and *Brachylophosaurus* both possess nasal ornaments, which are

morphologically divergent and as visually distinctive from each other as they are from outgroup taxa. Their co-occurrence in the Oldman Formation is thus a relevant data point in both discussions of dinosaur palaeobiogeography as well as the debate over species recognition as a driving factor in the evolution of cranial ornaments in dinosaurs (Padian and Horner 2011; Knell and Sampson 2011; Knapp et al. 2018).

3.5 Conclusions

TMP 2010.077.0030 is distinct from *Brachylophosaurus canadensis*, and represents a second taxon of brachylophosaurin saurolophine in the Comrey Sandstone Zone of the Oldman Formation in southern Alberta. Comparisons with other brachylophosaurin taxa support the referral of TMP 2010.077.0030 to *Maiasaura*, as the first Canadian occurrence of this taxon. Subtle differences between this specimen and *M. peeblesorum* from the Two Medicine Formation in Montana suggest that it may represent an unnamed new species in this genus or an anagenetic predecessor of *M. peeblesorum*, an hypothesis that could be tested by the recovery of further maiasaurin material from this locality. TMP 2010.077.0030 supports the cladogenetic divergence of separate lineages of *Maiasaura* and *Brachylophosaurus*, as predicted by recent phylogenetic analyses. The general geographic distribution of *Maiasaura* and *Brachylophosaurus* in Alberta and Montana remains consistent with the hypothesis of a more inland habitat preference for the former taxon; however, this hypothesis should be refined with more detailed palaeoenvironmental analysis.

Chapter 4: A new parasaurolophin (Hadrosauridae: Lambeosaurinae) from the Oldman Formation of southern Alberta

Abstract— Lambeosaurines are abundantly represented in the Dinosaur Park Formation of Alberta, but are poorly known from older units, including the underlying Oldman Formation (Upper Cretaceous: Campanian). A new partial skull roof and braincase from the Comrey Sandstone Zone (middle Oldman) at the Milk River Ridge Reservoir locality in southern Alberta represents the first diagnostic cranial material of an adult-sized lambeosaurine from the Oldman Formation. Derived characters of the frontal platform and braincase (including the steeply inclined frontal platform, anteroposteriorly short and boomerang-shaped post-platform dorsal surface of the frontals, and ventrolaterally pendent alar processes of the basisphenoid) support the referral of this specimen to the clade Parasaurolophini, as the stratigraphically lowest specimen with the skull roof and braincase preserved. A unique combination of characters, some resembling the inferred plesiomorphic condition for corythosaurians, supports the naming of a new species. These characters include a flat, triangular plateau on the dorsal parietal separating the interfrontal process from the sagittal crest, and the anterolaterodorsal orientation of the postorbital processes of the laterosphenoids. The prefrontal-postorbital contact is not strongly elevated, and the posterior margin of the frontal platform has only a small vertical projection that does not overhang the parietal or dorsotemporal fenestrae, resembling the condition described in an immature *Parasaurolophus* from Dinosaur Provincial Park, despite the large size and fused interfrontal contact of the Milk River

Ridge Reservoir braincase. This difference may be attributable to heterochrony, with the ancestral adult development of the prefrontal–postorbital and nasal–frontal contacts being attained relatively early, in the juvenile stage of the stratigraphically higher form. As one of the few diagnostic hadrosaurids in Alberta to predate the classic Dinosaur Park Formation taxa, the Milk River Ridge Reservoir parasaurolophin is a significant source of new information concerning the timing and process of this clade’s phylogenetic and morphological divergence from other corythosaurians, as well as the evolution of hadrosaurid communities in Laramidia.

4.1 Introduction

Hollow-crested hadrosaurs, belonging to the clade Lambeosaurinae, were widely distributed across the northern hemisphere towards the end of the Cretaceous (Horner et al. 2004; Prieto-Márquez et al. 2013; Brownstein and Bissell 2021; Longrich et al. 2021). Lambeosaurinae is inferred to have likely originated in Asia, where early-diverging members were present as early as the Santonian (Godefroit et al. 2003; Sues and Averianov 2009; Prieto-Marquez 2010a; Bell and Brink 2013). More derived lambeosaurines were present in western North America (Laramidia) by the early–middle Campanian (Gates et al. 2014; Beveridge et al. 2022; Ramírez Velasco 2022), and attained their greatest known abundance and diversity on that landmass later in the Campanian (Ramírez Velasco et al. 2021: table 1). An abundance of material is particularly noted in the Dinosaur Park Formation of Alberta (Ryan and Evans 2005), where up to thirteen species were historically recognized, all represented by complete or mostly complete skulls (Lull and Wright 1942). Modern studies considering the

ontogeny, variation, and stratigraphic distribution of Dinosaur Park Formation lambeosaurines recognize between four (Dodson 1975; Holland et al. 2021) and six (Brink et al. 2014; Mallon 2019) of these named species as valid. Lambeosaurines from the Dinosaur Park Formation are among the oldest well-represented examples of the derived lambeosaurine clade Corythosauria (Madzia et al. 2021), with Lambeosaurini represented by the genera *Corythosaurus* and *Lambeosaurus*, and Parasaurolophini represented by the less abundant genus *Parasaurolophus* (Ryan and Evans 2005). Other, geologically younger records of Lambeosaurinae from Alberta include the taxonomically indeterminate Spring Creek lambeosaurine from the upper Campanian Wapiti Formation (Holland et al. 2021), and the lambeosaurin *Hypacrosaurus altispinus* from the lower Maastrichtian of the Horseshoe Canyon Formation (Evans 2010).

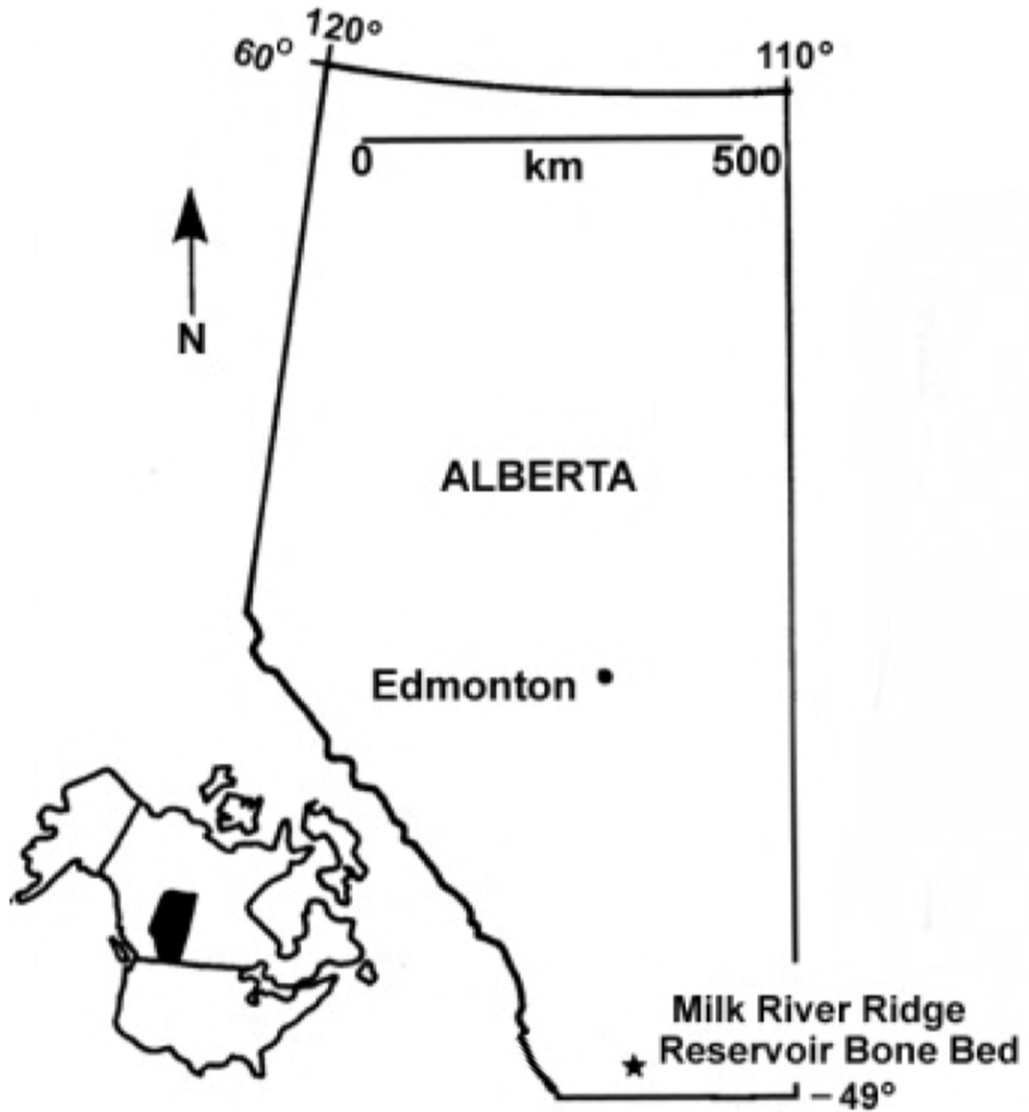
Despite their high abundance and diversity in the Dinosaur Park Formation, definitive records of Lambeosaurinae have been practically unknown from stratigraphically lower dinosaur-bearing units of Alberta. So far, no lambeosaurine fossils have been identified from the Milk River Formation, the Foremost Formation, or the informal lowest unit of the Oldman Formation. The poorer record of Albertan hadrosaurids in general in units below the Dinosaur Park Formation has been attributed, in part, to the smaller area of outcrops and less intensive prospecting (Thompson et al. 2021; Scott et al. 2022). Takasaki et al. (2019: table 1) listed three lambeosaurine supraoccipitals (UALVP 48, UALVP 53092, and UALVP 53106) as known from the Oldman Formation, but these are historically collected specimens from areas that also have Dinosaur Park Formation outcrops (not recognized as a distinct formation from the Oldman Formation at the dates of collection), and as such, cannot be definitively

assigned to a formation in the absence of more precise locality data. The lambeosaurine skeleton TMP 1978.016.0001 has also been cited as representing an undescribed new species from the Comrey Sandstone Zone (middle unit) of the Oldman Formation (Ryan and Russell 2001; Ryan and Evans 2005), but the quarry for this specimen has been relocated by David Evans (pers. comm.) and determined to be within the lowermost Dinosaur Park Formation. Embryonic lambeosaurine material from Devil's Coulee in southernmost Alberta was referred to *Hypacrosaurus stebingeri* and originally reported as being from the Two Medicine Formation (Horner and Currie 1994), but is now recognized as being from the upper Oldman Formation (Brink et al. 2014) that was deposited concurrently with the Dinosaur Park Formation (D. Evans, pers. comm.), rather than being evidence of pre-Dinosaur Park Formation lambeosaurines in Alberta.

Here, I describe the first diagnostic lambeosaurine material definitively from the Comrey Sandstone Zone of the Oldman Formation, representing a new taxon of Parasaurolophini. The specimen was collected along the Milk River Ridge Reservoir near Warner, Alberta (Fig. 4.1). Other dinosaur material from this locality includes abundant disarticulated elements of the ceratopsian *Coronosaurus* (Ryan and Russell, 2005), and a single partial skull referred to the brachylophosaurin hadrosaur *Maiasaura* (McFeeters et al. 2021a).

Institutional Abbreviations— **CMN**, Canadian Museum of Nature, Ottawa, Ontario, Canada; **CPC**, Colección Paleontológica de Coahuila (Paleontological Collection of Coahuila), Saltillo, Coahuila, Mexico; **DMNH**, Perot Museum of Nature and Science, Dallas, Texas, USA; **DMNH EVP**, Denver Museum of Nature and Science, Denver,

Figure 4.1 Map showing the location of the Milk River Ridge Reservoir bone bed in southern Alberta, Canada. Modified from Figure. 2 of Ryan and Russell (2005).



Colorado, USA; **GMH**, Geological Museum of Heilongjiang Province, Harbin, Heilongjiang, China; **NMMNH**, New Mexico Museum of Natural History, Albuquerque, New Mexico, USA; **ROM**, Royal Ontario Museum, Toronto, Ontario, Canada; **TMP**, Royal Tyrrell Museum of Palaeontology, Drumheller, Alberta, Canada; **UALVP**, University of Alberta, Edmonton, Alberta, Canada; **UCMP**, University of California Museum of Paleontology, Berkeley, California, USA.

4.2 Systematic Palaeontology

Lambeosaurinae Parks 1923

Corythosauria Madzia et al. 2021

Parasaurolophini Brett-Surman 1989 *vide* Evans and Resiz 2007

gen. et sp. nov.

Holotype— TMP 2016.023.0039, articulated posterior skull roof and braincase comprised of partial prefrontals, complete fused frontals, parietal, partial postorbitals, left squamosal fragment, and nearly complete neurocranium.

Horizon and Locality— Comrey Sandstone Zone of the Oldman Formation, Belly River Group (Campanian, ~77 Ma). Milk River Ridge Reservoir, near Warner, Alberta, Canada. GPS coordinates are on file at the TMP.

Diagnosis— Distinguishable from stratigraphically higher parasaurolophins by the retention of the following characters that are interpreted as plesiomorphic for

Corythosauria (shared with lambeosaurins): adult frontal platform does not overhang the remainder of the frontals or the parietal posteriorly; postorbital process of the laterosphenoid projects anterolaterally rather than laterally. Further distinguishable from *P. walkeri* in the more plesiomorphic orientation of the adult prefrontal–postorbital contact, which is well exposed dorsally and does not overlie the jugal process of the postorbital; from at least *P. walkeri* and *P. tubicen* in having a well-developed dorsal triangular region of the parietal separating the interfrontal process from the anteroposteriorly short sagittal crest; from at least *P. tubicen* and *P. cyrtocristatus* in having markedly stouter basiptyergoid processes of the parabasisphenoid, which have a complex lateral topography consisting of a distal anterior swelling continuous with the ventral lamina of the cultriform process, and posterior depression continuous with the lateral groove of the cultriform process (as in *Hypacrosaurus altispinus*), and also a relatively robust, subrectangular alar process (cannot be evaluated in *P. walkeri*); from at least *P. walkeri* and *Tlatolophus* by the mediolaterally long and shallow curve of the ventral margin of the paroccipital process ‘neck’ in posterior view (shared with *Charonosaurus*); from *Charonosaurus jiyinensis* in the markedly steeper angle of the frontal platform (shared with *Parasaurolophus* and *Tlatolophus*), and presence of a sagittal crest on the posterior parietal; and from *Tlatolophus galorum* in the absence of a tall, laminar supraoccipital crest.

4.3 Description and Comparisons

TMP 2016.023.0039 preserves the majority of an articulated posterior skull roof and braincase (Figs. 4.2–4.4). It is presently in two pieces, upper and lower, which are

Figure 4.2 Overview of the partial skull roof and braincase TMP 2016.023.0039 in A) right lateral; and B) left lateral view.

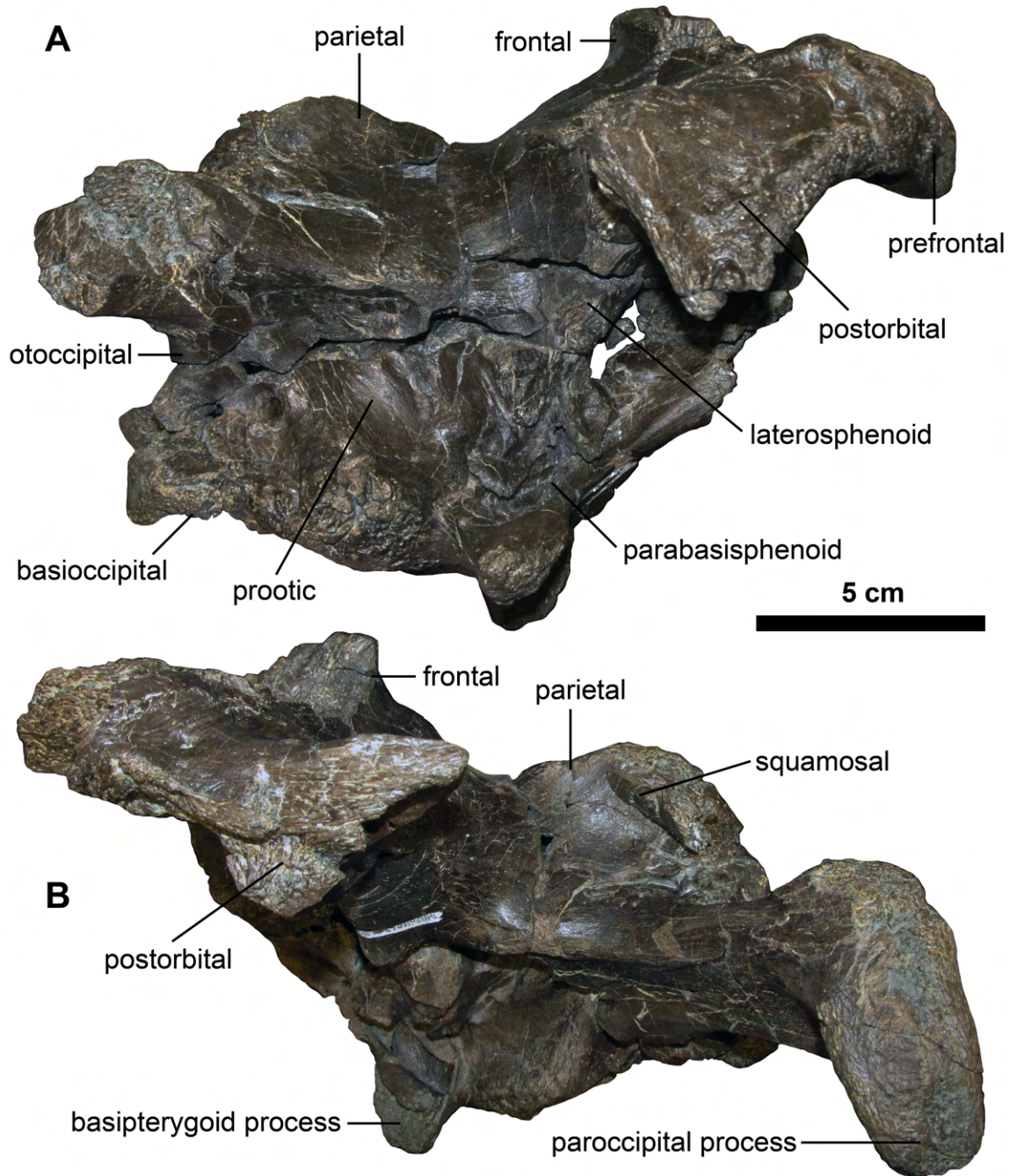


Figure 4.3 Overview of the partial skull roof and braincase TMP 2016.023.0039 in A) dorsal; and B) ventral view. The dorsal view was taken from a photo of only the upper part of the specimen.

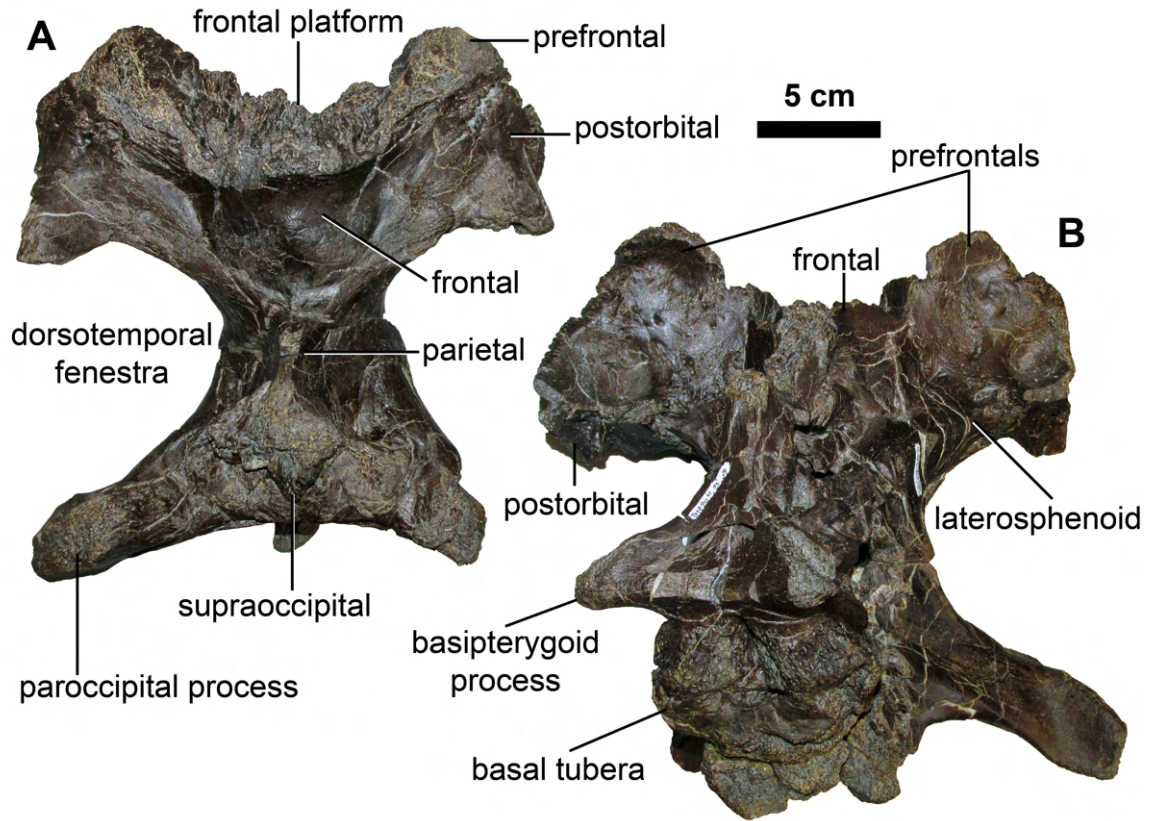
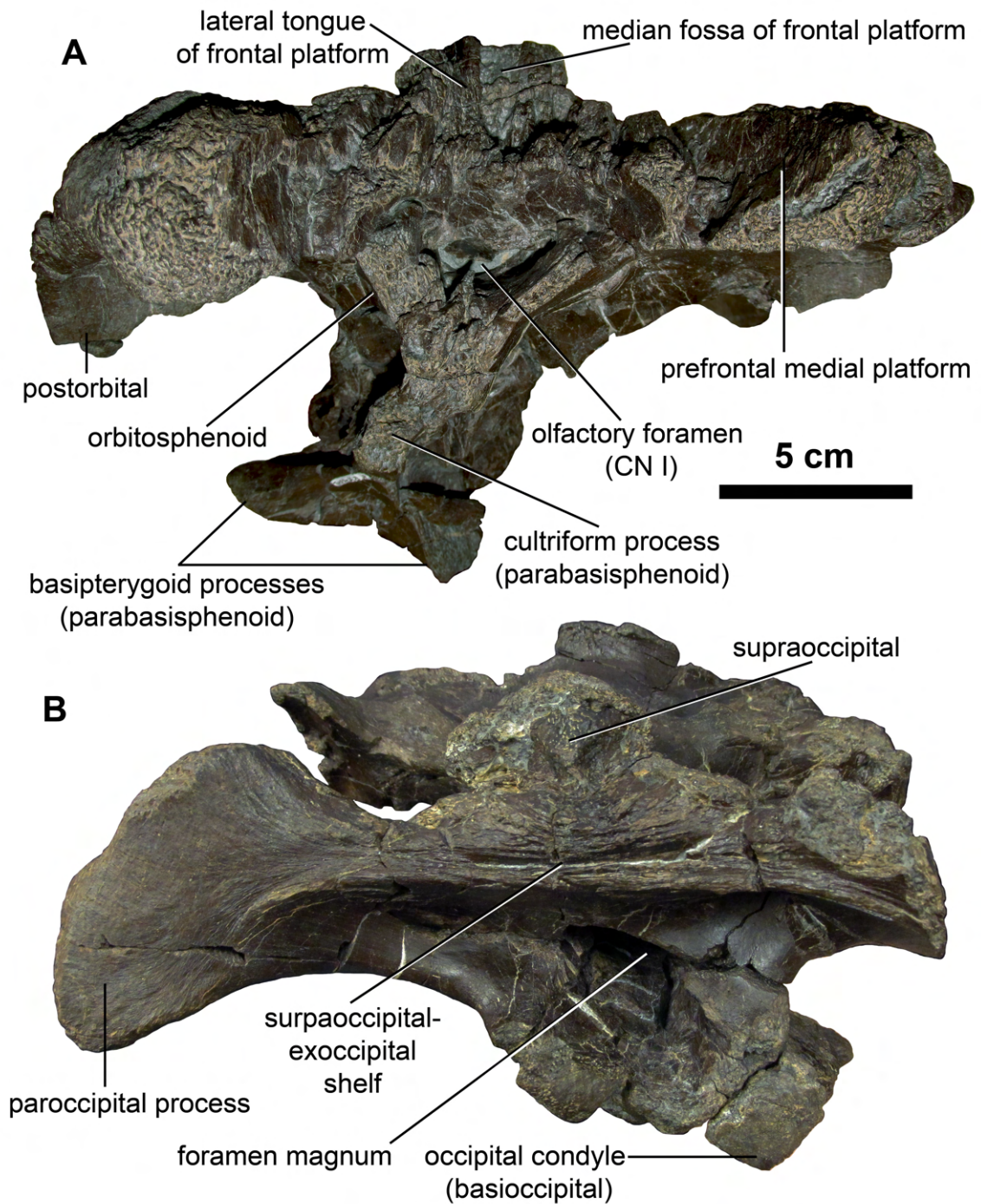


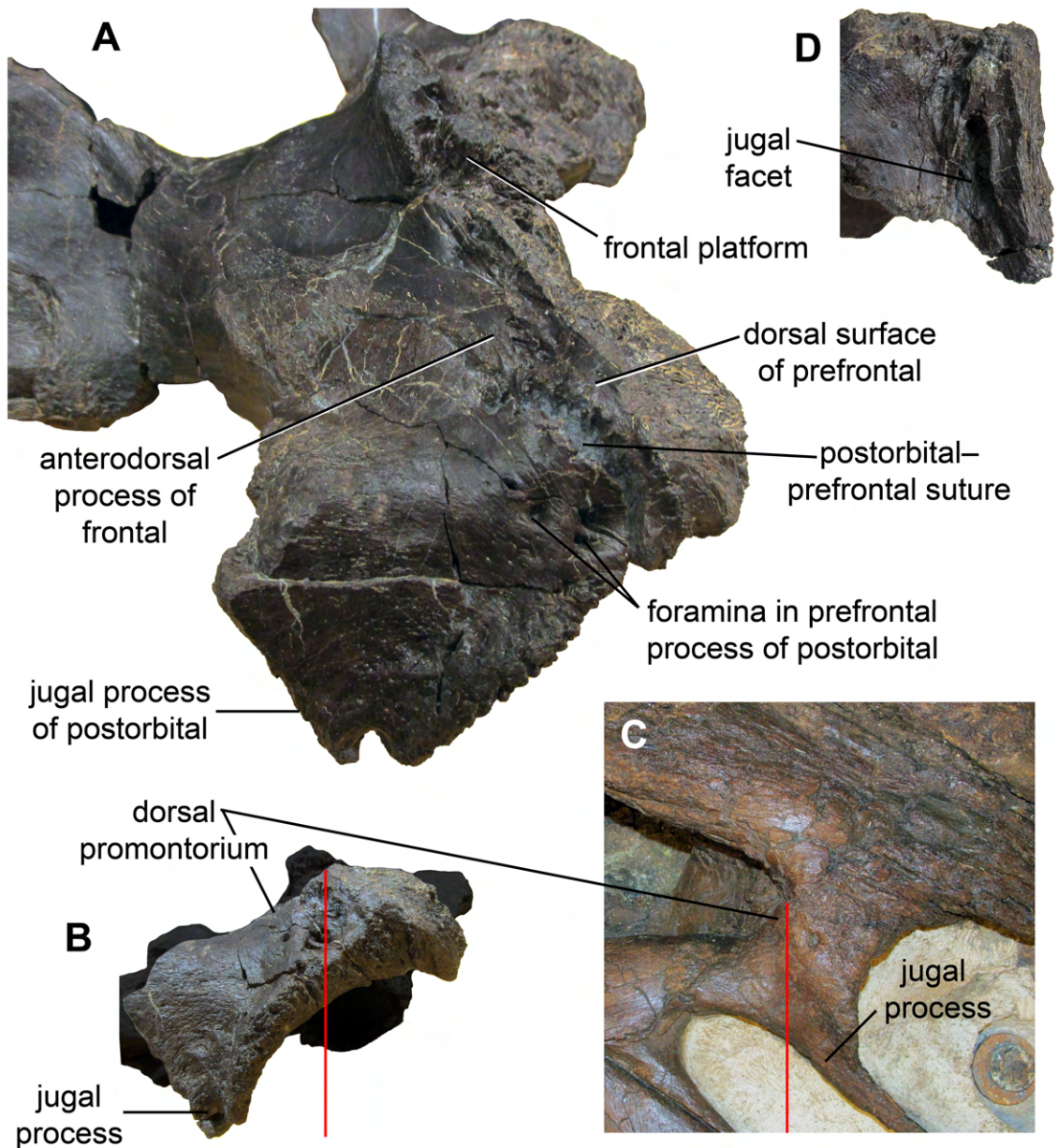
Figure 4.4 Overview of the partial skull roof and braincase TMP 2016.023.0039 in A) anterior; and B) posterior view.



separated by a natural break that cuts through the neurocranium wall approximately at the level of the cranial nerves V, VII, and VIII, and permits partial observation of the interior of the braincase. Although a small amount of bone has been lost along some regions of this break, there remain well-preserved breakage surfaces (such as through the right laterosphenoid) that allow for a precise reconnection of the upper and lower parts. The braincase is taphonomically deformed such that the neurocranium leans strongly to the right (Fig. 4.4). The left exoccipital condyloid is pushed beneath the midline of the skull roof, resulting in the foramen magnum being strongly skewed (Fig. 4.4B). Additionally, slight torsion of the neurocranium is apparent, which exposes a broken surface on the right laterosphenoid dorsally, and a broken surface on the left exoccipital ventrally.

Prefrontal— The preserved region of each prefrontal is a wedge-shaped element that inserts between the frontal platform and the anterolateral processes of the frontal, and continues anterolaterally in contact with the postorbital, forming at its lateral margin part of the orbital rim. Along with the frontal platform, the medial sides of the prefrontals form an expanded cradle for the nasal–premaxillary crest (Figs. 4.3A, 4.4A, 4.5A), with a preserved width of 117 mm. The exposed medial surface is close to vertical on the right prefrontal, whereas it is more inclined on the left. The prefrontals lack the heavily sculpturing of the frontal platform, and there is no prefrontal “clamp” (Gates et al. 2007). The anterior and dorsal surfaces of the prefrontals are damaged, so the contribution of the prefrontal to the side of the crest cannot be observed. However, at least a portion of the prefrontal directly anterior to the contact with the postorbital formed a relatively flat, essentially dorsally-facing surface (Fig. 4.5A), as in the lambeosaurins *Co. casuarius* (ROM 871), *Co. intermedius* (CMN 8503), *H. altispinus* (ROM 702), and subadult *L.*

Figure 4.5 Detail of the prefrontal-postorbital articulation in TMP 2016.023.0039: A) right postorbital region in oblique latero-dorsal view; B) right prefrontal and postorbital in lateral view, and compared to C), left prefrontal and postorbital of *Parasaurolophus walkeri* (ROM 768), reversed, with red line highlighting how the posterior limit of the prefrontal does or does not overlie the jugal process; D) detail of posterior surface of right postorbital. Not to scale.



lambei (ROM 869). The prefrontal also has a small, wedge-shaped dorsal exposure in *P. cyrtocristatus* (Gates et al. 2021: fig. 4) and in *P. tubicen* (ROM 65650, cast of NMMNH P-25100), in which it is more rugose than the laterally-facing flange. In contrast, the exterior surface of the prefrontal in *P. walkeri* (ROM 768) is oriented fully laterally, without a change in inclination between the orbital brow and the flange onto the crest (Fig. 4.5C). The prefrontal in TMP 2016.023.0039 has an open, interdigitating contact with the postorbital in dorsal view, but this contact is nearly obliterated by fusion ventrally. Laterally, the prefrontal–postorbital contact may correspond to a particularly pronounced groove on the orbital rim. The section of the orbital rim formed by the prefrontal is slightly thicker than that formed by the postorbital, and its ventral margin is gently concave in lateral view. The orbital rim of the prefrontal is robust, differing from the thinner condition in *Co. intermedius* (CMN 8503).

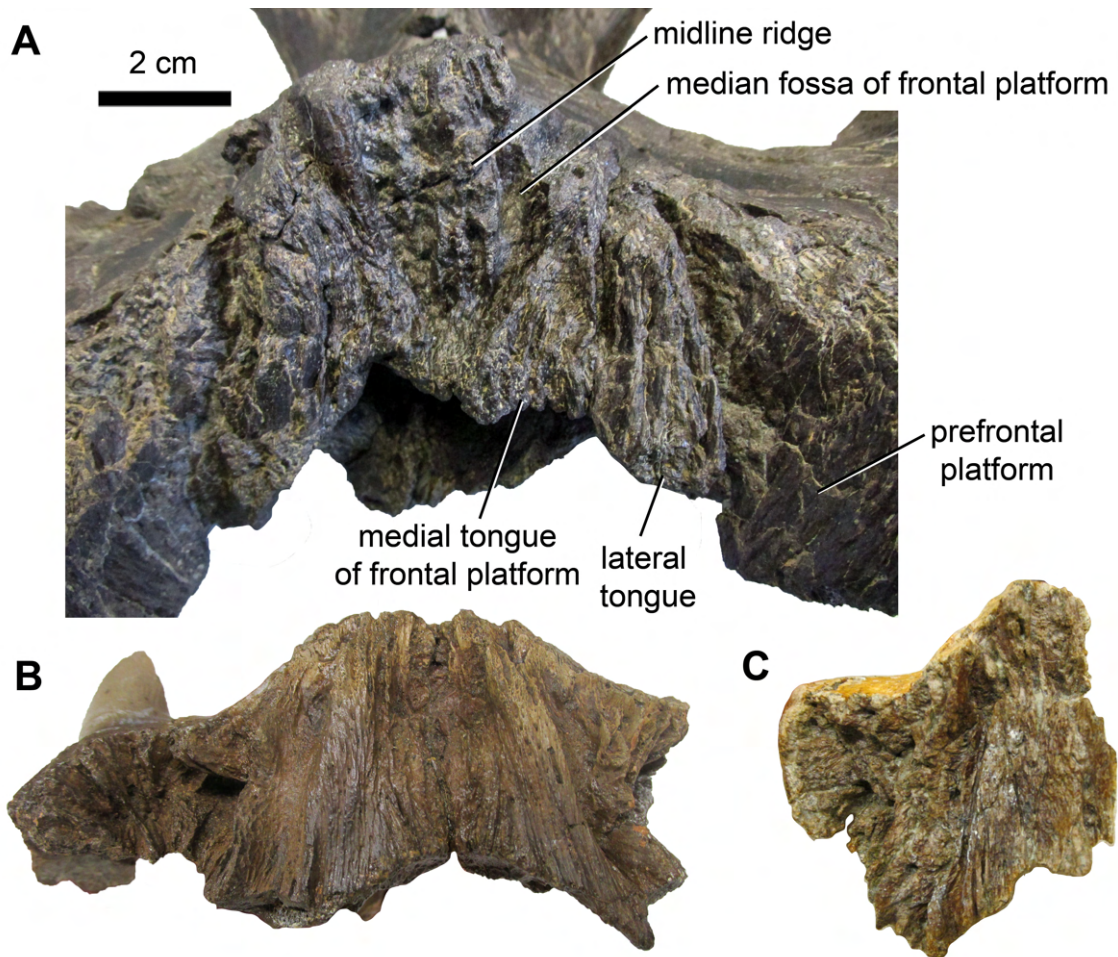
Postorbital— The prefrontal process of the postorbital is relatively short, as in *Parasaurolophus* (Evans et al. 2007) and *Charonosaurus* (Godefroit et al. 2001: fig. 6a), and bears several foramina near its contact with the prefrontal (Fig. 4.5A). The prefrontal process appears relatively longer in *Tlatolophus*, extending considerably farther anteriorly of these foramina (Ramírez Velasco et al. 2021: fig. 11a), but I have not independently confirmed the illustrated boundaries of this element in that taxon. The prefrontal process is angled anterodorsally approximately 25° with respect to the horizontal, but its contact with the prefrontal remains entirely anterior to the jugal process (Fig. 4.5A), as in CMN 8502, *P. cyrtocristatus* (Gates et al. 2021: fig. 4), *P. tubicen* (ROM 65650), and *Tlatolophus* (Ramírez Velasco et al. 2021: fig. 11). This differs from adult *P. walkeri* (ROM 768), in which the prefrontal–postorbital contact substantially

overlies the dorsal part of the jugal process, and the prefrontal process is swollen laterally with respect to the posterior region of the postorbital (Fig. 4.5C). The orbital margin of the postorbital is rugose, and the orbits are oriented slightly anterolaterally. The dorsal margin of the postorbital above the jugal process is slightly concave in lateral view. The jugal process, which is more completely preserved on the right postorbital, is T-shaped in cross-section. Its lateral surface is more rugose in comparison to the dorsal surface. The right jugal process has a small circular fossa near the convergence of the anterior and posterior margins, at which point the process is broken off ventrally. On the posterior side, part of the triangular slot for the jugal is preserved. As in *Parasaurolophus* (CMN 8502, ROM 768, ROM 65650, UCMP 143270; Evans et al. 2007: fig. 2c), this facet is deeply incised and extends high on the jugal process (Fig. 4.5D), whereas in the lambeosaurin *H. altispinus* (ROM 702), it is relatively faint and restricted to the ventral third of the process. The majority of the squamosal processes are broken off on both postorbitals, though it is slightly more complete on the left. The preserved part of the squamosal process is horizontal, approximately parallel to the crista prootica.

In dorsal view, the medial process contacting the frontals and parietal is exposed as a wedge approximately equal in area, but opposite in direction, to the anterolateral process of the frontal. On the ventral surface of the postorbital, the orbital and temporal cavities of the skull are divided by a ridge that spans from the jugal process to the socket for the laterosphenoid. In the posterolateral corner of the orbit, bounded by this ridge and the jugal process, there is a pronounced circular depression with a diameter of approximately 30 mm.

Frontal— The frontal platform is thickened and steeply angled, as in other parasaurolophins (Evans et al. 2007; Ramírez Velasco et al. 2021). It measures approximately 45 mm in length (along the horizontal axis of the skull), 80 mm wide at the anteroventral end, and 60 mm wide (estimated) at the posterodorsal end. As in lambeosaurins (e.g., CMN 57072, ROM 1940), a median fossa is present on the frontal platform, wedged between a pair of anteroventrally expanded, striated tongues (Fig. 4.6). However, unlike lambeosaurins, the midline of the fossa is raised as a narrow columnar ridge, which in its anteroventral half becomes subdivided into three finer ridges. The median ridge is separated from the fan-shaped tongue on either side by an inverted triangular depression that is bisected by a single, shallow ridge. The medial set of fan-shaped tongues each have a single, robust ridge posterodorsally, which branches into an array of very fine ridges anteroventrally. A more laterally positioned pair of fan-shaped tongues are similar in morphology to the medial pair, with anteroventrally branching ridges, though the quality of preservation makes it unclear if the ridges are as finely branched. In contrast, the entire frontal platform is much smoother in lambeosaurins (e.g., CMN 57072, ROM 1940). Along the anteroventral edge of the frontal platform, the right medial fan-shaped tongue is damaged, but if complete, it would form a straight edge with its counterpart on the left, and there would be practically no gap or cleft between the frontals. The lateral pair of fan-shaped tongues projects slightly farther anteriorly than the medial pair, so the overall anterior margin of the frontal platform is bracket-shaped in dorsal or ventral view. The overall morphology of the frontal platform in anterior view resembles that of the juvenile *Parasaurolophus* sp. specimen CMN 8502 (Evans et al. 2007: fig. 2d) and an

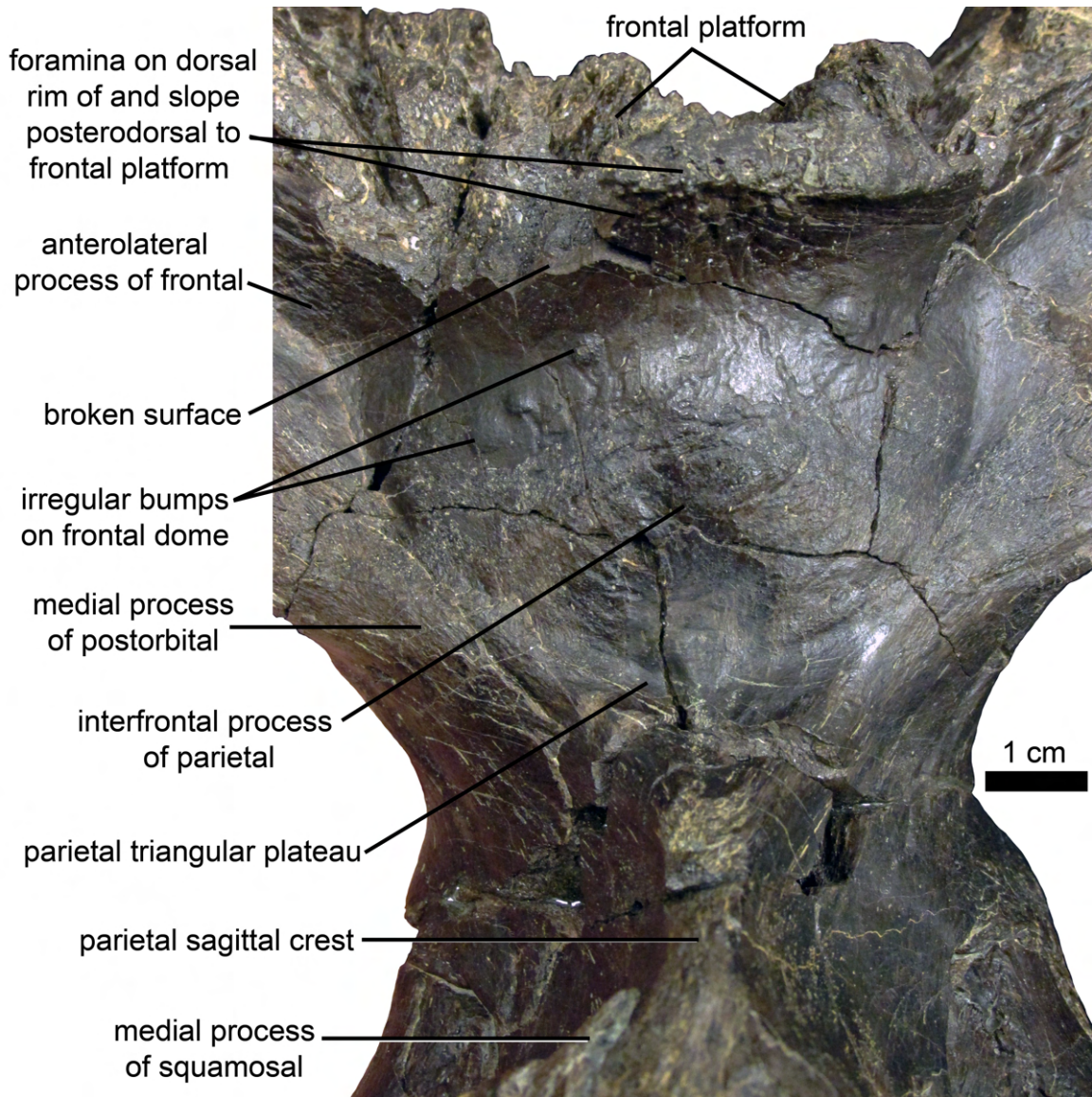
Figure 4.6 Detail of frontal platform of A) TMP 2016.023.0039 in anterior view, compared to B) *Parasaurolophus* sp. (Belly River Group), CMN 8502, and C) right frontal of *Parasaurolophus* sp. (Kaiparowits Formation), UCMP 556168.



undescribed *Parasaurolophus* frontal from the Kaiparowits Formation (UCMP 556168), but with more deeply corrugated ridges and grooves. As in those specimens (Evans et al. 2007: fig. 2a), the frontal forms a socket lateral to the frontal platform for articulation with the prefrontal.

The frontal platform of TMP 2016.023.0039 appears unusual among adult parasaurolophins in its lack of any posterodorsal extension overhanging the frontal dome and anterior parietal (Sullivan and Williamson 1999; Gates et al. 2021; Ramírez Velasco et al. 2021). Instead, the posterior wall of the frontal platform forms only a small dorsally projecting peak in lateral view, closely resembling the condition in the much smaller juvenile specimen CMN 8502 (Evans et al. 2007: fig. 2). This condition could be mimicked by breakage of the posterior extension, but there is reason to believe that the right side of the frontal platform apex in TMP 2016.023.0039 is not substantially damaged. The obvious breakage surface on the left side of the frontal platform shows a clear distinction between the lighter-coloured layer of cortical bone, approximately 2 mm thick, and the darker interior (Fig. 4.7). The right side, in addition to lacking any surface with this colour contrast, has no atypically sharp or irregular edges, which are commonly observed at breaks and fractures elsewhere on the specimen. A dense patch of small foramina concentrated along the midline of the steeply descending surface of the frontal posterior to the frontal platform, covering an area of approximately 1 cm², also continues anteriorly onto the dorsal rim of the platform, further supporting the interpretation that the original extent of the dorsal rim is preserved in this region (Fig. 4.7). That this steep posterior surface is not inclined beyond the vertical differs from the mature condition in *P. walkeri* (ROM 768), *P. cyrtocristatus* (Gates et al. 2021: fig. 4B), and *P. tubicen*

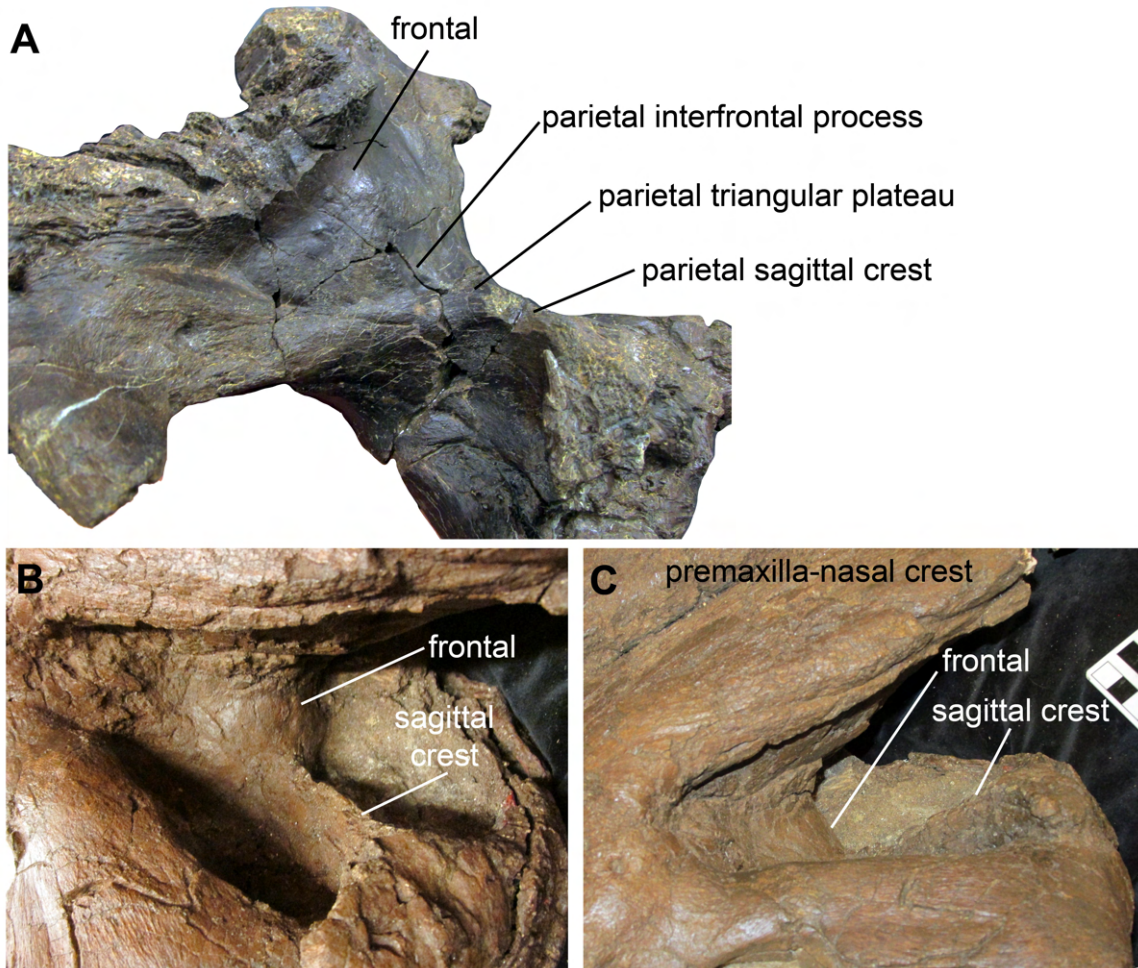
Figure 4.7 Detail of features of the middle skull roof (frontal and parietal) of TMP 2016.023.0039 in dorsal view.



(ROM 65650), in which the base of the frontal platform buttress forms a more sharply inflected posterior angle overhanging the frontal dome (Fig. 4.8). The posterodorsal margin of the frontal platform forms a gentle arc in dorsal view, with the convex side directed posteriorly.

The dorsal surface of both frontals excluding the frontal platform is crescent-shaped, with a combined width of approximately 133 mm. The interfrontal suture is completely obliterated by fusion, as also reported in *Tlatolophus* (Ramírez Velasco et al. 2021), but unlike that in large adult lambeosaurins (e.g., ROM 1940; the frontals of the holotype of *Sahaliyana elunchunorum* were interpreted as fused by Godefroit et al. 2008, but paired by Xing et al. 2022). The sutures with the postorbitals and parietal are also closed, but the boundaries of the frontal can be discerned through colour and textural differences: the frontals are slightly darker and with a less pronounced bone grain than the postorbitals, and are slightly lighter than the parietal (though similar in texture). The prefrontal–frontal contact is not tightly closed. The anterolateral processes of the frontals, which contact the prefrontals and postorbitals, are at nearly a right angle to each other. They are approximately 40 mm long, and taper to 13 mm wide (perpendicular to the long axis) anterolaterally. As in other lambeosaurines, the frontal is excluded from the orbital margin. However, in *P. walkeri* (ROM 768) and *P. tubicen* (ROM 65650), the frontals expand laterally nearer to the orbital margin than in TMP 2016.023.0039, and thus constitute a greater proportion of the total width of the skull roof. The region medial to the anterolateral processes is gently domed, with a central peak just anterior to the interfrontal process of the parietal. The frontal surface posterior to the frontal platform is mostly smooth, with the exception of a few irregularly positioned raised circular bumps.

Figure 4.8 Middle skull roof of A) TMP 2016.023.0039, and B) *Parasaurolophus walkeri* ROM 768 compared in oblique left postero-lateral view; C) same region of ROM 768 in left lateral view (compare to Figure 4.2). Not to scale.



There is one bump of approximately 5 mm diameter on the right frontal, and three bumps of approximately 3–4 mm diameter on the left frontal (Fig. 4.7).

The exposed ventral surface of the frontal is flat with a scattering of small foramina. The interdigitating frontal-prefrontal contact is partially open in ventral view. The frontal-postorbital contact is nearly obliterated, but can be loosely traced as an increased concentration of foramina. The relationships of these three elements are similar to those in CMN 8502 (Evans et al. 2007). The frontal–prefrontal contact is shorter than the prefrontal–postorbital contact, resulting in the prefrontal–postorbital contact being positioned relatively close to the anterior end of the frontal. Ventral to the frontal platform, the frontals roof the passage for the olfactory nerve (CN I). There is a rugose swelling on the ventral surface of the frontal at the entrance of the olfactory fenestra, inset 30 mm posteriorly from the anteroventral margin of the frontal platform. This distance is slightly greater in an immature individual of *P. cf. cyrtocristatus* with an overall smaller skull (UCMP 143270; 35 mm). The cerebral fossa is not visible, due to being covered by the attached orbitosphenoids, and remaining filled in by matrix. However, the cerebrum appears to have been a proportionately large part of the total endocranial volume, as in other lambeosaurines (Evans et al. 2009b; Lauters et al. 2013).

Parietal— As is typical of lambeosaurines (Godefroit et al. 2004a), the unpaired parietal is anteroposteriorly compact, measuring less than half of the interorbital width in length. The anterior end of the parietal inserts between the fused frontals as an anterodorsally inclined interfrontal process, which has a smooth surface. Remnants of the frontal-parietal contacts are visible as faint lineations perpendicular to the outline of this process (Fig. 4.7). In dorsal view, the interfrontal process is relatively long and narrow,

as in *Parasaurolophus* (CMN 8502, UCMP 143270), in contrast to the short and wide interfrontal process of lambeosaurins (ROM 694, ROM 1940, ROM 61784; Evans et al. 2007: fig. 3a). The dorsal surface of the parietal between the interfrontal process and the sagittal crest is down-warped below the level of the postorbital temporal bar. This region forms a triangular plateau in dorsal view, contributing to the overall hourglass shape of the parietal. A moderate to large triangular region of the parietal between the interfrontal process and the sagittal crest also occurs in immature (ROM 694) and adult (ROM 702, ROM 776, ROM 1940) lambeosaurins, and in the parasaurolophin *Tlatolophus* (Ramírez Velasco et al. 2021: fig. 12). It is greatly reduced in immature *Parasaurolophus* sp. (CMN 8502) and *P. cf. cyrtocristatus* (UCMP 143270), whereas in adult *P. walkeri* (ROM 768) and *P. tubicen* (ROM 65650) this flat triangular region of the parietal is absent (Fig. 4.8), and the interfrontal process and the sagittal crest meet directly at nearly a right angle (90–95°). The sagittal crest is at a broader obtuse angle to the interfrontal process in TMP 2016.023.0039, as in CMN 8502 (110–120°). The parallel-sided portion of the sagittal crest on the middle region of the parietal is short and stout, measuring approximately 20 mm long and 7–8 mm wide, compared to up to 60 mm long in ROM 768. Posteriorly, the sagittal crest is expanded into a triangular platform approximately 30 mm long and 40 mm wide. The posterodorsal surface of this region is damaged, and it is indeterminate whether the parietal would have been visible on the posterior surface of the complete skull.

Ventrally, the endocranial surface of the parietal is exposed. As in other lambeosaurines (Evans et al. 2009b), the endocranium is tilted anterodorsally when the skull roof is horizontal. There is a pronounced boundary between the cerebral and post-

cerebral regions. A foramen surrounded by a deep depression is visible internally towards the posterior end of the braincase wall, dorsal to the foramen for CN VII, which may correspond to the dorsal head vein (Evans et al. 2009b: fig. 5).

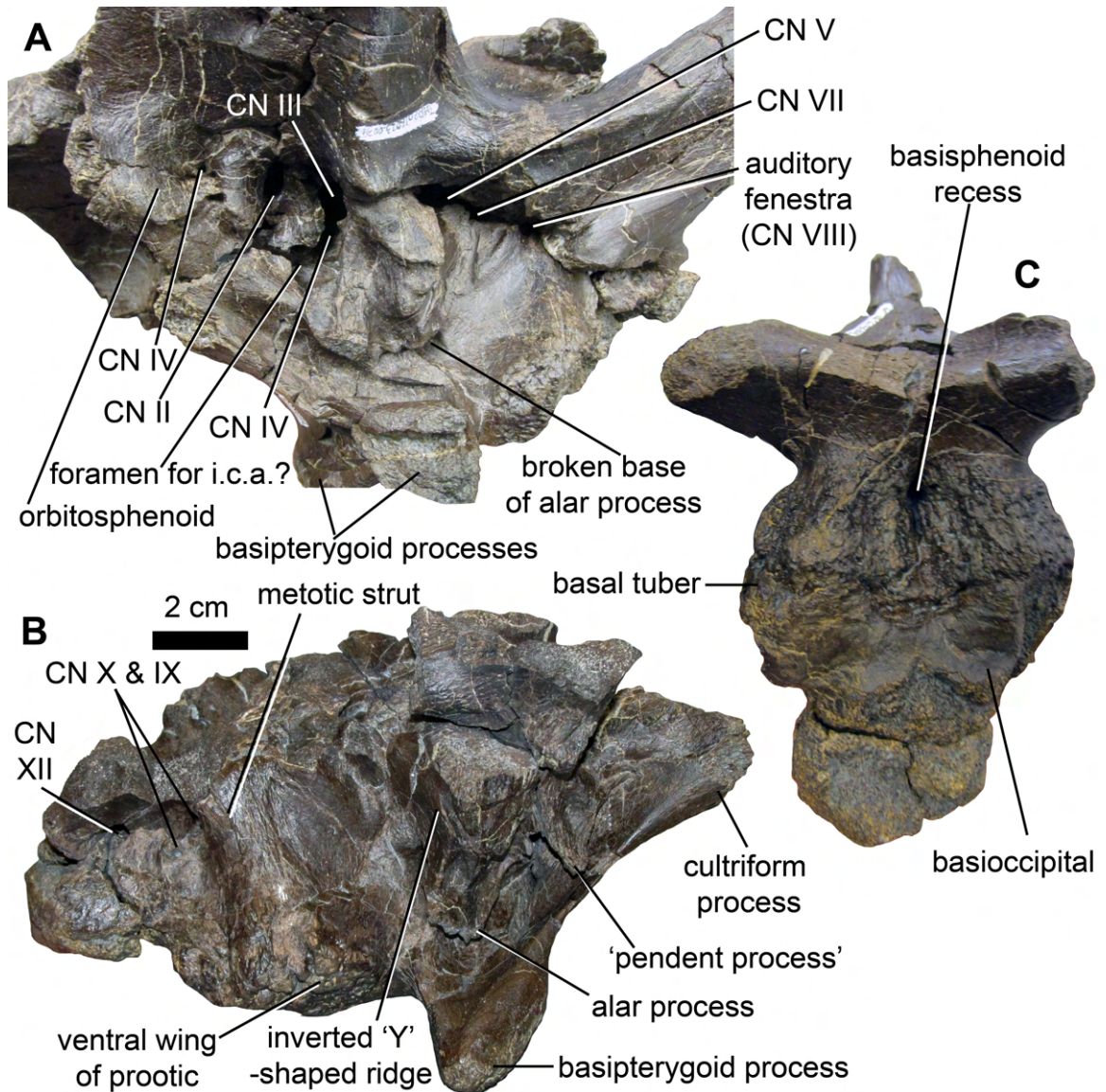
Squamosal— A wedge-shaped fragment of the medial process of the left squamosal is preserved in articulation with the posterior triangular expansion of the parietal. The anterior tip of the squamosal fragment does not cover the more anterior, unexpanded region of the sagittal crest, differing from the condition in *Velafrons*, in which the medial process of the squamosal is expanded to cover the entire side of the sagittal crest (Gates et al. 2007: fig. 7). The preserved fragment of the squamosal is not elevated in relation to the broken squamosal ramus of the postorbital, suggesting that the squamosals were not greatly elevated posteriorly, unlike *P. cyrtocristatus* and *P. tubicen* (Gates et al. 2021).

Presphenoid-Orbitosphenoid Complex— The orbitosphenoids as preserved here likely incorporate indistinguishably fused presphenoids, as in other adult lambeosaurines (Evans 2010). They contact the frontals, laterosphenoids, and parabasisphenoid. The sutures with the frontals and laterosphenoids are fused, but the approximate boundaries are shown by concentrations of dimple-like foramina. The boundary between the presphenoid-orbitosphenoid complex and the cultriform process of the parabasisphenoid is unclear. The paired orbitosphenoids converge medioventrally, forming the V-shaped floor of the olfactory fenestra, which has a midline ridge. The ventral portions of the orbitosphenoids are appressed, forming a “Y”-shaped unit in anterior view, but retain a visible boundary between the left and right elements (Fig. 4.4A).

On the lateral face of the orbitosphenoid, at approximately mid-length, there is a small recessed foramen, (Fig. 4.9A) corresponding to the trochlear nerve (CN IV). Although imperfectly preserved, especially on the right side, this foramen appears to be partitioned by septa. The optic nerve (CN II) enters the orbit through a larger foramen posteroventral to the trochlear foramen. Additional foramina within the orbit, ventral to the optic foramen, are not exclusively bounded by the orbitosphenoid, but are discussed here for convenience. The pattern of foramina within the orbit closely resembles that of *P. cf. cyrtocristatus* (UCMP 143270). The most posterior cranial nerve foramen within the orbit is the oculomotor (CN III) foramen. This foramen is taller than wide and opens anterolaterally, being situated between the more medial optic foramen on the lateral face of the orbitosphenoid, and the more lateral trigeminal foramen on the lateral face of the laterosphenoid. Immediately anteroventral to the oculomotor foramen is the abducens (CN VI) foramen. It is unclear whether the borders of these foramina were separate when complete, or merely pinched but confluent. On at least the left side, the ventral foramen is also pinched dorsally and ventrally, dividing it into anterior and posterior parts. This may imply a confluence of the abducens foramen and the foramen for the internal carotid artery, unlike the condition in the saurolophine *Edmontosaurus regalis* (Xing et al. 2017: fig. 15), in which they are widely separated. However, this cannot be verified on the right side, where the narrow condition of the ventral foramen is attributable to distortion.

Laterosphenoid— The laterosphenoids contact the orbitosphenoids, frontals, postorbitals, parietal, and prootics. All of these contacts except for that with the postorbital are fused and difficult to trace. The laterosphenoid-orbitosphenoid and laterosphenoid-frontal contacts are suggested by the distribution of foramina, with a deep

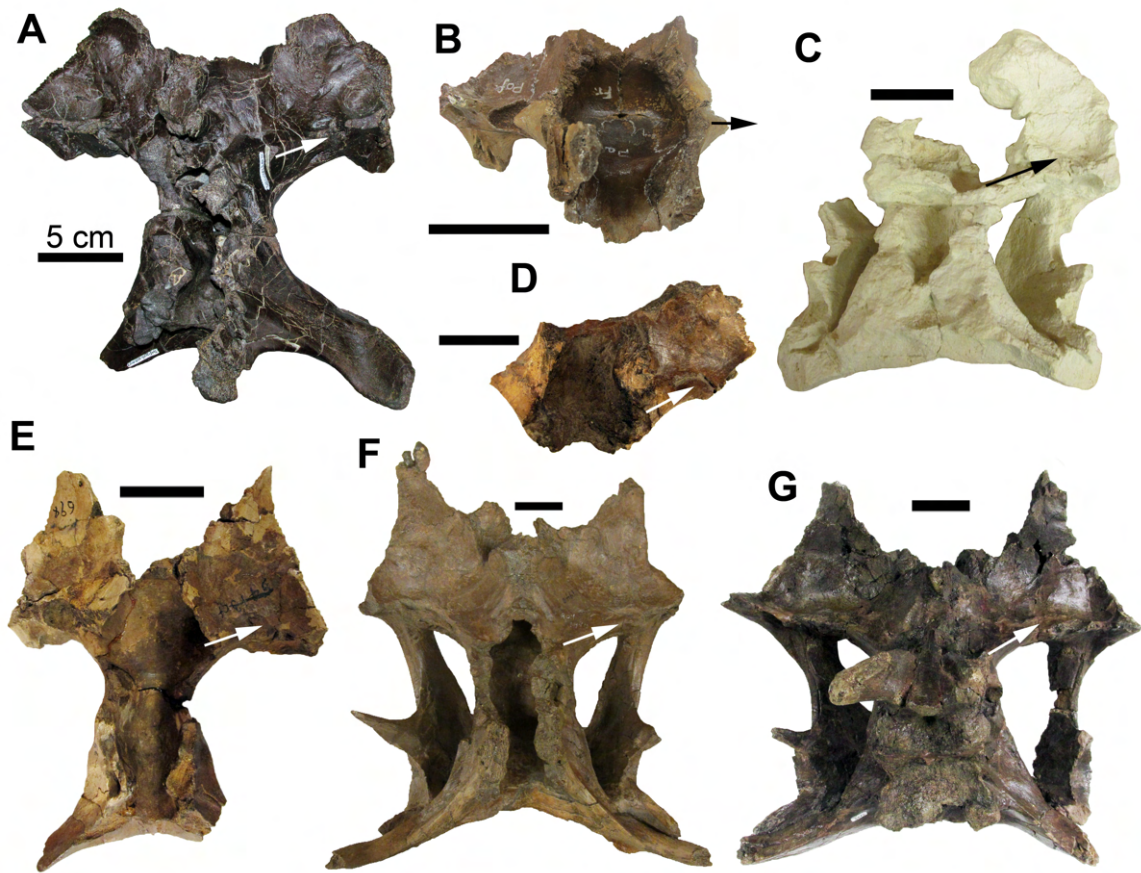
Figure 4.9 Detail of neurocranial features of TMP 2016.023.0039, in A) left antero-lateral view, photographed in articulation with the skull roof; B) right lateral view, photographed detached from the skull roof; C) ventral view, photographed detached from the skull roof. Abbreviations: CN = cranial nerve, i.c.a. = internal carotid artery.



foramen occurring at the probable junction of these three elements. A groove on either side of the braincase may represent the fused boundary between the laterosphenoid and the parietal. The triangular postorbital process of the laterosphenoid articulates with a socket on the postorbital via an expanded terminal knob, but since the frontal is fused to both the laterosphenoid and the postorbital, this joint could not have been kinetic (Holliday and Witmer 2008). The postorbital process is relatively elongate, in comparison to the proportionately short processes in the immature *Parasaurolophus* specimens CMN 8502 and UCMP 143270. These processes project anterolaterally with an interior angle of approximately 120° in ventral view (Fig. 4.10A), comparable to various immature and mature lambeosaurins including ROM 694, ROM 1940, ROM 23903, *H. altispinus* (CMN 8675, ROM 702), *H. stebingeri* (ROM 61784), and *Velafrons* (ROM, cast of CPC-59). In contrast, the postorbital processes in *Parasaurolophus* (CMN 8502, ROM 65650, UCMP 143270) and possibly other parasaurolophins (*Tlatolophus*, Ramírez Velasco et al. 2021: fig. 11B) project laterally with an internal angle of approximately 180°.

The laterosphenoid forms a pointed spur overhanging the anterior end of the orbital canal, which Holliday (2009) identified in *Brachylophosaurus* as an osteological correlate for the m. levator pterygoideus. This spur does not enclose the orbital canal, unlike the condition in *Lambeosaurus* (Ostrom 1961a: fig. 64b). The dorsal margin of the orbital canal forms a ledge on the side of the braincase continuous with the crista prootica. Ventral to the trigeminal foramen, there is a defined triangular region bounded by the orbital canal dorsally, and the groove variously interpreted as the maxillary ramus of the trigeminal nerve (Ostrom 1961a) or the

Figure 4.10 Corythosaurian skull roofs in ventral view, showing the orientation of the postorbital process of the laterosphenoid, indicated by an arrow: A) TMP 2016.023.0039; B) *Parasaurolophus* sp. CMN 8502; C) *Velafrons coahualiensis*, cast of CPC-59; D) Lambeosaurini indet. ROM 23903; E) Lambeosaurini indet. ROM 694; F) Lambeosaurini indet. ROM 1940; G) *Hypacrosaurus altispinus* CMN 8675. Scale bars = 5 cm.



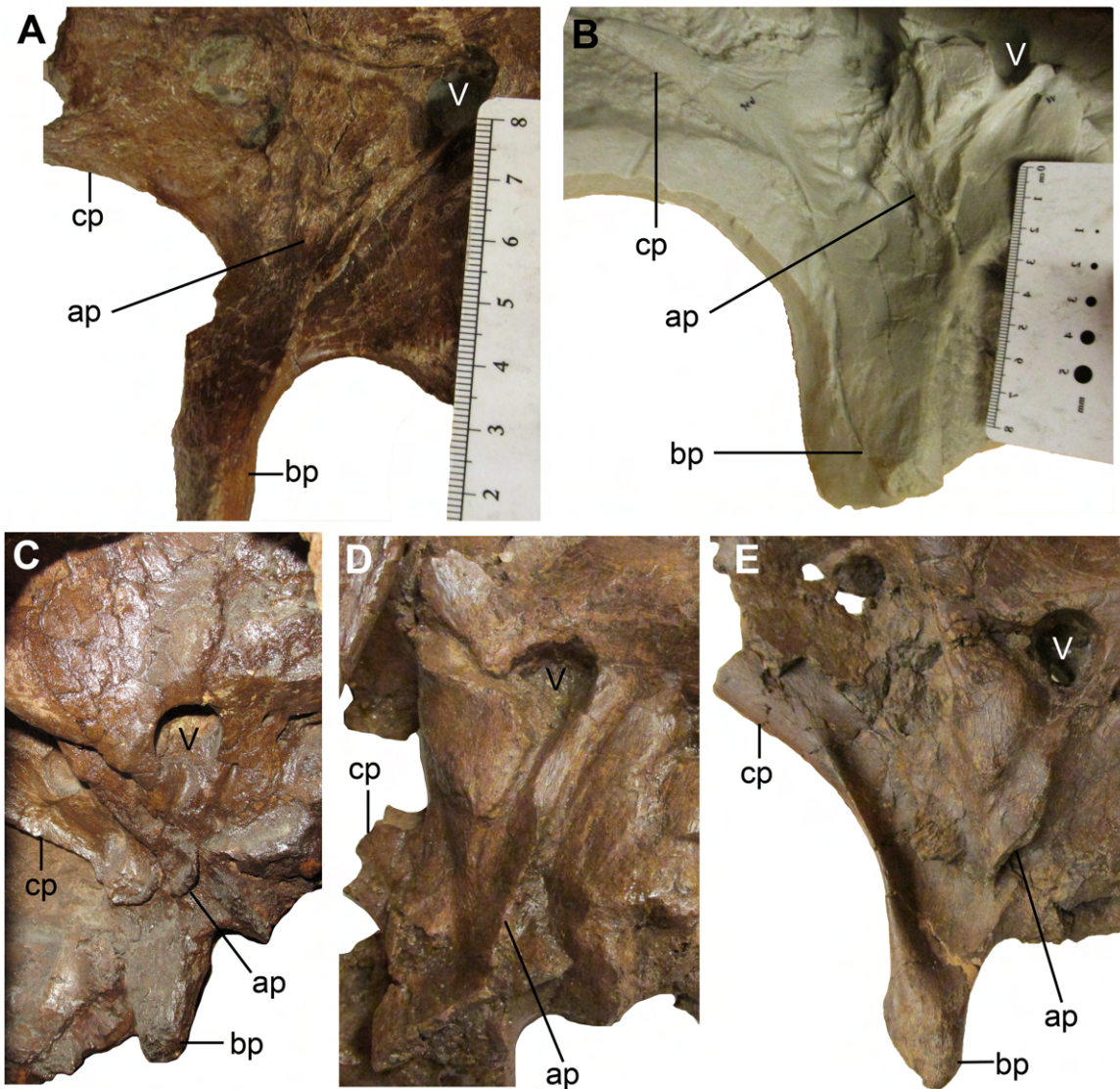
neurovascular bundle to the constrictor internalis dorsalis muscles (Holliday 2009) posteroventrally. The ventral tip of this surface is slightly but distinctly inset. The inset is slightly dorsal to the emergence of a prominent ridge that defines the posteroventral boundary of the groove descending ventrally from the trigeminal foramen. This ridge has an inverted “Y” shape, separating the ventral groove on the laterosphenoid from the fossa on the alar process of the basisphenoid (Fig. 4.9B), unlike the condition in *Corythosaurus* or *Lambeosaurus* (Ostrom 1961a: fig. 64). The region bound by the posterior margin of this ridge and the weakly defined vidian canal is confluent with the posterior face of the alar process. The vidian canal appears to be more sharply defined in *Charonosaurus* (Godefroit et al. 2001: fig. 4) and *P. cyrtocristatus* (Gates et al. 2021: fig. 9), though its prominence can be asymmetrical in a single individual in related taxa (e.g., *H. altispinus*, ROM 702).

Parasphenoid–Basisphenoid Complex (Parabasisphenoid)— The fused parasphenoid and basisphenoid form the anteroventral region of the braincase. The lateral surface of the anterodorsally projecting cultriform process is excavated by a smooth, shallow groove. Posteriorly, this groove is overhung by a faintly striated pendent process, ventral to the abducens foramen and anterior to the alar process, as previously noted by Evans (2010) in *H. altispinus*. This pendent process has a robust base with a triangular cross-section. Directly dorsal to the pendent process, there is a swelling that separates it from the abducens foramen. The posteroventral margin of the abducens foramen forms the notch between the posterodorsal margin of the cultriform process and the columnar base of the laterosphenoid. There is a deep, narrow cavity in basisphenoid opening

dorsally between the abducens foramina, which housed the pituitary gland (Ostrom 1961a).

The basiptyergoid processes are subtriangular in cross-section. The dorsolateral surface of the basiptyergoid process is continuous with the lateral surface of the cultriform process, while the anteroventral surface of the basiptyergoid process is continuous with the ventral surface of the cultriform process. The posteroventral surfaces of the basiptyergoid processes are joined across the midline on the underside of the basisphenoid. Above the basiptyergoid process, the boundary between these two surfaces is sharply laminar. Descending down the basiptyergoid process, this lamina expands into an asymmetrical, teardrop-shaped area that makes up the anterolateral part of the basiptyergoid process (Fig. 4.9B). As this anterolateral surface expands in width, the width of the triangular dorsolateral surface correspondingly diminishes. The anterolateral surface merges with the anteroventral surface of the basiptyergoid process proximally, but is more distinct from it distally. The overall shape of the basiptyergoid process, with its anteroventral expansion and posterolateral depression, closely resembles the *H. altispinus* specimen ROM 702 (Fig. 4.11E), and differs from the essentially flat lateral surface in *P. cf. cyrtocristatus* and *P. tubicen* (Fig. 4.11A, B), though a similar condition may be indicated in *Charonosaurus* (Godefroit et al. 2001: fig. 5). The distal ends of both basiptyergoid processes are abraded, with greater damage occurring on the left. The right process is reasonably complete, and its length does not appear to be significantly reduced; this is supported by the expansion of the anterolateral surface covering the width of the process in lateral view, which occurs only near the distal end. The ventral projection of the basiptyergoid processes is notably short, approximately 10 mm in lateral

Figure 4.11 Comparison of parabasisphenoid morphology in various corythosaurians, in left lateral view: A) *Parasaurolophus* cf. *cyrtocristatus* UCMP 143270; B) *Parasaurolophus tubicen*, ROM 65650 (right lateral view, reversed); C) *Lambeosaurus lambei*, CMN 8703; D) *Corythosaurus casuarius*, ROM 1933; E) *Hypacrosaurus altispinus*, ROM 702. Not to scale. Abbreviations: ap = alar process; bp = basiptyergoid process; cp = cultriform process; V = trigeminal foramen.



view. The shortest distance between the tip of the alar process and the tip of the basiptyergoid process is 34 mm, whereas this measurement is 43 mm in the immature *P. cf. cyrtocristatus* (UCMP 143270), and 80 mm in adult *P. tubicen* (ROM 65650). These processes are also longer and more pendent below the remainder of the basisphenoid, as well as having a longer subvertical anterodorsal edge, in *Charonosaurus* (Godefroit et al. 2001: fig. 4) and *P. cyrtocristatus* (DMNH EVP.132300; Gates et al. 2021: fig. 9). The basiptyergoid processes diverge from each other at a markedly obtuse angle of approximately 130°, in contrast to the acute angle observed in some other lambeosaurines, such as *Arenysaurus* (Pereda-Suberbiola et al. 2009: fig. 3B). The ventral margin of the interbasisphenoidal lamina is broad, connecting the left and right interbasiptyergoid processes relatively extensively, in contrast to the greater “free” length of the basiptyergoid processes in other specimens, such as DMNH EVP.132300 (Gates et al. 2021: fig. 5). The presence or absence of an interbasiptyergoid process is indeterminate, due to breakage.

The alar process is subrectangular, and more robust than the reduced “teardrop-shaped” processes of *P. tubicen* and *P. cyrtocristatus* (Gates et al. 2021), but does not appear to be as large as that of *Charonosaurus* (Godefroit et al. 2001: fig. 4–5), in which the prominence and symmetry of the alar process is considered diagnostic (Godefroit et al. 2001). The margin of the alar process is sharply demarcated anteriorly and ventrolaterally pendent, as in *P. tubicen* (ROM 65650), unlike the condition in *Co. casuarius* (ROM 1933) and *H. altispinus* (CMN 8675, ROM 702) in which the alar process merges onto the rest of the basisphenoid anteriorly and thus projects posterolaterally. The lateral surface of the alar process has a pronounced fossa bounded

dorsally by the “Y”-shaped ridge, described above with the laterosphenoid. This fossa does not appear to be well developed, if at all, in at least some *Parasaurolophus* specimens (e.g., DMNH EVP.132300; Gates et al. 2021: fig. 9A), *Tlatolophus* (Ramírez Velasco et al. 2021: fig. 13A), or other lambeosaurines, though there is a similar ridge on the lateral surface of the reduced alar process of *P. tubicen* (ROM 65650).

Ventromedially, the alar process is supported by a thin strut that separates the lateral concavity of the cultriform and basiptyergoid processes anteriorly from the foramen for the internal carotid artery posteriorly. This strut joins the base of the basiptyergoid process at the boundary between the latter’s dorsolateral and posteroventral surfaces.

The basisphenoid is hourglass-shaped in ventral view. The texture changes abruptly from smooth between the basiptyergoid processes, to very rugose on the region posterior to the middle constriction (Fig. 4.9C). This pattern of rugosity is observed in some other hadrosaurids, such as the *Gryposaurus notabilis* specimen AMNH 5350 (Prieto-Marquez 2010b: fig. 4), although the transition is less marked and the posterior surface less rugose in the *Parasaurolophus* specimens DMNH EVP.132300 and UCMP 143270 (Gates et al. 2021: figs. 9B and 13A). The posterior region of the basisphenoid has a narrow, elongated median fossa, as in *P. cyrtocristatus* (Gates et al. 2021) and *Tlatolophus* (Ramírez Velasco et al. 2021). In *Co. casuarius* (ROM 1933) and *H. altispinus* (CMN 8675), the posterior region of the basisphenoid has a broader, rounded concavity.

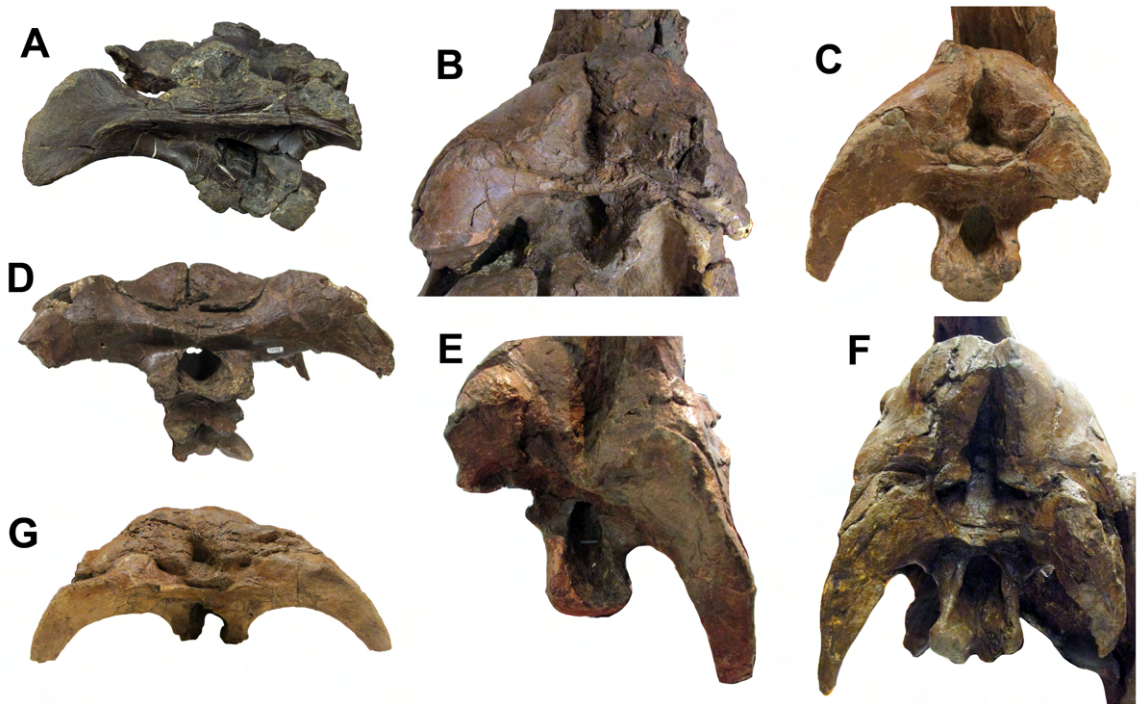
Prootic— The boundaries between the prootics and surrounding elements are difficult to discern, as is commonly the case in adult hadrosaurids (Ostrom 1961a), though the prootic presumably forms the posterior margin of the trigeminal (CN V) foramen, and contains the facial nerve (CN VII) foramen. On both sides, these foramina

and the auditory fenestrae occur on the break between the two pieces of the specimen. The lateral surface between the facial nerve foramen and the auditory fenestra forms a slightly convex triangular area. The prootic–otoccipital contact is faintly visible, as a subtle textural change, running posterodorsally across the lateral side of the braincase from the auditory fenestra to a point on the crista prootica dorsal to the vagus foramen. There is no indication of a prootic contribution to the posterior surface of the braincase, unlike the interpretation of this element in *Tlatolophus* by Ramírez Velasco et al. (2021).

Opisthotic–Exoccipital Complex (Otoccipital)— Three pairs of foramina penetrate the lateral walls of the otoccipitals (fused opisthotic–exoccipitals), as in most lambeosaurines (Ostrom 1961a; Evans 2010). The most anterior, which transmits the vagus nerve (CN X) and the jugular vein (Ostrom 1961a), is taller than wide and opens posterolaterally. It is within the lower piece of the specimen on the right side, and occurs on the break on the left. The middle foramen, variously identified with the accessory nerve (CN XI; Ostrom 1961a; Godefroit et al. 2001) or a branch of the hypoglossal nerve (CN XII; Evans 2010), is a small opening, less than half the maximum diameter of the preceding foramen, and opens farther ventrally on the lateral wall of the braincase, being within the lower piece of the specimen on both sides. It is positioned nearer to the preceding foramen than to the following one. The middle foramen is much closer in size to the other two in the *P. cyrtocristatus* specimen DMNH EVP.132300 (Gates et al. 2021: fig. 9), and has a more centered position between them. The most posterior foramen, which transmitted the hypoglossal nerve, is similar in size and elevation to the vagus foramen, but is slightly wider than tall. It is preserved within the lower piece of the specimen on the right side, but within the upper piece of the specimen on the left side.

The left and right otoccipitals are fused above the foramen magnum. There is a gentle concavity dorsolateral to the foramen magnum on either side. The exoccipital shelf is short, with its margin projecting approximately 22 mm posterodorsally from the foramen magnum. This shelf is slightly longer in a significantly smaller, immature individual of *P. cf. cyrtocristatus* (UCMP 143270; 27 mm). The margin of the shelf is straight in posterior view, and slightly bowed at its ends in dorsal view. The horizontal ridge formed by the exoccipital shelf ventral to its contact with the supraoccipital is wider than the supraoccipital, and extends laterally onto the paroccipital process, as in UCMP 143270 (Gates et al. 2021: fig. 13). The partially preserved left paroccipital process is damaged dorsally, laterally, and distally, precluding precise interpretation of its dimensions. The region of the otoccipital forming the ‘neck’ of the paroccipital process is mediolaterally elongate and shallowly curved ventrally in posterior view, similar to *Charonosaurus* (Godefroit et al. 2001: fig. 5), and the lambeosaurins CMN 57072, ROM 1940, *Amurosaurus* (Godefroit et al. 2004b: fig. 7), *H. altispinus* (CMN 8675), *Olorotitan* (Godefroit et al. 2012: fig. 4E), and *Sahaliyana* (Godefroit et al. 2008: fig. 3; this taxon regarded as a junior synonym of *Amurosaurus riabinini* by Xing et al. 2022), but not the lambeosaurins *Co. intermedius* (CMN 8503, ROM 776) and *L. lambei* (CMN 8703, ROM 794), in which this part of the otoccipital is mediolaterally shorter in relation to the braincase width, and more strongly arched in posterior view (Fig. 4.12). This region of the otoccipital is also notably shorter and more strongly arched in *P. walkeri* (ROM 768), *P. tubicen* (ROM 65650; Sullivan and Williamson 1999: figs. 16–17), *Tlatolophus* (Ramírez Velasco et al. 2021: fig. 13B), and to some extent *P. cyrtocristatus*

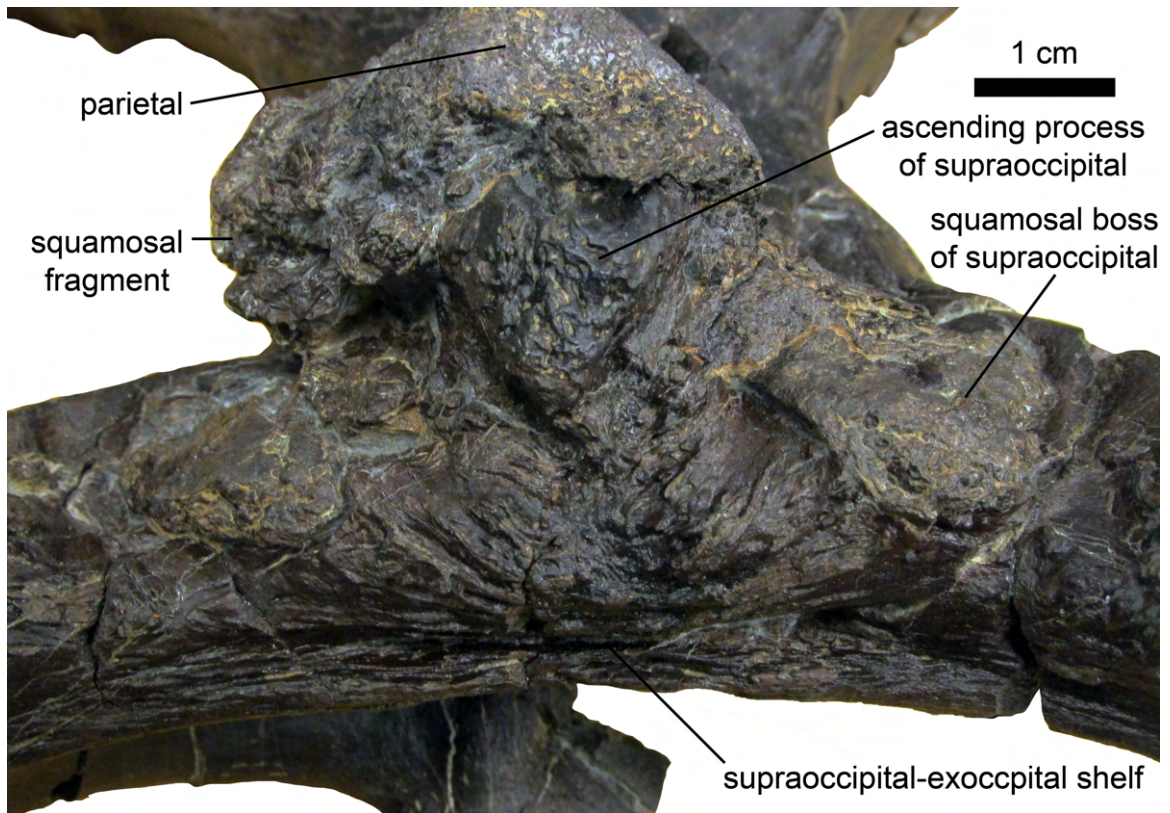
Figure 4.12 Comparison of corythinosaurian braincases in posterior view, illustrating the variation in the arching of the ventral margin of the otoccipital: A) TMP 2016.023.0039; B) *Parasaurolophus walkeri* ROM 768; C) *Parasaurolophus* cf. *cyrtocristatus* UCMP 143270; dD) *Hypacrosaurus altispinus* CMN 8675; E) *Lambeosaurus lambei* ROM 794; F) *Corythosaurus intermedius* ROM 776; g) *Lambeosaurini* indet. ROM 1940. Not to scale. See references in text for additional comparisons.



(Gates et al. 2021: fig. 5), though the immature *P. cf. cyrtocristatus* UCMP 143270 (Gates et al. Fig. 13C) may be scarcely distinguishable from TMP 2016.023.0039 in this character, if the distortion of the latter is taken into account (Fig. 4.12).

Supraoccipital— The supraoccipital is more exposed than in other Laramidian parasaurolophin skulls, due to the squamosals being mostly unpreserved (Fig. 4.13). The morphology of this element in dorsal view is generally similar to *Charonosaurus* (Godefroit et al. 2001: fig. 4A). The paired, oblong squamosal bosses are angled anterolaterally, and the maximum width of the supraoccipital, 85 mm, is across their anterolateral ends. The posterior ends of the squamosal bosses reach the posterior margin of the supraoccipital. There is no evidence of the otoccipital contributing to the squamosal bosses. The median ascending process is triangular in dorsal view, similar in size to the squamosal bosses, with a pointed posterior end that terminates 10 mm anterior to the posterior margin of the supraoccipital, similar to *P. tubicen* (ROM 65650). This differs from the Prince Creek Formation lambeosaurine DMNH 2014-12-266 (Takasaki et al. 2019: fig. 1A), in which the ascending process is more rounded posteriorly, much more massive than the squamosal bosses, and reaches the posterior margin of the supraoccipital. The dorsal surface of the ascending process slopes posteroventrally, and resembles a strawberry with its slightly bulbous, triangular shape and pitted texture, as in *P. tubicen*. The density of foramina on the ascending process is similar to that of the medial region of the frontals directly posterior to the frontal platform. The ascending process lacks the tall, laminar dorsal extension that divides the nuchal fossa in *Tlatolophus* (Ramírez Velasco et al. 2021). In posterior view, the ventral edge of the

Figure 4.13 Detail of supraoccipital in TMP 2016.023.0039, in oblique postero-dorsal view.



supraoccipital is straighter than in DMNH 2014-12-266, and the ascending process has a narrow, laminar pedestal that tapers more sharply ventrally. The squamosal bosses are relatively flat and much lower in posterior view than the ascending processes, as in *P. tubicen*, and differing from *Charonosaurus*, in which the squamosal bosses are more bulbous and closer in height to the ascending process (Godefroit et al. 2001: fig. 5b).

Basioccipital— The basioccipital is mostly exposed on the ventral side of the braincase. Its texture is relatively smooth, comparable to the anterior rather than the posterior part of the ventral basisphenoid. The width of the basioccipital across the basal tubera (73 mm) considerably exceeds its total length (55 mm), whereas in the immature *Parasaurolophus* UCMP 143270 this element is approximately as wide as it is long. Although much of the posterior surface is damaged, part of the surface of the occipital condyle is preserved. The preserved surface of the occipital condyle is flat, and approximately vertical in relation to the horizontal long axis of the basioccipital, apparently lacking the pronounced ventral deflection of the condyle present in *Tlatolophus* (Ramírez Velasco et al. 2021).

4.4 Discussion

Ontogenetic Assessment— A recent review of methods for assessing ontogeny in fossil reptiles recommended long bone histology as the most reasonable method for ornithomorphs, followed by (with caveats) some other methods including facial proportions, tooth counts, postcranial fusion, and tendon ossification (Griffin et al. 2021: table 1). These methods are, unfortunately, not applicable to the partial skull roof and braincase of TMP 2016.023.0039, and potentially more ambiguous methods must therefore be

considered. A morphologically mature ('adult') stage is tentatively supported on the basis of the combination of relatively large size, a deeply and complexly corrugated frontal platform, and advanced cranial fusion. The maximum width of the skull across the postorbitals is 211 mm, slightly exceeding the 200 mm estimated for the adult *P. walkeri* holotype, ROM 768 (Parks 1922), which can be considered a fairly typical-sized lambeosaurine for the Belly River Group. Although the posterior skull roof is incompletely preserved, the preserved portions of the postorbital temporal bar and paroccipital process suggest that the skull roof could have also been relatively wide posteriorly, producing a square-ish dorsal outline similar to other large, presumably 'adult' lambeosaurines (e.g., CMN 57072, ROM 1940), and unlike the narrower posterior skull roof of 'juveniles' and 'subadults' (e.g., CMN 2246, CMN 8633). The proportionately wide basioccipital, compared to the immature *Parasaurolophus* UCMP 143270, is also suggestive of the ontogenetic trend of this element observed in *M. peeblesorum* (McFeeters et al. 2021b), which may be typical for hadrosaurids. The well-developed frontal platform is deeply and complexly corrugated in comparison to the smaller, less mature *Parasaurolophus* specimens CMN 8502 and UCMP 556168, as well as in comparison to adult lambeosaurines. Although an ontogenetic series of the frontal platform has not been described for any individual parasaurolophin species, it is plausible that the platform became increasingly rugose with maturity as the crest enlarged. A comparable ontogenetic transformation is documented in the brachylophosaurin *Maiasaura peeblesorum*, which convergently evolved a more steeply inclined frontal platform, and more deeply corrugated frontal platform ridges than in closely related taxa (McFeeters et al. 2021b). Evans (2010) identified the fusion of the prootic with the

opisthotic-exoccipital complex as occurring only late in the ontogeny of *H. altispinus*, which may further support an ‘adult’ designation for TMP 2016.023.0039, even though immature hadrosaurids can show some degree of neurocranial fusion (Ostrom 1961a). Dorsal skull roof sutures are much less open in TMP 2016.023.0039 than in CMN 8502 (Evans et al. 2007: fig. 2). In particular, the obliteration of the interfrontal suture appears to be an uncommon late-ontogeny feature of some hadrosaurids that has not been observed in any immature specimens, but is present in large, presumably mature individuals of *T. galorum* (Ramírez Velasco et al. 2021), *M. peeblesorum* (McFeeters et al. 2021b), and *Edmontosaurus annectens* (ROM 64623; T. Dudgeon pers. comm. 2022).

Taxonomic Assessment— Derived lambeosaurine or corythosaurian characters present in TMP 2016.023.0039 include a moderately elevated rostral process of the postorbital with respect to the dorsal surface of the postorbital over the jugal process, the nasal articulation of the frontals forming a sloping frontal platform that is united across both frontals, the frontal excluded from the margin of the orbit by the prefrontal and postorbital, a proportionately short dorsal surface of the frontals that forms a slight dome, and an anteroposteriorly short parietal with a strongly down-warped sagittal crest (Horner et al. 2004; Evans and Reisz 2007; Gates et al. 2021). Within Corythosauria, several characters indicate affinities with Parasaurolophini rather than with Lambeosaurini. The anterior region of the frontal platform is short, and lacks the narrow cleft between the frontals that is present in lambeosaurins (Evans and Reisz 2007). The frontal platform is strongly inclined, with a slope similar to *Parasaurolophus* (Evans et al. 2007), and the peak of its elevation above the ancestral dorsal profile of the frontals is visible in lateral view. The dorsal surface of the frontals posterior to the frontal platform is boomerang-

shaped, with a very shortened length/width ratio of < 0.4 , as in *Parasaurolophus*, *Charonosaurus*, and *Tlatolophus* (Evans and Reisz 2007; Ramírez Velasco et al. 2021). Although not previously recognized as a parasaurolophin synapomorphy, the proportionately long and narrow dorsal exposure of the interfrontal process of the parietal may also link TMP 2016.023.0039 to *Parasaurolophus*, and distinguish it from lambeosaurins (e.g., Evans et al. 2007: fig. 2a vs. Fig. 3a). The dorsal exposure of the interfrontal process in the early non-corythosaurian lambeosaurine *Jaxartosaurus* appears relatively short and broad, as in lambeosaurins (Godefroit et al. 2004b: fig. 20), suggesting that to be the more likely ancestral condition for corythosaurians. However, this character is homoplastic on a broader scale, as a narrow dorsal exposure also occurs in the more distantly related hadrosaurid *Edmontosaurus* (CMN 2289, CMN 8509, CMN 8744). On the basisphenoid, TMP 2016.023.0039 shares with *Parasaurolophus* the condition of a pendent alar process that has a free anterior edge and projects primarily ventrolaterally, with (in at least some *Parasaurolophus*) a fossa defined by a stout ridge on the outer surface; in contrast to the condition found in lambeosaurins (e.g., *Corythosaurus*, ROM 776, ROM 1933; *Hypacrosaurus*, CMN 8675, ROM 702) and non-lambeosaurine hadrosaurids (e.g., *Edmontosaurus*, Xing et al. 2017: fig. 15; *Gryposaurus*, Prieto-Márquez 2010: fig. 8; *Maiasaura*, McFeeters et al. 2021b: fig. 8), in which the base of the alar process is attached to the braincase wall along a long, subvertical anterior edge and projects primarily posterolaterally, with a flat outer surface. The alar process is diminutive in *L. lambei* (CMN 8633, Fig. 4.11C), but appears to be oriented essentially as in other lambeosaurins. The supraoccipital, which is frequently poorly preserved or exposed in hadrosaurid fossils, has been underappreciated as a source

of taxonomically and phylogenetically informative characters, and was previously characterized as not varying greatly among lambeosaurines (Evans 2010). The supraoccipital of TMP 2016.023.0039 closely matches that of *Parasaurolophus*, and differs from that of *Hypacrosaurus* and the Prince Creek Formation lambeosaurine, in several characters such as the shape of the median process (triangular vs. rounded), the size of the median process in relation to the lateral (squamosal) processes (larger vs. subequal), and the distance between the median process and the posterior edge of the element. However, further sampling of supraoccipitals from a broader range of lambeosaurines, including non-corythosaurians, is needed to determine whether the character states in the parasaurolophins are synapomorphies or symplesiomorphies.

Though overall closely resembling *Parasaurolophus*, TMP 2016.023.0039 also exhibits some character states reminiscent of conditions in lambeosaurins. The prefrontal-postorbital contact differs from at least *P. walkeri* (ROM 768) in that the posterior prefrontal has a relatively flat, dorsally exposed area, and the prefrontal process of the postorbital is only moderately elevated, with the prefrontal-postorbital contact not directly overlying the jugal process, though this less derived condition is also shared with some other parasaurolophins. The frontal platform, although strongly inclined and elevated, is plesiomorphic in lacking a posterior expansion that overhangs the anterior parietal or the dorsotemporal fenestrae. As in lambeosaurins, the interfrontal process of the parietal is considerably separated from the sagittal crest by a distinct region of the dorsal parietal that forms a relatively flat, triangular plateau, contrasting with both the condition in *Parasaurolophus* in which the sagittal crest extends almost as far anteriorly as the interfrontal process (ROM 768, ROM 65650), convergent with the non-

hadrosaurid hadrosauroid *Sirindhorna* (Shibata et al. 2015), and *Charonosaurus*, in which the sagittal crest is absent (Godefroit et al. 2000). A novel character identified in this study is the orientation of the postorbital process of the laterosphenoid, which projects anterolaterodorsally in TMP 2016.023.0039 and lambeosaurins, but laterodorsally in *Parasaurolophus*, independently of ontogenetic stage. The anterolaterodorsally projecting condition is here considered the probable plesiomorphic state for Corythosauria, since it occurs in all examined lambeosaurins, as well as the stratigraphically lowest examined parasaurolophin (TMP 2010.023.0039), and potentially in the early-diverging lambeosaurine *Aralosaurus* (Godefroit et al. 2004a: fig. 2b). However, the distribution of this character among non-corythosaurian lambeosaurines remains poorly documented, and the deeper phylogenetic history of this character may be more complex, as shown by the entirely laterodorsally projecting laterosphenoids in at least some saurolophines (e.g., *Maiasaura*, ROM 66180), and even earlier-diverging hadrosauromorphs close to the origin of Hadrosauridae (e.g., *Gobihadros*, Tsogtbaatar et al. 2019: fig. 8; *Lophorhothon*, Gates and Lamb 2021: fig 6b). The complex topography of the basiptyergoid process of the basisphenoid in lateral view closely resembles *H. altispinus* (ROM 702, Fig. 4.11E), and differs from the simple, flat-sided basiptyergoid processes of *Parasaurolophus* (ROM 65650; UCMP 143270), though it is uncertain whether this is retained from the ancestral corythosaurian condition, as some lambeosaurins also have simple basiptyergoid processes (e.g., *L. lambei*, CMN 8703). The basisphenoid of TMP 2016.023.0039 is also distinct from the southern *Parasaurolophus* species, *P. cyrtocristatus* and *P. tubicen*, in the greater size and robustness of the alar process, and very short basiptyergoid process, but unfortunately it

cannot be determined at this time whether these characters differ from *P. walkeri*. The mediolaterally long, shallow curve of the ventral edge of the otoccipital ‘neck’ of the paroccipital process qualitatively differs from at least some specimens of *Parasaurolophus* and *Tlatolophus*, but resembles *Charonosaurus* and some lambeosaurins, and thus may also represent a taxonomically informative character state. However, the distribution of this character state in corythosaurians appears to be homoplastic, and may be susceptible to intraspecific or preservational variation.

The unique combination of morphological characters, combined with its lower stratigraphic position, indicates that TMP 2016.023.0039 represents a diagnostic new species within Parasaurolophini (see Systematic Palaeontology: Diagnosis). Genus-level systematics within Parasaurolophini are complicated in practice, sometimes resting on character states that have conflicting interpretations in the literature, or poorly understood distributions amongst the relevant taxa, the phylogenetic interrelationships of which are unstable. In particular, there is currently some ambiguity over whether certain skull roof characters diagnose *Parasaurolophus* or Parasaurolophini. Over the early decades of research, three species were assigned to *Parasaurolophus* (*P. walkeri*, Parks 1922; *P. tubicen*, Wiman 1931; *P. cyrtocristatus*, Ostrom 1961b), and these are retained in all recent diagnoses of the genus (Sullivan and Williamson 1999; Evans et al. 2007; Gates et al. 2021). Godefroit et al. (2000) described the monotypic genus *Charonosaurus* as the sister taxon of *Parasaurolophus*, but did not discuss or test implications for the monophyly of the latter, which was scored as a single operational taxonomic unit in their phylogenetic analysis. According to Godefroit et al. (2000: 879), “the frontal platform extending backwards above the rostral part of the parietal and supratemporal fenestra”

(their character 5) is a synapomorphy uniting *Charonosaurus* and *Parasaurolophus*. This derived condition was also scored as present in the monotypic genus *Tlatolophus* by Ramírez Velasco et al. (2021; their character 144), which has been recovered as a member of the *Charonosaurus* + *Parasaurolophus* clade, either closer to the former (Ramírez Velasco et al. 2021) or the latter (Ramírez Velasco 2022). Conversely, a posterior extension of the frontal platform overhanging the parietal is probably absent in TMP 2016.023.0039, which could support a more basal position for it within Parasaurolophini. However, Evans and Reisz (2007: Appendix 2) scored essentially the same character state (their character 41) as being absent in *Charonosaurus*, while occurring in *P. tubicen*. Although Godefroit et al. (2000, 2001) explicitly mentioned this condition in their text as present in *Charonosaurus*, it cannot be verified from any of their figures. Unfortunately, the original material of *Charonosaurus* was unavailable in the present study to resolve this discrepancy. The phylogenetic analysis of Evans and Reisz (2007) was the first to test and support the hypothesis of *Charonosaurus* as the sister taxon to all three species of *Parasaurolophus*, the monophyly of the latter genus unambiguously supported by the steeper angle of the thickened frontal platform (their character 40, in part). This character was retained in the generic diagnosis of *Parasaurolophus* by Gates et al. (2021). In this character, TMP 2016.023.0039 agrees with *Parasaurolophus*, and differs from *Charonosaurus*. The frontal platform appears to possibly be also steeply angled in *Tlatolophus* (Ramírez-Velasco et al. 2021: fig. 13a), at least from external appearances of the posterior projection of the platform, but details of the frontal platform in that genus are partially obscured by the articulated crest in the only known skull. Some phylogenetic analyses, beginning with Xing et al. (2014) and

including some more recent studies (e.g., Longrich et al. 2021; Xing et al. 2022), have found *Ch. jiyinensis* to be deeply nested within *Parasaurolophus*, making the traditional concept of *Parasaurolophus* paraphyletic. Gates et al. (2021) recovered a traditional monophyletic *Parasaurolophus*, and included in its revised diagnosis the following characters adapted from Evans et al. (2007): “precerebral region of frontal short, anterior processes of conjoined frontals meet at a widely obtuse angle in dorsal view and median cleft is poorly developed” and “olfactory depression of frontal is offset ventrally from roof of cerebral fossa” (Gates et al. 2021: 7). These character states are shared with TMP 2016.023.0039, but have a potentially broader distribution within Parasaurolophini. The anterior processes of the frontals also meet at a widely obtuse angle in *Ch. jiyinensis* (Godefroit et al. 2001: fig. 4A), which was scored the same as *Parasaurolophus* in lacking a bifurcated median cleft in the phylogenetic analysis of Gates et al. (2021; their character 137). The characters relating to the endocranial surface of the frontal (relatively length and ventral offset of the precerebral region) were not included in the phylogenetic analysis, and so far their states in *Ch. jiyinensis* and *T. galorum* cannot be determined from the literature, making it unclear what clade these characters diagnose.

Although TMP 2016.023.0039 was collected geographically and stratigraphically close to the known range of *P. walkeri*, and nothing noted in its morphology precludes it from representing a direct ancestor of that taxon, no morphological characters are identified in this study that would unambiguously nest TMP 2016.023.0039 within a clade that includes *P. walkeri*, *P. tubicen*, and *P. cyrtocristatus*, but exclude *Ch. jiyinensis* and *T. galorum*. The proposal of a new genus for TMP 2016.023.0039, although arguably separated from other parasaurolophins by only modest morphological

differences, is consistent with other recent studies that favour high generic diversity for a small number of similar, closely related species in other clades within Hadrosauridae (e.g., McDonald et al. 2021; Rozadilla et al. 2022). The name of the new taxon will be given in the eventual published version of this chapter.

Implications for Parasaurolophin Cranial Evolution— Previous studies have noted the relatively precocious development of the cranial crest and its platform in immature specimens of *Parasaurolophus*, compared to approximately contemporaneous, comparably mature individuals in the clade Lambeosaurini (Evans et al. 2007; Farke et al. 2013). Farke et al. (2013) hypothesized that the exceptionally large and morphologically derived crest of *Parasaurolophus* was a result of peramorphic heterochrony, with a predisplacement of crest development to an earlier ontogenetic stage than in the most recent common ancestor of parasaurolophins and lambeosaurins. However, it could not be shown with the data then available that the timing of crest development changed within the parasaurolophin clade over time. The peramorphism hypothesis predicts that if a stratigraphically lower, less derived member of the *Parasaurolophus* lineage were to be discovered, the development of the crest in adult individuals may resemble the development of the crest in less mature individuals from stratigraphically higher, more derived populations, analogous to the mechanism has been described for the independent lengthening of the frontal platform in the *Probrachylophosaurus-Brachylophosaurus* clade (Freedman Fowler and Horner 2015).

The specimen TMP 2016.023.0039 potentially fulfills this prediction by being the stratigraphically lowest record of a parasaurolophin skull roof, occurring slightly below the lowest record of *Parasaurolophus*, and having among the least derived development

of the prefrontal-postorbital contact and frontal platform for an adult-sized parasaurolophin. The similar development of these characters in TMP 2016.023.0039 to the much smaller and less mature *Parasaurolophus* specimen CMN 8502 from an unknown horizon in Dinosaur Provincial Park could further support the hypothesis of predisplacement, given the more likely stratigraphic position of CMN 8502 considered to be in the Dinosaur Park Formation (Evans et al. 2007), and thus higher in the Belly River Group than TMP 2016.023.0039. In this scenario, the immature ontogenetic stage of *Parasaurolophus* represented in the Dinosaur Park Formation by CMN 8502 potentially recapitulated the mature stage of an ancestor similar to TMP 2016.023.0039, but continued to develop into the more derived mature morphology typified by ROM 768 (*P. walkeri*). However, in the less likely event that CMN 8502 was collected from the Comrey Sandstone Zone of the Oldman Formation outcrops of Dinosaur Provincial Park, it could represent a less mature individual of the same species as TMP 2016.023.0039, which would instead imply that the mature morphologies of these skull roof characters were attained early in ontogeny in this taxon. Arguing against this hypothesis is the presence in CMN 8502 of a laterosphenoid postorbital process angle similar to geologically younger specimens of *Parasaurolophus* from the American southwest, and distinct from TMP 2016.023.0039. More material, with precise stratigraphic data, is needed to make a definitive argument for the predisplacement of these characters over time in Belly River Group parasaurolophins. As the characters that separate TMP 2016.023.0039 from *Parasaurolophus* partly relate to the hypertrophy of the hollow crest in the latter, it can be hypothesized that the unknown crest of TMP 2016.023.0039 was

likely less extreme in its development, though the steeply inclined frontal platform indicates that a considerably developed crest was present.

Evolution of Laramidian hadrosaurid assemblages—The Comrey Sandstone Zone yielding TMP 2016.023.0039 is younger than the oldest known Laramidian lambeosaurine, *Adelolophus hutchisoni* from the Coyote Point Member of the Wahweap Formation of Utah, while older than the diverse lambeosaurines of the Dinosaur Park Formation, though closer in age to the latter (Gates et al. 2014; Fowler 2017; Beveridge et al. 2022). *Adelolophus hutchisoni* has also been recovered as a member of Parasaurolophini (Longrich et al. 2021; Ramírez Velasco 2022), exclusively on the basis of the holotype maxilla, and cannot be compared to TMP 2016.023.0039 due to lack of overlapping elements. The approximately three-million-year age difference (Beveridge et al. 2022: fig. 9) suggests that they are unlikely to be the same species. TMP 2016.023.0039 is the oldest Laramidian lambeosaurine with skull roof and braincase elements preserved, and definitively corroborates that the basal split within Corythosauria between lambeosaurins and parasaurolophins had occurred at latest by middle Oldman time. It represents the second hadrosaurid taxon reported from the Comrey Sandstone Zone at the Milk River Ridge Reservoir locality, after the brachylophosaurin *Maiasaura* sp. (McFeeters et al. 2021a). Both *Maiasaura* (Horner 1983; McFeeters et al. 2021a) and *Parasaurolophus* (Evans et al. 2009a) have been interpreted as preferring more inland habitats compared to related hadrosaurids, but members of these lineages had not been reported from the same locality prior to the discovery of this material. All other Laramidian parasaurolophins are known from units where non-lambeosaurine

hadrosaurids are represented by members of Kritosaurini, as in the lower Dinosaur Park, Kaiparowits, Fruitland/Kirtland, and Cerro del Pueblo formations (Williamson 2000; Ryan and Evans 2005; Gates et al. 2013; Ramírez Velasco 2022). The Milk River Ridge Reservoir locality thus adds relevant new data for discussions of niche partitioning and competitive exclusion between various hadrosaurid lineages in the Campanian of Laramidia.

Species turnover between the ornithischian dinosaur assemblage of the Comrey Sandstone Zone and that of the lower Dinosaur Park Formation or chronostratigraphically equivalent upper Oldman Formation in southern Alberta has been previously recognized (Ryan and Evans 2005), but the relative importance of *in situ* anagenetic evolution versus replacement by populations arriving from elsewhere during this transition is unclear. The hadrosaurid genus *Gryposaurus* is documented in Alberta in both the lowest unit of the Oldman Formation and the lower Dinosaur Park Formation (Scott et al. 2022), but has yet to be reported from the intervening Comrey Sandstone Zone. Instead, both previously recognized hadrosaurid taxa in the Comrey Sandstone Zone belong to the clade Brachylophosaurini (Sternberg 1953; McFeeters et al. 2021a), which has yet to be recognized in the lowest part of the Dinosaur Park Formation, though a single specimen from probably around the middle of the Dinosaur Park Formation (CMN 52845; Evans et al. 2009a) may belong to this clade (pers. obs.). The only named Comrey Sandstone Zone ceratopsid, *Coronosaurus*, has been variably recovered in recent phylogenetic analyses either in a position compatible with a possible ancestral relationship to its stratigraphic successor *Centrosaurus* (Chiba et al. 2018; Wilson et al. 2020), or in a position that requires both to have distinct ghost lineages pre-dating the occurrence of *Xenoceratops* in

the underlying Foremost Formation (Dalman et al. 2021). The lambeosaurine TMP 2016.023.0039, though representing a morphologically distinct species (or chronospecies), appears closely related to stratigraphically higher parasaurolophins including *P. walkeri* from the lower Dinosaur Park Formation, and a possible ancestor-descendant relationship cannot be excluded on the basis of the available data. This taxon may thus eventually add further support for phyletic continuity within Belly River Group ornithischian populations, rather than replacement by non-locally evolved taxa, during this faunal turnover episode.

4.5 Conclusions

The first several million years of lambeosaurine evolution in Laramidia, from the occurrence of *Adelolophus* up until the diverse and abundant material of the Dinosaur Park Formation, continues to be largely unrepresented in the fossil record. The new parasaurolophin represented by the partial skull roof and braincase TMP 2016.023.0039 from the Comrey Sandstone Zone of the Oldman Formation provides a significant exception to this gap. This taxon is notable as the oldest lambeosaurine from northern Laramidia (or present-day Canada), the first lambeosaurine to be described on diagnostic adult-sized material from the Oldman Formation, and the oldest parasaurolophin globally for which the skull roof and braincase are preserved. The new taxon is diagnosed by a unique combination of characters, but does not appear to be strongly autapomorphic, and cannot be excluded as a potential ancestor to the parasaurolophin in the overlying Dinosaur Park Formation. In some senses, the morphology of the new taxon conforms to what could be predicted for a stratigraphically lower representative of Parasaurolophini:

the greater morphological similarity to members of Lambeosaurini is reflective of being temporally closer to the phylogenetic divergence from that clade, and the similarity to immature examples of later parasaurolophins is reflective of the heterochronic process hypothesized to have produced the exaggerated crests for which the group is known. In the course of this study, new characters were noted in the basisphenoid, laterosphenoid, supraoccipital, and otoccipital that are proposed to have potential taxonomic and phylogenetic utility for parasaurolophins. However, the precise probable phylogenetic position of TMP 2016.023.0039 within Parasaurolophini is difficult to evaluate at present, in part due to lack of available data on closely related members of this clade. As one of only a few ornithischian megaherbivores definitively known from the Comrey Sandstone Zone, the new parasaurolophin taxon provides a valuable new data point for the composition of this faunal assemblage, and the nature of its transition to the more familiar and intensely studied assemblage of the lower Dinosaur Park Formation.

Chapter 5: Phylogenetic Analysis of Distinctive Hadrosaurid Skull Roof and Braincase Material from the Belly River Group (Upper Cretaceous, Campanian) of Alberta

Abstract– A recent character-taxon matrix for Hadrosauoidea is modified to test the phylogenetic positions of three partial skulls from the Belly River Group of Alberta: TMP 2010.077.0030, described in Chapter 3 and hypothesized to represent a specimen of *Maiasaura* sp., TMP 2016.023.0039, described in Chapter 4 and hypothesized to represent a new parasaurolophin, and CMN 52845, a previously described specimen that was assigned to cf. *Parasaurolophus* sp. on the basis of other phylogenetic analyses. New characters sourced from the descriptions of these specimens are added to the phylogenetic dataset. The consensus trees of maximum parsimony and Bayesian analyses differ on some aspects of hadrosauroid phylogeny, but broadly agree on the positions of the newly added specimens. TMP 2010.077.0030 is closest to *Maiasaura peeblesorum*, and TMP 2016.023.0039 is a member of the *Parasaurolophus* + *Tlatolophus* clade that falls outside of *Parasaurolophus*, as hypothesized in the descriptive chapters. CMN 52845 is recovered for the first time as the sister taxon of *Brachylophosaurus canadensis*, and extends the stratigraphic range of Brachylophosaurini upwards in the Belly River Group.

5.1 Introduction

Hadrosaurids were a widespread and species-rich group of dinosaurs, and there has been much interest and effort into reconstructing their evolutionary tree. The history of research on hadrosaur phylogeny (up to the late 2000s) was reviewed by Prieto-Márquez

(2010a) in an influential paper that included the largest character-taxon matrix for hadrosaurs assembled up to that point. Since the beginning of the 2010s, over 50 quantitative analyses have been published that focused on testing the phylogenetic position of hadrosaurid material (Appendix 5.1), not including numerous other analyses focused on non-hadrosaurid hadrosauroid material that may use variations of the same datasets. Many of these studies are incremental modifications of previously published analyses to incorporate newly described or revisited material, a practice that is continued in this chapter. In the early years of the 2020s, hadrosaur researchers using matrices descended from varied “lineages” of previous analyses (see Appendix 5.1) have come to an increasing consensus on issues that were not settled in the early 2010s, such as the sister-group relationship between Saurolophini and Edmontosaurini, with Kritosaurini the next major clade out from those two; and that the Asian lambeosaurines *Amurosaurus* and *Olorotitan* are lambeosaurins, rather than either being basal to the split between lambeosaurins and parasaurolophins. However, there remains conflict between these recent results on other issues, such as the monophyly of the genus *Hypacrosaurus*; the monophyly of the genus *Parasaurolophus* (versus paraphyly with respect to *Charonosaurus*); and the relationships of the European lambeosaurines, such as *Arenysaurus* and *Blasisaurus*, to each other and as well as to lambeosaurines on other continents (Gates et al. 2021; Longrich et al. 2021; Ramírez Velasco 2022; Xing et al. 2022).

Quantitative phylogenetic analyses of Hadrosauridae have overwhelmingly relied on a maximum parsimony approach, beginning with the earliest computer-aided phylogenetic analyses of this clade in the 1990s (Weishampel et al. 1993). Prieto-

Márquez (2010a) compared the results of maximum parsimony and Bayesian likelihood analyses of hadrosaur phylogeny against their fit with the stratigraphic data, and concluded that the consensus tree produced by the parsimony analysis was more compatible with the fossil record. Of the two Bayesian analyses performed by Prieto-Márquez (2010a), the consensus tree produced with equal rates of character change (Mk model without the gamma parameter) had closer agreement with the most parsimonious trees, whereas the tree produced with variable rates of character change (Mk model with gamma parameter) was more strongly discordant with the stratigraphic evidence and conventional classifications. Gates and Scheetz (2015) revisited this problem using a modified version of the Prieto-Márquez (2010a) matrix. They found that the equal rate and variable rate models both produced consensus trees similar to that from the variable rate model in Prieto-Márquez (2010a), with Lambeosaurinae nested within a strongly paraphyletic “Saurolophinae,” and commented that the outcome of their Bayesian analyses, “given the current fossil record, seems quite unlikely” (Gates and Scheetz 2015: 720). These unusual early Bayesian results may have been influential in maximum parsimony continuing as the standard method across the majority of the hadrosaur phylogenetic literature. However, Evans (2010) used both maximum parsimony and Bayesian likelihood (Mk model with gamma parameter) algorithms to analyze a smaller dataset focused on relationships within Lambeosaurinae, and recovered essentially similar trees, crediting this to a strong phylogenetic signal in the data. More recently, Longrich et al. (2021) performed a tip-dated Bayesian phylogenetic analysis on a large dataset of Hadrosoidea (adapted from Kobayashi et al. 2019), and recovered a “standard” overall topology essentially similar to the most parsimonious trees.

The aim of this chapter is to test the phylogenetic positions of three distinctive hadrosaurid specimens consisting of skull roof and braincase elements from the Campanian Belly River Group of Alberta that were examined over the course of this thesis project. Two of these specimens, TMP 2010.077.0030 (Chapter 3) and TMP 2016.023.0039 (Chapter 4), were recently collected from the Comrey Sandstone Zone (“middle unit”) of the Oldman Formation at the Milk River Ridge Reservoir locality in southern Alberta and have not been included in any prior quantitative phylogenetic analysis. On the basis of the descriptions and comparisons made in the preceding chapters, TMP 2010.077.0030 was hypothesized to belong to the brachylophosaurin genus *Maiasaura*, and TMP 2016.023.0039 was hypothesized to represent a new parasaurolophin. The third specimen, CMN 52845, was collected in the Dinosaur Park Formation of Dinosaur Provincial Park and originally described by Evans et al. (2009a) as “cf. *Parasaurolophus* sp.” This identification was supported by the addition of CMN 52845 to the phylogenetic analyses of Evans and Reisz (2007) and Godefroit et al. (2008). However, Evans et al. (2009a) also noted characters of the specimen that would be unusual for a lambeosaurine, and considered the referral to *Parasaurolophus* merely tentative. The phylogenetic position of CMN 52845 has not been revisited in the literature since 2009, but new observations made during comparison to the other specimens in this project raised doubts about its published identity, and prompted its inclusion in this analysis. The use of both maximum parsimony and Bayesian approaches in this chapter is primarily intended to test whether the positions of the newly scored specimens are especially sensitive to variation in the assumptions of the chosen

algorithm, rather than taking on the much more complicated problem of which algorithm provides the overall more accurate modelling of hadrosaur phylogeny.

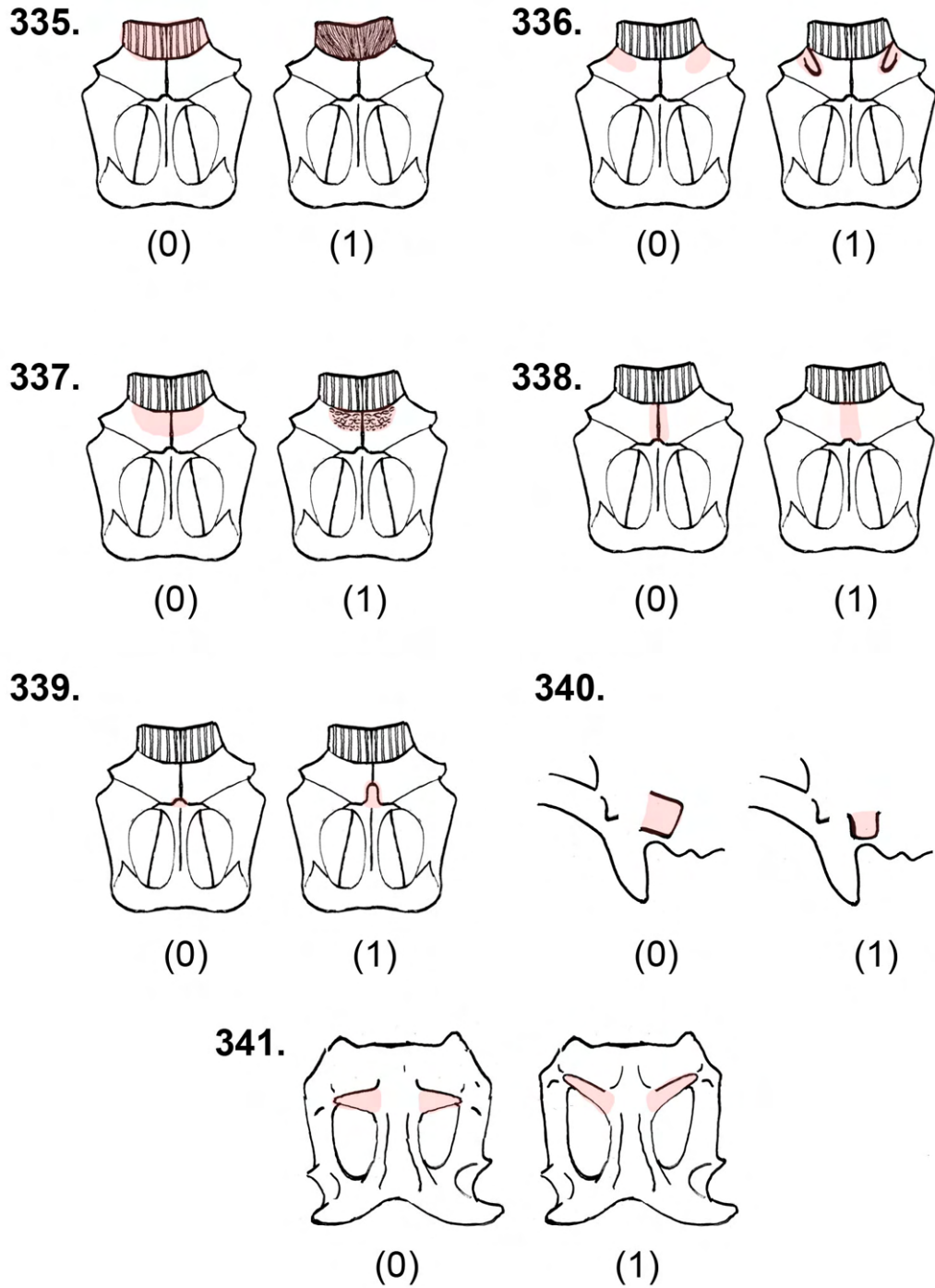
Institutional Abbreviations – **CMN**, Canadian Museum of Nature, Ottawa, Ontario, Canada; **MOR**, Museum of the Rockies, Bozeman, Montana, USA; **ROM**, Royal Ontario Museum, Toronto, Ontario, Canada; **TMP**, Royal Tyrrell Museum of Palaeontology, Drumheller, Alberta, Canada; **UCMP**, University of California Museum of Paleontology, Berkeley, California, USA.

5.2 Materials and Methods

The dataset for the phylogenetic analysis was modified from Ramírez Velasco (2022). This matrix is among the most recent to be published for hadrosaurids, and is a synthesis of data from Gates et al. (2021), Longrich et al. (2021), and Ramírez Velasco et al. (2021), as well as introducing some new data. Notably, it includes both the recently described parasaurolophin *Tlatolophus galorum* (Ramírez Velasco et al. 2021) and the recently described brachylophosaurin *Ornatops incantatus* (McDonald et al. 2021), which are potentially relevant to the hypothesized relationships of the newly scored specimens. Furthermore, all characters used by Ramírez Velasco (2022) are illustrated in the supplementary information, reducing the potential for incorrect character interpretations. The modified matrix includes 90 taxa, of which three are new, and 341 characters, of which two are modified to include additional states, and seven are new (Figure 5.1). For the sake of this discussion the new characters are appended to the end of the character list, rather than with other characters relating to the same element, to keep

Figure 5.1 Illustrations of new character states scored in the phylogenetic analysis.

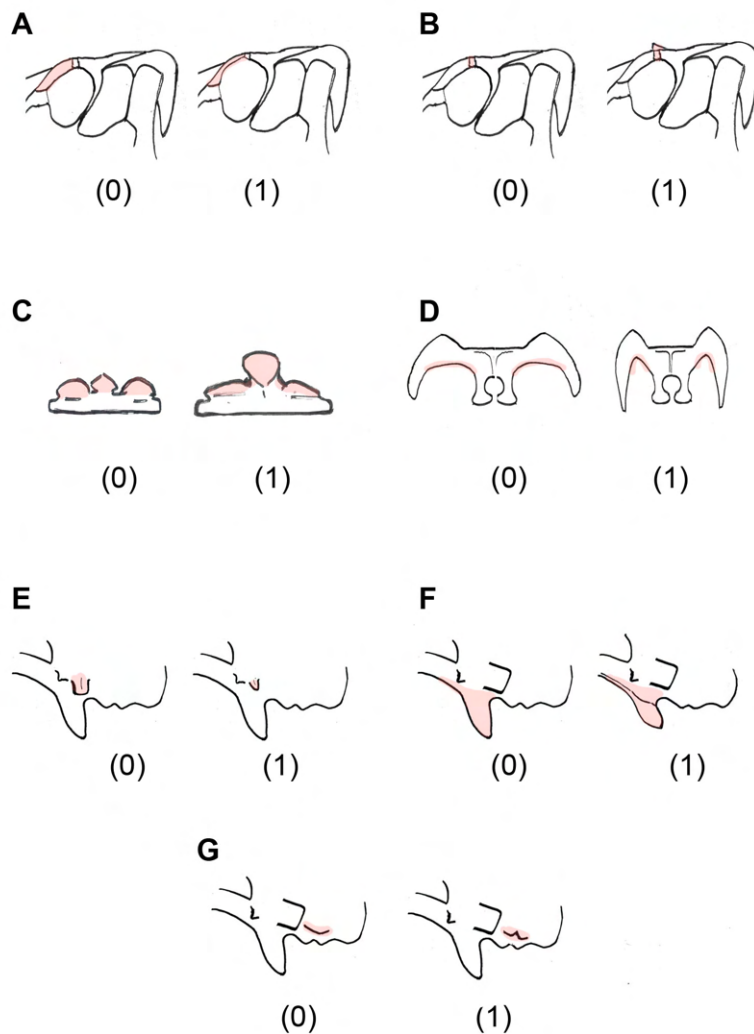
Numbers correspond to numbers in the text and data file. Drawings are schematic and do not represent actual specimens.



the numbering of the other characters consistent with Ramírez-Velasco (2022). This section also describes some considered characters that are currently unscored and excluded from the present analysis for various reasons, so that they might be revisited in future continuation of this work (Figure 5.2). Chiarenza et al. (2021) recently indicated a number of other new skull roof and braincase characters in the differential diagnosis of *Tethyshadros insularis*, which have yet to be incorporated into a character-taxon matrix. Characters were scored from firsthand observation of TMP 2010.077.0030, TMP 2016.023.0039, CMN 52845, and other hadrosaurid material available in the collections of the CMN and ROM. Unfortunately, restrictions on travel and collections visits during the development of this project necessitated a larger dependence on the literature, especially for the non-hadrosaurid taxa, which are mostly found outside of Canada. It is hoped that further data collection will continue to refine and improve this work, but that the distributions of character states sampled in this version are adequately representative for the purposes of the present chapter.

The maximum parsimony analysis was run using PAUP* version 4.0a169 for Macintosh (Swofford 2002). Commands and settings follow those of Ramírez Velasco (2022) to ensure comparability of results. *Iguanodon bernissartensis* was designated as the outgroup. The maximum number of trees was set to 10000, with no increase. A heuristic search was performed with random addition sequence for 1000 replicates, using branch swapping by tree-bisection-reconnection (TBR). A bootstrap analysis was performed with the default settings of 100 resamplings and a confidence value of 50. The Bayesian analysis was run using MrBayes v3.2.6 x64 (Ronquist and Huelsenbeck 2003), using the Markov k maximum-likelihood model (mcmc). The gamma-shape parameter

Figure 5.2 Illustrations of potential character states not scored in the phylogenetic analysis, in the order discussed in the text: A) thickness of the prefrontal rim; B) anterodorsal slope of the frontal; C) elevation of the median ascending process of the supraoccipital relative to the squamosal bosses; D) length and arching of the otoccipital ‘neck’ of the paroccipital processes; E) reduction of the alar process of the parabasisphenoid; F) distal swelling and lateral groove on the basipterygoid process; G) prootic forming a pit or pocket above the basal tubera. Drawings are schematic and do not represent actual specimens.



allowing variable rates was used, following Evans (2010). Prieto-Márquez (2010a) added a large number of parsimony-uninformative autapomorphic characters to the character-taxon matrix for the Bayesian analyses, which was not done for the present analysis. Prieto-Márquez (2010a: 450) stated that Müller and Reisz (2006) “showed that the implementation of the Mk model appears to be appropriate only if autapomorphies are included,” but what Müller and Reisz (2006: 503) more specifically found was that “the exclusive use of the Mk model appears suitable only if autapomorphic characters are included, whereas the Mk+gamma model performed well with or without autapomorphies.” The Bayesian analysis was run for 13.75 million generations (stopped when the average standard deviation of split frequencies of 0.007423, below the recommended 0.01), with a sample frequency of 100, print frequency of 100, and diagnostic frequency of 1000.

Updated Character Descriptions

Character descriptions are adapted from Ramírez Velasco (2022). For descriptions of unmodified characters, refer to the supplementary information of Ramírez Velasco (2022).

Rescored Characters

74. Nasal, ventral process, form, in non-lambeosaurines (Prieto-Márquez 2010a, Ch. 78): absent (0); long and high triangular process (1); short and thin triangular process (2). This character was originally scored “1” in both *Brachylophosaurus*

canadensis and *Maiasaura peeblesorum*, contrasting with state “2” in, for example, *Prosaurolophus maximus*. In Chapter 3, the small, slender nasal process of TMP 2010.077.0030 was contrasted with the larger, deeper nasal ventral process of *B. canadensis*, but compared favourably to the *M. peeblesorum* specimen ROM 66180 (Chapter 2). The development of the nasal ventral process in TMP 2010.077.0030 and ROM 66180 is not appreciably different from that in the *P. maximus* specimen CMN 2277 (pers. obs.), so all are here considered to have state “2.” However, it could not be ruled out that the original scoring is correct for a different specimen of *M. peeblesorum* (in ROM 44770, for example, these processes are incompletely preserved but appear potentially more similar to *B. canadensis*), so *M. peeblesorum* was cautiously rescored “1&2” rather than “2.”

149. Postorbital, temporal process, caudal end form (Prieto-Márquez 2010a, Ch. 132): oblong or wedge-shaped (0); bifid (1). In the unmodified matrix the distribution of character states corresponds to the inverse of the stated descriptions (Ramírez Velasco 2022, supplementary information), so the character description is modified to correct for this. *Brachylophosaurus canadensis* is also rescored as having non-bifid temporal processes (Cuthbertson and Holmes 2010; pers. obs. of CMN 8893).

157. Squamosal, occipital ramus, dorsoventral expansion in caudal view (Prieto-Márquez 2010a, Ch. 135): unexpanded, shallowly exposed (0); dorsocaudally expanded (1). This character was originally scored “0” in both *Brachylophosaurus canadensis* and *Maiasaura peeblesorum*. In Chapter 3, the dorsoventral expansion of the

squamosals in caudal view was figured as a character in which TMP 2010.077.0030 is more similar to *M. peeblesorum* than to *B. canadensis*. The condition in TMP 2010.077.0030 and *M. peeblesorum* (e.g., ROM 44770, ROM 66180) is no less pronounced than that in some lambeosaurines that are scored “1” for this character, such as *Hypacrosaurus stebingeri* (Brink et al. 2014: fig. 14.5), so *M. peeblesorum* is rescored from “0” to “1.”

165. Frontal, nasal articular facie, extension (Prieto-Márquez 2010a, Ch. 141): occupies the rostral part of the frontal (0); markedly extends caudodorsally and overhangs the parietal (1). This character was originally scored “1” in *Charonosaurus jiyinensis* and *Parasaurolophus walkeri*. Although the derived state is said to be present in the description of *Ch. jiyinensis*, the figures seemingly contradict this and show the frontal platform ending anterior to the frontal-parietal contact in dorsal view, and having a vertical, rather than overhanging, posterior wall in lateral view (Godefroit et al. 2001: fig. 4). Until this discrepancy can be resolved, *Ch. jiyinensis* is rescored from “1” to “?”. Regarding *P. walkeri*, Evans et al. (2009) noted that this character state is unclear in the holotype, ROM 768, due to poor preservation. The dorsal expansion of the frontal in ROM 768 does appear to have some posterior inclination, and thus at least overhangs at least part of itself (pers. obs.), but whether it extends far enough to overhang is parietal could not be determined. The certain presence of the derived state in CMN 58425 has been used to support the likelihood of its presence in ROM 768 (Evans et al. 2009). To properly test the position of CMN 58425, the scoring of the *P. walkeri* OTU should not

be influenced by any prior assumption of their relationship, so it is also cautiously rescored from “1” to “?”.

166. Frontal, nasal process, angle (between the articular nasal facie and the dorsal surface of the bone) (Xing et al. 2012, Ch. 186): up to 10° (0); greater than 10° and less than 25° (1); 25° to 35° (2); more than 35° (3). In the unmodified matrix, the distribution of derived character states was 1 in *Ornatops*, *Probrachylophosaurus*, *Brachylophosaurus*, *Jaxartosaurus*, most lambeosaurins for which known, and *Parasaurolophus cyrtocristatus*, 2 in both species of *Saurolophus* and *Parasaurolophus walkeri*, and 3 in *Maiasaura*, *Arenysaurus*, *Charonosaurus*, *Parasaurolophus tubicen*, and *Tlatolophus*. The low angle of the frontal platform scored for *P. cyrtocristatus* cannot be verified in the material referred to this species and *P. cf. cyrtocristatus* by Gates et al. (2021), with the orientation of the crests and posterior extensions of the frontals suggesting a higher angle more similar to other *Parasaurolophus*. However, the condition of the frontal platform in the *P. cyrtocristatus* holotype could not be verified in this study, either through direct observation or the literature. Pending further data, *P. cyrtocristatus* is rescored from “1” to “?”. The frontal platform is not directly exposed in the holotype of *P. walkeri*, but from external observation of the crest and frontals, does not show any indication of differing from the angle in *P. tubicen* or *Tlatolophus*. State 3 is present in the *Parasaurolophus* sp. specimen CMN 8502 (Figure 5.1A), also from Dinosaur Provincial Park. The “*Parasaurolophus walkeri*” OTU in the unmodified matrix evidently already incorporates some data from that specimen, since it is scored for characters that would be unknown if scored strictly from the holotype, and only

definitively assigned cranial specimen of *P. walkeri* in the literature (e.g., character 163, rostral margin of nasal processes of frontals; character 174, cerebral surface, annular ridge). *P. walkeri* is therefore rescored from “2” to “3,” with the understanding that the scoring of this OTU includes a (plausible) assumption about the affinity of CMN 8502. This is considered preferable to creating a separate OTU for CMN 8502, which is represents a clearly immature individual, or deleting all data based on CMN 8502 from the analysis, since this it is the only available Albertan *Parasaurolophus* specimen to preserve certain informative characters. Finally, at least on the basis of the published figures (Godefroit et al. 2001: figs. 4 & 5), the frontal platform in *Charonosaurus* appears distinctly less steep than in *Parasaurolophus*, which was reflected in it being scored differently from *Parasaurolophus* for character 40 in the analysis of Evans and Reisz (2007). It is rescored here from “3” to “1”.

168. Frontal, nasal process, median fossa (Prieto-Márquez 2010a, Ch. 142): absent (0); present (1). In the unmodified matrix this character was scored “0” in species of *Parasaurolophus*. This could not be confirmed in *P. cyrtocristatus* or *P. tubicen*. In the description of TMP 2016.023.0039 (Chapter 4), it was noted that the median fossa was present, but ridged, thus representing a potential transitional state between the typical lambeosaurin and parasaurolophin conditions. Whether the homologous region of the platform in CMN 8502 exhibits the “same” state as TMP 2016.023.0039 is to some extent subjective. Problematically, the “0” state for this character encompasses multiple non-equivalent states, such as a medially continuous ridged frontal platform as in brachylophosaurins, or a frontal platform split by a process of the ectofrontal surface, as

in *Jaxartosaurus*. Pending further refinement of this character, all of the *Parasaurolophus* OTUs were rescored from “0” to “?”.

179. Parietal, sagittal crest, extension relative to its body, in dorsal view (Prieto-Márquez 2010a, Ch. 150): remains sharp, defined rostrally (0); sharpness fades away rostrally (1); rostral half of parietal lacks ridge, flattened (2). In the unmodified matrix, this character was scored 0 in most non-hadrosaurids and all saurolophines for which it is known, and *Hypacrosaurus altispinus*, 1 in *Tethyshadros* and most lambeosaurines for which it is known, including *Hypacrosaurus stebingeri*, *Tlatolophus* and all species of *Parasaurolophus*, and 2 in *Amurosaurus*, *Sahaliyana*, and *Charonosaurus*. However, this distribution does not match personal observations, or the interpretation of a similar character by Shibata et al. (2015). Since it is possible that I am interpreting the character states differently from previous authors, the original scorings were all deleted. This approach resulted in an increase in missing data for this character, which does not reflect true uncertainty in the fossil record, but rather a cautious approach to the literature to avoid introducing unverified or falsified data into the matrix. In the revised matrix, state 0 is interpreted as only including taxa in which the sagittal crest reaches either the frontal-parietal contact, or the interfrontal process of the parietal. Shibata et al. (2015) considered this state to be an autapomorphy of *Sirindhorna khoratensis*, distinct from the sagittal crest being separated from the frontal in other basal hadrosauroids such as *Jinzhousaurus* and *Probactrosaurus*. The sagittal crest also covers essentially the maximum possible length of the parietal, excluding the interfrontal process, in *Parasaurolophus walkeri* and *Parasaurolophus tubicen* (Chapter 4, pers. obs.

of ROM 768, ROM 65650). In contrast, state 1 is here interpreted as including all taxa with an identifiable region of the parietal, forming a triangular “plateau,” between the frontal contact and the anterior end of the sagittal crest. In examined material of *Hypacrosaurus altispinus* (ROM 702, CMN 8675) this region is comparable in size to that of *Hypacrosaurus stebingeri* (Brink et al. 2014: fig. 14.6) or TMP 2016.023.0039 (Chapter 4), and distinctly larger than in *P. walkeri*. This character state encompasses some variation the size of the triangular plateau; it is proportionately larger in *Corythosaurus* (CMN 8704, ROM 776, ROM 1933) than in *Hypacrosaurus*, in some cases possibly verging on the state 2 condition (though here tentatively retained as state 1). In some brachylophosaurins including *Maiasaura* (e.g., ROM 66180, Chapter 2), the sagittal crest reaches the anterior end of the parietal on top of a triangular parietal expansion; this is scored as state 0. State 2 is the same as in the original character. Based on the published figures (McDonald et al. 2021: figs. 6 & 7), *Ornatops* is tentatively rescored “2,” but this condition is not mentioned in its description, and requires further confirmation.

185. Parabasisphenoid, preotic wing, anterior pendent process: absent (0); present (1). In the unmodified matrix, state 0 was described as a “semicircular” preotic wing, and state 1 was described a “bilobate” preotic wing. The latter condition was scored as present in *Brachylophosaurus*, *Maiasaura*, *Amurosaurus*, and all parasaurolophins in which known. From the illustrations and distributions of this character, the anterior lobe of the “bilobate” state appears to be equivalent to the presence on the parabasisphenoid of what Holliday (2006: 172) described as a “short, striated spur” in *Corythosaurus*

casuarius (CMN 8676), *Lambeosaurus lambei* (CMN 2869), *Brachylophosaurus*, and *Maiasaura*, and what Evans (2010: 419) described as a “pendent process” in *Hypacrosaurus altispinus* (CMN 2246, ROM 702). This character was thus rescored from “0” to “1” in *C. casuarius*, *L. lambei*, and *H. altispinus*, as well as in *Sahaliyana* based on the redescription by Xing et al. (2022). Other scores of “0” within Lambeosaurinae were considered suspect and tentatively rescored as “?”, since this structure is commonly poorly preserved or overlooked, and further investigation is needed to confirm its absence in any lambeosaurine taxon. This character was not rescored outside of Lambeosaurinae, but it is noted here that the given distribution within Brachylophosaurini is homoplastic in the consensus trees, and further confirmation may be necessary for taxa such as *Ornatops* and *Probrachylophosaurus*.

193. Prootic, ventral wing, cover the lateral side of the sphenoccipital tuber

(Ramírez Velasco 2022): absent (0); present (1). In the unmodified matrix the derived state is scored as present only in *Charonosaurus* and *Tlatolophus*. It is not evident from figures of *Charonosaurus* (Godefroit et al. 2001: figs. 4 & 5) that the prootic extends as far ventrally as in *Tlatolophus* (Ramírez Velasco et al. 2021: fig. 13A), and at least the *Parasaurolophus* cf. *cyrtocristatus* specimen UCMP 143270 appears close to the *Tlatolophus* condition (pers. obs.), potentially more so than that of *Charonosaurus*. *Parasaurolophus cyrtocristatus* was thus rescored from “0” to “1”, based on the observation of UCMP 143270, and *Parasaurolophus tubicen* was rescored from “0” to “?” pending further observation.

Modified Characters

145. Postorbital, dorsal promontorium, in adults (Prieto-Márquez 2010a, Ch. 128): absent (0); moderate development with prefrontal contact not overlying body of jugal process (1); extreme development with prefrontal contact dorsally positioned, overlying body of jugal process (2) (ordered). As noted in Chapter 4, the elevation of the dorsal promontorium in TMP 2016.023.0039 is similar to that in *Tlatolophus* and lambeosaurins, but markedly less than that in *Parasaurolophus walkeri*. An additional ordered state (“2”) was added to this character to recognize the mature condition in *Parasaurolophus walkeri* (ROM 768), *Parasaurolophus tubicen* (Sullivan and Williamson 1999: fig. 8), and *Charonosaurus* (Godefroit et al. 2001: fig. 6). *Parasaurolophus cyrtocristatus* was rescored from “1” to “?” because the observed material was immature. *Tethyshadros* was rescored from “0” to “1”, following Chiarenza et al. (2021).

173. Frontal, ectocranial surface, length/width ratio (without count its nasal process) (Prieto-Márquez 2010a, Ch. 145): greater than 0.8 (0); 0.8 or less, but greater than 0.4 (1); less than 0.4 (2); dorsal ectocranial surface reduced to basically nonexistent (3) (ordered). Evans et al. (2009) noted that CMN 52845 shares with *Brachylophosaurus*, but not *Parasaurolophus*, a frontal platform that covers the entire length of the frontal, such that there is basically no frontal exposure on the dorsal surface of the skull (except at the margins of the orbits, in *Brachylophosaurus*). However, this observation was not represented in either of their phylogenetic analyses. A new state for this character (“3”) is thus created for the condition in CMN 52845 and

Brachylophosaurus. The ordering of this character is justified by the ontogenetic series of *Brachylophosaurus canadensis*, which progresses through the states of having a short, but present frontal ectocranial surface posterior to the frontal platform (Freedman Fowler and Horner 2015: fig. 11B–D). This character is also rescored from “0” to “1” in *Probrachylophosaurus* (Freedman Fowler and Horner 2015: fig. 11A) and *Maiasaura* (see Chapter 2).

New Characters (Figure 5.1)

335. Frontal, nasal process, development of striations on sloping frontal platform: relatively widely spaced, subparallel (0); densely spaced fine ridges, rostrally

diverging (1). Evans et al. (2009: 797) noted the “long, straight striations that form the nasal articulation surface on the frontal platform” as a character of CMN 52845 that is unusual for Lambeosaurinae, but more similar to solid-crested taxa such as

Brachylophosaurus. However, this observation was not represented in either of their phylogenetic analyses. State 0 occurs in CMN 52845, *Brachylophosaurus canadensis*

(Freedman Fowler and Horner 2015: fig. 11), *Maiasaura peeblesorum* (ROM 60260,

ROM 60261, ROM 66181), *Ornatops incantatus* (McDonald et al. 2021: fig. 8),

Probrachylophosaurus bergei (Freedman Fowler and Horner 2015: fig. 11), and

tentatively *Saurolophus osborni* (Bell 2011a: fig. 9). State 1 occurs in TMP

2016.023.0039, *Corythosaurus intermedius* (ROM 776), *Hypacrosaurus altispinus*

(CMN 8675), *Hypacrosaurus stebingeri* (Brink et al. 2014: fig. 14.6), *Parasaurolophus*

sp. (CMN 8502), and more tentatively from the literature, *Amurosaurus riabinini*

(Godefroit et al. 2004b: fig. 6), *Charonosaurus jiyinensis* (Godefroit et al. 2001: fig. 4A), and *Jaxartosaurus aralensis* (Godefroit et al. 2004b: fig. 20). The striations appear to be more prominently developed in parasaurolophins than in other lambeosaurines, but this has generally not been described in such a way that can be incorporated into character scoring. Taxa that were scored as having state 0 for character 167 (sloping frontal platform absent) lack either form of ridges on the nasal facet and were scored “-” for character 335, to avoid effectively scoring the absence of the platform more than once (Brazeau 2011).

336. Frontal, distinct depressions at anterolateral corners: absent (0); present (1).

Freedman Fowler and Horner (2015) noted that frontal depressions are a widespread feature of brachylophosaurins, including *Acristavus*. The morphology of these depressions is ontogenetically variable in *Maiasaura peeblesorum* (see Chapter 2), but their presence in some form is consistent for ‘adult’-sized individuals. Distinct frontal depressions (opposed to a lateral region of the frontal that is relatively concave in correlation with a convex medial region, but lacking a clearly definable outline) have also been noted in *Jinzhousaurus* (Barrett et al. 2009), *Kritosaurus navajovius* (Prieto-Márquez 2014a), *Sahaliyana* (Godefroit et al. 2008), and *Velafrons* (Gates et al. 2007), but appear to be absent in most other hadrosauroids.

337. Frontal, ectocranial surface, texture directly posterior to nasal contact: smooth (0); tessellate (1). As noted in Chapter 3, the frontal of TMP 2010.077.0030 shares with mature individuals of *Maiasaura peeblesorum* (e.g., ROM 60260, ROM 66180) a

distinctive mosaic-like texture on the sloping region of the frontal posterior to the nasal contact, which is not seen on other skull roof elements, or well-preserved frontals of most other hadrosaur taxa. A somewhat similar irregular blister-like texture occurs on part of the posterior sloping region of the frontals in the immature *Parasaurolophus* cf. *cyrtocristatus* specimen UCMP 143270 (pers. obs.), but was not scored as the same character state.

338. Frontal, interfrontal suture in adult: present (0), absent due to fusion of frontals to each other (1). Both TMP 2010.077.0030 (Chapter 3) and TMP 2016.023.0039 (Chapter 4) were noted to have fused frontals, as in *Maiasaura peeblesorum* (Chapter 2) and *Tlatolophus* (Ramírez Velasco et al. 2021). This character was found to be ontogenetically dependent in *Maiasaura* (Chapter 2), but appears to also have some taxonomic signal. For example, Barrett et al. (2009) considered fusion of the frontals to be an autapomorphy of *Jinzhousaurus*, contrasting with the separate frontals of *Iguanodon*, *Probactrosaurus*, *Eolambia*, *Protohadros*, and most hadrosaurids. The frontals were described as fused in the holotype of *Sahaliyania* in the original description by Godefroit et al. (2008), but separate in the redescription by Xing et al. (2022), so *Sahaliyania* is scored “?” here. This character was deliberately left unscored in taxa for which the examined material was immature, such as *Parasaurolophus cyrtocristatus* and *Velafrons*.

339. Parietal, interfrontal process, shape of dorsal exposure: short (wider than long) (0); elongate (longer than wide). As noted in Chapter 4, TMP 2016.023.0039 shares

with *Parasaurolophus* a proportionately narrow, anteroposteriorly elongated interfrontal process, in contrast with the short, mediolaterally wide interfrontal process present in lambeosaurins, basal lambeosaurines, and most other hadrosauroids. An elongate interfrontal process is also present in *Edmontosaurus annectens* (CMN 8509) and *Edmontosaurus regalis* (CMN 2289). The outlines of the parietals in the figures of *Charonosaurus* (Godefroit et al. 2001: fig. 4A) and *Tlatolophus* (Ramírez Velasco et al. 2021: fig. 12C) are suggestive of state “0”, but this has not been independently verified by looking at the fossils without interpretive lines, and these taxa were cautiously scored “?”.

340. Parabasisphenoid, alar process, orientation: attaches to braincase wall along anterior side and projects posterolaterally (0); free anterior edge and projects ventrally (1).

As noted in Chapter 4, TMP 2016.023.0039 shares with *Parasaurolophus cyrtocristatus* and *Parasaurolophus tubicen* a ventrally pendent alar process with a substantial anterior edge detached from the surrounding parabasisphenoid, whereas in lambeosaurins the anterior edge of the alar process is attached along the braincase wall and the process projects more posterolaterally, as in non-lambeosaurines (eg.

Maiasaura). State 1 has not been observed outside of putative parasaurolophins. Based on the published figures, state 1 is possibly present in *Charonosaurus* (Godefroit et al. 2001: fig. 4B and 5A) and *Tlatolophus* (Ramírez Velasco et al. 2021: fig. 13), but this has not been confirmed through direct observation, and these taxa were cautiously scored “?”.

341. Laterosphenoid, postorbital process orientation: projects dorsolaterally, such that the angle between the left and right postorbital processes approximately 180° in ventral view (0); projects anterodorsolaterally, such that the angle between the left and right postorbital processes is approximately 120–130° in ventral view (1). As noted in Chapter 4, TMP 2016.023.0039 resembles lambeosaurins, but differs from *Parasaurolophus*, in having the postorbital processes of the laterosphenoids angled anterodorsolaterally rather than straight out dorsolaterally. The scoring of the “*Parasaurolophus walkeri*” OTU as “0” is based on the tentatively referred specimen CMN 8502, using the justification explained for character 166. The outline of the laterosphenoid in the figure of *Tlatolophus* (Ramírez Velasco et al. 2021: fig. 11B) is also suggestive of state 0, but this has not been independently verified by looking at the fossil without interpretive lines, and this taxon was cautiously scored “?”. State 0 is also usually present in non-lambeosaurines. A possible exception scored “1” from the literature is *Eolambia* (McDonald et al. 2012: fig. 19F), which one preliminary phylogenetic analysis did recover as a basal lambeosaurine (Kirkland 1998), though not by using this character.

Currently Unscored Characters (Figure 5.2)

Prefrontal, thickness of orbital rim: robust with dorsoventrally thick lateral edge (0); thin, with laminar lateral edge (1). Both TMP 2010.077.0030 (Chapter 3) and TMP 2016.023.0039 (Chapter 4) were noted to have especially thick prefrontals when contrasted with *Brachylophosaurus* and *Corythosaurus*, respectively. However, only the posterior portion of the prefrontal in each specimen is preserved, so the complete shape

of this element cannot be described. Further reasons for excluding this character from the present analysis include the unclear dividing line between the “thick” and “thin” states, the unevaluated potential for ontogenetic or individual variation, and the difficulty in distinguishing from photographs, especially when the edge of the prefrontal rim may be displaced or distorted. The thickness of the rim of the prefrontal may still have some phylogenetically informative signal in hadrosaurids, but the distribution of variation has not been determined satisfactorily.

Frontal, slope of ectocranial surface: flat or slightly sloping posterodorsally (0); prominently sloping anterodorsally (1). As noted in Chapter 3, the preserved portion of the frontal in TMP 2010.077.0030 is sloped anterodorsally over much of its preserved length, which was cited as a shared character with *Maiasaura peeblesorum*. In *Maiasaura*, the strongly anterodorsally sloping ectocranial surface of the frontal appears to develop later in ontogeny than the high-angled frontal platform (char. 166: 3), with ROM 66181 showing weak development of the former, but strong development of the latter (Chapter 2). However, in the fully developed crest these could be argued to merely describe opposite sides of the same character state, which is already adequately represented in the character list as the cranial crest being composed primarily of the nasals and frontals (char. 220: 1), and correlated with the solid crest form being a folded transverse crest (char. 221: 3), which is a character state exclusive to *Maiasaura peeblesorum* in this matrix. An additional character state unique to the formation of the *Maiasaura* crest could be criticized as overweighting. Unfortunately, without the nasal contact preserved, TMP 2010.077.0030 cannot be scored as having either of those

character states without interpreting it as a *Maiasaura*-like hadrosaur *a priori*, because as an isolated character state, the condition of an anterodorsally sloping ectocranial region of the frontal also describes some lambeosaurines, such as *Parasaurolophus*, which have a very different crest composition and morphology. In some sense an anterodorsally sloping ectocranial region of the frontal can be considered widely occurring in lambeosaurines, even in the absence of a very steep frontal platform, such as in *Lambeosaurus lambei* (ROM 794). However, the externally visible slope of the dorsal surface of the frontal can be modified in at least two ways: increasing the thickness of the frontal bone, and dorsal expansion/reorientation of the underlying endocranial cavity. In TMP 2010.077.0030 it is the former, but in a specimen that does not have an accessible view of the anterior this could be ambiguous, and the character would risk conflating two states that are not equivalent, or be widely unscorable. The exclusion of this character is thus uncertain, but may be reworkable with more data collection as an independent character relating to the anterodorsal thickening of the frontal bone behind the nasal articulation producing a slope, with the derived state restricted to *Maiasaura*-like and *Parasaurolophus*-like forms (including TMP 2016.023.0039).

Supraoccipital, elevation of ascending process: similar to height of squamosal bosses (0); dorsal to squamosal bosses (1), or similar characters. As noted in Chapter 4, variation in the supraoccipital of lambeosaurines, and possibly hadrosauroids generally, is underappreciated in phylogenetic analyses. An example of a variable character is the dorsal elevation of the median ascending process, which has been figured as similar to the height of the squamosal bosses in some taxa such as *Aralosaurus* (Godefroit et al.

2004a: fig. 2C) and *Amurosauros* (Godefroit et al. 2004b: fig. 7C), but projects much higher in TMP 2010.023.0039 (Chapter 4). Unfortunately, such characters would be unscorable in many examined skulls due to obfuscation by the articulated squamosals, insufficient preparation, or poor preservation of this region.

Otoccipital, paroccipital process “neck” in posterior view: mediolaterally long with a shallowly curved ventral margin (0); mediolaterally compact with a strongly

arched ventral margin (1). As noted in Chapter 4, the ventral margin of the otoccipital between the supraoccipital and the paroccipital process in TMP 2016.023.0039 is

relatively long and shallowly curved, as in *Charonosaurus* and some other

lambeosaurines, differing from the more compact, arched condition that brings the

paroccipital process closer to the braincase wall in *Tlatolophus* (Ramírez Velasco et al.

2021: fig. 13B), *Parasaurolophus walkeri* (ROM 768), and some other lambeosaurines.

Although this may be a phylogenetically informative character at its end points, it has not yet been established where the line between the two states should be drawn in the case of specimens not clearly at either extreme, so there is a risk of scorings being ambiguous or

subjective. This character may also be particularly sensitive to postdepositional

deformation, and is expressed asymmetrically in some lambeosaurine specimens, such as

the holotype of *Parasaurolophus tubicen* (Sullivan and Williamson 1999: fig. 8E). The

braincase in TMP 2016.023.0039 itself is clearly asymmetrically deformed and missing

the paroccipital process on the right side, so the appropriateness of this character for

determining its phylogenetic position should at least be further examined.

Parabasisphenoid, form of alar process: medium-to-large (or symmetrical) (0); very reduced (or asymmetrical). Gates et al. (2021) noted that *Parasaurolophus cyrtocristatus* and *Parasaurolophus tubicen* share a tiny, teardrop-shaped alar process of the parabasisphenoid that is among the most reduced in size compared to other lambeosaurines (unknown in *Parasaurolophus walkeri*). In TMP 2016.023.0039, the alar process is larger and more rectangular, which is probably plesiomorphic and suggests that it is not a member of the *P. cyrtocristatus* + *P. tubicen* clade. If scored on the basis of size, this proposed character has essentially the same absence state as character 186 (a moderately developed, “standard issue” alar process), so could logically be combined into an ordered multistate character making the “tiny” condition state 0, the medium condition state 1, and the enlarged condition state 2. This would require a complete revisitation of all taxa currently scored “0” to decide on the appropriate boundaries between the states and which taxa to promote to the new state “1,” which would be difficult to confidently complete from the literature (measurements of this process are not typically included in descriptions). Separating the character states by shape, between symmetrical/asymmetrical or rectangular/triangular may also be a viable approach, but would require a cautious avoidance of scoring from specimens in which this thin process has acquired a misleading shape through damage.

Parabasisphenoid, lateral surface of basipterygoid process: relatively flat surface (0); distinct anterodistal swelling continuous with the ventral lamina of the cultriform process, bounded by a posterodorsal groove (1). As noted in Chapter 4, TMP 2016.023.0039 shares a distinctive morphology of the basipterygoid process with

Hypacrosaurus altispinus, which is absent in some other lambeosaurines. The distribution of this character state observed so far is not suggestive of the currently recognized phylogenetic relationships, but the character may have some phylogenetic signal when investigated in greater detail.

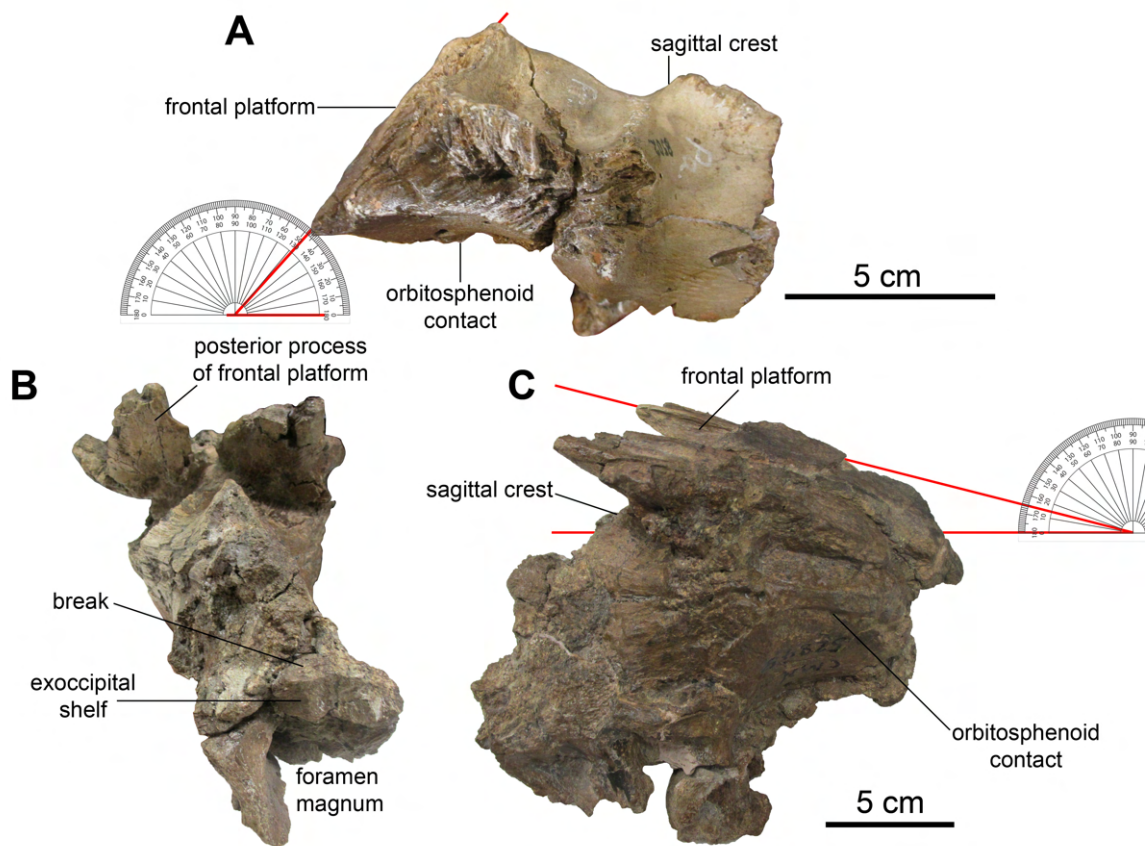
Prootic, ventral wing, forming a pit- or pocket-like fossa dorsal to the basal tubera:

absent (0); present (1). This character was originally proposed as an autapomorphy of *Maiasaura peeblesorum* Hickie et al. (2015), based on observation of ROM 66180. Further observations support this being a consistent feature of the braincase in that taxon, but also present in the holotype of the closely related taxon *Brachylophosaurus canadensis* (Chapter 2). The presence of a similar pit was noted in TMP 2010.077.0030 as a character that may link it to brachylophosaurins (Chapter 3). However, the distribution of this character state among hadrosauroids has been difficult to conclusively establish, both because it is a small feature that can easily be ambiguous in published figures, and because it can also be difficult to evaluate directly on specimens that are broken, weathered, or insufficiently prepared in this region. The functional significance of this structure, if any, has not been determined. Pending further information, it is excluded from the present analysis.

Notes on Character Scoring in CMN 52845— The anatomy of CMN 52845 was described in detail by Evans et al. (2009a), so it was not deemed necessary to fully redescribe it here, apart from reinterpretations that affect the character scoring. Evans et al. (2009a) did not describe their method for orienting the horizontal axis of the

braincase, which due to the fragmentary condition of the specimen is not immediately obvious. However, the orientation of the ventral edge of the frontal can be standardized using the contact along the orbitosphenoid, which is approximately horizontal in other hadrosaurid braincases examined (Figure 5.3). Evans et al. (2009a) interpreted CMN 52845 as having a very steep frontal platform (character 40 of Evans and Reisz 2007; character 166 of Ramírez Velasco 2022 and this study), which was scored as being the same character state as in *Parasaurolophus*, and used to support the referral of this specimen to cf. *Parasaurolophus* sp. The inclination of the frontal platform in CMN 52845 cannot be measured with ideal precision, because the braincase is distorted (Figure 5.3B), and there has been minor reconstruction with plaster fill at the connection between the frontal platform and the rest of the braincase. However, the angle of frontal platform is clearly much shallower in relation to the frontal-orbitosphenoid contact than in the *Parasaurolophus* specimen CMN 8502 (Figure 5.3), and they are scored as different states for this character in the present analysis. Reorienting the specimen so that the frontal-orbitosphenoid contact approximates the horizontal also rotates the parietal such that the anterior part of the sagittal crest is no longer strongly inclined posterodorsally (character 44 of Evans and Reisz 2007; character 4 of Godefroit et al. 2008; character 178 of Ramírez Velasco 2022 and this study), another character that Evans et al. (2009a) cited in favour of a lambeosaurine affinity for CMN 52845. Because so little of the sagittal crest is actually preserved, its posterodorsal inclination is scored here as unknown, rather than absent. Finally, the extent of the exoccipital above the foramen magnum has an apparently conflicting interpretation in Evans et al. (2009a). The “relatively long ridge that marks the midline contact of the exoccipitals above the foramen magnum” is

Figure 5.3 Comparison of hadrosaurid braincases, showing differences in the inclination of the frontal platform (red lines): A) CMN 8502 (*Parasaurolophus* sp.) in left lateral view, showing a high angled frontal platform (character 166, state 3); B) CMN 52845 (Brachylophosaurini) in posterior view, showing distortion of the braincase; C) CMN 52845 in right lateral view, showing a lower angled frontal platform (character 166, state 1).

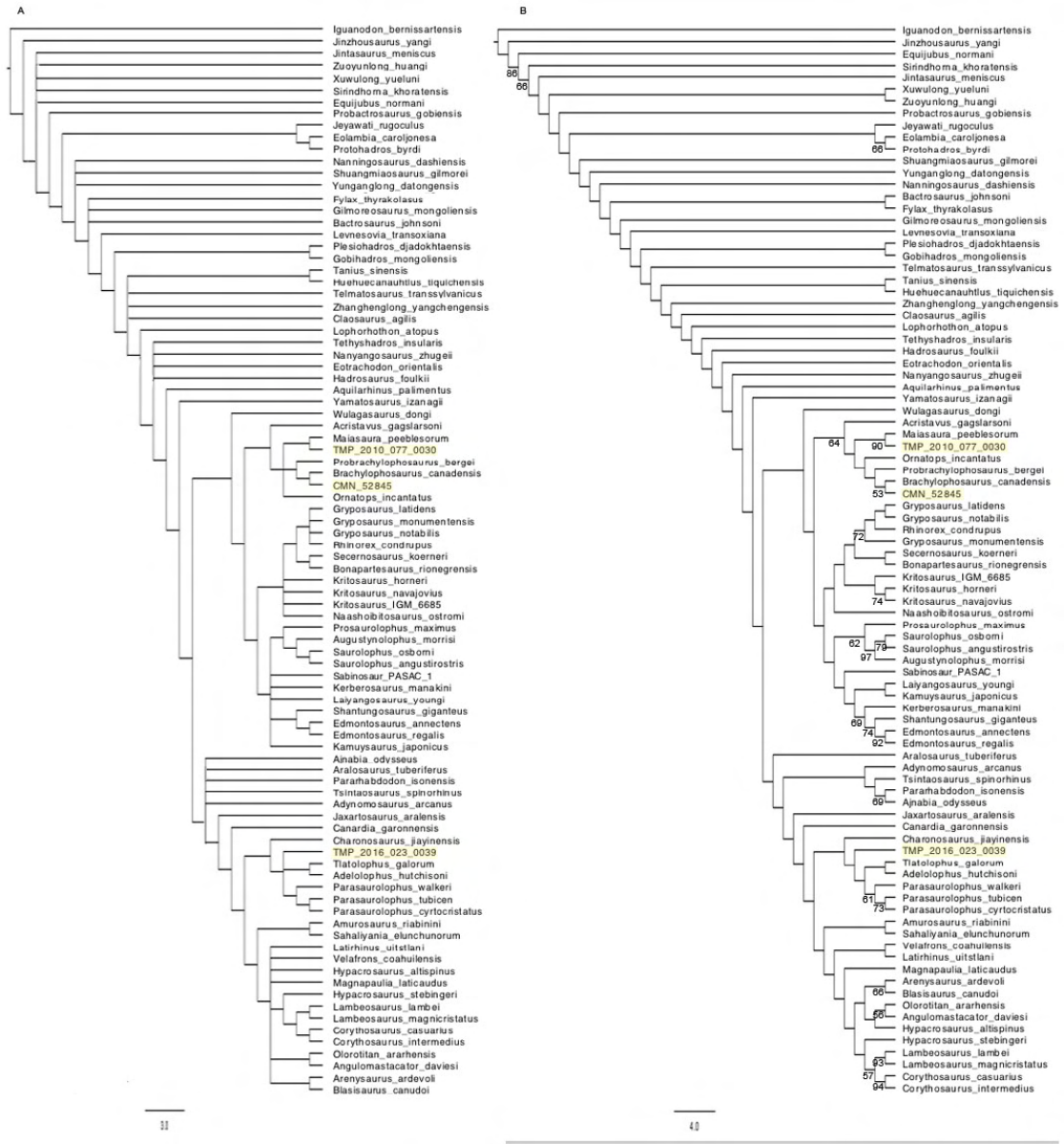


mentioned in the text as evidence against a lambeosaurine identity (Evans et al. 2009a: 797), but in the phylogenetic analysis CMN 52845 was scored as having the lambeosaurine condition of a limited exoccipital shelf above the foramen magnum (character 26 of Godefroit et al. 2008, character 181 of Ramírez Velasco 2022 and this study). In CMN 52845 the exoccipitals above the foramen magnum are badly damaged (Figure 5.3B), but the morphology of the preserved region would be just as consistent with resembling *Brachylophosaurus* (CMN 8893). This character is scored as unknown.

5.3 Results

The maximum parsimony analysis retained 100 most parsimonious trees with a length of 1424 steps. The consistency index (CI) was 0.3427 (0.3394 excluding uninformative characters) and the retention index (RI) was 0.7660, both similar to the values reported by Ramírez Velasco (2022). In the strict consensus tree (Figure 5.4A), TMP 2010.077.0030 is recovered within Brachylophosaurini as the sister taxon of *Maiasaura peeblesorum*, TMP 2016.023.0039 is recovered within Parasaurolophini in a polytomy with *Parasaurolophus* and the *Adelolophus* + *Tlatolophus* clade, and CMN 52845 is recovered within Brachylophosaurini as the sister taxon of *Brachylophosaurus canadensis*. The strict consensus tree otherwise resembles that of Ramírez Velasco (2022), except that the basal hadrosauromorph region of the tree is slightly more resolved (agreeing with the 50% majority-rule consensus tree of Ramírez Velasco 2022), and *Ornatops* is in an unresolved polytomy with the *Maiasaura* and *Brachylophosaurus* clades, rather than definitively closer to *Brachylophosaurus* than to *Maiasaura*. In the 50% majority-rule consensus tree (Figure 5.4B), TMP 2016.023.0039 is further resolved

Figure 5.4 Consensus trees of the maximum parsimony analysis: A) strict consensus tree; B) 50% majority-rule consensus tree. Bootstrap supports over 50% are shown below nodes.



as the sister taxon of a *Parasaurolophus* + *Tlatolophus* + *Adelolophus* clade. The 50% majority-rule consensus tree is also similar to that of Ramírez Velasco (2022), with the following minor differences: *Fylax* is recovered as the sister taxon of *Bactrosaurus* rather than the sister taxon of *Gilmoreosaurus*, *Gryposaurus notabilis* is recovered as the sister taxon of *Gryposaurus latidens* rather than the sister taxon of *Gryposaurus monumentensis*, the Mexican kritosaurin is recovered as the sister taxon of *Kritosaurus* exclusively, rather than the sister taxon of *Kritosaurus* + *Gryposaurus*, and *Latirhinus* is recovered as the sister taxon of *Velafrons*, rather than closer to the clade including *Lambeosaurus* than to *Velafrons*. The bootstrap 50% majority-rule consensus tree retained the TMP 2016.023.0039 + *Maiasaura peeblesorum* and CMN 52845 + *Brachylophosaurus canadensis* clades with bootstrap support values of 90 and 53, respectively. The clade Brachylophosaurini including these taxa, *Acristavus*, *Ornatops*, and *Probrachylophosaurus* was retained as a polytomy with a bootstrap support value of 64. The parasaurolophin clade of TMP 2016.023.0039 + *Parasaurolophus* + *Tlatolophus* + *Adelolophus* collapsed in the bootstrap analysis, with these taxa forming a large polytomy with other hadrosauroids more derived than *Equijubus*. However, the bootstrap tree did retain a resolved, monophyletic *Parasaurolophus* (*P. walkeri* + *P. cyrtocristatus* + *P. tubicen*) with a bootstrap support value of 61, and a *P. tubicen* + *P. cyrtocristatus* clade with a bootstrap support value of 73, supporting the inference that TMP 2016.023.0039 is not nested within the traditionally recognized genus *Parasaurolophus*.

The Bayesian majority-rule consensus tree (Figure 5.5) recovered TMP 2010.077.0030 within Brachylophosaurini as the sister taxon of *Maiasaura peeblesorum* (posterior probability of 0.98), TMP 2016.023.0039 within Parasaurolophini as the sister

Figure 5.5 Majority-rule consensus tree of the Bayesian phylogenetic analysis, with posterior probabilities displayed at nodes.



taxon of *Tlatolophus galorum* (posterior probability of 0.33), and CMN 52845 within Brachylophosaurini as the sister taxon of *Brachylophosaurus canadensis* (posterior probability of 0.79). The Laramidian parasaurolophin clade common to both analyses had a posterior probability of 0.8. This tree differs from the strict consensus tree of the maximum parsimony analysis in various aspects including the positions of *Fylax* and *Jintasaurus* outside of and within Hadrosauromorpha, respectively; the position of Brachylophosaurini (including *Wulagasaurus*) outside of Euhadrosauria; the position of *Bonapartesaurus* within Lambeosaurinae; the taxa comprising Lambeosaurini in the most parsimonious trees instead forming a paraphyletic grade with respect to Parasaurolophini; and the novel, essentially “inverted” topology of the Laramidian parasaurolophin clade, including a different position for TMP 2010.023.0039.

5.4 Discussion and Conclusions

Comparison of maximum parsimony and Bayesian results— Although differing in other details, the maximum parsimony and Bayesian consensus trees agree that TMP 2010.077.0030 is the sister taxon of *Maiasaura peeblesorum*; TMP 2016.023.0039 is a member of a Laramidian parasaurolophin clade that also includes *Parasaurolophus*, *Tlatolophus*, and *Adelolophus*; and CMN 52845 is the sister taxon of *Brachylophosaurus canadensis*. These results support a major premise of this thesis: that even incomplete hadrosaur specimens preserving only skull roof and braincase characters contain sufficient information to be placed in phylogenetic context with reasonable degrees of precision and repeatability, and thus be able to inform hypotheses of hadrosaur evolution.

The most parsimonious trees did not strongly differ from those resulting from a similar matrix without the addition of the new taxa and characters (Ramírez Velasco 2022). The Bayesian consensus tree in this analysis is somewhat reminiscent of the unconventional Bayesian topologies reported by Prieto-Márquez (2010a) and Gates and Scheetz (2015), in that the usual content of “Saurolophinae” is paraphyletic with respect to Lambeosaurinae, and the usual content of “Lambeosaurini” is paraphyletic with respect to Parasaurolophini. However, in this analysis the majority of core Saurolophinae (Kritosaurini + Saurolophini + Edmontosaurini) is still recovered as monophyletic with the conventional internal topology, and only Brachylophosaurini falls outside of Euhadrosauria. A similar topology was recovered, but not discussed, in the strict consensus tree of the maximum parsimony analysis of Serrano-Brañas and Prieto-Márquez (2022). The earliest (pre-middle Campanian) stages of the euhadrosaurian radiation remain comparatively poorly represented in the fossil record (Prieto-Márquez et al. 2020), and such alternative topologies are thus more difficult to assess and dismiss as being biostratigraphically or palaeobiogeographically incongruent. Other aspects of the Bayesian consensus tree that differ from the most parsimonious trees also have some precedent in the literature, for example, the position of the hadrosauroid *Jintasaurus* as a hadrosauromorph in the same region of the tree as *Telmatosaurus* and *Claosaurus* is similar to its position recovered in the maximum parsimony analysis of Prieto-Márquez et al. (2016).

Relationship of TMP 2010.077.0030 to *Maiasaura peeblesorum*— A sister-group relationship between TMP 2010.077.0030 and *Maiasaura peeblesorum* is supported by the mosaic-like texture on the ectocranial region of the frontals (char. 337: 1), the fusion

of the interfrontal suture (char. 338: 1), the dorsoventral expansion of the squamosals in posterior view (char. 157: 1), an anterior spur on the preotic wing of the parabasisphenoid (char. 185: 1; optimized as convergently present in *Brachylophosaurus canadensis*, but scorings in other brachylophosaurins may need further verification), and possibly the small, slender ventral process of the nasal (char. 74: 2), though this may be variable in *M. peeblesorum*. The frontal slope character discussed under unscored characters would also optimize as a synapomorphy of this clade, if included. The long, preserved portion of the alar process (char. 186: 1) provides additional support for a general brachylophosaurin affinity. The recovered phylogenetic position of TMP 2010.077.0030 is consistent with its proposed taxonomic referral to *Maiasaura* sp. (Chapter 3). This analysis is not designed to test whether or not TMP 2010.077.0030 falls within an appropriate range of morphological and stratigraphic variation to be included within the species *M. peeblesorum*.

Relationships of TMP 2016.023.0039 within Parasaurolophini— The inclusion of TMP 2016.023.0039 in the Laramidian parasaurolophin clade containing *Parasaurolophus* and *Tlatolophus* is unambiguously supported by the very steep frontal platform (char. 166: 3), assuming that the rescoring of *Charonosaurus* as having a shallower frontal platform is correct. General parasaurolophin characters of TMP 2016.023.0039 include a proportionately short ectocranial surface of the frontal (char. 173: 2), and potentially the fusion of the interfrontal suture (char. 338: 1), a narrow interfrontal process of the parietal (char. 339: 1), a ventrally pendent alar process on the parabasisphenoid (char. 340: 1), and the ventral wing of the prootic covering the lateral side of the basal tubera (char. 193: 1), though the distributions of the latter four characters

in parasaurolophins require further confirmation. A *Parasaurolophus* + *Tlatolophus* clade excluding TMP 2016.023.0039, as recovered in the 50% majority-rule consensus tree of the maximum parsimony analysis, is supported by the presence in those taxa of an extension of the frontals overhanging the parietal (char. 165: 1, assuming that the absence of this character state in TMP 2016.023.0039 is real and not preservational), and potentially by the reversion from anterodorsolaterally to dorsolaterally projecting postorbital processes of the laterosphenoids (char. 341: 0), though the latter character was unscored in *Tlatolophus* for this run. However, if *Tlatolophus* is confirmed to have a short, wide interfrontal process of the parietal (char. 339: 0), as seems likely from the description and figures (Ramírez Velasco 2021: fig. 12C), that character would lend support to an alternate topology in which TMP 2016.023.0039 and *Parasaurolophus* form a clade to the exclusion of *Tlatolophus*. None of the individual characters considered in this analysis unambiguously support a sister-group relationship between TMP 2016.023.0039 and *Tlatolophus*, as recovered (albeit with low posterior probability) in the Bayesian consensus tree. However, these two parasaurolophins do present a similar overall combination of skull roof characters that includes a modestly elevated prefrontal process on the postorbital (char. 145: 1), a very steep frontal platform (char. 166: 3), and a triangular plateau on the parietal between the interfrontal process and the sagittal crest (char. 179: 1). They are also the only two parasaurolophins presently scored as having fused frontals (char. 338: 1), as this was cautiously left unscored in *Charonosaurus* and all species of *Parasaurolophus*. The uncertain position of TMP 2016.023.0039 among Laramidian parasaurolophins is probably exacerbated by the uncertainties in scoring of some of the other taxa in this clade, with some characters scored overly cautiously, or

potentially, incorrectly. Although *Charonosaurus* was consistently recovered as the earliest-diverging parasaurolophin in this study, other recent analyses have recovered it as deeply nested within *Parasaurolophus* (Longrich et al. 2021; Xing et al. 2022), which could potentially affect the polarization of character states that determine the phylogenetic position of TMP 2016.023.0039. As there is some conflicting information in the literature on its morphology, and the knowledge base of other parasaurolophins has improved considerably since its last description (Evans et al. 2007; Gates et al. 2021; Ramírez Velasco et al. 2021; Chapter 4), a thorough redescription of the *Charonosaurus* material may be justified.

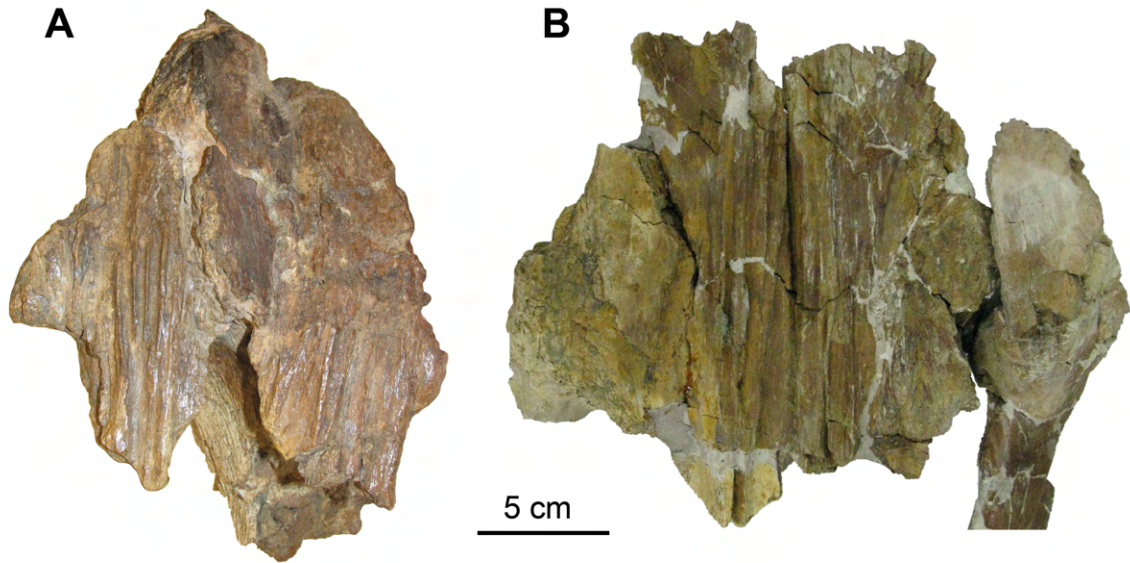
In Chapter 4, I suggested that no anatomical evidence is known to exclude the possibility of TMP 2016.023.0039 representing a taxon directly ancestral to *Parasaurolophus*. In the 50% majority-rule consensus tree, *Parasaurolophus* is recovered as sharing a more recent common ancestry with the geologically older *Adelolophus* than with TMP 2016.023.0039, implying that the divergence of the *Parasaurolophus* and TMP 2016.023.0039 lineages had already occurred prior to the deposition of the Oldman Formation. However, since *Adelolophus* and TMP 2016.023.0039 are each known from quite limited material that does not overlap, it is certainly possible that when more complete remains of these taxa are known, the balance of character evidence will shift to supporting a most parsimonious topology that does not require three separate parasaurolophin lineages (*Parasaurolophus*, *Adelolophus-Tlatolophus*, and TMP 2016.023.0039) existed at the same time in middle Campanian Laramidia.

Ramírez Velasco (2022) performed a Statistical Dispersal-Vicariance analysis and concluded that although lambeosaurines arrived in Laramidia from Asia, Laramidian

parasaurolophin evolution occurred preferentially in the southern Laramidian zone, and *Parasaurolophus walkeri* represents a single dispersal event into northern Laramidia. The present analysis did not recover a sister-group relationship between the two northern Laramidian taxa (TMP 2016.023.0039 and *P. walkeri*), which could suggest either that parasaurolophins had an even more complex palaeobiogeographic history in Laramidia than previously recognized, or alternatively that a strong north-south provincialism may have simply not meaningfully existed during at least some stages of their evolution.

Relationship of CMN 52845 to *Brachylophosaurus canadensis*— A sister-group relationship between CMN 52845 and *Brachylophosaurus canadensis* is unambiguously supported by practically the entire dorsal length of the frontals being covered by the frontal platform (char. 173: 3). CMN 52845 differs from the holotype of *B. canadensis* (CMN 8893) in the possession of a posterior extension of the frontal platform overhanging the parietal (char. 165: 1), which is here interpreted as convergently evolved in *Parasaurolophus*. In CMN 8893, the frontals are prevented from overhanging the parietals by the posteromedial expansion of the prefrontals, which wrap around the posterior limit of the frontal platform to provide additional support for the solid nasal crest. However, in this aspect CMN 52845 appears to closely resemble MOR 720 (Figure 5.6), a specimen from the upper Judith River Formation of Montana that is referred in the literature to *B. canadensis* (Freedman Fowler and Horner 2015; McDonald et al. 2021). Notably, Freedman Fowler and Horner (2015: 22–23) described the posterior extension of the platform supporting the nasal crest in MOR 720 as being composed of the frontals, rather than the prefrontals as in other specimens included in *B. canadensis*, and overhanging the dorsotemporal fenestrae by “at least 5 cm,” similar to CMN 52845.

Figure 5.6 Brachylophosaurin skull roofs in dorsal view: A) CMN 52845; B) MOR 720, from Freedman Fowler and Horner 2015: Fig. 11E, reproduced under the terms of the Creative Commons Attribution License.



Rescoring character 165 in *B. canadensis* as “0&1” to include the state in MOR 720 does not change the topology of the consensus tree in the maximum parsimony analysis. A more complete description of MOR 720 is needed to determine whether its referral to *B. canadensis* is justified, or if it and CMN 52845 could represent a new brachylophosaurin taxon occurring stratigraphically higher than *B. canadensis*, and diagnosable by the posterior extension of the frontal platform over the parietal.

CMN 52845 is among the stratigraphically highest records of Brachylophosaurini, and constitutes the first record of a brachylophosaurin in the Dinosaur Park Formation (Ryan and Evans 2005). The middle of the Dinosaur Park Formation is approximately coeval with the lower unit of the Kaiparowits Formation in the southern Utah (Roberts et al. 2005), which has produced an isolated jugal identified as the stratigraphically highest “brachylophosaur” by Gates et al. (2013). The occurrence of a brachylophosaurin in the Dinosaur Park Formation is nonetheless surprising, given the abundant and well-studied hadrosaur record of this formation, and highlights how study of even fragmentary skull roof and braincase material can provide significant new insights into hadrosaur diversity.

Chapter 6: Conclusions

In this thesis I sought to investigate the morphology, ontogeny, and evolution of skull roof and braincase characters in hadrosaurids from the Campanian of northern Laramidia (Alberta and Montana), a setting in which they have been historically recognized as having a high abundance and diversity (Horner et al. 2004; Ryan and Evans 2005). I predicted that the description of new material would clarify the distribution and informativeness of morphological character states, allow further testing of previous hypotheses about how the ontogenetic development of these characters evolved within clades, and enable the identification of previously unrecorded taxa, potentially including those implied to have existed during this time by ghost lineages. Material described included a series of *Maiasaura peeblesorum* from a bone bed in the Two Medicine Formation of Montana documenting the ontogenetic development of the cranial crest (Chapter 2), and two new specimens from the middle Oldman Formation of southern Alberta referred to *Maiasaura* sp. (Chapter 3) and a new genus and species of Parasaurolophini (Chapter 4), both representing previously unknown taxa in that assemblage and providing new insights into this comparatively little-known assemblage occurring stratigraphically below the more intensively studied hadrosaurids of the Dinosaur Park Formation. A phylogenetic analysis including these specimens (Chapter 5) supported these identifications, as well as recovering the previously described “cf. *Parasaurolophus* sp.” specimen CMN 54825 in a novel phylogenetic position beside *Brachylophosaurus canadensis* within Brachylophosaurini. A general congruence

between the maximum parsimony and Bayesian consensus trees in the positions of the newly added taxa adds to the confidence of the phylogenetic conclusions.

6.1 New Findings on Skull Roof and Braincase Morphology

The skull roof and braincase morphology of *Maiasaura peeblesorum* is now well characterized on the basis of multiple individuals. Braincase anatomy is similar to other brachylophosaurins, although the presence at large size of a well-defined ventral channel on the overhanging crista prootica may be autapomorphic. Minor differences in the positions of cranial nerve foramina do not appear taxonomically significant. The description of the skull roof and braincase anatomy of *M. peeblesorum* allows one of the specimens from the Milk River Ridge Reservoir locality, TMP 2010.077.0030, to be referred to *Maiasaura* sp. based on multiple shared characters that differ from *Brachylophosaurus*, including the thickened posterior slope and ornamented texture of the dorsal surface of the fused frontals, and relationship between the postorbital and squamosal in the construction of the temporal bar. The other new specimen from the Milk River Ridge Reservoir locality, TMP 2016.023.0039, has a diagnostic unique combination of parasaurolophin synapomorphies such as a very steeply sloping frontal platform and anteroposteriorly short, boomerang-shaped ectocranial region of the frontal, and character states more common seen in lambeosaurins such as *Hypacrosaurus*, including anterolaterally projecting postorbital processes of the laterosphenoids, a triangular plateau on the parietal between the interfrontal process and the short sagittal

crest, and potentially a distinctive morphology of the basipterygoid processes. This taxon is interpreted as representing a more plesiomorphic parasaurolophin morphology than the stratigraphically higher *Parasaurolophus*. The problematic *Brachylophosaurus*-like characters of the “cf. *Parasaurolophus* sp.” specimen CMN 54845 that were previously noted by Evans et al. (2009a) are here interpreted as synapomorphies placing it in the *Brachylophosaurus* clade (as used here to refer to hadrosaurs sharing a more recent common ancestry with *B. canadensis* than with *M. peeblesorum*). The condition of the extended frontal platform overhanging the parietal, once uniquely shared between CMN 54845 and *Parasaurolophus*, is now also reported in a referred specimen of *Brachylophosaurus* (Freedman Fowler and Horner 2015).

The description of new *Maiasaura* and parasaurolophin material highlights a morphological convergence between the skull roofs of these taxa that is not commonly remarked upon. Although these clades evolved very dissimilar cranial crest morphologies with respect to the roles of the premaxillae, nasals, and prefrontals, both developed a very steeply angled frontal platform, with a similar thickening of the frontals behind the platform forming a transversely broad, sloping posterior wall or buttress of the crest. This morphology is different from the recruitment of the frontals into the crest in *Saurolophus*, which involved a pair of narrow processes rising dorsally from flat frontals (Bell 2011a: Fig. 5). Fusion of the frontals along the midline is observed in mature specimens of *Maiasaura* and at least some parasaurolophins, but is rare among other hadrosaurids. *Maiasaura* differs from stratigraphically lower, more plesiomorphic brachylophosaurins

such as *Acristavus* (Gates et al. 2011) in the mature frontals being proportionately short and compact posterior to the nasal contact, and the moderate dorsomedial expansion of the squamosals posteriorly, both characters shared with lambeosaurines including *Parasaurolophus*. In stratigraphically higher members of the *Parasaurolophus* lineage, the sagittal crest of the parietal is extended to the anterior end of the element, and the postorbital processes of the laterosphenoids project straight outwards away from one another, superficially reminiscent of some non-lambeosaurines including *Maiasaura*, in contrast to the more lambeosaurin-like conditions of these characters in TMP 2016.023.0039, which are potentially plesiomorphic for corythosaurians. Despite having some similarities, though, the skull roofs and braincases of these clades remain morphologically distinguishable. For example, *Maiasaura* retains the long, angled, posterolaterally oriented parabasisphenoid alar processes of other brachylophosaurins, regardless of frontal crest development, whereas in parasaurolophins such as TMP 2016.023.0039, the alar process is modified into a short, ventrally pendent structure. This variability of character combinations suggests that the overall morphology of the hadrosaur braincase was determined by a complex interaction of factors.

The variation found in the hadrosaurid braincase, especially in characters that are informative for diagnosing and distinguishing clades or species, is interesting from a functional perspective. Hadrosaurs in general are distinguished from basal ornithomids by the greater development and complexity of the preotic pendant of the parabasisphenoid, on which the protractor pterygoideus attaches to the braincase and is bounded posteriorly

by the alar process (Holliday 2006; Holliday and Witmer 2008). The parallel lateral ridges described on the parabasisphenoid of the Oldman Formation *Maiasaura* sp. are of uncertain taxonomic significance, but add to the diversity of morphological features, and potential soft tissue correlates, associated with this region. The alar process itself is interpreted as the ossified end of a ligament that connected the braincase and the palate (Holliday 2006). The basiptyergoid processes, which also show morphological diversity between hadrosaurid taxa, also connect the braincase to the palate by articulating with the pterygoid. The new Oldman Formation parasaurolophin is diagnosed in part by a unique combination of characters relating to the braincase/palate connection, supportive of a parasaurolophin affinity but distinct from stratigraphically higher specimens belonging to *Parasaurolophus*. The selective pressures that resulted in the observed diversity in the size, shape, and orientation of these structures on the hadrosaurid braincase is not often discussed in the literature describing new specimens or taxa, but hints that functional variation in the braincase/palate connection may have been important in the finer-level diversification of this clade, and its adaptation to changing environments.

6.2 New Findings on Distributions and Palaeoecology

Prior to this work, the “*Maiasaura* clade” (hadrosaurs sharing a more recent common ancestry with *Maiasaura peeblesorum* than with *Brachylophosaurus canadensis*) was represented exclusively by *M. peeblesorum* from the Two Medicine Formation of northwestern Montana. The referral of TMP 2010.077.0030 from the

Oldman Formation (Comrey Sandstone Zone, or middle unit) of southern Alberta to *Maiasaura* sp. is a slight geographic range extension for this taxon, occurring approximately 200 km north of the original localities, and is the first specimen referable to the genus collected in Canada. Freedman Fowler and Horner (2015: table 1) recalibrated the radiometric date of a bentonite associated with an *M. peeblesorum* bone bed in the upper middle Two Medicine Formation to 76.66 Ma, more than one million years younger than a sample from near the top of the Comrey Sandstone zone in the Dinosaur Provincial Park area (77.76 Ma), and close in age to a sample from the middle part of the Dinosaur Park Formation, also in the Dinosaur Provincial Park area (76.45 Ma). The material from the Comrey Sandstone Zone at the Milk River Ridge Reservoir locality was estimated by Ryan and Russell (2005) to be slightly older than a bone bed from the same unit in Dinosaur Provincial Park. This makes TMP 2010.077.0030 potentially the oldest known specimen of *Maiasaura*, and confirms the temporal overlap of the *Maiasaura* clade with *Brachylophosaurus*, as predicted by phylogenies that have *Maiasaura* diverging from *Brachylophosaurus* before *Probrachylophosaurus*. However, a caveat to this is that the complete stratigraphic range of *Maiasaura peeblesorum* in the Two Medicine Formation is not well dated, and it is possible that some referred specimens (e.g., ROM 44770) are older than 76.66 Ma by an undetermined amount (Freedman Fowler and Horner 2015: table 2). It should also be noted here that the Jackson Coulee bentonite near the base of the Dinosaur Park Formation near its contact with the Oldman Formation in Dinosaur Provincial Park has recently been dated 76.32

Ma (Brown et al. 2021), slightly younger than the ages given by Freedman Fowler and Horner (2015) for the middle of the Dinosaur Park Formation and the Two Medicine Formation *M. peeblesorum* bonebed. More work may thus be needed to establish what the absolute age difference is between the Two Medicine Formation material of *M. peeblesorum* and TMP 2010.077.0030.

The new parasaurolophin from the Comrey Sandstone Zone represented by TMP 2016.023.0039 is older than *Parasaurolophus walkeri* from the lower Dinosaur Park Formation, and is currently the oldest known member of Parasaurolophini and Lambeosaurinae from Canada. Globally, the oldest known parasaurolophin may be *Adelolophus hutchisoni* from the Wahweap Formation of southern Utah, which is the oldest known Laramidian lambeosaurine (Gates et al. 2014; Longrich et al. 2021; Beveridge et al. 2022; Ramírez Velasco 2022). Geographically, TMP 2016.023.0039 falls within the quite extensive established range of the genus *Parasaurolophus*, which is known from as far north as Dinosaur Provincial Park in Alberta, and from as far south as the San Juan Basin of New Mexico (Gates et al. 2021). However, the presence of TMP 2016.023.0039 as a relatively early, plesiomorphic parasaurolophin taxon in the northern zone of Laramidia may be notable, since Ramírez Velasco (2022) identified the diversification of this clade as occurring mainly in southern Laramidia.

The reassignment of CMN 52845 from “cf. *Parasaurolophus* sp.” to a member of the *Brachylophosaurus* clade makes it the stratigraphically highest brachylophosaurin in Alberta, occurring in roughly the middle of the Dinosaur Park Formation (Evans et al.

2009a), whereas *B. canadensis* is from the middle unit of the underlying Oldman Formation. Using the recalibrated radiometric dates for the middle Dinosaur Park Formation and Oldman Formation in Dinosaur Provincial Park provided by Freedman Fowler and Horner (2015: table 1), the stratigraphic range of the *Brachylophosaurus* clade in the Belly River Group is extended upwards by over one million years. Whether CMN 52845 represents the youngest member of the *Brachylophosaurus* clade globally depends on the exact ages and affinities of the stratigraphically high brachylophosaurin specimens in the upper Judith River and lower Kaiparowits formations (Gates et al. 2013; Freedman Fowler and Horner 2015). CMN 52845 is from the same general geographic area as the holotype of *B. canadensis*, also from Dinosaur Provincial Park (Ryan and Evans 2005).

The co-occurrence of TMP 2010.077.0030 and TMP 2016.023.0039 at the Milk River Ridge Reservoir locality is notable in that both *Maiasaura* and *Parasaurolophus* have previously been interpreted as hadrosaurs that preferred drier, inland habitats (Horner 1983; Evans et al. 2009a), but this is the first documented occurrence of a maiosaur and a parasaurolophon at the same locality. *B. canadensis* also occurs in Oldman Formation of southern Alberta at approximately the same stratigraphic level (Cuthbertson and Holmes 2010), so this unit is the first to document the probable co-occurrence of two brachylophosaurin taxa, which may have influenced the divergent evolution of the visual display structures. The slightly more western occurrence of *Maiasaura* than *Brachylophosaurus* in the Oldman Formation of southern Alberta is consistent with

previous ideas about habitat partitioning, and this hypothesis could be tested with further geological and palaeoenvironmental studies of the Milk River Ridge Reservoir locality. The full palaeoecological implications of CMN 52845 being a member of the *Brachylophosaurus* clade are unclear, because its stratigraphic position in the Dinosaur Park Formation can be only approximated (Evans et al. 2009a). It is possible that it falls within the stratigraphic range of *Prosaurolophus maximus* determined by Lowi-Merri and Evans (2020), in which case it would be an apparently rare exception to the generally observed stratigraphic segregation of saurolophine taxa in the Dinosaur Provincial Park area. However, if CMN 52845 was collected from the gap between the known ranges of *Gryposaurus notabilis* and *P. maximus* in the Dinosaur Park Formation (Lowi-Merri and Evans 2020), the seeming rarity of this taxon could be more a reflection of insufficient sampling of this interval, and a more complex history of faunal turnover than supported by the current data.

6.3 New Findings on Ontogeny and Heterochrony

The ontogeny of the skull roof was previously studied in the brachylophosaurins *Probrachylophosaurus bergei* and *Brachylophosaurus canadensis*, and it was proposed that the evolution of the latter taxon from the former involved heterochronic development of the crest (Freedman Fowler and Horner 2015). In *Maiasaura peeblesorum*, skull roof ontogeny resembles that of other crested brachylophosaurins in that the transformation from crestless to crested occurs at a relatively late ontogenetic stage, in individuals with

skulls already more than half of the mature size. This contrasts with the ontogenetically earlier development of the crest in saurolophins (Bell 2011b; Drysdale et al. 2019) and lambeosaurines (Evans 2010; Farke et al. 2013).

In the smallest subadult studied, the frontal platform is shallow and weakly ridged, and the posterior skull roof is narrow and not dorsally elevated. The frontal platform becomes steeply inclined and more strongly ridged prior to projecting dorsally above the skull roof. In the largest individuals, the prefrontals flare laterally, the frontal depressions deepen, and the frontals expand dorsally and fuse along the midline. As in *B. canadensis*, the length of the frontal ectocranial surface becomes proportionately shorter, the midline of the nasals flatten, and small ledges of the skull roof overhang the anterior margins of the dorsotemporal fenestrae. Ontogenetic changes were also observed in the neurocranium, including a proportional broadening of the basioccipital. Unlike the trend described in *P. bergei* and *B. canadensis*, the ontogeny of the frontal platform in *M. peeblesorum* does not recapitulate the adult morphology of any other known taxon, and at no point in its ontogeny does *M. peeblesorum* possess the paddle-shaped crest of its sister clade. However, the ontogenetic trends shared with *B. canadensis* are perhaps suggestive of some type of crest in their common ancestor, consistent with the recovery of a “crested brachylophosaurin” clade in the phylogenetic analysis. It is unfortunately not determinable whether any differences existed between the ontogeny of *M. peeblesorum* in the Two Medicine Formation and *Maiasaura* sp. in the Oldman Formation, since the

latter is represented by a single crushed specimen lacking that does not preserve the nasal articulation of the frontal platform.

Heterochronic evolution of the crest in parasaurolophins was previously inferred from the observation that juvenile parasaurolophin specimens have more developed crests (or supporting platforms for crests) than lambeosaurins of comparable ontogenetic stage, suggestive of predisplacement of growth (Evans et al. 2007; Farke et al. 2013). However, it was not possible to compare ontogenetic series of different parasaurolophin species to demonstrate that heterochrony occurred within this clade, and the scant evidence available from basal lambeosaurines does not necessarily confirm that the lambeosaurin condition was ancestral (Bell and Brink 2013). A previous study of CMN 8502, an immature skull roof from Dinosaur Provincial Park referred to *Parasaurolophus* sp., indicated that the characteristic steep frontal platform was present relatively early in ontogeny, prior to the development of its posterior extension overhanging the parietal, or the more strongly elevated dorsal promontorium of the postorbital (Evans et al. 2007). Potentially supporting previous inferences of heterochrony in parasaurolophins, the adult morphology of the new taxon represented by TMP 2016.023.0039 is reminiscent of CMN 8502, with a similar steep frontal platform, but no extension overhanging the parietal, or strongly elevated dorsal promontorium. Its relatively low stratigraphic position, and phylogenetic position recovered outside of *Parasaurolophus*, are consistent with the hypothesis that these crest-related character states appeared in the same order phylogenetically as recapitulated ontogenetically. A caveat to this conclusion is that

CMN 8502 has not been definitively established to be stratigraphically higher in the Belly River Group than TMP 2016.023.0039, although the distribution of Dinosaur Park versus Oldman Formation outcrops in Dinosaur Provincial Park suggests that it probably is (Evans et al. 2007), and the different orientation of the postorbital process of the laterosphenoid is consistent with this (this character not seeming to vary greatly with ontogeny in other taxa examined). This issue will be resolved as more parasaurolophin specimens from these formations are collected and described.

The removal of CMN 52845 from *Parasaurolophus* means that there is no longer any reason to speculate that the crest was not fully expressed in the holotype of *Parasaurolophus walkeri* (Evans et al. 2009a), or that the dorsal ectrofrontal surface underwent further reduction in the ontogeny of that taxon. If CMN 52845 is taxonomically distinct from the stratigraphically lower *Brachylophosaurus canadensis*, it may reveal that the peramorphic trend of the brachylophosaurin frontal platform described by Freedman Fowler and Horner (2015) continued to an even further extreme in late members of this clade, in that the posteriorly extended frontal platform does not merely occupy the entire ancestral length of the frontals, but extends beyond.

6.4 Discussion and Conclusions

This research adds three taxa to the list of hadrosaurs known from the Belly River Group: *Maiasaura* sp. and a new parasaurolophin in the Oldman Formation, and a member of the *Brachylophosaurus* clade in the Dinosaur Park Formation. However, all

three are presently represented in these units by very incomplete material, especially in comparison to their better-known contemporaries. I hope that by recognizing that these taxa occur, the search images will be planted to accelerate the identification of additional material referable to them, whether in the field or already in museum collections. With more complete skulls, it may be possible to resolve such unanswered questions as: Does *Maiasaura* in the Oldman Formation represent a new species, or fall within the range of variation for *Maiasaura peeblesorum*? Or, what was the shape of the crest in the new parasaurolophin? Continued collecting of the abundant *Maiasaura peeblesorum* material in the Two Medicine Formation may also eventually provide a dataset large enough to approach such questions as sexual dimorphism in the development of cranial ornamentation, which is a possible explanation for some of the variation observed here, but about which very little can be currently known.

Phylogenetic analyses, especially of extinct clades like hadrosaurs with incomplete but constantly growing morphological datasets, are by nature works in progress. In future analyses, the skull roof and braincase characters identified in this study can be more comprehensively scored across hadrosauroids, and new ones identified and added. As alluded to above, the functional implications of different character states could be explored in greater depth, leading to a richer understanding of their significance in the evolution of these dinosaurs.

Appendices

Appendix 5.1: Overview of published phylogenetic analyses with a member of Hadrosauridae as the main taxon of interest, 2010 to present.

Reference:	Main taxon of interest:	Matrix modified from:	Analytical method(s):
Bell and Evans 2010	<i>Augustynolophus morrisoni</i>	Godefroit et al. 2008	Parsimony
Cruzado-Caballero et al. 2010	<i>Blasisaurus canudoii</i>	Sues and Averianov 2009	Parsimony
Cuthbertson and Holmes 2010	<i>Brachylophosaurus canadensis</i>	Horner et al. 2004	Parsimony
Evans 2010	<i>Hypacrosaurus altispinus</i>	Evans and Reisz 2007	Parsimony, Bayesian
Prieto-Márquez 2010a	Hadrosauridae	various/new	Parsimony, Bayesian
Prieto-Márquez 2010b	“ <i>Glishades ericksoni</i> ”	Prieto-Márquez 2010a	Parsimony
Prieto-Márquez and Salinas 2010	<i>Secernosaurus koernereri</i>	variant of Prieto-Márquez matrix	Parsimony
Bell 2011a	<i>Saurolophus osborni</i>	various/new	Parsimony
Bell 2011b	<i>Saurolophus angustirostris</i>	Bell 2011a	Parsimony
Gates et al. 2011	<i>Acristavus gagslarsoni</i>	Horner et al. 2004	Parsimony
Prieto-Márquez 2011	<i>Barsboldia sicinskii</i>	Prieto-Márquez 2010a	Parsimony
Godefroit et al. 2012a	<i>Olorotitan arharensis</i>	Evans and Reisz 2007	Parsimony
Godefroit et al. 2012b	<i>Kundurosaurus nagorny</i>	Prieto-Márquez 2010a	Parsimony
Prieto-Márquez 2012	<i>Gryposaurus latidens</i>	Prieto-Márquez 2010a	Parsimony
Prieto-Márquez and Wagner 2013	<i>Augustynolophus morrisoni</i>	Prieto-Márquez 2010a	Parsimony
Prieto-Márquez et al. 2012	<i>Magnapaulia laticaudus</i>	Prieto-Márquez 2010a	Parsimony
Xing et al. 2012	<i>Wulagasaurus dongi</i>	various/new	Parsimony
Campione et al. 2013	“ <i>Glishades ericksoni</i> ”	Prieto-Márquez 2010b	Parsimony

Cruzado-Caballero et al. 2013	<i>Arenysaurus ardevoli</i>	Godefroit et al. 2012a	Parsimony
McGarrity et al. 2013	<i>Prosaurolophus maximus</i>	Godefroit et al. 2012b	Parsimony
Prieto-Márquez and Wagner 2013	<i>Augustynolophus morrissi</i>	Prieto-Márquez 2010a	Parsimony
Prieto-Márquez et al. 2013	<i>Canardia garonnensis</i>	Prieto-Márquez et al. 2012	Parsimony
Gates et al. 2014	Wahweap Formation WBH locality material	Gates et al. 2011	Parsimony
Prieto-Márquez 2014a	<i>Kritosaurus navajovius</i> / Kritosaurini	Prieto-Márquez and Wagner 2012	Parsimony
Prieto-Márquez 2014b	<i>Edmontosaurus annectens</i> (immature)	Prieto-Márquez 2014a	Parsimony
Xing et al. 2014b	Edmontosaurini	Xing et al. 2012 (via Xing et al. 2014a)	Parsimony
Gates and Scheetz 2015	<i>Rhinorex condrupus</i>	Prieto-Márquez 2010a	Parsimony, Bayesian
Freedman Fowler and Horner 2015	<i>Probrachylophosaurus bergei</i>	Prieto-Márquez 2010a and Gates et al. 2011	Parsimony
Prieto-Márquez et al. 2015	<i>Augustynolophus morrissi</i>	Prieto-Márquez 2014a	Parsimony
Lehman et al. 2016	? <i>Gryposaurus alsatei</i>	Prieto-Márquez 2014a	Parsimony
Mori et al. 2016	" <i>Ugrunaaluk kuukpikensis</i> "	Prieto-Márquez 2014a and Xing et al. 2014b	Parsimony
Prieto-Márquez and Gutarra 2016	Careless Creek kritosaurin	Prieto-Márquez et al. 2016	Parsimony
Prieto-Márquez et al. 2016	<i>Eotrachodon orientalis</i>	update of Prieto-Márquez matrix	Parsimony
Cruzado-Caballero and Powell 2017	<i>Bonapartesaurus rionegrensis</i>	Xing et al. 2014a	Parsimony
Xing et al. 2017	<i>Edmontosaurus regalis</i>	Xing et al. 2014a (via Wang et al. 2017)	Parsimony
Takasaki et al. 2018	<i>Nipponosaurus sachalinensis</i>	Mori et al. 2016 (from Xing et al. 2014b)	Parsimony
Kobayashi et al. 2019	<i>Kamuysaurus japonicus</i>	Xing et al. 2017	Parsimony
Prieto-Márquez et al. 2019	<i>Adynomosaurus arcanus</i>	update of Prieto-Márquez matrix	Parsimony

Zhang et al. 2019	<i>Laiyangosaurus youngi</i>	Prieto-Márquez et al. 2016	Parsimony
Conti et al. 2020	Els Nerets lambeosaurine	Prieto-Márquez et al. 2019	Parsimony
Prieto-Márquez et al. 2020	<i>Aquilarhinus palimentus</i>	update of Prieto-Márquez matrix	Parsimony
Takasaki et al. 2020	“ <i>Ugrunaaluk kuukpikensis</i> ”	Kobayashi et al. 2019	Parsimony
Zhang et al. 2020	“ <i>Tanius laiyangensis</i> ”	Xing et al. 2017	Parsimony
Brownstein 2021	Merchantville Formation hadrosaurs	Prieto-Márquez et al. 2016	Parsimony
Gates et al. 2021	<i>Parasaurolophus cyrtocristatus</i>	Prieto-Márquez et al. 2019	Parsimony
Kobayashi et al. 2021	<i>Yamatosaurus izanagii</i>	Takasaki et al. 2020	Parsimony
Longrich et al. 2021	<i>Ajnabia odysseus</i>	Kobayashi et al. 2019	Bayesian, Parsimony
McDonald et al. 2021	<i>Ornatops incantatus</i>	McDonald et al. 2017	Parsimony
Ramírez Velasco et al. 2021	<i>Tlatolophus galorum</i>	various/new	Parsimony
Rozadilla et al. 2021	<i>Kelumapusaura machi</i>	Kobayashi et al. 2021 (but cited as Takasaki et al. 2020)	Parsimony
Thompson et al. 2021	Foremost Formation brachylophosaurin	Xing et al. 2017	Parsimony
Ramírez-Velasco 2022	Mexican hadrosauroids	various/new	Parsimony
Serrano-Brañas and Prieto-Márquez 2022	<i>Latirhinus uitstlani</i>	update of Prieto-Márquez matrix	Parsimony
Xing et al. 2022	<i>Amurosaurus riabinini</i>	various/new	Parsimony

Appendix 5.2: List of modifications to the matrix of Ramírez Velasco (2022).

Iguanodon bernissartensis: **179**: 0 → ?, **336**: 0, **338**: 0

Jinzhousaurus yangi: **179**: ? → 1, **336**: 1, **338**: 1

Equijubus normani: **179**: 0 → ?, **338**: 0

Sirindhorna khoratensis: **179**: ? → 0, **336**: 0, **337**: 0, **338**: 0, **340**: 0, **341**: 0

Probactrosaurus gobiensis: **179**: 0 → 1, **338**: 0

Eolambia caroljonesa: **179**: 0 → 1, **336**: 0, **338**: 0, **340**: 0, **341**: 1

Protohadros byrdi: **336**: 0, **338**: 0

Jintasaurus meniscus: **179**: ? → 1, **336**: 0, **337**: 0, **338**: 0, **339**: 0, **340**: 0

Yunganglong datongensis: **341**: 0

Levnesovia transoxiana: **179**: ? → 1, **336**: 0, **337**: 0, **338**: 0, **339**: 0, **340**: 0, **341**: 0

Tanius sinensis: **179**: 0 → ?

Tethyshadros insularis: **145**: 0 → 1, **179**: 1 → ?

Plesiohadros djadokhtaensis: **336**: 0

Gobihadros mongoliensis: **336**: 0, **337**: 0, **339**: 0, **341**: 0

Eotrachodon orientalis: **179**: 0 → 1, **336**: 0, **337**: 0, **338**: 0, **339**: 0

Lophorhothon atopus: **179**: 0 → ?, **339**: 0, **341**: 0

Acristavus gagslarsoni: **336**: 1, **337**: 0, **338**: 0, **339**: 0, **340**: 0

Ornatops incantatus: **179**: 0 → 2, **335**: 0, **337**: 0, **340**: 0, **341**: 0

Probrachylophosaurus bergei: **173**: 0 → 1, **335**: 0, **336**: 1, **337**: 0, **338**: 0, **340**: 0

Brachylophosaurus canadensis: **149**: 1 → 0, **173**: 0 → 3, **335**: 0, **336**: 1, **338**: 0, **339**: 0,
340: 0

Maiasaura peeblesorum: **74**: 1 → (1&2), **157**: 0 → 1, **173**: 0 → 1, **335**: 0, **336**: 1, **337**: 1,
338: 1, **339**: 0, **340**: 0, **341**: 0

Gryposaurus monumentensis: **179**: 0 → ?

Gryposaurus notabilis: **179**: 0 → 1, **336**: 0, **337**: 0, **338**: 0, **339**: 0, **340**: 0, **341**: 0

Rhinorex condrupus: **179**: ? → 1, **338**: 0

Kritosaurus horneri: **166**: no change [accidentally entered as “?” instead of “0” in the version of the matrix that was run, but will be corrected in subsequent runs before publication], **179**: 0 → ?

Kritosaurus navajovius: **166**: no change [accidentally entered as “1” instead of “0” in the version of the matrix that was run, but will be corrected in subsequent runs before publication], **179**: 0 → ?, **336**: 1, **338**: 0, **340**: 0

Secernosaurus koeneri: **179**: 0 → ?, **338**: 0, **339**: 0, **341**: 0

Prosaurolophus maximus: **179**: 0 → 1, **336**: 0, **337**: 0, **338**: 0, **339**: 0

Saurolophus osborni: **179**: 0 → 1, **335**: 0

Saurolophus angustirostris: **179**: 0 → 1, **338**: 0, **339**: 0

Augustynolophus morrisoni: 179: 0 → 1, 341: 0

“Sabinosaur” PASAC 1: 179: 0 → ?

Kerberosaurus manakini: 179: 0 → ?

Shantungosaurus giganteus: 179: 0 → ?

Kamuysaurus japonicus: 179: 0 → ?

Edmontosaurus annectens: 179: 0 → 1, 336: 0, 337: 0, 338: 1, 339: 1

Edmontosaurus regalis: 179: 0 → 1, 336: 0, 337: 0, 338: 0, 339: 1

Aralosaurus tuberiferus: 179: ? → 1, 341: 1

Arenysaurus ardevoli: 339: 0

Jaxartosaurus aralensis: 179: ? → 1, 335: 1, 336: 0, 338: 0, 339: 0

Tsintaosaurus spinorhinus: 179: 1 → ?, 336: 0, 338: 0, 339: 0

Amurosaurus riabinini: **335**: 1, **339**: 0 [accidentally entered as “1” in the version of the matrix that was run, but will be corrected in subsequent runs before publication], **340**: 0, **341**: 1

Sahaliyana elunchunorum: **185**: 0 → 1, **336**: 1, **339**: 0, **340**: 0

Olorotitan arharensis: **340**: 0, **341**: 1

Charonosaurus jiyinensis: **145**: 1 → 2, **165**: 1 → ?, **166**: 3 → 1, **335**: 1

Parasaurolophus walkeri: **145**: 1 → 2, **165**: 1 → ?, **166**: 2 → 3, **168**: 0 → 1, **179**: 1 → 0, **335**: 1, **336**: 0, **337**: 0, **339**: 1, **341**: 0

Parasaurolophus tubicen: **145**: 1 → 2; **168**: 0 → ?, **179**: 1 → 0, **193**: 0 → ?; **340**: 1, **341**: 0

Parasaurolophus cyrtocristatus: **145**: 1 → ?, **166**: 1 → ?, **168**: 0 → ?, **179**: 1 → ?, **193**: 0 → 1; **339**: 1, **340**: 1, **341**: 0

Tlatolophus galorum: **338**: 1

Lambeosaurus lambei: **185**: 0 → 1, **336**: 0, **337**: 0, **340**: 0

Lambeosaurus magnicristatus: 179: 1 -> ?

Corythosaurus casuarius: 185: 0 -> 1, 340: 0, 341: 1

Corythosaurus intermedius: 185: 0 -> ?, 335: 1, 336: 0, 337: 0, 338:0, 339: 0, 340: 0,
341: 1

Hypacrosaurus altispinus: 179: 0 -> 1, 185: 0 -> 1, 335: 1, 336: 0, 337: 0, 338:0, 339: 0,
340: 0, 341: 1

Hypacrosaurus stebingeri: 185: 0 -> ?, 335: 1, 338:0, 339: 0, 340: 0, 341: 1

Velafrons coahualiensis: 179: 1 -> ?, 336: 1, 339: 0, 341: 1

TMP 2010.077.0030: 71: 0, 72: 0, 74: 2, 78: 0, 136: 0, 137: 0, 143: 0, 144: 0, 145: 0, 146:
0, 147: 1, 148: 0, 149: 1, 150: 1, 151: 0, 152: 0, 154: 0, 155: 0, 157: 1, 165: 0, 169: 0,
171: 0, 173: 1, 176: 0, 177: 2, 178: 0, 181: 1, 185: 1, 186: 1, 187: 1, 188: 1, 191: 0, 192:
1, 193: 0, 194: 0, 195: 0, 201: 0, 202: 1, 203: 0, 205: 1, 241: 0, 242: 0, 244: 0, 336: 1,
337: 1, 338: 1, 340: 0

TMP 2016.023.0039: 141: 0, 143: 0, 144: 0, 145: 1, 147: 1, 148: 0, 151: 0, 163: 0, 165: 0,
166: 3, 167: 1, 168: 1, 169: 0, 171: 1, 173: 2, 175: 0, 176: 0, 177: 0, 178: 1, 179: 1, 181:
0, 182: 1, 183: 0, 184: 0, 185: 1, 186: 0, 187: 1, 189: 0, 190: 0, 191: 1, 192: 1, 193: 1,

194: 0, 195: 0, 219: 1, 242: 1, 335: 1, 336: 0, 337: 0, 338: 1, 339: 1, 340: 1, 341: 1

**CMN 52845: 71: {1/2}, 165: 1, 166: 1, 167: 1, 169: 0, 173: 3, 176: 0, 179: 0, 194: 0, 219:
1, 335: 0**

011?0000?00?0000101000-
00?01001001000?0????0001000000000000--0-00000-
000001100000??0000-
11????00?0???000000?0?00??0?1000000000011000000000-
0000000000000?110?00-????000000-
000?0010?000?1?0?????0?0??????010200--00--0-00--00-0---?--
00-?-?-
100000?00000?0?00????????????????????????????00000000100000
-?000?0????????????????????????????????????-??0???

Sirindhorna_khoratensis

01??01001?0?101?10??0??00101002000??00000001?0???0??00100?0
????0?????0????0??000?0?0??110?0010???00000?0?0?0000?0???
00??01?0?10?????0?????????0??000??1?0????0???0000??000????
00?0101?0111000?00?????????????????????0-
????????????????????????????001????????????????????????????
??
??-000-00

Xuwulong_yueluni

011?01001?0?10101?0000?00111002001??000001?1?0???00000100?0
????0?????0??00??000?0?0??11????????????0000?0?0??0?1??1??
1???02?0?1010000000?00?0000?00100?01??0???0???0000??000????
0?00101?0?????0??00?????010201??????0-

00?0????????????????0?0?0000?000101????????????????????
??????00000?00000000-
0?00?000?0?00010000?????1????1????????????-??????

Probactrosaurus_gobiensis

00101100100?1??0?00001010?100010010000000101?0?0?0?000?0000
--0?00000?0000??00?00??0??-
????10000000?00?000000??0?????00000?????1000?0??????00000?
?000?????00-01??00000-
000?0010100????????????0?0??0??010??-0?--0-0????0-?---?--
00-?-?-
?00100001??10?0101000000200000000011??01?11?00000000100000
-000010001201???1111?001011000000???1000-??0???

Zuoyunlong_huangi

??
??
??
??
??
??0000?00000000-
0?0010??

Eolambia_caroljonesa

0010120110101010100011310??21(12)200100000001010010001{01}?

000000--0-0000?-00000010000???0010-
?20010000000010000010010000???100?0(01)30(12)10100000??????
0000000?000100000-?1????00000-
0000002011010000001100010??0??010200--00--0-00--00-?---?--
00-?-?-
??0?000????01010101000000200100000000??01110000000100112010
-000000000000000101111210010?001000?1000-0?0?01

Protohadros_byrdi

00??1201101?111000?0113111021220110000001101001000111000000
--0-00000-000010?00001000010-
11001001000001000?010010100???100?010012001000000-
?000000?00??001?????????0??00000-
00000????0????????????????????000010200--00--0-00--00-?---?--
00-?-?-
1?0?00?0????????????????????????????000????????????????????
??1????-0?0???

Jintasaurus_meniscus

??
??
????????????????????????????????0?10100??1??0??0??0000??0000??
011010?001?11?0000????????????????????0????????????????????

????01??
??-00000?

Yunganglong_datongensis

??
??
??
????0100????11?0?00??
??
??1????????????????0

Levnesovia_transoxiana

0???11011?0?111?10000??1????001??1?????00??1?11??0?????????
????????????????????????0????????????0?1??1????010??0?1?01?1?????
10??0????00?111?000?00?0000?101100?0??0??0??0000??0000??
0100100?01110?0?00??
????00??????0?????0?0?0?????????0?????????????????0?010??????
?????000???11?10?????????????????????0???10-000000

Tanius_sinensis

????????????1??
????????????????000??
100000001?01??0?????0?000001011001???0??01?1100000-
000?0010??0100001?10?0000001???1?????-??--????????0-----?--

??-?-?-

????000?11??2????????????110000000100????????12010101111111
1001000????????????????????1??1??????-??????

Shuangmiaosaurus_gilmorei

0?????????0?111????????????1012000???000?101?????????????
????????????????????????????0??100?1??1???0???0?0?0011?1?????
10???
??
??
??1????????????????

Bactrosaurus_johnsoni

0110(12)(12)0210011(01)101001010101020110010(01)00000101011
001110010000--0-00000-10000?10000?000010-
1100101110000000000100101001001000011010101110000-
00000000001100000000-01?1100000-
00000010100110001120?0000??1??010?0?--00--0-00--00-----?--
00-?-?-

0?00000?00??10?10010000001100101010100??10?1?12001101111(01
)111000010001210110111111110210011110010010-??????

Gilmoreosaurus_mongoliensis

01102??1??0111100?0001010???001?01???0000101???????????????

????????????0000?????0?00?010-
12001011100000000?01011010010010?00??0??101110000-
???0000?????0???00?0-
????????????00??0????????????????????????????10?0??-00--0-
0????0??--??--??-?-?-
??1??????????1?????2000000100010101011{01}??1?????12101101112
011100101(01)?????01?1111101110110001110011000???????

Nanningosaurus_dashiensis

0???1?001?0111????????????????????2?????011??1?1?????????????????
????????????????????????0??0?0??1?1?1??1???00000???1011?1?????
????????????????????1????????????????110??1??0?????????????????????
?????11???
????????????????????????????????0?00?????????????????????????????
????????????????????10?????1???0??1?????????????????

Telmatosaurus_transsylvanicus

01??12001101110????????????100000100010011?0?11001110000000
--0-00000-100??0100?0????010-
120010111000011000021110100???10?00?????0101??01??????0000??
???011?0000-?0?1100000-
000?0010?1?100?????101??00??1??0102?0--00--0-0??-?0-----?--
00-?-?-

1?1?0000?0????????????????1????????????????????????????????
????????????????????0????1??????0?????-??????

Tethyhadros_insularis

111?11101011110010000000011?00??001?0???01?00111011{01}0000
000--00000?0-
100000100000????000110????1??0?011??0?2?????0?1001000?03002
101121000-00000010100001000000-10?0?00000-
000?0001?101??0??????00?????010?0{01}--00--0-000-00-----
?--0--?-?-00100000100011110020000010101-?0000000111-
1111211310201?110-2000?001001011000010111?00--11?0??10110-
??????

Plesiohadros_djadokhtaensis

1???12011?0111?0210001211???101??1??011111?1??????????3100?1
0?????????1?????????0???0?0????0?1?????????????????????1?????
?????000??10112?000?00????0?101101?0??0?????1??0000??000????
???010000??20?000000??
?1?00??1100????????????????
??1111?-0??????

Gobihadros_mongoliensis

011?12001?0111?1100011211101000001??0?????101?????????00100?0
????0?????0????001??000??0?10?110?1??1???01110?0?100101?01??

10??0000?0101111000?00?0000?10110000??0???01??0001??000????
010?1000?1120000?00??0000?0200???0??0-
00??0????????????????1???00001?001011112011?01?10010001??10
101101111101?02012000-
??11?01412??111?000?????1???1?0?0011110-00?0?0

Nanyangosaurus_zhugei

??
??
??
??
????????????????10????????????????????00??10?11011????????????
????????????????????????????????????00?1110????????

Zhanghenglong_yangchengensis

021?12111?01111????????????2002001???0011101????????????
????????????????????0???0?1??110????1???00110?0?2012?1????
?0??22?0?2??
??
????????????????????????1?000?00????1????????????????
??

Eotrachodon_orientalis

{01}0{01}0121111{01}111101110111101010010010001110101111101

100310010--

000000001000?11000000010221110010111000(01)0100011012010010

11000122101101121100-10000000101100100000-12?1100000-

000?00111001?0?0011??1?00?????010212--00--0-01100-----?--

00-?-?-

2110000110??1??

???????1?1011101100001120??---??1???????-0000??

Claosaurus_agilis

????1??????111????????????????????????????0????????????????????

??

????????????????????????????????0?10??0????????????????????????

????????????????????????????1????????????????????????????????-

????????????????????????????????1?001-000{0

1}0?00?????????021211?2012010-

?010?0????????????????????????????1????1?0????????????

Huehuecanauhtlus_tiquichensis

?110?2021?01112??

????????????????????????????????????1?01?1?0????????????011?1?????

??

??

?????????0?011????????????????????????????????????11011?010111113

10011110?1?11?1??

Jeyawati_rugoculus

1{01}??12011?1?101????0?????10220010000101101????????0??
????????????????????????0????010-
?100?01???0?0?????0011?0????????????????001000?????????0?
0???1??1????
?-0?--?0????????????-??????-
?0???
????????????????????????????????????0?????????????

Lophorhodon_atopus

????22111?0?111????????????????????????????????????1????
?0?000???100???100?0?????00-
?2?????????111000?10??????0110?01?????101110100-
000000?00?10012??0??10?1100000-
0000001???01?0??????01?0?00??010????-00--0-0100104-0--?--
00-?-?-???1000?1?????00010000001001-
00000210??10?1?12?02102?1??10-?010111??1101??110201????0---
1010011000-???0?0

Hadrosaurus_foulkii

????131110??111???
??2??????
??

00-?-?-(12)11110000110111101211121121(01)1-
01101112111121112022203012110-2011111211111111010112110---
111{01}01101101-000?

Maiasaura_peebleorum

12202312101211?1211121111111211101111111201111101121111111
00000000-1001(12)1000101002010-120011-
2100?1110112202201001001111222111101120100-
10100000101100100010-1220003100-
001?10(12)0001100111120?100010100010110--00--0-0200113-00-
?--00-?-?-111110000110111??12111?112111-
01101111111?21112022203012110-201111121111111101?112110---
111001?0110111000

Aquilarhinus_palimentus

11(12)?12121010112????????????1(12)1(01)100?1?1111201??????
?????????????0??????000100?020?0??000-
12??1012100011101?220120100???10001021201??????0????????????
????????????????2????????????????????????????????????00001021?
--00--0-0101100000---
?00??11111?1??????
??????10-2011??

Gryposaurus_latidens

13200311101211????????????22211011101111201111101121311??1
000000110100010??02001110220130011-
21000111010220320100???20002130021??????00-
??00?0?0???000120000-
1????000????0???0??????0??????1?????1??01021?--00--0-
0101100000-?--00-?-?-??1?0????0??0111?121111111011-
111(01)1201??1????11?12112112210-
2011111411111?012????????0---???1????10-??????

Gryposaurus_monumentensis

13201312101211201101013111012211011?011112?1111101111311011
0000001111000100102001120220130?11-
210001110102203201002012110223112101120100-
1000000101000120000-1?01000000-
000?1020?0?1?00?111001000001??010213--00--0-0101100100-?--
00-?-?-
211101011??2???
?????????????????????????????---??????????-???????

Gryposaurus_notabilis

13201212101211?0200101311101(12)(12)(01)?011101111211111101
1113110110000000111100010010200??20220130?11-
2100?111?1022?32010020121(01)0213112101120100-

10000000101000120000-1101000000-
0000102010210000111001000001??010213--00--0-0101100100-?--
00-?-?-2110010110100111?121111111011-
111(12)1(12)11111111111221120122?????11111411111???2010112
100---1111011110-000000

Rhinorex_condrupus

?32?131210????????????????????????????1???1112?1?????1111311011
000000011?100010??0200???0220130?11-
?100?111?1022032?10?20?2100?2??121??????00-
?0?0000010100?1?0?00-11??000000-
000??0201????????????1?0??????01021?--00--0-010-100000-?--
00-?-?-
21?10101??
??-??0???

Kritosaurus_horneri

??202312?022????????????????????????????1????1????????????????
??0?0000??00010100?0011?022113??11-2100?
1110?0220????0??0121102???0????????00-
1000000010110?1???0??1???000000-
?00?1010????????????0??????????01021?--00--0-0200104-00-?--
00-?-?-

211001011??
??-???????

Kritosaurus_navajovius

12202312102211?01??101311??1020100(01)1011112011111011??3??
????????00?0??00??0100200??0{12}2113??1??2??0?1110?0?2032?
?0?2??21102231021011201?0-?0?0000010110?120000-1?0?000000-
00001010?0?1?0??10?001?10?01??0102??--00--0-0??????-????--
00-?-?-

211001011??2???
??-1?0?0?

Kritosaurus_IGM_6685

????????????????011?1013??10?120100????????????????????01311011
0000??01110?0?????201??
??
????????????????????????????????????102????00????????????????????????2
??
???

Naashoibitosaurus_ostromi

???02312??22112????????????????????????1????????????????????
??0?00?????000?0100?001110120120011-
2100?11101022032?10??002110213111101120100-

1000000010110?120100-11??000000-
100?1010??210???1?00???00?01??010?1??-00--0-0111100000-?--
0?-?-?-
?111000?1?1????????????????????????1??2????????????????????
??-???????

Secernosaurus_koernerii

12??2312101?11???1????????????021?011101?1120??1?1?11????????
????????????00????1??0????020-1???11-
210001110??2201201?0????????????????????????00-
1000000?10??001???0??1??1000000-
00001?20?02100001?0001000??????1?????-0?--?-0????????????--
0?-?-?-??????0?1???1??1?11011111011-
11????1???1????111221021121113111111401111201202?112120---
111??1????-??00?0

Bonapartesaurus_rionegrensis

??
??
??
??
????????????????211????????????????????????0????????000222020122113
1011111410?1??012????????0---1101111???????????

Prosaurolophus_maximus

23212312102211?0(23)101113111111(01)01001101111201111101121
311011000100001010022110020010?0120120111-
2100?11101022032010020121002(01)3002101111100-
101000011011(0 1)0120000-1100000000-
100000201?21000011000100000???010312--00--0-0210104-00-?--
00-?-?-011110001?1001110121112111111-
11111(12)1111111111212(23)212112210-
20111114011112012020112110---1110011110?0000??

Saurolophus_osborni

23212312102211?0310101311??020010011011112?1111101111311011
00010100101102210002001??0120120?11-
2100?11101022?320100201210020300(12)101111100-
10100111101110120012-
121001211101?0?00?1102100001?00?1000001??010312--00--0-
0310102-11-?--00-?-?-011110002111011??121112112111-
01?21{01}01111??1112123212012210-
2011111411111??110??1???10---11110111100??????

Saurolophus_angustirostris

23211312102211?02101013111102001001101111201111101111311011
0001010020110221000200???0120120?11-
2100?11101022?32?10?201210020300(12)101111100-

10100111101110120010-
12100121110110?002110210000??00?1000??1??010312--00--0-
0310102-11-?--00-?-?-0111100021110111?121112111111-
01221001111?11112123212012210-2011111411111??1102?112010---
1111011110-??00-?

Augustynolophus_morrisi

23?11312102211????????????00201?00110111?201?11101??1311011
00?10???10110???00?20?????0120120?11-
?100??11???22?32?10?????210020??0210111?100-
??????0010?100?????1??12?00?????111?0?0021102?????????0?????0??
???010?????-00--0-0301102-11-?--?0-?-?-
0??100002?????????1???????1??11-
?11211???1??1??
?????1?????????????0

Sabinosaur_PASAC_1

232????????221????????????????0110?001101111201?????11?????????
????????????????????????0?????012??20?11-
?10??111?1?22?320100?????????????????011211?0-
??????0?10??001???0??1?????????????????20?02100??100001?1??0
?????10?????-0?--?-0??????????-?--??-?-?-
??1??????????11???111??2?01101-

11????????????????122212012110-?011111401111211202?112100---
111????????????????

Kerberosaurus_manakini

13????????2211????????????????{01}???11011112?1??????1?????
????????????????002????220?11?01??120?11-
2100011101122032?10????21002030111011211?0-
1000000?10?0(01)0110001-
1??1?00000?0000?120?0210??0???0???0???1??01011??-00--0-012-
00?----?--0?-?-?-?11????????????1????????1??11-
111?021????????02121302012110?2011111{23}?0111101202?112100
---??????????-??????

Laiyangosaurus_youngi

2??0??????11102????????????211010011011112011111????41??11
?10????????100221??120010?0{01}20120011-
2100011101?220320100???20001020101??????0????????????????2
??0??0
??
??
????????????

Shantungosaurus_giganteus

232013121022112?2???0?????2{2
3}0210011011112?1?????11??4???11110?000??-
?002???0220????001-
120?1??2?00?11101??2032?10?????????????11121100-
0000?00110111?111?00-1(12)?1?000-0-
000?0121?021?00????0010?0?????010????-00--0-012-00?----?--
00-?-?-0111100?1??01101?121111011011-
0121111111??1?12122312012110-2011111310111111002?112110---
1110010010-??????

Kamuysaurus_japonicus

????33121???112????????????1110100110111120111111?????????
????????????????????2???0????????????2????????????3201?0???
2110102001111120100?000??0011010000???0?-1111?00100-
001?0??0?0?10????????????0?01????????????0?????????????
????????110000?0?100?1??11111110011-
111012111111??1???2?11012110?201111????????????0?????????
11100?11100??????

Edmontosaurus_annectens

232013121022112011?11131111130(01)1001101111201111101121411
11111000000-100221002201102001-120?11-
210001110112203201002002100203021101121100-
10001001211100111001-1111000000-

00000120102100001110?1001011??010111--00--0-012-00?----?--
00-?-?-0111100000100111012111211{1 2}111-
01(12)111(01)111111112122312012110-
2011111310111101202?112(01)00---1110011010-0011??

Edmontosaurus_regalis

232023121022112011?11131111130(01)1001101111201111101121411
11111000000-100221002201102001-120111-
210001110112203201002002100203021101121100-
10001001211100111001-1111000000-
000001201021000011100100101100010111--00--0-012-00?----?--
00-?-?-01111000001001110121111112111-
0121111111111112022312012110-2011111310111101102?111100---
1110011010-000100

Aralosaurus_tuberiferus

12202(23)12111111(12)????????????011??111011112?1?????????
??????????00?????01?????????---112012??11-
2100?11102?22012?110???2010213011111111?00-
100000010110010??01?1????00000-
00000101?0????????????0????????????0??0?????1??-
0?0????000?0-
?111?0101??
??-?????1

Canardia_garonnensis

???0220210?1112????????????????????????????????????1111????????????
 ??????????????????????????---112012??11-
 3100111112?221321110????2??02????????111?11111010?00????????????
 ???
 ???-????????????????????-
 ?????????????????1????????1??????01?1????????????????????????
 ???

Arenysaurus_ardevoli

11?032121?1?112?????????????1002?01111111101?111111????????
 ?????????????2????????1---
 ?????????????????????????1???2?1??????1????????01??????1111101
 0002101100110011012?1003110-
 111?0001100110?00?00?1000?????10????????????????---
 1???0????????????-
 ?1?1?21?1??12????12?1121110001????????????????????????????
 ???????011??1???10????????????11????????????0??

Blasisaurus_canudo

112?331211?2112?????????????20020011101111101?1111????????
 ?????????????????????1---
 ??????????1????????????????????????10?310?1212031101????????????

??
??-
??
??

Adynomosaurus_arcanus

1{12}??2???11????????????????????????????1??????1101111201????????????????
??
??
??
?-
????????????????????0?????????10000110?????????????????2023302112?10
-????11?????????????2110?????????11?1?????????????????

Jaxartosaurus_aralensis

??
????????????????????00??
?????????????????????110010?000210110?11??0??1??0001100-
101?00101?0100?01100???00?????????1?????????????????????????-0-
?????????????-
???1101?1??
??10?00??

Tsintaosaurus_spinorhinus

1120(23)311101?11?021011121110111200011011112?111100110131?
010--?-32?-1-1103--00021----001-111211-
4111111102?221320100???512?21100(1
2)1101111100?0?0000????1001???0??10?00000?0-
101?0001?00100001?00?1??0??1??1?1?0?0??0??10?---12?-
0?30????00?0-
?111?0201?1111000120110111100100221112??11?1112022302112111
1{12}01111011011111?1021?1110110101111110110-0?00??

Pararhabdodon_isonensis

??1?????????
????????????????????0??1----001111?211-
3111111112?221321100???
???
?????????-?????????????-
????????????????11????????????1???01002{12}11?????????????????????
????????????????????????2????????1???1111????????????????

Ajnabia_odysseus

????????????0?102???
????????????????????????1----0???1???11-
3111111112?1?1321??0?????2???
???

??
??
????????????

Amurosaurus_riabinini

1{2
3}20221210111110211111211??1112010110111121111101111121000
--1-22?-1-121?--00021----001-121211-
31001111021221320100?1?31?12110101111011111010?001010??101?
00?10???1?01110-111??01120010010011011000?????101-2-
11????10{12}---12?-0-3?010?????-
211???10????1??0?1?111211?11010022110??11????02?213021?2?10
-2???1101101?????0?201????????1111?1????1???001

Sahaliyana_elunchunorum

11?0221210????????????????????21120111101111211????????????????
????????????????????????1----001-11??11-
3?001?11?2?211???00????3121211?1011100?11?1????????????????
?????????1?0111?-
??1???00?2001?010???0?1000?????????????????????????---
????????????????????-
?????????????????1?????1??1??001002211?????????02121312112110
-20111101101111011?1?112011?????1?????????1???00?

Olorotitan_ararhensis

1?203211112211??31?111?111111110?11101111211111111111210000
 --1-220-1-12??--?0021----001-111211-
 3100111102122132010?3??512120101111???1?1110?0?0?1??????1?
 10?111??????0-111?00?1?0?1000????0?1?0000???101-2-
 2??1??101---12?-0-3?01?010?1-
 11110210?011?2?1012111111211010022101???????12021312112111
 02011?1??????????2101120110?0111????????????01

Charonosaurus_jiayinensis

112?33121????????????????2?1100111011112111111?11?????????
 ???????-???21?--00???-
 ???0???1???1??3??????1?????1??0??????31212010101??????111??
 0?0?201012001?0011?12?00?11?0-
 1121001120010010??1011100??1??10?-?-??????1??---1??-0-
 ??????????-
 ?111??101?????1????????1??1111010012111???10???120223?2112010
 -201111?????11??1?2101??0?1111111111?1??1??????

Parasaurolophus_walkeri

1220????1???111031?11131110211200111011112?1111111111210000
 --1-???-1-122?--00021----011-111?11-
 3100?11102022132??0?310412120102011000111110102002110110012
 0?11?12?00?31?0-112100010001????????????00??1??101-2-

410111112---12?-0-22100000-
00211110101?1111???1211111111100012210011110011120233121120
10-2011?111101111?1021?112011?1111???????0100?1?0

Parasaurolophus_tubicen

122032111012111????????11??2?120011111112111111111????????
??1????-???22?--00021----011-111211-
3100111102?221320101310412120102011?00111110102002110110012
1112-?2?00131?0-1?21000100010010100011?00??102101-2-
?10111112---12?-0-22100000-
01?111?2101??1?2?
??10

Parasaurolophus_cyrtocristatus

?220221110????????????11?????????1?01?112?1???1?11??????0?
??1?323-???225--0002?-
????????????????????????????????????310????????????????11101
0200?1101100121112-11?001?1?0-
112?0001?0010010100011100?????101-2-?10111112---12?-0-
22100000-
00?1?1?21?1?11110????????11110101221001111????121233121120
10-20111111011111020?01102111111111??10????110

Tlatolophus_galorum

1?20221211121120211111211101122001111111211??????21410000
 --1-323-1-1223--00021----001-120111-
 3100111102?221320101310????????????????1110102001110110010
 1112-12?00131?0-112?00111011001010001110000?02101-2-
 410111112---12?-0?12100000-
 0?2111?0112??
 ???1???

Adelolophus_hutchisoni

??
 ?????????????????????????1----?11-1?0?11-
 3101111102???1320??1????????????????????????????????
 ???
 ???
 ???
 ????????????

Angulomastacator_daviesi

??????????2?1????????????????????????????????????
 ?????????????????????????1----?1-11??11-
 310?111102?2213201?0?????2????????????????????
 ???
 ???

??
????????????

Lambeosaurus_lambeii

1(12)20(23)21111(12)21110(23)10111(23)1110111100111011112?1
11111111210000--1-222-1-1213--00021----001-
1(12)1?1??3100?11102122132?10?31031212(01)10111100011111010
1001010110011??1??1211001110-
11110001100100101100?1010001??101-2-101110101---12?-0-
3213110101-
11110210101111010121111112100100??111{12}111111112022312112
110-20111111?011111112101120110101111111110?00??0?

Lambeosaurus_magnicristatus

1?20?21?1?(12)2111?(23)1011121110111100111011112?11111?1111
210000--1-222-1-1213--00021----001-121?11-
3100111102122032??0?310312120101111000111110101001010110011
0?110121?001110-11??0001?001?0?????0?1?1???1??101-2-
10?1?0101---12?-0-3213110111-
11110210??11??01?1??????12100100221112111?11112022312112110
-20111111101111?1121?1120210101111?1??10???????

Corythosaurus_casuaris

12202211111211?03101112111021(12)(01)0011101111211111111111

210000--1-121-1-1214--00021----001-121111-
3100111102122032010031031212(01)101111000111110102001010110
011001101211001110-11110001100100101100?1000001??101-2-
101100101---12?-0-3202101011-
(01)11102101011110101211111211010022101211111112022312112
110-201111110111111121?1120210101111110110?????01

Corythosaurus_intermedius

12202211111211?031011121110211(01)00111011112?1111111111210
000--1-121-1-1214--00021----001-121?11-
3100?11102122032?10?31031212(01)101111000111110102001010110
011?01??1211001110-11110001100100?01100?100000111101-2-
101100101---12?-0-3202101001-
(01)1110210101111?1?12111111211010022101211111112022312112
110-2011111110111111121?11202101011111101101000001

Magnapaulia_laticaudus

1120221?1012111????????????1??1?0?1????11211??????111210000
--1-???-1-1???--?0?21----001-12??11-
3100111102?220320100???312120???1????????????????????????1?
????????????????-????????????????????????????????101-2-
2?????????---1??-0-????????????-
??1????????12?0??12111111??001002111????????12021312112?1?
???111101101111110210112021010111????????????

Hypacrosaurus_altispinus

112?32121112112?311111211??111(12)001?101?112111111?1111210
000--1-122-1-1214--00021----001-121211-
3100111102122032010031051212(01)101111000111110102001010010
011001111211001110-11110001100100100100?10(01)0001??101-2-
311100101---12?-0-3201101001-
(01)111021011112101?12111111210010022101211111112022312112
11121011110110111111021?11102111011111101101000001

Hypacrosaurus_stebingeri

112?32(01)111221??03101112111011120011101111211111111111210
000--1-121-1-1214--00021----001-121211-
3100111102122032?10?310312121101111000111110102001010110011
001101211001110-11110001100100?0110011000??111101-2-
111100101---12?-0-3201101011-
111102101???21?1?121111111100100221012???????12022312112111
02011110110111111021?11?011010111?1101101??0001

Velafrons_coahuilensis

1?2012111?12111021?111211??11120011101111211?????1101210000
--1-121-1-1214--00021----001-111111-
31001111021220220100???31?121101011100111100?0200001010001?
0011112?10011?0-11110001?00?????000?????????111101-2-

211100101---12?-0-3102101000-

211101101?1??1???12011{01}1????010?{12}2111?0010?1?12121212

1120112101111?1??111111?210112011000111111110?1??0?1

Latirhinus_uitstlani

??

????????????????????????????-

??

??

??11100?11?

?00100211010111??1??11212121122110201?11????????????????????2

1100111111????????????

Yamatosaurus_izanagii

121?221210????????????????????111??01????11120111110????????????

??

??

??

????????????????????210001????????????????????????????????????

??

Fylax_thyrakolasus

011?210210????????????????????10?1?0?1010100001????0????????????

??

??
??
??
??

TMP_2010_077_0030

??
????????????????00?2???0??
????????????????????????00-????0000101100?00?1?????????0???0-
0?1??020??1???1111??01000?????010?1?-
??00?0????????????????????????????
??
????????????????111?0?

TMP_2016_023_0039

??
??
????????????????????????????0?001?10??0????????????????0?03110-
1?2?00011?0100101?0011100????????????????????????????????1????????????
????????????????1??
??1001111

CMN_52845

??
????????????????{12}??
??111?0-
??3??0??0??1????????????
??
??0?-????

References

- Barrett, P. M., Butler, R. J., Wang X.-L., and Xu X. 2009. Cranial anatomy of the iguanodontoid ornithopod *Jinzhouosaurus yangi* from the Lower Cretaceous Yixian Formation of China. *Acta Palaeontologica Polonica* 54:35–48.
- Baziak, B. 2008. Comparative osteohistology of *Maiasaura peeblesorum* (Hadrosauridae) from the Two Medicine Formation (Campanian) Camp-O-Saur bonebed of Montana. *Journal of Vertebrate Paleontology* 28: 49A.
- Bell, P. R. 2011a. Redescription of the skull of *Saurolophus osborni* Brown, 1912 (Ornithischia: Hadrosauridae). *Cretaceous Research* 32: 30–44.
- Bell, P. R. 2011b. Cranial osteology and ontogeny of *Saurolophus angustirostris* from the Late Cretaceous of Mongolia with comments on *Saurolophus osborni* from Canada. *Acta Palaeontologica Polonica* 56: 703–722.
- Bell, P. R. 2014. A review of hadrosaurid skin impressions. In: D.A. Eberth and D.C. Evans (eds.), *Hadrosaurs*, 572–590. Indiana University Press, Bloomington.
- Bell, P. R. and Evans, D. C. 2010. Revision of the status of *Saurolophus* (Hadrosauridae) from California, USA. *Canadian Journal of Earth Sciences* 47:1417–1426.

Bell, P. R., Fanti, F., Currie, P. J., and Arbour, V. M. 2014. A mummified duck-billed dinosaur with a soft-tissue cock's comb. *Current Biology* 24: 70–75.

Bertozzo, F., Dal Sasso, C., Fabbri, M., Manucci, F., and Maganuco, S. 2017.

Redescription of a remarkably large *Gryposaurus notabilis* (Dinosauria: Hadrosauridae) from Alberta, Canada. *Memorie della Società Italiana di Scienze Naturali e del Museo Civico di Storia Naturale di Milano* 43: 1–56.

Bertozzo, F., Manucci, F., Dempsey, M., Tanke, D. H., Evans, D. C., Ruffell, A., and Murphy, E. 2021. Description and etiology of paleopathological lesions in the type specimen of *Parasaurolophus walkeri* (Dinosauria: Hadrosauridae), with proposed reconstructions of the nuchal ligament. *Journal of Anatomy* 238:1055–1069.

Bertozzo, F., Bolotsky, I., Bolotsky, Y. L., Poberezhskiy, A., Ruffell, A., Godefroit, P., and Murphy, E. 2022. A pathological ulna of *Amurosaurus riabinini* from the Upper Cretaceous of Far Eastern Russia. *Historical Biology*,
doi:10.1080/08912963.2022.2034805

Beveridge, T. L., Roberts, E. M., Ramezani, J., Titus, A. L., Eaton, J. G., Irmis, R. B., and Sertich, J. J. W. 2022. Refined geochronology and revised stratigraphic nomenclature of the Upper Cretaceous Wahweap Formation, Utah, U.S.A. and the age of early Campanian vertebrates from southern Laramidia. *Palaeogeography, Palaeoclimatology, Palaeoecology* 591:110876, 1–22.

Bolotsky, Y. L. and Godefroit, P. 2004. A new hadrosaurine dinosaur from the Late Cretaceous of Far Eastern Russia. *Journal of Vertebrate Paleontology* 24: 351–365.

Brett-Surman, M. K. 1989. A revision of the Hadrosauridae (Reptilia: Ornithischia) and their evolution during the Campanian and Maastrichtian. PhD thesis, George Washington University, Washington D.C. 192 pp.

Brink, K. S., Zelenitsky, D. K., Evans, D. C., Therrien, F., and Horner, J. R. 2011. A sub-adult skull of *Hypacrosaurus stebingeri* (Ornithischia: Lambeosaurinae): anatomy and comparison. *Historical Biology* 23: 63–72.

Brazeau, M. D. 2011. Problematic character coding methods in morphology and their effects. *Biological Journal of the Linnean Society* 104:489–498.

Brown B. 1914a. *Anchiceratops*, a new genus of horned dinosaurs from the Edmonton Cretaceous of Alberta. With discussion of the origin of the ceratopsian crest and the brain casts of *Anchiceratops* and *Trachodon*. *Bulletin of the American Museum of Natural History* 33:539–548.

Brown B. 1914b. *Corythosaurus casuarius*, a new crested dinosaur from the Belly River Cretaceous, with provisional classification of the family Trachodontidae. *American Museum of Natural History Bulletin* 33:559–565.

Brown, B. 1916. A new crested trachodont dinosaur *Prosaurolophus maximus*. *Bulletin of the American Museum of Natural History* 35: 701–708.

Brown, C. 2022. Hadrosaur Variations II. NIME: International Conference on New Interfaces for Musical Expression 2022. doi:10.21428/92fbeb44.fa9fd7a0

Brown, C. M., Ryan, M. J., and Evans, D. C. 2015. A census of Canadian dinosaurs: more than a century of discovery. In *All Animals Are Interesting: A Festschrift in Honour of Anthony P. Russell*. Edited by O.R.P. Bininda-Emonds, G.L. Powell, H.A. Jamniczky, A.M. Bauer, and J. Theodor. BIS Verlag. pp. 151–191.

Brown, C. M., Herridge-Berry, S., Chiba, K., Vitkus, A., and Eberth, D. A. 2021. High-resolution (centimetre-scale) GPS/GIS-based 3D mapping and spatial analysis of in situ fossils in two horned-dinosaur bonebeds in the Dinosaur Park Formation (Upper Cretaceous) at Dinosaur Provincial Park, Alberta, Canada. *Canadian Journal of Earth Sciences* 58:225–246.

Brownstein, C. D. 2021. Dinosaurs from the Santonian–Campanian Atlantic coastline substantiate phylogenetic signatures of vicariance in Cretaceous North America. *Royal Society Open Science* 8:210127, 1–23.

Brownstein, C. D. and Bissell, I. 2021. An elongate hadrosaurid forelimb with biological traces informs the biogeography of the Lambeosaurinae. *Journal of Paleontology* 95:367–375.

Bullar, C. M., Zhao, Q., Benton, M. J., and Ryan, M. J. 2019. Ontogenetic braincase development in *Psittacosaurus lujiatunensis* (Dinosauria: Ceratopsia) using micro-computed tomography. *PeerJ* 7: e7217.

Burnham, D. A., Derstler, K. L., and Linster, C. J. 1997. A new specimen of *Velociraptor* (Dinosauria: Theropoda) from the Two Medicine Formation of Montana. In: D.L.Wolberg, E. Stump, and G.D. Rosenberg (eds.), *Dinofest International: Proceedings of a Symposium Sponsored by Arizona State University*, 73–75. The Academy of Natural Sciences, Philadelphia.

Burnham, D. A., Derstler, K. L., Currie, P. J., Bakker, R. T., Zhou, Z., and Ostrom, J. H. 2000. Remarkable new birdlike dinosaur (Theropoda: Maniraptora) from the Upper Cretaceous of Montana. *The University of Kansas Paleontological Contributions* 13: 1–14.

Campbell, J. A., Ryan, M. J., Holmes, R. B., and Schröder-Adams, C. J. 2016. A re-evaluation of the chasmosaurine ceratopsid genus *Chasmosaurus* (Dinosauria: Ornithischia) from the Upper Cretaceous (Campanian) Dinosaur Park Formation of western Canada. *PLoS One* 11:e0145805

Campione, N. E. and Evans, D. C. 2011. Cranial growth and variation in edmontosaurs (Dinosauria: Hadrosauridae): implications for latest Cretaceous megaherbivore diversity in North America. PLoS One 6: e25186.

Campione, N. E., Brink, K. S., Freedman, E. A., McGarrity, C. T., and Evans, D. C. 2013. “*Glishades ericksoni*”, an indeterminate juvenile hadrosaurid from the Two Medicine Formation of Montana: implications for hadrosauroid diversity in the latest Cretaceous (Campanian–Maastrichtian) of western North America. Palaeobiodiversity and Palaeoenvironments 93: 65–75.

Carpenter, K. 1999. *Eggs, Nests, and Baby Dinosaurs: A Look at Dinosaur Reproduction*. 336 pp. Indiana University Press, Bloomington.

Chiarenza, A. A., Fabbri, M., Consorti, L., Muscioni, M., Evans, D. C., Cantalpedrea, J. L., and Fanti, F. 2021. An Italian dinosaur Lagerstätte reveals the tempo and mode of hadrosauriform body size evolution. Scientific Reports 11:23295, 1–15.

Chiba, K., Ryan, M. J., Fanti, F., Loewen, M. A., and Evans, D. C. 2018. New material and systematic re-evaluation of *Medusaceratops lokii* (Dinosauria, Ceratopsidae) from the Judith River Formation (Campanian, Montana). Journal of Paleontology 92:272–288.

Christison, B. E., Tanke, D. H., and Mallon, J. C. 2020. Canada's first known dinosaurs: palaeontology and collecting history of Upper Cretaceous vertebrates in southern Alberta and Saskatchewan, 1874–1889. *Earth Sciences History* 39:184–218.

Conti, S., Vila, B., Sellés, A. G., Galobart, À., Benton, M. J., and Prieto-Márquez, A. 2020. The oldest lambeosaurine dinosaur from Europe: insights into the arrival of Tsintaosaurini. *Cretaceous Research* 107: 104286, 1–15.

Coombs, W.P. 1988. The status of the dinosaurian genus *Diclonius* and the taxonomic utility of hadrosaurian teeth. *Journal of Vertebrate Paleontology*, 62: 812–817.

Cope, E.D. 1869. Synopsis of the extinct Batrachia, Reptilia, and Aves of North America. *Transactions of the American Philosophical Society*, 14(1): 1–252.

Cruzado-Caballero, P. and Powell, J. 2017. *Bonapartesaurus rionegrensis*, a new hadrosaurine dinosaur from South America: implications for phylogenetic and biogeographic relations with North America. *Journal of Vertebrate Paleontology* e1289381, 1–16.

Cruzado-Caballero, P., Pereda-Suberbiola, X., and Ruiz-Omeñaca, J. I. 2010. *Blasisaurus canudo* gen. et sp. nov., a new lambeosaurine dinosaur (Hadrosauridae) from the Latest Cretaceous of Arén (Huesca, Spain). *Canadian Journal of Earth Sciences* 47:1507–1517.

Cruzado-Caballero, P., Lecuona, A., Cerda, I., and Díaz-Martínez, I. 2021. Osseous paleopathologies of *Bonapartesaurus rionegrensis* (Ornithopoda, Hadrosauridae) from Allen Formation (Upper Cretaceous) of Patagonia Argentina. *Cretaceous Research* 124:104800.

Cullen, T. M., and Evans, D. C. 2016. Palaeoenvironmental drivers of vertebrate community composition in the Belly River Group (Campanian) of Alberta, Canada, with implications for dinosaur biogeography. *BMC Ecology*, 16(52): 1–35.

Cullen, T. M., Zhang, S., Spencer, J., and Cousens, B. 2022. Sr-O-C isotope signatures reveal herbivore niche-partitioning in a Cretaceous ecosystem. *Palaeontology* 65 (2):e12591.

Cuthbertson, R. S. and Holmes, R. B. 2010. The first complete description of the holotype of *Brachylophosaurus canadensis* Sternberg, 1953 (Dinosauria: Hadrosauridae) with comments on intraspecific variation. *Zoological Journal of the Linnean Society* 159: 373–397.

Dalman, S. G., Lucas, S. G., Jasinski, S. E., Lichtig, A. J., and Dodson, P. 2021. The oldest centrosaurine: a new ceratopsid dinosaur (Dinosauria: Ceratopsidae) from the Allison Member of the Menefee Formation (Upper Cretaceous, early Campanian), northwestern New Mexico, USA. *PalZ* 95:291–335.

Dilkes, D.W. 2001. An ontogenetic perspective on locomotion in the Late Cretaceous dinosaur *Maiasaura peeblesorum* (Ornithischia: Hadrosauridae). *Canadian Journal of Earth Sciences* 38: 1205–1227.

Dodson, P. 1975. Taxonomic implications of relative growth in lambeosaurine hadrosaurs. *Systematic Zoology* 24: 37–54.

Dodson, P. 1995. *An Alphabet of Dinosaurs*. 64 pp. (pages unnumbered) Scholastic Inc., New York.

Dollo, L. 1888. Iguanodontidae et Camptosauridae. *Comptes Rendus de l'Academie des Sciences*, 106: 775–777.

Drysdale, E. T., Therrien, F., Zelenitsky, D. K., Weishampel, D. B., and Evans, D. C. 2019. Description of juvenile specimens of *Prosaurolophus maximus* (Hadrosauridae, Saurolophinae) from the Upper Cretaceous Bearpaw Formation of southern Alberta, Canada, reveals ontogenetic changes in crest morphology. *Journal of Vertebrate Paleontology* 39: e1547310.

Eberth, D. A. 2005. The geology. In *Dinosaur Provincial Park: A Spectacular Ancient Ecosystem Revealed*, Edited by P.J. Currie, and E.B. Koppelhus. Indiana University Press. pp. 54–82.

Eberth, D. A., Evans, D. C., Brinkman, D. B., Therrien, F., Tanke, D. H., and Russell, L. S. 2013. Dinosaur biostratigraphy of the Edmonton Group (Upper Cretaceous), Alberta, Canada: evidence for climate influence. *Canadian Journal of Earth Sciences*, 50(7): 701–726.

Evans, D. C. 2006. Nasal cavity homologies and cranial crest function in lambeosaurine dinosaurs. *Paleobiology* 32: 109–125.

Evans, D. C. 2010. Cranial anatomy and systematics of *Hypacrosaurus altispinus*, and a comparative analysis of skull growth in lambeosaurine hadrosaurids (Dinosauria: Ornithischia). *Zoological Journal of the Linnean Society* 159: 398–434.

Evans, D. C. and Reisz, R. R. 2007. Anatomy and relationships of *Lambeosaurus magnicristatus*, a crested hadrosaurid dinosaur (Ornithischia) from the Dinosaur Park Formation, Alberta. *Journal of Vertebrate Paleontology* 27:373–393.

Evans, D. C. and Ryan, M. J. 2015. Cranial anatomy of *Wendiceratops pinhornensis* gen. et sp. nov., a centrosaurine ceratopsid (Dinosauria: Ornithischia) from the Oldman Formation (Campanian), Alberta, Canada, and the evolution of ceratopsid nasal ornamentation. *PLoS One* 10:e0130007

Evans, D.C., Forster, C.A., and Reisz, R.R. 2005. The type specimen of *Tetragonosaurus erectofrons* (Ornithischia: Hadrosauridae) and the identification of juvenile lambeosaurines. In: P.J. Currie and E.B. Koppelhus (eds.), *Dinosaur Provincial Park: A Spectacular Ancient Ecosystem Revealed*, 349–366. Indiana University Press, Bloomington.

Evans, D. C., Reisz, R. R., and Dupuis, K. 2007. A juvenile *Parasaurolophus* (Ornithischia: Hadrosauridae) braincase from Dinosaur Provincial Park, Alberta, with comments on crest ontogeny in the genus. *Journal of Vertebrate Paleontology* 27: 642–650.

Evans, D. C., Bavington, R., and Campione, N. E. 2009a. An unusual hadrosaurid braincase from the Dinosaur Park Formation and the biostratigraphy of *Parasaurolophus* (Ornithischia: Lambeosaurinae) from southern Alberta. *Canadian Journal of Earth Sciences* 46:791–800.

Evans, D. C., Ridgely, R., and Witmer, L. M. 2009b. Endocranial anatomy of lambeosaurine hadrosaurids (Dinosauria: Ornithischia): a sensorineural perspective on cranial crest function. *The Anatomical Record* 292:1315–1337.

Farke, A. A. and Herrero, L. 2014. Variation in the skull roof of the hadrosaur *Gryposaurus* illustrated by a new specimen from the Kaiparowits Formation (late

Campanian) of southern Utah. In: D.A. Eberth and D.C. Evans (eds.), *Hadrosaurs*, 191–199. Indiana University Press, Bloomington.

Farke, A. A., Ryan, M. J., Barrett, P. M., Tanke, D. H., Braman, D. R., Loewen, M. A., and Graham, M. R. 2011. A new centrosaurine from the Late Cretaceous of Alberta, Canada, and the evolution of parietal ornamentation in horned dinosaurs. *Acta Palaeontologica Polonica* 56:691–702.

Farke, A. A., Chok, D. J., Herrero, A., Scolieri, B., and Werning, S. 2013. Ontogeny in the tube-crested dinosaur *Parasaurolophus* (Hadrosauridae) and heterochrony in hadrosaurids. *PeerJ* 1: e182.

Freedman Fowler, E. A. and Horner, J. R. 2015. A new brachylophosaurin hadrosaur (Dinosauria: Ornithischia) with an intermediate nasal crest from the Campanian Judith River Formation of northcentral Montana. *PLoS One* 10: e0141304.

Fondevilla, V., Dalla Vecchia, F. M., Gaete, R., Galobart, À., Moncunill-Solé, B., and Köhler, M. 2018. Ontogeny and taxonomy of the hadrosaur (Dinosauria, Ornithopoda) remains from Basturs Poble bonebed (late early Maastrichtian, Tremp Syncline, Spain). *PLoS One* 13:e0206287

Fowler, D. W. 2017. Revised geochronology, correlation, and dinosaur stratigraphic ranges of the Santonian–Maastrichtian (Late Cretaceous) formations of the Western

Interior of North America. PLoS One 12:e0188426, 1–20.

Gates, T. A. and Lamb, J. P. 2021. A redescription of *Lophorhothon atopus* (Ornithopoda: Dinosauria) from the Late Cretaceous of Alabama based on new material. Canadian Journal of Earth Sciences 58:918–935.

Gates, T. A. and Sampson, S. D. 2007. A new species of *Gryposaurus* (Dinosauria: Hadrosauridae) from the late Campanian Kaiparowits Formation, southern Utah, USA. Zoological Journal of the Linnean Society 151: 351–376.

Gates, T. A., and Scheetz, R. 2015. A new saurolophine hadrosaurid (Dinosauria: Ornithopoda) from the Campanian of Utah, North America. Journal of Systematic Palaeontology, 13(8): 711–725.

Gates, T. A., Sampson, S. D., Delgado De Jesús, C. R., Zanno, L. E., Eberth, D. A., Hernandez-Rivera, R., Aguillón Martínez, M. C., and Kirkland, J. I. 2007. *Velafrons coahuilensis*, a new lambeosaurine hadrosaurid (Dinosauria: Ornithopoda) from the late Campanian Cerro del Pueblo Formation, Coahuila, Mexico. Journal of Vertebrate Palaeontology 27: 917–930.

Gates, T. A., Horner, J. R., Hanna, R. R., and Nelson, C. R. 2011. New un-adorned hadrosaurine hadrosaurid (Dinosauria, Ornithopoda) from the Campanian of North America. Journal of Vertebrate Paleontology 31: 798–811.

Gates, T. A., Lund, E. K., Boyd, C. A., DeBlieux, D. D., Titus, A. L., Evans, D. C., Getty, M. A., Kirkland, J. I., and Eaton, J. G. 2013. Ornithopod dinosaurs from the Grand Staircase-Escalante National Monument Region, Utah, and their role in paleobiogeographic and macroevolutionary studies. In *At the Top of the Grand Staircase: The Late Cretaceous of Southern Utah*. Edited by A. L. Titan and M. A. Loewen. Indiana University Press. pp. 463–481.

Gates, T. A., Jinnah, Z., Levitt, C., and Getty, M. A. 2014. New hadrosaurid specimens from the lower-middle Campanian Wahweap Formation of Utah. In *Hadrosaurs*. Edited by D. A. Eberth and D. C. Evans. Indiana University Press. pp. 156–173.

Gates, T. A., Evans, D. C., and Sertich, J. J. W. 2021. Description and rediagnosis of the crested hadrosaurid (Ornithopoda) dinosaur *Parasaurolophus cyrtocristatus* on the basis of new cranial remains. *PeerJ* 9:e10669, 1–35.

Godefroit, P., Zan S. and Jin L. 2000. *Charonosaurus jiayinensis* n.g., n.sp., a lambeosaurine dinosaur from the Late Maastrichtian of northeastern China. *C. R. Acad. Sci. Paris, Sciences de la Terre et desplanètes/Earth and Planetary Sciences* 330:875–882.

Godefroit, P., Zan S. and Jin L. 2001. The Maastrichtian (Late Cretaceous) lambeosaurine dinosaur *Charonosaurus jiayinensis* from north-eastern China. *Bulletin de l'Institut Royal des Sciences Naturelles de Belgique, Sciences de la Terre* 71:119–168.

- Godefroit, P., Alifanov, V., and Bolotsky, Y. 2004a. A re-appraisal of *Aralosaurus tuberiferus* (Dinosauria, Hadrosauridae) from the Late Cretaceous of Kazakhstan. *Bulletin de l'Institut Royal des Sciences Naturelles de Belgique, Sciences de la Terre* 74 (Suppl.):139–154.
- Godefroit, P., Bolotsky, Y. L., and Van Itterbeeck, J. 2004. The lambeosaurine dinosaur *Amurosaurus riabinini*, from the Maastrichtian of Far Eastern Russia. *Acta Palaeontologica Polonica* 49: 585–618.
- Godefroit, P., Shulin, H., Tingxiang, Y., and Lauters, P. 2008. New hadrosaurid dinosaurs from the uppermost Cretaceous of northeastern China. *Acta Palaeontologica Polonica*, 53(1): 47–74.
- Godefroit, P., Bolotsky, Y. L., and Bolotsky, I Y. 2012a. Osteology and relationships of *Olorotitan arharensis*, a hollow-crested hadrosaurid dinosaur from the latest Cretaceous of far eastern Russia. *Acta Palaeontologica Polonica* 57:527–560.
- Godefroit, P., Bolotsky, Y. L., and Lauters, P. 2012b. A new saurolophine dinosaur from the latest Cretaceous of far eastern Russia. *PLoS One*, 7(5): e36849.

Griffin, C. T., Stocker, M. R., Colleary, C., Stefanic, C. M., Lessner, E. J., Riegler, M., Formoso, K., Koeller, K., and Nesbitt, S. J. 2021. Assessing ontogenetic maturity in extinct saurian reptiles. *Biological Reviews* 96:470–525. DOI: 10.1111/brv.12666

Guenther, M. F., Macmillan, A., and Bank, N. 2018. The influence of heterochrony on the evolution of the hadrosauroid dentary. *Journal of Vertebrate Paleontology, Program and Abstracts*, 2018: 138.

Heck, C. T. and Woodward, H. N. 2018. Using bone microstructure to infer intraskeletal growth and postural shifts in the hadrosaurid dinosaur *Maiasaura peeblesorum*. *Journal of Vertebrate Paleontology, Program and Abstracts*, 2018: 144.

Heck, C.T. and Woodward Ballard, H. 2019. An arm and a leg: testing ontogenetic posture change in *Maiasaura peeblesorum* through limb scaling and osteohistology. *Journal of Vertebrate Paleontology, Program and Abstracts*, 2019: 116.

Hickie, E., Evans, D. C., and Maddin, H. C. 2015. Braincase anatomy of *Maiasaura peeblesorum*. *Journal of Vertebrate Paleontology, Program and Abstracts*, 2015: 142.

Holland, B., Bell, P. R., Fanti, F., Hamilton, S. M., Larson, D. W., Sissons, R., Sullivan, C., Vavrek, M. J., Wang, Y., and Campione, N. E. 2021. Taphonomy and taxonomy of a juvenile lambeosaurine (Ornithischia: Hadrosauridae) bonebed from the late Campanian Wapiti Formation of northwestern Alberta, Canada. *PeerJ* 9:e11290, 1–38.

Holliday, C. M. 2006. Evolution and function of the jaw musculature and adductor chamber of archosaurs (crocodilians, dinosaurs, and birds). PhD thesis, Ohio University. 326 pp.

Holliday, C. M. 2009. New insights into dinosaur jaw muscle anatomy. *The Anatomical Record* 292: 1246–1265.

Holliday, C. M. and Witmer, L. M. 2008. Cranial kinesis in dinosaurs: intracranial joints, protractor muscles, and their significance for cranial evolution and function in diapsids. *Journal of Vertebrate Paleontology* 28:1073–1088.

Holliday, C. M., Porter, W. R., Vliet, K. A., and Witmer, L. M. 2020. The frontoparietal fossa and dorsotemporal fenestra of archosaurs and their significance for interpretations of vascular and muscular anatomy in dinosaurs. *The Anatomical Record* 303: 1060–1074.

Holmes, R. B., Forster, C., Ryan, M., and Shepherd, K. M. 2001. A new species of *Chasmosaurus* (Dinosauria: Ceratopsia) from the Dinosaur Park Formation of southern Alberta. *Canadian Journal of Earth Sciences* 38:1423–1438.

Hone, D. W. E. and Mallon, J. C. 2017. Protracted growth impedes the detection of sexual dimorphism in non-avian dinosaurs. *Palaeontology* 60: 535–545.

Hopson, J. A. 1975. The evolution of cranial display structures in hadrosaurian dinosaurs. *Paleobiology* 1: 21–43.

Horner, J. R. 1983. Cranial osteology and morphology of the type specimen of *Maiasaura peeblesorum* (Ornithischia: Hadrosauridae), with discussion of its phylogenetic position. *Journal of Vertebrate Paleontology* 3: 29–38.

Horner, J. R. 1988. A new hadrosaur (Reptilia, Ornithischia) from the Upper Cretaceous Judith River Formation of Montana. *Journal of Vertebrate Paleontology* 8: 314–321.

Horner, J. R. 1992. Cranial morphology of *Prosaurolophus* (Ornithischia: Hadrosauridae) with descriptions of two new hadrosaurid species and an evaluation of hadrosaurid phylogenetic relationships. *Museum of the Rockies Occasional Paper* 2: 1–119.

Horner, J. R. 1999. Egg clutches and embryos of two hadrosaurian dinosaurs. *Journal of Vertebrate Paleontology* 19: 607–611.

Horner, J. R., and Currie, P. J. 1994. Embryonic and neonatal morphology and ontogeny of a new species of *Hypacrosaurus* (Ornithischia, Lambeosauridae) from Montana and Alberta. In *Dinosaur Eggs and Babies*. Edited by K. Carpenter, K. F. Hirsch, and J. R. Horner. Cambridge University Press. pp. 312–336.

Horner, J. R. and Makela, R. 1979. Nest of juveniles provides evidence of family structure among dinosaurs. *Nature* 282: 296–298.

Horner, J. R., De Ricqlès, A., and Padian, K. 2000. Long bone histology of the hadrosaurid dinosaur *Maiasaura peeblesorum*: growth dynamics and physiology based on an ontogenetic series of skeletal elements. *Journal of Vertebrate Paleontology* 20: 115–129.

Horner, J. R., Weishampel, D. B., and Forster, C. A. 2004. Hadrosauridae. In: D. B. Weishampel, P. Dodson, and H. Osmólska (eds.), *The Dinosauria. Second Edition*, 438–463. University of California Press, Berkeley.

Kirkland, J. I. 1998. A new hadrosaurid from the upper Cedar Mountain Formation (Albian-Cenomanian: Cretaceous) of eastern Utah – the oldest known hadrosaurid (Iambeosaurine?). *New Mexico Museum of Natural History and Science Bulletin* 14:283–295.

Knapp, A., Knell, R. J., Farke, A. A., Loewen, M. A., and Hone, D. W. E. 2018. Patterns of divergence in the morphology of ceratopsian dinosaurs: sympatry is not a driver of ornament evolution. *Proceedings of the Royal Society B*, 285: 20180312.

Knell, R. J., and Sampson, S. 2011. Bizarre structures in dinosaurs: species recognition or sexual selection? A response to Padian and Horner. *Journal of Zoology*, 283(1): 18–22.

Kobayashi, Y., Nishimura, T., Takasaki, R., Chiba, K., Fiorillo, A. R., Tanaka, K., Chinzorig, T., Sato, T., and Sakurai, K. 2019. A new hadrosaurine (Dinosauria: Hadrosauridae) from the marine deposits of the Late Cretaceous Hakobuchi Formation, Yezo Group, Japan. *Scientific Reports* 9: 12389.

Kobayashi, Y., Takasaki, R., Kubota, K., and Fiorillo, A. R. 2021. A new basal hadrosaurid (Dinosauria: Ornithischia) from the latest Cretaceous Kita-ama Formation in Japan implies the origin of hadrosaurids. *Scientific Reports* 11:8547, 1–15.

Lambe L. M. 1918. On the genus *Trachodon* of Leidy. *Ottawa Naturalist* 31:135–139.

Lauters, P., Vercauteren, M., Bolotsky, Y. L., and Godefroit, P. 2013. Cranial endocast of the lambeosaurine hadrosaurid *Amurosaurus riabinini* from the Amur Region, Russia. *PLoS One* 8:e78889.

Langston, W. 1960. The vertebrate fauna of the Selma Formation of Alabama. Part VI: The dinosaurs. *Fieldiana: Geology Memoirs* 3: 315–359.

Larson, D W., Campione, N. E., Brown, C. M., Evans, D. C., and Ryan, M. J. 2014. Hadrosauroid material from the Santonian Milk River Formation of southern Alberta, Canada. In *Hadrosaurs*. Edited by D. A. Eberth and D. C. Evans. Indiana University Press. pp. 136–152.

Lehman, T. M., Wick, S. L., and Wagner, J. R. 2016. Hadrosaurian dinosaurs from the Maastrichtian Javelina Formation, Big Bend National Park, Texas. *Journal of Paleontology* 90:333–356.

Leidy J. 1858. *Hadrosaurus foulkii*, a new saurian from the Cretaceous of New Jersey, related to *Iguanodon*. *Proceedings of the Academy of Natural Sciences of Philadelphia* 10:213–218.

Longrich, N. R. 2010. *Mojoceratops perifania*, a new chasmosaurine ceratopsid from the late Campanian of western Canada. *Journal of Paleontology* 84:681–694.

Longrich, N. R. 2014. The horned dinosaurs *Pentaceratops* and *Kosmoceratops* from the upper Campanian of Alberta and implications for dinosaur biogeography. *Cretaceous Research* 51:292–308.

Longrich, N. R., Pereda Suberbiola, X., Pyron, R. A., and Jalil, N.-E. 2021. The first duckbill dinosaur (Hadrosauridae: Lambeosaurinae) from Africa and the role of oceanic dispersal in dinosaur biogeography. *Cretaceous Research* 120:104678, 1–15.

Lowi-Merri, T. M. and Evans, D. C. 2020. Cranial variation in *Gryposaurus* and biostratigraphy of hadrosaurines (Ornithischia: Hadrosauridae) from the Dinosaur Park Formation of Alberta, Canada. *Canadian Journal of Earth Sciences* 57: 765–779.

Madzia, D., Arbour, V. M., Boyd, C. A., Farke, A. A., Cruzado-Caballero, P., and Evans, D. C. The phylogenetic nomenclature of ornithischian dinosaurs. *PeerJ* 9:e12362, 1–98.

Maidment, S. C. R. and Barrett, P. M. 2011. A new specimen of *Chasmosaurus belli* (Ornithischia: Ceratopsidae), a revision of the genus, and the utility of postcrania in the taxonomy and systematics of ceratopsid dinosaurs. *Zootaxa* 2963:1–47.

Mallon, J. C. 2017. Recognizing sexual dimorphism in the fossil record: lessons from nonavian dinosaurs. *Paleobiology* 43: 495–507.

Mallon, J. C. 2019. Competition structured a Late Cretaceous megaherbivorous dinosaur assemblage. *Scientific Reports* 9:15447, 1–18.

Mallon, J. C., Evans, D. C., Ryan, M. J., and Anderson, J. S. 2012. Megaherbivorous dinosaur turnover in the Dinosaur Park Formation (upper Campanian) of Alberta, Canada. *Palaeogeography, Palaeoclimatology, Palaeoecology* 350–352:124–138.

Mallon, J. C., Ott, C. J., Larson, P. L., Iuliano, E. M., and Evans, D. C. 2016. *Spiclypeus shipporum* gen. et sp. nov., a boldly audacious new chasmosaurine ceratopsid (Dinosauria: Ornithischia) from the Judith River Formation (Upper Cretaceous: Campanian) of Montana, USA. *PLoS One* 11:e0154218

Martin, J. E., Hassler, A., Montagnac, G., Therrien, F., and Balter, V. 2021. The stability of dinosaur communities before the Cretaceous–Paleogene (K–Pg) boundary: A perspective from southern Alberta using calcium isotopes as a dietary proxy. *Geological Society of American Bulletin*, doi:10.1130/B36222.1

Maryńska, T. and Osmólska, H. 1979. Aspects of hadrosaurian cranial anatomy. *Lethaia* 12: 267–273.

Marsh, O. C. 1881. Principal characters of American Jurassic dinosaurs. Part IV. *American Journal of Science*, 21(125): 417–423.

McDonald, A. T., Bird, J., Kirkland, J. I., and Dodson, P. 2012. Osteology of the basal hadrosauroid *Eolambia caroljonesa* (Dinosauria: Ornithopoda) from the Cedar Mountain Formation of Utah. *PLoS One* 7:e45712, 1–38.

McDonald, A. T., Gates, T.A., Zanno, L.E., and Makovicky, P.J. 2017. Anatomy, taphonomy, and phylogenetic implications of a new specimen of *Eolambia caroljonesa* (Dinosauria: Ornithopoda) from the Cedar Mountain Formation, Utah, USA. *PLoS One* 12:e0176896.

McDonald, A.T., Wolfe, Douglas, G., and Freedman Fowler, E.A. 2019. A new crested brachylophosaurin (Dinosauria: Hadrosauridae) from the Upper Cretaceous Menefee Formation of New Mexico and Judith River Formation of Montana. In *Cretaceous &*

beyond: paleontology of the western interior [abstracts]. Dickinson Museum Center.

Available from http://dickinsonmuseumcenter.com/cret_and_beyond-abs10-

[mcdonald_et_al/](http://dickinsonmuseumcenter.com/cret_and_beyond-abs10-mcdonald_et_al/)

McDonald, A. T., Wofle, D. G., Freedman Fowler, E. A., and Gates, T. A. 2021. A new brachylophosaurin (Dinosauria: Hadrosauridae) from the Upper Cretaceous Menefee Formation of New Mexico. *PeerJ* 9:e11084, 1–28.

McFeeters, B. D., Evans, D. C., Ryan, M. J., and Maddin, H. C. 2021a. First occurrence of *Maiasaura* (Dinosauria, Hadrosauridae) from the Upper Cretaceous Oldman Formation of southern Alberta, Canada. *Canadian Journal of Earth Sciences* 58:286–296.

McFeeters, B. D., Evans, D. C., and Maddin, H. C. 2021b. Ontogeny and variation in the skull roof and braincase of the hadrosaurid dinosaur *Maiasaura peeblesorum* from the Upper Cretaceous of Montana, USA. *Acta Palaeontologica Polonica* 66:485–507.

McGarrity, C. T., Campione, N. E., and Evans, D. C. 2013. Cranial anatomy and variation in *Prosaurolophus maximus* (Dinosauria: Hadrosauridae). *Zoological Journal of the Linnean Society* 167: 531–568.

McKenna, M. F., Cranford, T. W., Berta, A., and Pyenson, N. D. 2012. Morphology of the odontocete melon and its implications for acoustic function. *Marine Mammal Science* 28: 690–713.

Mori, H., Druckenmiller, P. S., and Erickson, G. M. 2016. A new Arctic hadrosaurid from the Prince Creek Formation (lower Maastrichtian) of northern Alaska. *Acta Palaeontologica Polonica* 61:15–32.

Müller, J. and Reisz, R. R. 2006. The phylogeny of early eureptiles: comparing parsimony and Bayesian approaches in the investigation of a basal fossil clade. *Systematic Biology* 55:503–511.

Murphy, N. L., Trexler, D., and Thompson, M. 2007. “Leonardo,” a mummified *Brachylophosaurus* (Ornithischia: Hadrosauridae) from the Judith River Formation of Montana. In *Horns and Beaks: Ceratopsian and Ornithopod Dinosaurs*. Edited by K. Carpenter. Indiana University Press. pp. 117–133.

Norell, M. A. 1993. Tree-based approaches to understanding history: comments on ranks, rules, and the quality of the fossil record. *American Journal of Science* 293-A:407–417.

Norman, D. B. Iguanodonts from the Wealden of England: Do they contribute to discussion concerning hadrosaur origins? In *Hadrosaurs*. Edited by D. A. Eberth and D. C. Evans. Indiana University Press. pp. 10–43.

Ostrom, J. H. 1961a. Cranial morphology of the hadrosaurian dinosaurs of North

America. *Bulletin of the American Museum of Natural History* 122: 33–186.

Ostrom, J. H. 1961b. A new species of hadrosaurian dinosaur from the Cretaceous of New Mexico. *Journal of Paleontology* 35:575–577.

Padian, K., and Horner, J. R. 2011. The evolution of ‘bizarre structures’ in dinosaurs: biomechanics, sexual selection, social selection or species recognition? *Journal of Zoology*, 283(1): 3–17.

Parks, W. A. 1922. *Parasaurolophus walkeri*, a new genus and species of crested trachodont dinosaur. *University of Toronto Studies, Geological Series* 13:1–32.

Parks, W. A. 1923. *Corythosaurus intermedius*, a new species of trachodont dinosaur. *University of Toronto Studies, Geological Series* 15:5–57.

Pereda-Suberbiola, X., Canudo, J. I., Cruzado-Caballero, P., Barco, J. L., López-Martínez, N., Oms, O., and Ruiz-Omeñaca, J. I. 2009. The last hadrosaurid dinosaurs of Europe: A new lambeosaurine from the uppermost Cretaceous of Aren (Huesca, Spain). *Comptes Rendus Palevol* 8: 559–572.

Prieto-Márquez, A. 2005. New information on the cranium of *Brachylophosaurus canadensis* (Dinosauria, Hadrosauridae), with a revision of its phylogenetic position. *Journal of Vertebrate Paleontology* 25: 144–156.

Prieto-Márquez, A. 2007. Postcranial osteology of the hadrosaurid dinosaur *Brachylophosaurus canadensis* from the Late Cretaceous of Montana. In *Horns and Beaks: Ceratopsian and Ornithopod Dinosaurs*. Edited by K. Carpenter. Indiana University Press. pp. 91–115.

Prieto-Márquez, A. 2010a. Global phylogeny of Hadrosauridae (Dinosauria: Ornithopoda) using parsimony and Bayesian methods. *Zoological Journal of the Linnean Society* 159:435–502.

Prieto-Márquez, A. 2010b. Global historical biogeography of hadrosaurid dinosaurs. *Zoological Journal of the Linnean Society* 159:503–525.

Prieto-Márquez, A. 2010c. *Glishades ericksoni*, a new hadrosauroid (Dinosauria: Ornithopoda) from the Late Cretaceous of North America. *Zootaxa* 2452:1–17.

Prieto-Marquez, A. 2010d. The braincase and skull roof of *Gryposaurus notabilis* (Dinosauria, Hadrosauridae), with a taxonomic revision of the genus. *Journal of Vertebrate Paleontology* 30: 838–854.

Prieto-Márquez, A. 2011. A reappraisal of *Barsboldia sicinskii* (Dinosauria: Hadrosauridae) from the Late Cretaceous of Mongolia. *Journal of Paleontology* 85:468–477.

Prieto-Márquez, A. 2012. The skull and appendicular skeleton of *Gryposaurus latidens*, a saurolophine hadrosaurid (Dinosauria: Ornithopoda) from the early Campanian (Cretaceous) of Montana, USA. *Canadian Journal of Earth Sciences* 49:510–532.

Prieto-Márquez, A. 2014a. Skeletal morphology of *Kritosaurus navajovius* (Dinosauria: Hadrosauridae) from the Late Cretaceous of the North American southwest, with an evaluation of the phylogenetic systematics and biogeography of Kritosaurini. *Journal of Systematic Palaeontology* 12: 133–175.

Prieto-Márquez, A. 2014b. A juvenile *Edmontosaurus* from the late Maastrichtian (Cretaceous) of North America: Implications for ontogeny and phylogenetic inference in saurolophine dinosaurs. *Cretaceous Research* 50:282–303.

Prieto-Márquez, A. and Guenther, M.F. 2018. Perinatal specimens of *Maiasaura* from the Upper Cretaceous of Montana (USA): insights into the early ontogeny of saurolophine hadrosaurid dinosaurs. *PeerJ* 6: e4734.

Prieto-Márquez, A. and Gutarra, S. 2016. The ‘duck-billed’ dinosaurs of Careless Creek (Upper Cretaceous of Montana, USA), with comments on hadrosaurid ontogeny. *Journal of Paleontology* 90:133–146.

Prieto-Márquez, A. and Salinas, G. C. 2010. A re-evaluation of *Secernosaurus koernerii*

and *Kritosaurus australis* (Dinosauria, Hadrosauridae) from the Late Cretaceous of Argentina. *Journal of Vertebrate Paleontology* 30:813–837.

Prieto-Márquez, A. and Serrano Brañas, C. I. 2012. *Latirhinus uitstlani*, a “broad-nosed” saurolophine hadrosaurid (Dinosauria, Ornithopoda) from the late Campanian (Cretaceous) of northern Mexico. *Historical Biology* 24: 607–619.

Prieto-Márquez, A. and Wagner, J. R. 2013. A new species of saurolophine hadrosaurid dinosaur from the Late Cretaceous of the Pacific coast of North America. *Acta Palaeontologica Polonica* 58:255–268.

Prieto-Márquez, A., Chiappe, L. M., and Joshi, S. H. 2012. The lambeosaurine dinosaur *Magnapaulia laticaudus* from the Late Cretaceous of Baja California, northwestern Mexico. *PLoS One* 7:e38207, 1–32.

Prieto-Márquez, A., Dalla Vecchia, F. M., Gaete, R., and Galobart, À. 2013. Diversity, relationships, and biogeography of the lambeosaurine dinosaurs from the European Archipelago, with description of the new aralosaurin *Canardia garonnensis*. *PLoS One* 8:e69835, 1–44.

Prieto-Márquez, A., Erickson, G. M., and Ebersole, J. A. 2016. A primitive hadrosaurid from southeastern North America and the origin and early evolution of ‘duck-billed’ dinosaurs. *Journal of Vertebrate Paleontology* e1054495, 1–10.

Prieto-Márquez, A., Fondevilla, V., Sellés, A. G., Wagner, J. R., and Galobart, A. 2019. *Adynomosaurus arcanus*, a new lambeosaurine dinosaur from the Late Cretaceous Ibero-Armorican Island of the European archipelago. *Cretaceous Research* 96: 19–37.

Prieto-Márquez, A., Wagner, J. R., and Lehman, T. 2020. An unusual “shovel-billed” dinosaur with trophic specializations from the early Campanian of Trans-Pecos Texas, and the ancestral hadrosaurian crest. *Journal of Systematic Palaeontology* 18: 461–498.

Ramírez Velasco, A. A. 2022. Phylogenetic and biogeography analysis of Mexican hadrosauroids. *Cretaceous Research* 138:105267, 1–14.

Ramírez Velasco, A. A., Aguilar, F. J., Hernández-Rivera, R., Gudiño Maussán, L. G., Rodríguez, M. L., and Alvarado-Oretega, J. 2021. *Tlatolophus galorum*, gen. et sp. nov., a parasaurolophin dinosaur from the upper Campanian of the Cerro del Pueblo Formation, Coahuila, northern Mexico. *Cretaceous Research* 126:104884, 1–33.

Reid, M. 1990. *The Last Great Dinosaurs: An Illustrated Guide to Alberta's Dinosaurs*. Red Deer College Press.

Roberts, E. M., Deino, A. L., and Chan, M. A. 2005. $^{40}\text{Ar}/^{39}\text{Ar}$ age of the Kaiparowits Formation, southern Utah, and correlation of contemporaneous Campanian strata and vertebrate faunas along the margin of the Western Interior Basin. *Cretaceous Research*

26:307–318.

Romano, M. and Farlow, J. 2018. Bacteria meet the “titans”: horizontal transfer of symbiotic microbiota as a possible driving factor of sociality in dinosaurs. *Bollettino della Società Paleontologica Italiana* 57: 75–79.

Ronquist, F. and Huelsenbeck, J. P.. 2003. MRBAYES 3: Bayesian phylogenetic inference under mixed models. *Bioinformatics* 19:1572-1574.

Rozadilla, S., Brissón-Egli, F., Agnolín, F. L., Aranciaga-Rolando, A. M., and Novas, F. E. 2021. A new hadrosaurid (Dinosauria: Ornithischia) from the Late Cretaceous of northern Patagonia and the radiation of South American hadrosaurids. *Journal of Systematic Palaeontology* 19:1207–1235.

Russell, D.A. 1989. *An Odyssey in Time: The Dinosaurs of North America*. 240 pp. University of Toronto Press, Toronto.

Ryan, M. J. 2007. A new basal centrosaurine ceratopsid from the Oldman Formation, southeastern Alberta. *Journal of Paleontology* 81:376–396.

Ryan, M. J., and Chiba, K. 2020. Reassessment of *Coronosaurus brinkmani* from the Oldman Formation (Campanian) of southern Alberta. *Vertebrate Anatomy Morphology*

Palaeontology, 8: 54–55.

Ryan, M. J., and Evans, D. C. 2005. Ornithischian dinosaurs. In *Dinosaur Provincial Park: A Spectacular Ancient Ecosystem Revealed*. Edited by P.J. Currie and E.B. Koppelhus. Indiana University Press. pp. 312–348.

Ryan, M. J., and Russell, A. P. 2001. Dinosaurs of Alberta (exclusive of Aves). In *Mesozoic Vertebrate Life: New Research Inspired by the Paleontology of Philip J. Currie*. Edited by D. H. Tanke, and K. Carpenter. Indiana University Press. pp. 279–297.

Ryan, M. J., and Russell, A. P. 2005. A new centrosaurine ceratopsid from the Oldman Formation of Alberta and its implications for centrosaurine taxonomy and systematics. *Canadian Journal of Earth Sciences* 42:1369– 1387.

Ryan, M. J., Eberth, D. A., Brinkman, D. B., Currie, P. J., and Tanke, D. H. 2010. A new *Pachyrhinosaurus*-like ceratopsid from the upper Dinosaur Park Formation (Late Campanian) of southern Alberta, Canada. In: M.J. Ryan, B.J. Chinnery–Allgeier, and D.A. Eberth (eds.), *New Perspective on Horned Dinosaurs*, 141–155. Indiana University Press, Bloomington.

Ryan, M. J., Evans, D. C., and Shepherd, K. M. 2012. A new ceratopsid from the Foremost formation (middle Campanian) of Alberta. *Canadian Journal of Earth Sciences*, 49(10): 1251–1262.

Ryan, M. J., Evans, D. C., Currie, P. J., and Loewen, M. A. 2014. A new chasmosaurine from northern Laramidia expands frill disparity in ceratopsid dinosaurs. *Naturwissenschaften* 101:505–512.

Ryan, M. J., Holmes, R., Mallon, J., Loewen, M., and Evans, D. C. 2017. A basal ceratopsid (Centrosaurinae: Nasutoceratopsini) from the Oldman Formation (Campanian) of Alberta, Canada. *Canadian Journal of Earth Sciences* 54:1–14.

Saitta, E. T., Stockdale, M. T., Longrich, N. R., Bonhomme, V., Benton, M. J., Cuthill, I. C., and Makovicky, P. J. 2020. An effect size statistical framework for investigating sexual dimorphism in non-avian dinosaurs and other extinct taxa. *Biological Journal of the Linnean Society* 131: 231–273.

Sampson, S. D., Loewen, M. A., Farke, A. A., Roberts, E. M., Forster, C. A., Smith, J. A., and Titus, A. L. 2010. New horned dinosaurs from Utah provide evidence for intracontinental dinosaur endemism. *PLoS One* 5:e12292

Schmitt, J. G., Jackson, F. D., and Hanna, R. R. 2014. Debris flow origin of an unusual Late Cretaceous hadrosaur bonebed in the Two Medicine Formation of western Montana. In: D.A. Eberth and D.C. Evans (eds.), *Hadrosaurs*, 486–501. Indiana University Press, Bloomington.

Schott, R. K., Evans, D. C., Goodwin, M. B., Horner, J. R., Brown, C. M., and Longrich, N. R. 2011. Cranial ontogeny in *Stegoceras validum* (Dinosauria: Pachycephalosauria): a quantitative model of pachycephalosaur dome growth and variation. PLoS One 6: e21092.

Scott, E. E., Chiba, K., Fanti, F., Saylor, B. Z., Evans, D. C., and Ryan, M. J. 2022. Taphonomy of a monodominant *Gryposaurus* sp. bonebed from the Oldman Formation (Campanian) of Alberta, Canada. Canadian Journal of Earth Sciences, in press.

Serrano, J. F., Sellés, A. G., Vila, B., Galobart, À., and Prieto-Márquez, A. 2021. The osteohistology of new remains of *Pararhabdodon isonensis* sheds light into the life history and paleoecology of this enigmatic European lambeosaurine dinosaur. Cretaceous Research 118:104677.

Serrano-Brañas, C. I. and Prieto-Márquez, A. 2022. Taphonomic attributes of the holotype of the lambeosaurine dinosaur *Latirhinus uitstlani* from the late Campanian of Mexico: Implications for its phylogenetic systematics. Journal of South American Earth Sciences 114:103689, 1–16.

Shibata, M., Jintasakul, P., Azuma, Y., and You, H.-L. 2015. A new basal hadrosauroid dinosaur from the Lower Cretaceous Khok Kruat Formation in Nakhon Ratchasima

Province, northeastern Thailand. PLoS One 10:e0145904, 1–28.

Słowiak, J., Szczygielski, T., Ginter, M., and Fostowicz-Frelik, Ł. 2020. Uninterrupted growth in a non-polar hadrosaur explains the gigantism among duck-billed dinosaurs. *Palaeontology* 63: 579–599.

Słowiak, J., Szczygielski, T., Rothschild, B. M., and Surmik, D. 2021. Dinosaur senescence: a hadrosauroid with age-related diseases brings a new perspective of “old” dinosaurs. *Scientific Reports* 11:11947.

Sternberg, C. M. 1935. Hooded hadrosaurs of the Belly River Series of the Upper Cretaceous. *National Museum of Canada Bulletin* 77:1–38.

Sternberg, C. M. 1953. A new hadrosaur from the Oldman Formation of Alberta: discussion of nomenclature. *National Museum of Canada Bulletin* 128:275–286.

Sues, H.-D. and Averianov, A. 2009. A new basal hadrosauroid dinosaur from the Late Cretaceous of Uzbekistan and the early radiation of duck-billed dinosaurs. *Proceedings of the Royal Society B: Biological Sciences* 276:2549–2555.

Sullivan, R. M. and Williamson, T. E. 1999. A new skull of *Parasaurolophus* (Dinosauria: Hadrosauridae) from the Kirtland Formation of New Mexico and a revision

of the genus. *New Mexico Museum of Natural History and Science Bulletin* 15:1–52.

Swofford, D. L. 2002. PAUP*. *Phylogenetic Analysis Using Parsimony (*and Other Methods)*. Version 4. Sinauer Associates, Sunderland, Massachusetts.

Takasaki, R., Chiba, K., Kobayashi, Y., Currie, P. J., and Fiorillo, A. R. 2018. Reanalysis of the phylogenetic status of *Nipponosaurus sachalinensis* (Ornithopoda: Dinosauria) from the Late Cretaceous of Southern Sakhalin. *Historical Biology* 30:694–711.

Takasaki, R., Fiorillo, A. R., Kobayashi, Y., Tykoski, R. S., and McCarthy, P. J. 2019. The first definitive lambeosaurine bone from the Liscomb Bonebed of the Upper Cretaceous Prince Creek Formation, Alaska, United States. *Scientific Reports* 9:5384, 1–11.

Takasaki, R., Fiorillo, A.R., Tykoski, R.S., and Kobayashi, Y. 2020. Re-examination of the cranial osteology of the Arctic Alaskan hadrosaurine with implications for its taxonomic status. *PLoS One* 15: e0232410.

Thompson, M. G. W., Ryan, M. J., and Schröder-Adams, C. J. 2020. The first record of the hadrosaur *Probrachylophosaurus* in the foremost formation, representing the oldest occurrence of a brachylophosaurin in Alberta. *Vertebrate Anatomy Morphology Palaeontology*, 8: 58–59.

Thompson, M. G. W., Bedek, F. V., Schröder-Adams, C., Evans, D. C., and Ryan, M. J. 2021. The oldest occurrence of brachylophosaurin hadrosaurids in Canada. *Canadian Journal of Earth Sciences* 58:993–1004.

Trexler, D.L. 1995. A Detailed Description of Newly-discovered Remains of *Maiasaura peeblesorum* (Reptilia: Ornithischia) and a Revised Diagnosis of the Genus. 235 pp. M.Sc. Thesis, Department of Biological Sciences, University of Calgary, Calgary.

Trexler, D. L. 2001. Two Medicine Formation, Montana: geology and fauna. In: D.H. Tanke and K. Carpenter (eds.), *Mesozoic Vertebrate Life*, 298– 309. Indiana University Press, Bloomington.

Tsogtbaatar, K., Weishampel, D. B., Evans, D. C., and Watabe, M. 2019. A new hadrosauroid (Dinosauria: Ornithopoda) from the Late Cretaceous Baynshire Formation of the Gobi Desert (Mongolia). *PLoS One* 14: e0208480.

Varricchio, D.J. and Horner, J.R. 1993. Hadrosaurid and lambeosaurid bone beds from the Upper Cretaceous Two Medicine Formation of Montana: taphonomic and biologic implications. *Canadian Journal of Earth Sciences* 30: 997–1006.

Waldman, M. 1969. On an immature specimen of *Kritosaurus notabilis* (Lambe), (Ornithischia: Hadrosauridae) from the Upper Cretaceous of Alberta, Canada. *Canadian Journal of Earth Sciences* 6: 569–576.

Wallace, J. 1987. *The Rise and Fall of the Dinosaur*. 143 pp. Michael Friedman Publishing Group, Inc., New York.

Wang, R.-F., You, H.-L., Wang, S.-Z., Xu, S.-C., Yi, J., Xie, L.-J., Jia, L., and Xing, H. 2017. A second hadrosauroid dinosaur from the early Late Cretaceous of Zuoyun, Shanxi Province, China. *Historical Biology* 29:17–24.

Weishampel, D. B., Norman, D. B., and Grigorescu, D. 1993. *Telmatosaurus transylvanicus* from the Late Cretaceous of Romania: the most basal hadrosaurid dinosaur. *Palaeontology* 36:361–385.

Wagner, J. R. and Lehman, T. M. 2009. An enigmatic lambeosaurine hadrosaur (Reptilia: Dinosauria) from the Upper Shale Member of the Campanian Aguja Formation of Trans-Pecos Texas. *Journal of Vertebrate Paleontology* 29:605–611.

Williamson, T. E. 2000. Review of Hadrosauridae (Dinosauria, Ornithischia) from the San Juan Basin, New Mexico. *New Mexico Museum of Natural History and Science Bulletin* 17:191–214.

Wilson, J. P., Ryan, M. J., and Evans, D. C. 2020. A new, transitional centrosaurine ceratopsid from the Upper Cretaceous Two Medicine Formation of Montana and the

evolution of the ‘*Styracosaurus*-line’ dinosaurs. *Royal Society Open Science* 7:200284, 1–25.

Woodward, H.N. 2019. *Maiasaura* (Dinosauria: Hadrosauridae) tibia osteohistology reveals non-annual cortical vascular rings in young of the year. *Frontiers in Earth Science* 7: 50.

Woodward, H. N., Freedman Fowler, E. A., Farlow, J. O., and Horner, J. R. 2015. *Maiasaura*, a model organism for extinct vertebrate population biology: a large sample statistical assessment of growth dynamics and survivorship. *Paleobiology* 41: 503–527.

Wosik, M., Chiba, K., Therrien, T., and Evans, D. 2020. Testing size-frequency distributions as a method of ontogenetic aging: a life-history assessment of hadrosaurid dinosaurs from the Dinosaur Park Formation of Alberta, Canada, with implications for hadrosaurid paleoecology. *Paleobiology* 46: 379–404.

Wosik, M. and Evans, D. C. 2022. Osteohistological and taphonomic life-history assessment of *Edmontosaurus annectens* (Ornithischia: Hadrosauridae) from the Late Cretaceous (Maastrichtian) Ruth Mason dinosaur quarry, South Dakota, United States, with implication for ontogenetic segregation between juvenile and adult hadrosaurids. *Journal of Anatomy* 241:272–296.

Wyenberg-Henzler, T., Patterson, R. T., and Mallon, J. C. 2022. Ontogenetic dietary shifts in North American hadrosaurids (Dinosauria: Ornithischia). *Cretaceous Research* 135:105177.

Xing, L., Niu, K., Yang, T.-R., Wang, D., Miyashita, T., and Mallon, J. C. 2022. Hadrosauroid eggs and embryos from the Upper Cretaceous (Maastrichtian) of Jiangxi Province, China. *BMC Ecology and Evolution* 22:60.

Xing, H., Prieto-Márquez, A., Gu, W., and Yu, T.-X. 2012. Re-evaluation and phylogenetic analysis of *Wulagasaurus dongi*, a hadrosaurine dinosaur from the Maastrichtian of northeast China. *Vertebrata Palasiatica*, 50: 160–169.

Xing, H., Wang, D., Han, F., Sullivan, C., Ma, Q., He, Y., Hone, D. W. E., Yan, R., Du, F., and Xu, X. 2014a. A new basal hadrosauroid dinosaur (Dinosauria: Ornithopoda) with transitional features from the Late Cretaceous of Henan Province, China. *PLoS One* 9:e98821, 1–23.

Xing, H., Zhao, X., Wang, K., Li, D., Chen, S., Mallon, J. C., Zhang, Y., and Xu, X. 2014b. Comparative osteology and phylogenetic relationship of *Edmontosaurus* and *Shantungosaurus* (Dinosauria: Hadrosauridae) from the Upper Cretaceous of North America and East Asia. *Acta Geologica Sinica (English Edition)* 88:1623–1652.

Xing, H., Mallon, J. C., and Currie, M. L. 2017. Supplementary cranial description of the

types of *Edmontosaurus regalis* (Ornithischia: Hadrosauridae), with comments on the phylogenetics and biogeography of Hadrosaurinae. PLoS One 12: e075253.

Xing, H., Gu, W., Hai, S., Yu, T., Han, D., Zhang, Y., and Zhang, S. 2022. Osteological and taxonomic reassessments of *Sahaliyania elunchunorum* (Dinosauria, Hadrosauridae) from the Upper Cretaceous Yuliangzi Formation, northeast China. Journal of Vertebrate Paleontology e2085111:1–23.

Zhang, J., Wang, X., Wang, Q., Jiang, S., Cheng, X., Li, N., and Qiu, R. 2019. A new saurolophine hadrosaurid (Dinosauria: Ornithopoda) from the Upper Cretaceous of Shandong, China. Anais da Academia Brasileira de Ciências (2019) 91(Suppl. 2): e20160920, 1–20.

Zhang, Y.-G., Wang, K.-B., Chen, S.-Q., Liu, D., and Xing, H. 2020. Osteological re-assessment and taxonomic revision of “*Tanius laiyangensis*” (Ornithischia: Hadrosauroidae) from the Upper Cretaceous of Shandong, China. The Anatomical Record 303:790–800.

Zhu, X., Wang, Q., and Wang, X. 2022. Restudy of the original and new materials of *Stromatoolithus pinglingensis* and discussion on some Spheroolithidae eggs. Historical Biology 34:283–297.